Fakultät für Elektrotechnik und Informationstechnik
Technische Universität München

Modelling space harmonics in induction machines for real-time applications

Julien Alexandre Cordier

Vollständiger Abdruck der von der Fakultät für Elektrotechnik und Informationstechnik der Technischen Universität München zur Erlangung des akademischen Grades eines

Doktor-Ingenieurs (Dr.-Ing.)

genehmigten Dissertation.

Vorsitzender:

Prof. Dr.-Ing. Ulrich Wagner

Prüfer:

1. Prof. Dr.-Ing. Dr. h. c. Ralph Kennel
2. Prof. Dr. Jean-Luc Thomas
   Conservatoire National des Arts et Métiers, Paris

Die Dissertation wurde am 19.11.2019 bei der Technischen Universität München eingereicht und durch die Fakultät für Elektrotechnik und Informationstechnik am 01.01.2020 angenommen.

Abstract

The present work examines a modelling approach for space harmonics in low-power off-the-shelf induction machines. These cost-saving machines usually exhibit a radial flux density distribution over the air-gap circumference far from sinusoidal. The flux density harmonics give rise to additional stator current components resulting in unwanted torque oscillations. At the same time, they also provide instrumental information for condition monitoring or rotor speed estimation. Taking advantage of these properties to achieve better drive performance necessitates a more accurate, yet simple machine description. These aspects are challenging, as generally no information about internal structure and magnetic characteristics is available for off-the-shelf machines, whereas the physical phenomena considered are complex.

The approach presented in this thesis constitutes a trade-off between these requirements. We primarily focus on space harmonics arising from the non-sinusoidal conductor distribution over the air-gap circumference and assume linear magnetic properties and a constant air-gap length. Using the winding function theory and key mathematical properties of Fourier series, we obtain a simple relation between currents and flux linkages including the contribution of flux density harmonics. The concept of interconnection matrices allows us to account for various types of winding configurations and therefore greatly simplifies the derivation of state-space models including flux density harmonics for specific machines.

In a further step, we derive a coordinate transformation combining interconnection matrices with the discrete Fourier transform to reduce the model order. The transformation allows for a substantial decrease of computational effort and makes the modelling approach presented promising for torque ripple reduction applications. More broadly, it provides a general means of analysing space harmonics and potentially opens new possibilities for multiphase drive applications.

Kurzfassung

Die vorliegende Arbeit untersucht einen Modellierungsansatz für Raumharmonische in handelsüblichen Asynchronmaschinen kleiner Leistung. In diesen kostengünstigen Maschinen ist die radiale Flussdichteverteilung über den Luftspalt meistens nicht sinusförmig. Die Oberwellen der Flussdichteverteilung verursachen zusätzliche Statorstromharmonische, die Drehmomentschwingungen hervorrufen. Gleichzeitig stellen sie eine hilfreiche Informationsquelle für Zustandsdiagnose und Drehzahlschätzung dar. Die Nutzung dieser Eigenschaften zur Erhöhung der Antriebsperformanz erfordert eine genauere, jedoch simple Maschinenbeschreibung. Im Falle handelsüblicher Maschinen stellen diese Aspekte aufgrund fehlender Daten über internen Aufbau sowie magnetische Eigenschaften eine Herausforderung dar, zumal die betrachteten physikalischen Phänomene komplex sind.

Der in dieser Dissertation beschriebene Ansatz stellt einen Kompromiss zwischen diesen Anforderungen dar. Wir befassen uns vorrangig mit Raumharmonischen, welche von der nicht sinusförmigen Leiterverteilung am Luftspaltumfang herrühren. Lineare magnetische Eigenschaften werden vorausgesetzt und die Luftspaltlänge wird als konstant angenommen. Der Ansatz der Wicklungsverteilungsfunktion sowie entscheidende mathematische Eigenschaften von Fourier-Reihen ermöglichen die Herleitung eines einfachen Zusammenhangs zwischen Strömen und Flussverkettungen, welcher den Beitrag der Flussdichteoberwellen berücksichtigt. Die Verwendung von Verschaltungsmatrizen bietet die Möglichkeit, verschiedene Arten von Wicklungskonfigurationen in Betracht zu ziehen. Dies vereinfacht die Herleitung von Zustandsraummodellen unter Berücksichtigung Harmonischer der Flussdichteverteilung für spezielle Maschinen deutlich.

Im Weiteren wird eine Koordinatentransformation durch Kombination der Verschaltungsmatrizen mit der diskreten Fourier-Transformation zur Reduzierung der Modellordnung hergeleitet. Die Transformation bietet eine wesentliche Verringerung des Rechenaufwands und macht den beschriebenen Modellierungsansatz vielversprechend für Anwendungen zur Verringerung von Drehmomentschwankungen. Im Allgemeinen stellt die Transformation eine systematische Methode zur Analyse von Raumharmonischen dar und eröffnet unter Umständen neue Möglichkeiten für Anwendungen mit Mehrphasenmaschinen.

Acknowledgements

This doctoral dissertation constitutes a summary of my research activities carried out during my time at the Chair of Electrical Drive Systems and Power Electronics, Technical University of Munich. I would like to pay tribute to those who, through their kind help and support, contributed to this thesis become reality.

I am extremely grateful to Professor Ralph Kennel, head of the Chair of Electrical Drive Systems and Power Electronics, for allowing me to perform my doctoral studies at his institute. I particularly appreciated the possibility of working on a research topic I truly feel passionate about as well as the great latitude granted in organizing and conducting my research work. I am highly honoured that Prof. Kennel offered me the opportunity of assisting him with the management of the institute, which enabled me to acquire fundamental skills for my professional development beyond the scientific scope.

I express my profound gratitude to Professor Jean-Luc Thomas (Conservatoire National des Arts et Métiers, Paris) for his ardent interest in the research topic and his tremendous enthusiasm to provide supportive expertise. This includes in particular the numerous in-depth technical conversations over the phone despite his busy schedule. I also warmly thank Prof. Thomas for accepting to be a reviewer in my doctoral examination process.

I am grateful to Professor Ulrich Wagner, head of the Chair of Energy Economy and Application Technology at the Technical University of Munich, for chairing the examination committee.

Part of my research activities was funded by the German Research Foundation (DFG). In addition, the company dSPACE GmbH generously provided an FPGA board essential to the experiments presented in the dissertation. I wish to acknowledge these contributions.

My thanks go to my colleagues and former colleagues for the pleasant atmosphere at work. I feel especially grateful to Professor Christoph Hackl (Hochschule München/Munich University of Applied Sciences) for his valuable advice as well as to Dr.-Ing. Daniel Glose and Dr.-Ing. Saeid Saeidi for the fruitful technical exchanges and the good time spent in the office. I remain deeply indebted to M. Sc. Alexander Florian and M. Sc. Stefan Klass for their decisive help and support, a tiny bit of which includes proofreading the present document. I sincerely thank Ms. Sabine Prucker for taking great care of the administrative procedure leading to my doctoral examination and ensuring the latter could take place on the scheduled day.

I dedicate this work to my parents, as there is no word strong enough to make up for the considerable debt of gratitude I owe to them.

Munich in January 2020

Contents

List of figures

List of tables

Nomenclature

Physical constants

μ_0	permeability of vacuum

Symbols

α	air-gap geometric coordinate
δt	step size
δ	air-gap length
δ_0	ideal air-gap length
γ	normalized air-gap coordinate
ω	angular velocity
Ψ, ψ	flux linkage
Ψ_σ	leakage flux
$\widetilde{\Psi}$, $\widetilde{\psi}$	main flux linkage
Θ	magnetomotive force (MMF)
θ_r	rotor mechanical angle
B	magnetic flux density
C_W	coefficient of friction
f	frequency
f_{sw}	inverter switching frequency
H	magnetic field strength
h	harmonic order
i	current
J_M	rotor moment of inertia
L	inductance
l	rotor lamination stack length
L_σ	leakage inductance
M	mutual inductance
M_L	load torque
M_M	electromechanical torque
m_r	number of rotor circuits
m_s	number of stator circuits

N_r	number of rotor slots/bars
N_s	stator slot number
P_{el}	electrical power
R	resistance
r	air-gap mean radius
s	slip
t	time
T_s	sampling period
U	rms voltage
u	voltage
W_R	number of turns of a rotor winding coil
w_r	number of rotor windings
W_S	number of turns of a stator winding coil
w_s	number of stator windings
Z_p	pole pair number

Mathematical objects

$\mathbb{C}$	set of complex numbers
$\mathbf{C}$	interconnection matrix, output matrix
$C_{2\pi}$	set of 2π-periodic continuous functions from $\mathbb{R}$ to $\mathbb{C}$
$\mathcal{W}_{\mathrm{m}}$	$m \times m$ Fourier matrix ($m \in \mathbb{N}^\star$)
$E_{2\pi}$	set of 2π-periodic piecewise continuous functions from $\mathbb{R}$ to $\mathbb{C}$
$\gamma_{r0,n}$	shift angle between conductor distribution functions of rotor circuits $n \in [\![0,\, m_r - 1]\!]$ and 0
$\gamma_{s0,m}$	shift angle between conductor distribution functions of stator circuits $m \in [\![0,\, m_s - 1]\!]$ and 0
$\mathbf{I_m}$	$m \times m$ identity matrix ($m \in \mathbb{N}^\star$)
$\mathfrak{Im}[\cdot]$	imaginary part of a complex number
$\langle \cdot \vert \cdot \rangle$	Hermitian inner product
$[\![a,\, b]\!]$	for $(a, b) \in \mathbb{Z}^2$, such that $a \leqslant b$, $[\![a,\, b]\!] = \{k \in \mathbb{Z} \mid a \leqslant k \leqslant b\}$
$\widetilde{L}_{r,\,h}$	rotor main inductance for wavelength of order $h \in \mathbb{N}^\star$
$\widetilde{L}_{s,\,h}$	stator main inductance for wavelength of order $h \in \mathbb{N}^\star$
$\widetilde{\mathbf{L}}_{\mathbf{h}}$	main inductance matrix associated with wavelength h (non-interconnected circuits)
$\widetilde{\mathbf{L}}_{\mathbf{r\,h}}$	rotor main inductance matrix associated with wavelength h (non-interconnected circuits)
$\widetilde{\mathbf{L}}_{\mathbf{rs\,h}}$	coupling inductance matrix associated with wavelength h (non-interconnected circuits)
$\widetilde{\mathbf{L}}_{\mathbf{s\,h}}$	stator main inductance matrix associated with wavelength h (non-interconnected circuits)
$\widetilde{\mathbf{L}}_{\mathbf{sr\,h}}$	$\widetilde{\mathbf{L}}_{\mathbf{sr\,h}} = \widetilde{\mathbf{L}}_{\mathbf{rs\,h}}^{\top}$
$\mathbf{L}$	inductance matrix of a set of non-interconnected circuits

$\mathcal{H}$	set of wavelength orders considered in a model, $\mathcal{H} \subset \mathbb{N}^\star$
$\mathcal{M}_{m,\,n}(\mathbb{C})$	set of $m \times n$ matrices with entries in $\mathbb{C}$ ($(m,\,n) \in (\mathbb{N}^\star)^2$)
$\mathcal{T}_{\mathcal{W}m}$	transformation operator based on the $m \times m$ Fourier matrix
$\mathbf{A}$	system matrix
$\mathbf{B}$	input matrix
$\mathbf{L}'$	inductance matrix of a network of interconnected circuits
$\mathbf{R}'$	resistance matrix of a network of interconnected circuits
$\mathbb{N}$	set of natural numbers (including zero)
$\|\cdot\|$	norm
$\mathbb{N}^\star$	$\mathbb{N}^\star = \mathbb{N} \setminus \{0\}$
$\widetilde{\psi}_{rn_0,\,h}$	contribution of wavelength h to the main flux of rotor circuit $n_0 \in [\![0,\,m_r - 1]\!]$
$\widetilde{\psi}_{sm_0,\,h}$	contribution of wavelength h to the main flux of stator circuit $m_0 \in [\![0,\,m_s - 1]\!]$
$\mathbb{R}$	set of real numbers
$\mathbb{R}^+$	set of positive real numbers including zero, i.e. $\mathbb{R}^+ = \{x \in \mathbb{R} \mid x \geqslant 0\}$
$\mathfrak{Re}[\cdot]$	real part of a complex number
$\mathbf{R}$	resistance matrix of a set of non-interconnected circuits
$\mathcal{Z}_{\mathrm{s}}$	transformation matrix in presence of circuit interconnections
φ_h	$\varphi_h = \varphi_{s0,\,h} - \varphi_{r0,\,h}$, for $h \in \mathbb{N}^\star$
$\varphi_{r0,\,h}$	argument of the Fourier coefficient of order h of conductor distribution function W_{r0}
$\varphi_{s0,\,h}$	argument of the Fourier coefficient of order h of conductor distribution function W_{s0}
$\vec{\widetilde{\Psi}}$	main flux linkage vector
$\vec{\widetilde{\Psi}}_h$	main flux linkage vector for wavelength $h \in \mathbb{N}^\star$
$\vec{\widetilde{\psi}}_{r,\,h}$	rotor main flux linkage vector for wavelength $h \in \mathbb{N}^\star$
$\vec{\widetilde{\psi}}_{s,\,h}$	stator main flux linkage vector for wavelength $h \in \mathbb{N}^\star$
$\vec{\Psi}$	flux linkage vector
$\vec{i}$	current vector of a set of non-interconnected circuits
$\vec{i}'$	vector of *independent* currents in a network of interconnected circuits
$\vec{u}$	voltage vector of a set of non-interconnected circuits
$\vec{u}'$	vector of *independent* voltages in a network of interconnected circuits
$\mathbb{Z}$	set of integers
$\mathbb{Z}^\star$	$\mathbb{Z}^\star = \mathbb{Z} \setminus \{0\}$
$B(\gamma_s)$	flux density distribution function in stator coordinates
$B'(\gamma_r)$	flux density distribution function in rotor coordinates
$c_h(f)$	Fourier coefficient of order $h \in \mathbb{Z}$ of the function f
$L_{M,\,h}$	coupling inductance between stator and rotor for wavelength of order $h \in \mathbb{N}^\star$
W	conductor distribution function
W_0	basic winding distribution function

Subscripts

α	stator direct axis component
β	stator quadrature axis component
$\mathcal{H}$	denotes quantities computed using only the wavelength orders present in set $\mathcal{H}$
σ	leakage
d	rotor direct axis component
q	rotor quadrature axis component
r	rotor
s	stator

Superscripts

$\natural$, $\sharp$, $\flat$	denote transformed quantities
$\prime$	denotes electrical quantities in a network of interconnected circuits
r	rotor
s	stator

Introduction

Induction machines are omnipresent in our modern society, with applications in the residential, industrial as well as the transportation sector. Although showing lower power densities as their permanent magnet synchronous counterparts, induction machines are highly robust, comparatively cheap and not depending on rare earth materials, a criterion of crucial importance with respect to the development of electromobility. Simultaneously, the currently raising concerns about climate change and the need for a more responsible use of energy motivates the development of more efficient control strategies for electric drives.

The present work focuses on a particular, yet extremely common case in this wide context which is applications involving off-the-shelf induction machines in a power range of up to around ten kilowatts. The radial flux density distribution over the air-gap circumference of these low-power machines generally displays a high amount of harmonics which produce unwanted stator current components, torque oscillations and losses. Simultaneously, they also provide useful information for monitoring the machine condition or estimating the rotor speed.

The consideration of these so-called 'space harmonics' in control schemes to achieve better drive performance creates interesting challenges as Park's modelling approach to AC machines is not applicable anymore and a more precise machine model is required. In addition, usually no information about internal structure and magnetic properties is available for off-the-shelf machines. Moreover, the new model must be real-time compliant to meet an essential need of drive control applications. The modelling strategy described in the thesis aims at finding a compromise between these constraints.

After presenting the context and setting the objectives of the study in the first chapter, we will introduce the fundamental modelling concepts in chapter 2 and propose the first version of an extended model including the effect of space harmonics in induction machines.

In chapter 3, we will concentrate on space harmonics caused by the non-sinusoidal conductor distribution over the air-gap circumference. We assume linear magnetic properties and a constant air-gap length. These hypotheses will allow for simplifications and are a first step towards real-time compliance.

We will then propose and discuss a coordinate transformation for the magnetically linear model in chapter 4. We will show by means of concrete examples that this transformation enables a substantial reduction of the model complexity.

The practical potential of the transformed model will be assessed in chapter 5 and conclusions will be drawn on its ability to fulfil the initial objectives.

Chapter 1
Scope and objectives of the thesis

Overview of chapter

This introductory chapter presents the context of the investigations carried out in the frame of the thesis. This aspect includes the existing applications in the considered field. As we focus on off-the-shelf machines with unknown internal structure, the use of methods such as finite element analysis is not possible. We will therefore review alternative modelling techniques for taking space harmonics into account and discuss their benefits and drawbacks.

This will allow us to set the objectives of the present study.

1.1 Considered problem and general assumptions

The considerations in the present work essentially focus on inverter drives featuring *off-the-shelf* squirrel cage induction machines for which no information about internal geometry or magnetic properties is available. These inexpensive yet robust machines often exhibit a radial air-gap flux density distribution far from sinusoidal and thus do not satisfy the fundamental hypothesis of Park's modelling approach.

The harmonics present in the air-gap flux density distribution, known as *space harmonics*, induce additional voltage and current components in the electrical conductors of the machine (see for instance [1, chapt. 10]). On the one hand, this results in increased iron losses as well as unwanted torque oscillations leading to vibrations and noise. On the other, some of the extra stator current components arising from the presence of space harmonics can provide valuable information to detect the rotor speed or position.

As we will see next, these characteristics provide the foundation for real-time control applications such as encoderless control (commonly known as sensorless control), machine condition monitoring and current (or torque) harmonic reduction. The present study targets:

1.) current and torque harmonic reduction primarily;

2.) encoderless control applications to a lesser extent.

We presume that the power of the drive is low enough to allow for the use of inverters with a switching frequency of at least 10 kHz, a condition typically met by IGBT inverters up to a few tens of kilowatts. This enables us to consider the inverter dynamic performance as sufficiently high to generate the voltage reference waveforms needed in order to damp the current harmonics mentioned above. We will therefore regard the inverter as ideal and ignore the parasitic high-frequency components in its output voltages. The modelling approach will be centred on the machine.

1.2 Air-gap flux density harmonics in induction machines

1.2.1 Physical origin

The nature, origin and impact of air-gap flux density harmonics in induction machines have been investigated since the beginning of the 20^{th} century and are well-documented in the literature. Extensive analyses of the phenomenon can be found in particular in the works of Kron (cf. [2], [1, chapt. 10]), Liwschitz [3], Alger [4] or White and Woodson [5, chapt. 10 and 11]. We will therefore only briefly mention a few important facts here.

The non-ideal distribution of the air-gap flux density in real induction machines results essentially from two effects:

1.) the discrete distribution of electric conductors, concentrated in slots on the stator as well as on the rotor;

2.) the variation of permeance due to slot opening, eccentricity or saturation of the lamination stack.

1.2.2 Space harmonics related to the discrete conductor distribution

In a machine with uniform air-gap, fed by a set of balanced sinusoidal voltages in which only the first of the aforementioned effects is considered, the fundamental of the resulting stator currents produces a stepwise magnetomotive force (MMF) distribution along the air-gap circumference. This results in a rotating air-gap flux density distribution being the superposition of many waves with different wavelengths (or pairs of poles), some of which induce voltages and currents in the rotor conductors. The latter generate a stepwise MMF and air-gap flux density contributions inducing current components in the stator conductors which in turn generate a stepwise MMF etc. Kron has described this process of harmonic generation in detail in [1, chapt. 10] and proposed an equivalent machine representation in which the different waves of the air-gap flux density distribution are modelled as virtual machines with corresponding pole pair numbers, all rotating at the same speed. We will take a closer look at this approach in section 1.4.

References [6] and [7] present a concise mathematical description of flux density waves arising from the discrete conductor distribution and summarize the conditions for them to generate additional frequency components in the stator currents. Of major interest are the well-known *principal slot harmonics (PSH)*, the frequency of which depends on the rotor angular velocity. In the case of three-phase cage induction machines, the corresponding frequencies are [7]:

- Lower principal slot harmonic:

$$f_{\mathrm{LPSH}} = \left[1 - \frac{N_r}{Z_p}(1-s)\right] f \tag{1.1a}$$

- Upper principal slot harmonic:

$$f_{\mathrm{UPSH}} = \left[1 + \frac{N_r}{Z_p}(1-s)\right] f \tag{1.1b}$$

where N_r represents the number of rotor bars, Z_p the machine pole pair number, s the slip and f the supply frequency. As flux density waves can only induce currents on the stator side if their pole pair number corresponds to an harmonic order present in the stator winding MMF, the lower and upper PSHs will not appear for any number of rotor bars. In a three-phase machine, the conditions to be met by N_r for a lower PSH to show up is $N_r \in \mathcal{R}_{\mathrm{LPSH}} = \{k \in \mathbb{N}^\star \mid k = Z_p(6p+2),\, p \in \mathbb{N}\}$. In contrast, an upper PSH will be visible if $N_r \in \mathcal{R}_{\mathrm{UPSH}} = \{k \in \mathbb{N}^\star \mid k = Z_p(6p-2),\, p \in \mathbb{N}\}$. Both PSHs may appear if N_r is multiple of $6Z_p$ [7].

1.2.3 Influence of permeance variations

In a real machine, slot openings, eccentricity and magnetic saturation cause the permeance to depend on the position considered along the air-gap circumference. The interaction of MMF waves with the variable permeance distribution leads to additional flux density waves. The non-constant permeance resulting from slot openings on the stator and the rotor leads to specific stator current components with the same frequency as the lower and upper PSH, thus impacting on their amplitude [7].

Besides slot openings, an eccentric rotor will also influence the permeance distribution and give rise to additional stator current components. This effect has been investigated in detail in [8–10].

The impact of magnetic saturation occurring in the lamination stack can be modelled as a periodic permeance distribution function with a number of periods over the air-gap circumference equal to the number of poles of the machine [7, 8, 11]. Saturation may produce stator current harmonics as well.

1.3 Significance of space harmonics for drive control applications

This section is intended to provide a brief overview of drive control applications with off-the-shelf induction machines, in which harmonics of the air-gap flux density play a significant role. There are predominantly three types of applications of interest:

- encoderless speed or position control;
- machine condition monitoring;
- current, torque and vibration suppression.

1.3.1 Encoderless control

Since the frequency of some additional stator current components caused by air-gap flux density harmonics is directly related to the rotor speed, the latter may be gained from a spectral analysis of the stator currents. The authors of [12] proposed a rotor speed detector extracting the frequency of slotting and eccentricity harmonics in stator currents, in order to extend encoderless control schemes based on Park's model which are known for being unreliable at low-speed due to measurement noise and inverter non-linearities. They compared the performance of several signal processing techniques to perform the required spectrum analysis in [13]. The detection of the rotor speed by processing current harmonics was reported more recently in [14] and [15].

As the current components arising from air-gap flux density harmonics vanish at zero-speed, traditional encoderless control methods for off-the-shelf induction machines at low speed detect permeance variations using an additional high-frequency test signal to estimate the rotor speed or position [16–19]. An alternative consists in using the voltage transients generated by the inverter pulse width modulation (PWM) [20–22].

1.3.2 Condition monitoring

Changes in the machine structure such as winding faults, broken rotor bars and eccentricity affect the air-gap flux density distribution and the time harmonics present in the stator currents. The analysis of stator currents in induction machines for the purpose of condition monitoring, known as 'motor signature current analysis' goes back to the 1990s with the publication by Toliyat and Lipo of an extended model based on the winding function approach which enables to take defective stator windings and rotor cages into account [23].

The research in the field includes the processing of stator current harmonics to detect inter-turn short circuits [24, 25], broken rotor bars [26–28], bearing faults [29] or rotor eccentricity [10, 30]. [31] proposes a method of detecting rotor bar failures in inverter-driven induction machines making use of a transient voltage excitation. Recent research activities appear to concentrate on improving the performance of the signal processing algorithms to enhance the identification of the current harmonics associated with specific types of faults [32, 33].

1.3.3 Current and torque harmonic reduction

Besides providing instrumental information for encoderless control and fault detection, current harmonics resulting from the discrete conductor distribution and permeance variations also generate

undesirable torque oscillations leading to vibrations and noise [2]. Although time harmonics originating from inverter supplies are the primary matter of concern with respect to current and torque ripple, some recent applications reported in the literature address the compensation of oscillations produced by space harmonics, in particular in the context of fault-tolerant drives [34, 35].

In a broader context going beyond the scope of the present study, the recent work presented in [36] discusses modelling strategies for reducing noise and vibrations in induction machine drives using time and space harmonic compensation. This shows the interest of the industry in the topic.

1.4 Review of modelling methods of interest

1.4.1 Context-related constraints

Since Park's model does not account for air-gap flux density harmonics (see for example [37, chapt. 2]), it is not appropriate for designing control algorithms intended for the aforementioned applications. Thus, a more accurate representation of magnetic and geometric characteristics is necessary, in order to derive a relation between currents and flux linkages taking into account the discrete conductor distribution as well as permeance variations. Owing to the considerations in section 1.1, the use of finite elements analysis for this purpose is not realistic, as the required machine data is not available.

Potentially effective modelling approaches to overcome this limitation are:

- the extension of Park's model to account for specific space harmonics;
- Kron's approach to modelling space harmonics;
- the winding function theory.

We will review them briefly in the next sections.

1.4.2 Extension of Park's model to account for space harmonics

Park's model, also known as 'fundamental model', since it assumes a sinusoidally distributed radial component of the air-gap flux density and therefore sinusoidal and continuous conductor distributions over the rotor circumference, has been extremely popular in drive control applications in the past decades. It relies on the concept of *space vector* and the Clarke transformation, which allow to represent the machine using a set of two orthogonal windings, one on the stator, the other on the rotor. We will only summarize the main features of the model. An in-depth description may be found for instance in [37, chapt. 2].

The model equations, using the stator and rotor current space vectors as state variables, are given below:

$$\begin{cases} \underline{u}_s^s = R_s \underline{i}_s^s + L_s \dfrac{\mathrm{d}\underline{i}_s^s}{\mathrm{d}t} + M \dfrac{\mathrm{d}\underline{i}_r^s}{\mathrm{d}t} & \text{(1.2a)} \\ \underline{0} = R_r \underline{i}_r^r + L_r \dfrac{\mathrm{d}\underline{i}_r^r}{\mathrm{d}t} + M \dfrac{\mathrm{d}\underline{i}_s^r}{\mathrm{d}t} & \text{(1.2b)} \\ M_M = \dfrac{3}{2} Z_p M \underline{i}_s^{s\top} \mathbf{J} \underline{i}_r^s & \text{(1.2c)} \\ \dfrac{\mathrm{d}\omega_r}{\mathrm{d}t} = \dfrac{1}{J_M}(M_M - M_L) & \text{(1.2d)} \end{cases}$$

where

$$\underline{u}_s^s = \begin{bmatrix} u_{s\alpha} & u_{s\beta} \end{bmatrix}^\top \in \mathbb{R}^2; \qquad \underline{i}_s^s = \begin{bmatrix} i_{s\alpha} & i_{s\beta} \end{bmatrix}^\top \in \mathbb{R}^2; \qquad \underline{i}_r^r = \begin{bmatrix} i_{rd} & i_{iq} \end{bmatrix}^\top \in \mathbb{R}^2; \qquad \mathbf{J} = \begin{bmatrix} 0 & -1 \\ 1 & 0 \end{bmatrix}$$

M_M and ω_r represent the electromechanical torque and the rotor angular velocity, respectively. The model parameters are: the stator resistance and inductance, (R_s and L_s resp.), the rotor resistance and inductance (R_r and L_r resp.), the mutual inductance M as well as the rotor inertia, J_M.

Considering the above relations, the success of Park's approach in drive control applications becomes apparent:

1.) the model involves few state variables (in the present case, the stator and rotor currents as well as the angular velocity and the rotor angle). Hence, it is not computationally demanding, a key criterion in real-time control applications;

2.) it has few parameters which can be determined easily in practice, for instance by means of a no-load and blocked rotor test.

In addition, Park's model provides a straightforward understanding of the transient and steady-state machine behaviour.

The above characteristics make Park's model ideal for drive control applications and constitute probably the reason why empirical extensions have been proposed to take specific air-gap flux density harmonics into account. This is mainly the case in encoderless control at low speed where air-gap permeance variations provide instrumental information about the rotor and flux position. A common technique consists in replacing the scalar inductance parameters in (1.2) by matrices to account for permeance differences in the main and quadrature axis (see for instance [16–18, 20]).

While these strategies are efficient and successful in tackling the problems of the respective applications, the empirical extension of concepts relying on very specific assumptions may appear as a limiting factor and raise concerns about general validity. The notion of space vector, the Clarke transformation and therefore Park's model equations are indeed inherently dependent on the hypothesis of sinusoidal air-gap flux density distribution.

These observations suggest giving up this assumption in the first place might be valuable to develop more general and potentially new solutions for control applications in which space harmonics play a crucial role.

1.4.3 Kron's method

Besides a generalized theory of electric machines based on tensorial analysis published in [38], Kron proposed a description of the current harmonic generation process caused by air-gap flux density waves arising from the discrete conductor distribution and slot openings (cf. [1, chapt. 10]). Kron's approach models each wave as a virtual machine with a number of pole pairs equal to the one of the wave. All virtual machines rotate at the mechanical speed of the real machine. Each of them features a set of two orthogonal sinusoidally distributed windings on the stator as well as on the rotor and its electrical equations are thus of the same form as the ones describing Park's model (compare eq. (1.2)). The inductances of a virtual machine are gained from the Fourier series representation of the air-gap flux density [39].

In a second step, the windings of the virtual machines are interconnected to account for the behaviour of the real machine, a process illustrated in fig. 1.1. The parameter P represents the pole pair number of the real machine, while Q is twice the product of the pole pair number and the number of stator

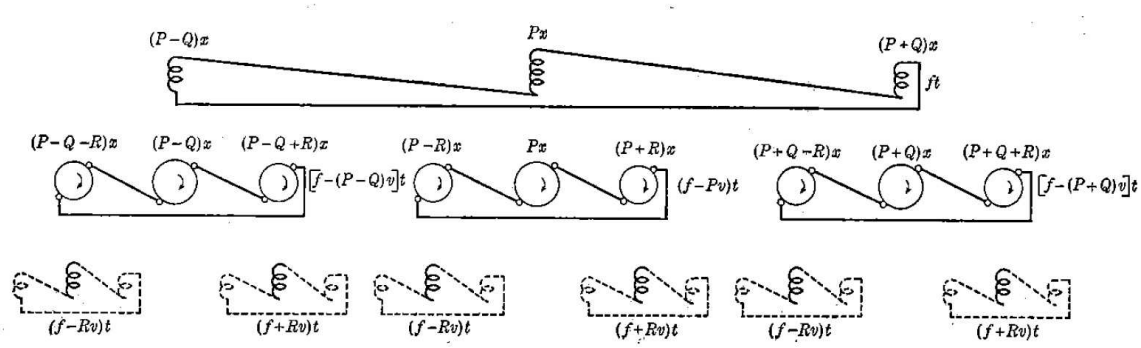

Figure 1.1: Interconnection of virtual machines to account for space harmonics [1, p. 183] ($P = Z_p$, $Q = 2Z_p w_s$, $R = N_r$)

windings w_s. R corresponds to the number of rotor bars. The top layer in the diagram models the presence of air-gap flux density waves generated by the fundamental stator currents and which induce currents in the rotor cage. This is achieved by connecting the stator windings of the virtual machines in series (on the first layer) and their rotor windings in parallel (on the second layer). The interaction of induced rotor currents with the stator is accounted for by introducing further virtual machines, the rotor of which is connected in series on the second layer, whereas their stators are connected in parallel on the third layer. The influence of the new stator current components on the rotor is considered by means of a fourth layer etc.

Note that the approach relies on the superposition principle and therefore assumes magnetic linearity. Originally intended for steady-state analysis, the method was extended by Vernet to obtain a state-space model of the induction machine including space harmonics [39, 40]. The strategy offers the possibility of considering the current components arising from space harmonics as specific states in the model. An application including the design of a Kalman filter to estimate the current component induced on the rotor side by a stator space harmonic is presented in [40].

Vernet's method appears particularly promising for torque ripple reduction or encoderless control, since it isolates the effect of given space harmonics in dedicated model states. A model for encoderless control could include for instance extra states assigned to rotor speed-dependent current components, while a torque ripple reduction scheme might feature states modelling unwanted current components with the aim of eliminating them through proper controller design.

One should, however, be aware of the increase in parameter number with each additional virtual machine required to model a particular current component. While clear rules apply to the inductances of the virtual machines (see above), the determination of their resistances is challenging. Modelling a stator current harmonic component requires at least three virtual machines, leading to roughly 15 parameters. In a context involving off-the-shelf machines with no structural data available, the tuning of such a set of parameters is problematic.

1.4.4 Winding function theory

The winding function approach started to gain importance in the 1990s and its use to model machines with concentrated windings or non-uniform air-gap [11, 23, 41, 42]. It consists in a simplified analysis of magnetic processes which are considered in a machine cross-section along the air-gap. The fundamental assumptions of the winding function theory are summarized as follows:

- the air-gap field and flux density have no component along the machine axis [42, 43]. This

justifies the restriction of the magnetic analysis to a cross-section;

- the permeability of iron is assumed infinite. Magnetic saturation is modelled with a variable air-gap length [7, 11].

As we will see in chapter 2, the conductor distribution is represented using 'turn functions' (compare [44]). The radial component of the air-gap flux density is computed by means of Ampere's law. The flux linking each winding with the others and the corresponding inductances are calculated by integrating the product of the turn function and the radial flux density distribution over the rotor circumference.

The principal advantage of the method is that it allows to adjust the degree of precision depending on the situation considered. In case the geometric characteristics of the machine are known, they can be taken into account in the model (cf. [45, 46]). Furthermore, the technique offers the possibility to model various types of machines. References [47, 48] investigate for instance axial flux machines. It also plays an essential role in fault analysis [9, 49, 50].

The winding function theory seems to be also an interesting modelling strategy if only basic information about the machine under investigation is available, such as the number of rotor bars and a rough estimate of the stator winding configuration. In the context of off-the-shelf squirrel cage machines, this is an option worth considering.

1.5 Objectives of the present work

The considerations in section 1.4 have pointed out some concerns about the general validity of extended Park models when space harmonics are relevant. An alternative, state-space models based on Kron's method, seems difficult to realize with off-the-shelf machines owing to the numerous model parameters.

The primary goal of the investigations to be discussed in the following chapters is to develop a mathematically consistent and systematic method of modelling air-gap flux density harmonics in induction machines with respect to the targeted applications, especially the reduction of current and torque harmonics. Thus, the model proposed should meet the subsequent requirements:

1.) real-time compliance;

2.) state controllability and observability;

3.) if possible, the model should only have a limited number of parameters which should be easy to determine.

The assessment of the results presented in this study will be carried out by means of simulations and experiments. The latter were performed using two 2.2 kW inverter-fed induction machines, in the following referred to as *induction machine 1* (IM1) and *induction machine 2* (IM2). The characteristics of the respective machines are given in appendix A.1. The inverter was controlled using a dSPACE DS1006 real-time system and inverter dead-time effects were compensated appropriately.

Summary

This first chapter was intended to put the study in context, the aim of which is to develop an innovative modelling strategy taking into account space harmonics in off-the-shelf induction machines with unknown internal structure. The main applications targeted are the compensation of current and torque oscillations caused by space harmonics and, in a longer term perspective, encoderless control.

A brief review of existing modelling approaches pointed out the possible limitations of empirical extensions of Park's model to integrate space harmonics. A potentially interesting alternative, Kron's method, appears to be difficult to implement owing to the number of parameters involved. The winding function approach seems to be the most promising option and will be the foundation of the subsequent investigations.

Chapter 2
A winding function based machine model

Overview of chapter

Among the modelling methods discussed in the previous chapter, the winding function theory appears to be the most encouraging with respect to our objectives, as it constitutes a compromise between accuracy and simplicity. We will therefore derive the first version of an extended model of induction machines using this method and assess its ability to meet our requirements.

The present chapter introduces the fundamental concepts and the methodology to develop a model taking into account conductor distribution, slot, eccentricity as well as saturation harmonics. We will only briefly review the geometric and magnetic aspects, as they have already been addressed extensively in the literature. In contrast, we will focus on the more challenging matter of winding interconnections.

A model of the machine IM1 is to be discussed from the perspective of accuracy and efficiency. The results will provide valuable information to determine which strategy to follow in further steps.

2.1 General assumptions and modelling strategy

2.1.1 Considered problem

In order to derive a general model first, we consider the case of an induction machine having Z_p pairs of poles and w_s stator windings distributed in N_s slots. The machine might have a wound rotor with w_r windings and N_r slots or a cage with N_r rotor bars.

The magnetic behaviour of the machine is described using the winding function theory mentioned in section 1.4. Consequently, the following fundamental simplifying hypotheses are made:

1.) the air-gap field and flux density have only a radial component, magnetic effects are analysed in a cross-section of the machine;

2.) neither magnetic hysteresis nor eddy currents in the iron core are considered.
Magnetic saturation is accounted for by means of a variable air-gap length, while the permeability of the iron core is assumed infinite (see [11] and [7]).

The above assumptions might appear restrictive but they constitute a compromise between the model accuracy and the need for computational efficiency in a context with unknown internal machine structure.

2.1.2 Concept of electrical circuit

The w_s stator windings are modelled as a set of m_s electrical circuits. Such an electrical circuit might only represent a subset of the coils belonging to a specific winding rather than the whole winding itself. This approach provides additional degrees of freedom with respect to the geometric description of the machine and will prove to be instrumental when optimizing the model in chapter 3 and 4. Similarly, the w_r windings of a wound rotor are described as an electrical network consisting of m_r circuits. For squirrel cage rotors, each circuit corresponds to a coil having one turn and a pitch equal to the rotor slot pitch, the number of circuits then being equal to the number of bars, i.e. $m_r = N_r$. We will see later on why this representation of a rotor cage makes sense.

In a first step, we will assume each electrical circuit to be independent, i.e. the voltage at the terminals of stator circuit number $m \in [\![0,\, m_s - 1]\!]$, u_{sm} (or the voltage at the terminals of rotor circuit number $n \in [\![0,\, m_r - 1]\!]$, u_{rn}) can be impressed freely. The current flowing through each circuit is an independent variable as well. Fig. 2.1 shows a schematic of a stator (resp. rotor) circuit for this virtual machine configuration.

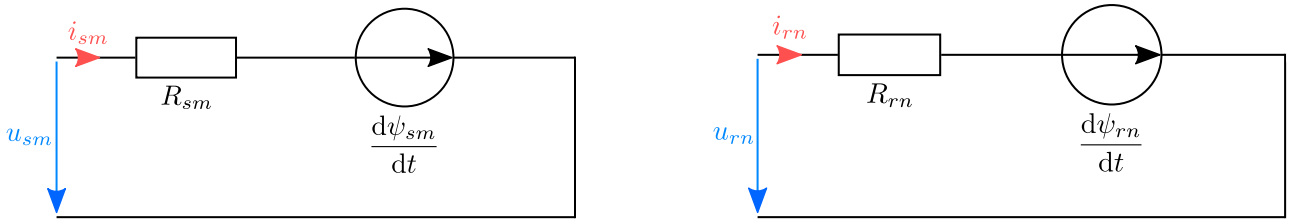

(a) stator circuit $m \in [\![0,\, m_s - 1]\!]$

(b) rotor circuit $n \in [\![0,\, m_r - 1]\!]$

Figure 2.1: Schematics of the electrical circuits considered in the model

This approach allows us to derive the model of a virtual machine configuration with the same geometric and magnetic properties as the real machine but without electrical constraints. The subsequent

determination of the equations describing the behaviour of the real machine is straightforward using the interconnection transformation defined by Kron in [38, pp. 230–232]. This technique is particularly convenient as the relations between currents and flux linkages can be determined based exclusively on the machine geometry. The model of the virtual configuration forms the basis for a given geometry and is then adapted to account for the specific characteristics of the machine under investigation.

2.2 Model of the virtual machine without circuit interconnections

2.2.1 Electrical equations

We start by setting up the equations describing the electrical behaviour of stator and rotor circuits without interconnections. Table 2.1 provides an overview of the quantities involved.

Symbol	Meaning
u_{sm}	Voltage at the terminals of stator circuit $m \in [\![0,\, m_s - 1]\!]$
u_{rn}	Voltage at the terminals of rotor circuit $n \in [\![0,\, m_r - 1]\!]$
i_{sm}	Current flowing through stator circuit m
i_{rn}	Current flowing through rotor circuit n
ψ_{sm}	Flux linkage of stator circuit m
ψ_{rn}	Flux linkage of rotor circuit n
R_{sm}	Resistance of stator circuit m
R_{rn}	Resistance of rotor circuit n

Table 2.1: Overview of the electrical quantities used in the model

Applying Kirchhoff's second law to stator circuit number m yields the following differential equation:

$$\forall\, m \in [\![0,\, m_s - 1]\!],\; u_{sm} = R_{sm} i_{sm} + \frac{\mathrm{d}\psi_{sm}}{\mathrm{d}t} \tag{2.1}$$

Similarly, the voltage at the terminals of rotor circuit n is:

$$\forall\, n \in [\![0,\, m_r - 1]\!],\; u_{rn} = R_{rn} i_{rn} + \frac{\mathrm{d}\psi_{rn}}{\mathrm{d}t} \tag{2.2}$$

Introducing the vectors:

$$\vec{u}_s = \begin{bmatrix} u_{s0} & \cdots & u_{sm} & \cdots & u_{sm_s-1} \end{bmatrix}^\top \qquad \vec{u}_r = \begin{bmatrix} u_{r0} & \cdots & u_{rn} & \cdots & u_{rm_r-1} \end{bmatrix}^\top$$

$$\vec{i}_s = \begin{bmatrix} i_{s0} & \cdots & i_{sm} & \cdots & i_{sm_s-1} \end{bmatrix}^\top \qquad \vec{i}_r = \begin{bmatrix} i_{r0} & \cdots & i_{rn} & \cdots & i_{rm_r-1} \end{bmatrix}^\top$$

$$\vec{\psi}_s = \begin{bmatrix} \psi_{s0} & \cdots & \psi_{sm} & \cdots & \psi_{sm_s-1} \end{bmatrix}^\top \qquad \vec{\psi}_r = \begin{bmatrix} \psi_{r0} & \cdots & \psi_{rn} & \cdots & \psi_{rm_r-1} \end{bmatrix}^\top$$

as well as the stator and rotor resistance matrices:

$$\mathbf{R_s} = \begin{bmatrix} R_{s0} & & 0 \\ & \ddots & \\ 0 & & R_{sm_s-1} \end{bmatrix}; \quad \mathbf{R_r} = \begin{bmatrix} R_{r0} & & 0 \\ & \ddots & \\ 0 & & R_{rm_r-1} \end{bmatrix}$$

leads to the systems of differential equations:

$$\begin{cases} \text{stator voltage:} & \vec{u}_s = \mathbf{R_s}\vec{i}_s + \dfrac{\mathrm{d}\vec{\psi}_s}{\mathrm{d}t} \quad (2.3a) \\ \text{rotor voltage:} & \vec{u}_r = \mathbf{R_r}\vec{i}_r + \dfrac{\mathrm{d}\vec{\psi}_r}{\mathrm{d}t} \quad (2.3b) \end{cases}$$

Using the definitions:

$$\vec{u} = \begin{bmatrix} \vec{u}_s^\top & \vec{u}_r^\top \end{bmatrix}^\top; \qquad \vec{i} = \begin{bmatrix} \vec{i}_s^\top & \vec{i}_r^\top \end{bmatrix}^\top; \qquad \vec{\Psi} = \begin{bmatrix} \vec{\psi}_s^\top & \vec{\psi}_r^\top \end{bmatrix}^\top;$$

$$\mathbf{R} = \begin{bmatrix} \mathbf{R_s} & \mathbf{0} \\ \mathbf{0} & \mathbf{R_r} \end{bmatrix}$$

eq. (2.3a) and (2.3b) can be combined into one:

$$\vec{u} = \mathbf{R}\vec{i} + \frac{\mathrm{d}\vec{\Psi}}{\mathrm{d}t} \tag{2.4}$$

The differential system (2.4) describes the electrical behaviour of the virtual machine configuration without interconnections. A relation between the current and flux vectors as well as an expression of the electromechanical torque need to be found. This step requires the machine geometry and its magnetic properties to be taken into account and will be discussed next.

2.2.2 Relation between currents and flux linkages

Air-gap flux density distribution

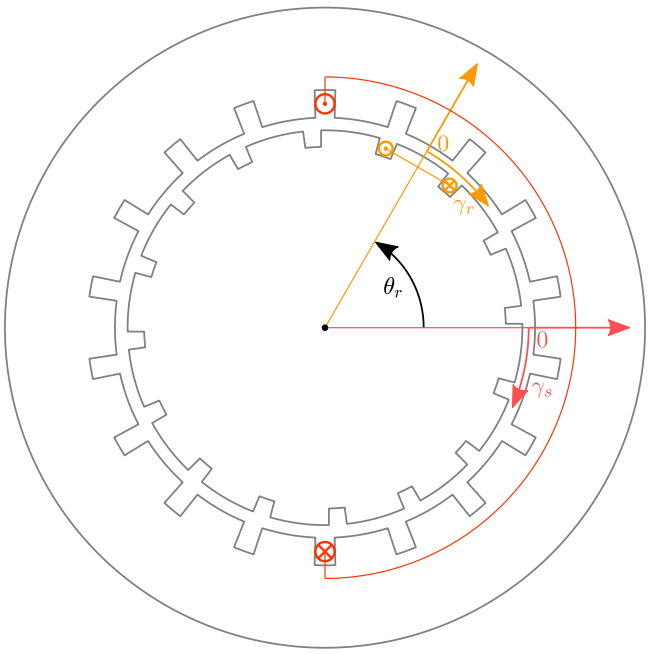

Figure 2.2: Definition of stator and rotor air-gap coordinates as well as rotor angle

A basic model of magnetic processes is derived using the winding function approach. According to the hypotheses formulated in section 2.1.1, the magnetomotive force (MMF) Θ as well as the air-gap field

$\vec{H}$ and flux density $\vec{B}$ depend only on the position along the air-gap. In addition, $\vec{H}$ and $\vec{B}$ exhibit only a radial component, denoted by H and B respectively.

We introduce the stator (and rotor) normalized air-gap coordinate γ_s (γ_r resp.) according to fig. 2.2 and with values in the interval $[0, 2\pi]$. Note that γ_s and γ_r are positive when moving clockwise from their respective origin.

The schematic of the machine cross section in fig. 2.2 shows the case of one stator and one rotor coil as an example. In order to illustrate the concept of electrical circuit introduced in section 2.1.2, we assume that the red coil centred on the origin of the stator air-gap coordinate γ_s has W_S turns and is the geometric equivalent of stator circuit number 0. We assign to this circuit the conductor distribution function W_{s0} depicted in fig. 2.3 which represents the turn number of the coil as a continuous function of the coordinate γ_s. W_{s0} is equal to W_S on the coil axis and decreases linearly to 0 when moving past the coil side towards π. Such a conductor distribution function therefore assumes a constant current density within the slots in which the coil sides are located.

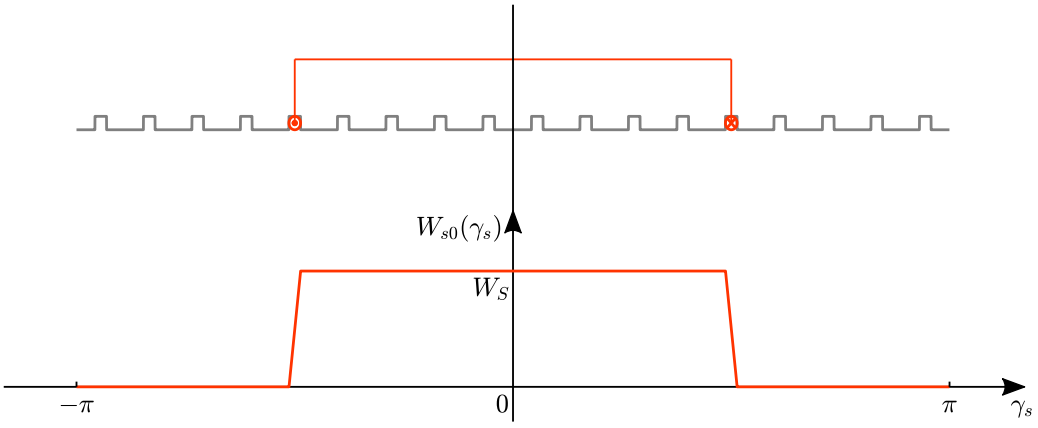

Figure 2.3: Example of conductor distribution function for stator circuit 0

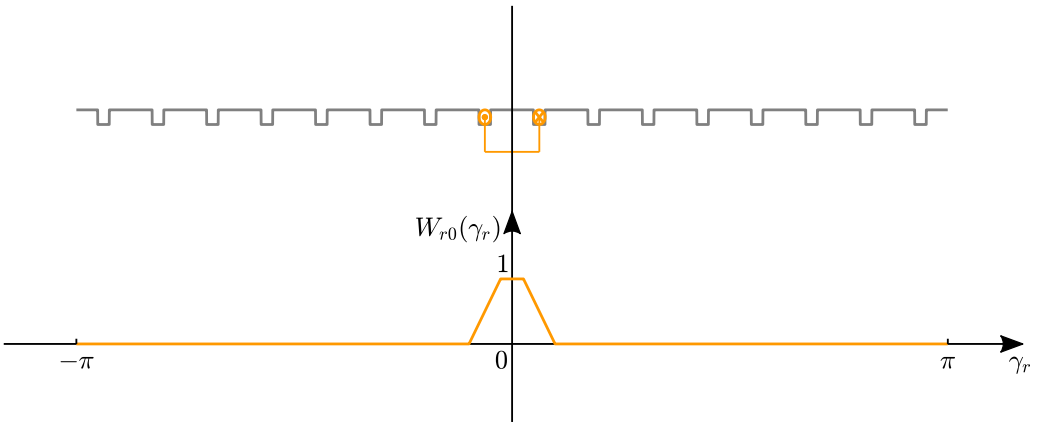

Figure 2.4: Conductor distribution function of rotor circuit 0

Similarly, the orange coil centred on the origin of the rotor air-gap coordinate γ_r in fig. 2.2 corresponds to rotor circuit 0. The conductor distribution function assigned to this circuit, W_{r0}, is shown in fig. 2.4. As we will see in section 2.3.4, this particular shape for W_{r0}, with a maximum $W_R = 1$, is used for modelling a section of a rotor cage consisting of two consecutive bars and the end ring segments joining them. Notice that the shape of W_{r0} also suggests that the current density distribution is non-zero outside the relevant slots. This provides a basic way of accounting for the rotor skew.

Remark:
The conductor distribution function is generally referred to as 'turn function' in the literature, such as in [43]. We prefer the former terminology as it avoids confusion, given that the corresponding function can also have non-integer or negative values (see for instance fig. A.8).

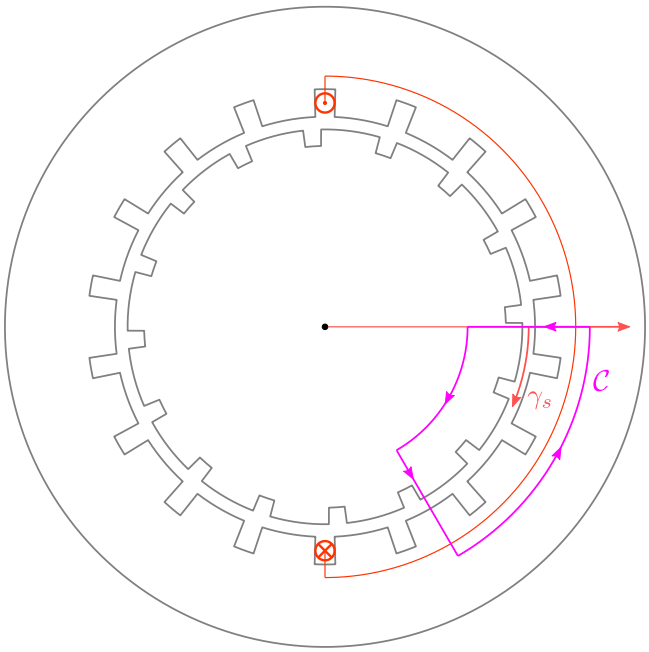

Figure 2.5: Integration path for determining the air-gap flux density generated by a circuit at a given instant

Following the above examples, we assign to each stator circuit $m \in [\![0,\, m_s - 1]\!]$ (and each rotor circuit $n \in [\![0,\, m_r - 1]\!]$) the conductor distribution function W_{sm} (W_{rn} resp.). For a given magnetic state of the machine and a given rotor angle θ_r, the air-gap field H_{sm} produced by current i_{sm} flowing through stator circuit number m is determined using Ampere's law [43]:

$$\Theta_{sm}(\gamma_s) = W_{sm}(\gamma_s) i_{sm} = \oint_{\mathcal{C}} \vec{H}_{sm} \cdot \mathrm{d}\vec{l} = H_{sm}(\gamma_s)\delta(\vec{i},\, \gamma_s) - H_{sm}(0)\delta(\vec{i},\, 0) \tag{2.5}$$

where Θ_{sm} represents the MMF distribution generated by current i_{sm} and δ the air-gap length function. Owing to the considerations in section 2.1.1, the shape of δ depends on the saturation state of the machine, i.e. on the total current vector, $\vec{i}$, and on the rotor angle due to the relative position of stator and rotor slots as well as possible rotor eccentricity.

From (2.5) follows:

$$H_{sm}(\gamma_s) = \frac{1}{\delta(\vec{i},\, \gamma_s)} \Big[\Theta_{sm}(\gamma_s) + H_{sm}(0)\delta(\vec{i},\, 0) \Big] \tag{2.6}$$

In order to determine the value of the term $H_{sm}(0)\delta(0)$, we use the condition

$$\oiint_{\mathcal{S}} \vec{B} \cdot d\vec{S} = 0 \tag{2.7}$$

and integrate on the surface $\mathcal{S}$ of a cylinder of radius equal to the air-gap mean radius r and length corresponding to the lamination stack length l, which leads to

$$r \cdot l \cdot \int_0^{2\pi} \mu_0 H_{sm}(\gamma_s)\, \mathrm{d}\gamma_s = 0$$

$$\iff \int_0^{2\pi} \frac{1}{\delta(\vec{i},\,\gamma_s)} \Big[\Theta_{sm}(\gamma_s) + H_{sm}(0)\delta(\vec{i},\,0)\Big]\,\mathrm{d}\gamma_s = 0 \tag{2.8}$$

From the above relation follows:

$$H_{sm}(0)\delta(\vec{i},\,0) = -\frac{\displaystyle\int_0^{2\pi} \frac{\Theta_{sm}(\gamma_s)}{\delta(\vec{i},\,\gamma_s)}\,\mathrm{d}\gamma_s}{\displaystyle\int_0^{2\pi} \frac{1}{\delta(\vec{i},\,\gamma_s)}\,\mathrm{d}\gamma_s} \tag{2.9}$$

Consequently, the flux density distribution B_{sm} generated by current i_{sm} is

$$B_{sm}(\gamma_s) = \frac{\mu_0\, i_{sm}}{\delta(\vec{i},\,\gamma_s)} \left[W_{sm}(\gamma_s) - \frac{\displaystyle\int_0^{2\pi} \frac{W_{sm}(\gamma_s)}{\delta(\vec{i},\,\gamma_s)}\,\mathrm{d}\gamma_s}{\displaystyle\int_0^{2\pi} \frac{1}{\delta(\vec{i},\,\gamma_s)}\,\mathrm{d}\gamma_s} \right] \tag{2.10}$$

Remark:
The term in square brackets in relation (2.10) is called 'winding function' of circuit m (see [43]).

For a specific rotor position and magnetic state of the machine, assumption 2 in section 2.1 allows to make use of the superposition principle, as the magnetic state is entirely defined by the air-gap length function δ. Thus, the total air-gap flux density B generated by all the currents flowing through the stator and rotor circuits is:

$$B(\gamma_s) = \sum_{m=0}^{m_s-1} B_{sm}(\gamma_s) + \sum_{n=0}^{m_r-1} B'_{rn}(\gamma_s) \tag{2.11}$$

where B'_{rn} denotes the contribution of rotor circuit n to the air-gap flux density as a function of the stator coordinate γ_s.

Flux linkage of a single circuit

The main flux linkage of a coil is the surface integral of the air-gap flux density distribution over the area spanned by the coil multiplied by the number of turns. In the case of a circuit, we can take advantage of the conductor distribution function to account for the number of turns and integrate over an interval of 2π since the conductor distribution function is zero outside the area spanned by the coils associated with the circuit. Thus, the main flux linking stator circuit m is:

$$\widetilde{\psi}_{sm} = r \cdot l \cdot \int_0^{2\pi} W_{sm}(\gamma_s) B(\gamma_s)\,\mathrm{d}\gamma_s \tag{2.12}$$

Similarly, the main flux linkage of rotor circuit n is given by the relation:

$$\widetilde{\psi}_{rn} = r \cdot l \cdot \int_0^{2\pi} W_{rn}(\gamma_r) B'(\gamma_r)\,\mathrm{d}\gamma_r \tag{2.13}$$

where B' represents the air-gap flux density distribution as a function of the rotor coordinate γ_r.

Relation between current and flux linkage vectors

Relations (2.12) and (2.13) allow to determine the components of the *main* flux vector, $\vec{\widetilde{\Psi}}$, defined as follows:

$$\vec{\widetilde{\Psi}} = \begin{bmatrix} \widetilde{\psi}_{s0} & \cdots & \widetilde{\psi}_{sm} & \cdots & \widetilde{\psi}_{sm_s-1} & \widetilde{\psi}_{r0} & \cdots & \widetilde{\psi}_{rn} & \cdots & \widetilde{\psi}_{rm_r-1} \end{bmatrix}^\top \tag{2.14}$$

Assuming that small variations of the currents around the operating point do not influence the magnetic state of the machine and that the leakage flux of a circuit does not link with others, we introduce the leakage inductances $L_{\sigma sm}$ of stator circuit $m \in [\![0,\, m_s - 1]\!]$ and $L_{\sigma rn}$ of rotor circuit $n \in [\![0,\, m_r - 1]\!]$. Thus, the *total* flux linkage vector, $\vec{\Psi}$, is the sum of $\vec{\tilde{\Psi}}$ and the *leakage* flux vector, $\vec{\Psi}_\sigma$:

$$\vec{\Psi} = \vec{\tilde{\Psi}} + \vec{\Psi}_\sigma = \vec{\tilde{\Psi}} + \mathbf{L}_\sigma \vec{i} \tag{2.15}$$

where $\mathbf{L}_\sigma = \mathrm{diag}[L_{\sigma s0} \quad \dots \quad L_{\sigma sm} \quad \dots \quad L_{\sigma sm_s-1},\, L_{\sigma r0} \quad \dots \quad L_{\sigma rn} \quad \dots \quad L_{\sigma rm_r-1}]$.

Using the above relations, the Jacobian matrix $\partial\vec{\Psi}/\partial\vec{i}$, i.e. the differential inductance matrix, can be determined for the considered operating point. We denote the differential inductance matrix by $\mathbf{L}(\vec{i},\, \theta_r)$ and obtain the subsequent relation between the current and flux linkage vectors:

$$\vec{\Psi} = \mathbf{L}(\vec{i},\, \theta_r)\vec{i} \tag{2.16}$$

Owing to the reciprocity property of magnetically coupled circuits, $\mathbf{L}(\vec{i},\, \theta_r)$ is symmetric. Moreover, since the quadratic form $\frac{1}{2}\vec{i}^{\top}\mathbf{L}(\vec{i},\, \theta_r)\vec{i}$ represents the instantaneous value of magnetic energy stored in the field generated by the electrical circuits, $\mathbf{L}(\vec{i},\, \theta_r)$ is positive definite. It is therefore invertible, which yields:

$$\vec{i}(\vec{\Psi},\, \theta_r) = \mathbf{L}^{-1}(\vec{\Psi},\, \theta_r)\vec{\Psi} \tag{2.17}$$

Relations (2.16) and (2.17) constitute a simplified model of the magnetic and geometric properties of the machine.

2.2.3 Mechanical equations

The electromechanical torque M_M produced by the machine can be derived from an energy balance equation applied to the magnetic field coupling the different electrical circuits [51]. This approach leads to the subsequent expression given the above hypothesis of magnetic linearity (refer to appendix A.2.1 for a detailed proof):

$$M_M = \frac{1}{2}\vec{i}^{\top}\frac{\partial\vec{\Psi}}{\partial\theta_r} \tag{2.18}$$

The rotor angular velocity, ω_r, is determined by the following equation:

$$\frac{\mathrm{d}\omega_r}{\mathrm{d}t} = \frac{1}{J_M}(M_M - C_W\omega_r - M_L) \tag{2.19}$$

where C_W denotes the coefficient of friction and M_L the external load torque. The rotor angle θ_r is obtained by integrating the angular velocity.

2.2.4 State-space equations of the model without interconnections

The components of $\vec{\Psi}$, the rotor angular velocity ω_r and the rotor angle θ_r are chosen as state variables. Combining equations (2.4), (2.17), (2.18) and (2.19) leads to the subsequent state-space model of the

machine:

$$\begin{cases} \dfrac{\mathrm{d}\vec{\Psi}}{\mathrm{d}t} = \vec{u} - \mathbf{R}\mathbf{L}^{-1}(\vec{\Psi}, \theta_r)\vec{\Psi} & \text{(2.20a)} \\ \dfrac{\mathrm{d}\omega_r}{\mathrm{d}t} = \dfrac{1}{J_M}\left[\dfrac{1}{2}\left[\mathbf{L}^{-1}(\vec{\Psi}, \theta_r)\vec{\Psi}\right]^\top \dfrac{\partial \vec{\Psi}}{\partial \theta_r} - C_W\omega_r - M_L\right] & \text{(2.20b)} \\ \dfrac{\mathrm{d}\theta_r}{\mathrm{d}t} = \omega_r & \text{(2.20c)} \end{cases}$$

The model dimension is $m_s + m_r + 2$. It can already be seen from the form of the equations that the implementation of the model in a simulation will require the inverse of the differential inductance matrix $\mathbf{L}^{-1}$ to be calculated at each time step. This is not of particular concern as $\mathbf{L}$ is symmetric positive definite. Consequently, there exists a unique upper triangular matrix $\mathbf{\Delta}$ with strictly positive diagonal elements such that:

$$\mathbf{L} = \frac{\partial \vec{\Psi}}{\partial \vec{i}} = \mathbf{\Delta}^\top \mathbf{\Delta} \tag{2.21}$$

The factorization (2.21) is known as *Cholesky decomposition*. It enables a more efficient way of computing $\mathbf{L}^{-1}$ than general methods of solving linear systems of equations [52, p. 96].

2.3 Accounting for electrical connections between circuits

2.3.1 Impact of electrical connections on the model

The considerations so far have focused exclusively on geometric and magnetic aspects and assumed that the currents flowing through the electric circuits as well as the voltage at their terminals were independent. However, in order to obtain a valid model, the circuits must be interconnected to account for the actual arrangement of electric conductors existing in a real machine. For example, stator windings are typically connected in star or delta, while rotor windings might be short-circuited (as are the conductors of a rotor cage).

The interconnection process will introduce constraints between the electrical quantities associated with each circuit, expressed by Kirchhoff's laws. Therefore, the $m_s + m_r$ components of the current vector $\vec{i}$ are not independent. Neither are the components of $\vec{u}$ which can therefore not easily be used as model inputs in general. For these reasons, the previous method which led to the differential system (2.20) is not applicable without performing a change of variables.

In available literature references, the crucial step of selecting appropriate variables is either performed empirically using an application specific approach, as in [24, 42, 53], or not addressed explicitly (see for example [49, 54–56]). In contrast, we will use the systematic method of electrical circuit analysis developed by Kron [38, pp. 230–232].

2.3.2 Definition of new electrical variables

Interconnecting the circuits introduced in section 2.2.1 to build a network representing a specific winding configuration results in a set of constraints between the components of the current vector $\vec{i}$. These constraints are obtained by applying Kirchhoff's first law, an operation which can be described mathematically by a vector-matrix relation:

$$\vec{i} = \mathbf{C}\vec{i'} \tag{2.22}$$

in which the original or *old* current vector $\vec{i}$ is expressed as the product of a rectangular *interconnection matrix* $\mathbf{C}$ and a *new* vector $\vec{i}'$. The components of $\vec{i}'$ represent the *independent* currents in the network of interconnected circuits and will be referred to as *new* currents. $\mathbf{C}$ has m_s+m_r rows and $m' \leqslant m_s+m_r$ columns while its rank is equal to m'. Eq. (2.22) enables to compute the set of *old* currents required in the above magnetic and geometric analysis using the *new* independent currents.

The definition of a *new* voltage vector is achieved using the expression of the electric power of the network [38, p. 231] which is given by:

$$P_{el} = \vec{u}^\top \vec{i} \tag{2.23}$$

Combining (2.22) and (2.23) leads to:

$$\begin{aligned} P_{el} = \vec{u}^\top \mathbf{C} \vec{i}' = \left[\vec{u}^\top \mathbf{C} \vec{i}'\right]^\top = \vec{i}'^\top \mathbf{C}^\top \vec{u} \\ = \vec{i}'^\top \vec{u}' = \vec{u}'^\top \vec{i}' \end{aligned}$$

where

$$\vec{u}' = \mathbf{C}^\top \vec{u} \tag{2.24}$$

The processes described by (2.22) and (2.24) constitute a change of variables. As in general

$$\operatorname{rank}(\mathbf{C}) < m_s + m_r,$$

$\mathbf{C}$ is not invertible and $\vec{i}'$ cannot be calculated from $\vec{i}$ by means of (2.22). Conversely, it is not possible to determine $\vec{u}$ from $\vec{u}'$ using (2.24). Such operations are, however, not necessary to establish the model of the machine with interconnected circuits, as we will see later on.

For the sake of clarity, it is often useful to handle stator and rotor circuits separately. Following the foregoing procedure, the vectors $\vec{i}'_s$ and $\vec{u}'_s$ of independent stator currents and voltages are introduced alongside a stator interconnection submatrix $\mathbf{C_s}$. $\mathbf{C_s}$ has m_s rows and m'_s columns with $m'_s \leqslant m_s$. Similarly, $\vec{i}'_r$, $\vec{u}'_r$ and $\mathbf{C_r}$ are used for describing interconnections on the rotor side, $\mathbf{C_r}$ being an $m_r \times m'_r$ matrix with $m'_r \leqslant m_r$. In such case, (2.22) and (2.24) become:

$$\vec{i} = \begin{bmatrix} \vec{i}_s \\ \vec{i}_r \end{bmatrix} = \begin{bmatrix} \mathbf{C_s} & \mathbf{0} \\ \mathbf{0} & \mathbf{C_r} \end{bmatrix} \begin{bmatrix} \vec{i}'_s \\ \vec{i}'_r \end{bmatrix} = \vec{i}' = \mathbf{C} \begin{bmatrix} \vec{i}'_s \\ \vec{i}'_r \end{bmatrix} = \vec{i}' \tag{2.25a}$$

and

$$\vec{u}' = \begin{bmatrix} \vec{u}'_s \\ \vec{u}'_r \end{bmatrix} = \begin{bmatrix} \mathbf{C_s}^\top & \mathbf{0} \\ \mathbf{0} & \mathbf{C_r}^\top \end{bmatrix} \begin{bmatrix} \vec{u}_s \\ \vec{u}_r \end{bmatrix} = \mathbf{C}^\top \vec{u} \tag{2.25b}$$

We will examine next how to make use of the above considerations to describe the practically relevant case of star-connected stator windings as well as the one of squirrel cage rotors.

2.3.3 Example of star-connected windings

We consider a set of w_s stator windings connected in star, each of them modelled using *one* circuit as depicted in fig. 2.6. In this particular case, $m_s = w_s$ stator circuits are necessary.

Applying Kirchhoff's first law to the network in fig. 2.6, the current in circuit $m_s - 1$, i_{sm_s-1}, can be expressed as a linear combination of the currents flowing through the others:

$$i_{sm_s-1} = -\sum_{m=0}^{m_s-2} i_{sm}$$

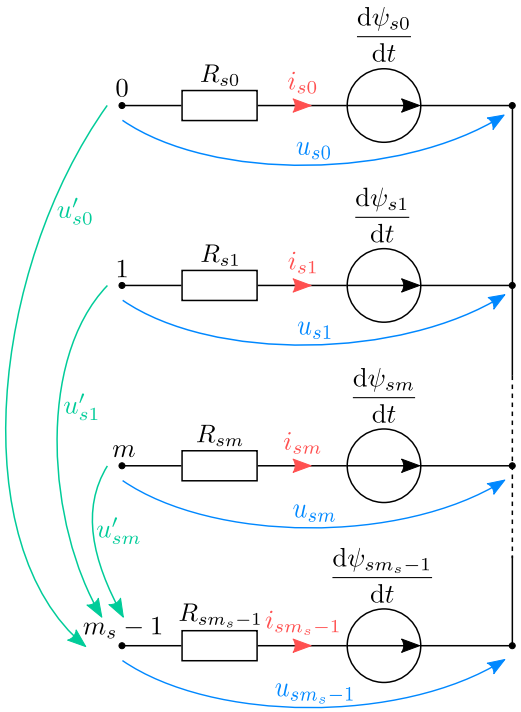

Figure 2.6: Schematic of star-connected stator electrical circuits

Thus, the vector of stator currents $\vec{i}_s$ can be written as follows:

$$\vec{i}_s = \begin{bmatrix} i_{s0} \\ \vdots \\ i_{sm_s-1} \end{bmatrix} = \begin{bmatrix} 1 & & 0 \\ 0 & \ddots & \\ -1 & \dots & -1 \end{bmatrix} \begin{bmatrix} i_{s0} \\ \vdots \\ i_{sm_s-2} \end{bmatrix}$$

Owing to the considerations in section 2.3.2, we introduce a *new* vector of independent stator currents, $\vec{i}'_s$, and a *stator interconnection matrix*, $\mathbf{C_s}$, as follows:

$$\vec{i}'_s = \begin{bmatrix} i'_{s0} \\ \vdots \\ i'_{sm_s-2} \end{bmatrix} = \begin{bmatrix} i_{s0} \\ \vdots \\ i_{sm_s-2} \end{bmatrix} \quad \text{and} \quad \mathbf{C_s} = \begin{bmatrix} 1 & & 0 \\ 0 & \ddots & \\ -1 & \dots & -1 \end{bmatrix}$$

The *old* vector of stator currents, $\vec{i}_s$, is expressed using the *new* one, $\vec{i}'_s$:

$$\vec{i}_s = \mathbf{C_s}\vec{i}'_s \tag{2.26a}$$

$\mathbf{C_s}$ is a matrix of dimension $m_s \times (w_s - 1)$, while $\vec{i}'_s$ has the dimension $w_s - 1$.

The new voltage vector $\vec{u}'_s$ corresponding to the star-connection is defined using relation (2.25b):

$$\vec{u}'_s = \begin{bmatrix} u'_{s0} \\ \vdots \\ u'_{sm_s-2} \end{bmatrix} = \mathbf{C_s}^\top \vec{u}_s = \begin{bmatrix} 1 & & 0 & -1 \\ 0 & \ddots & & \vdots \\ & & 1 & -1 \end{bmatrix} \begin{bmatrix} u_{s0} \\ \vdots \\ u_{sm_s-1} \end{bmatrix} = \begin{bmatrix} u_{s0} - u_{sm_s-1} \\ \vdots \\ u_{sm_s-2} - u_{sm_s-1} \end{bmatrix} \tag{2.26b}$$

i.e. (2.26b) refers the potential of the free terminals $m \in [\![0,\, m_s - 2]\!]$ to the one of terminal $m_s - 1$.

It is important to remember that the number of stator circuits m_s does not have to be equal to the number of stator windings w_s. In practice, a winding might for instance consist of a set of coil groups

connected in series, each of the latter being itself a series connection of coils. In this case, a circuit could be defined as a coil or as a coil group. Depending on the situation, one alternative can appear more convenient than the other when it comes to determining the flux linking a circuit to the others using the method described in the previous sections. We will make use of this degree of freedom when establishing the model of IM2 in section 3.7.1.

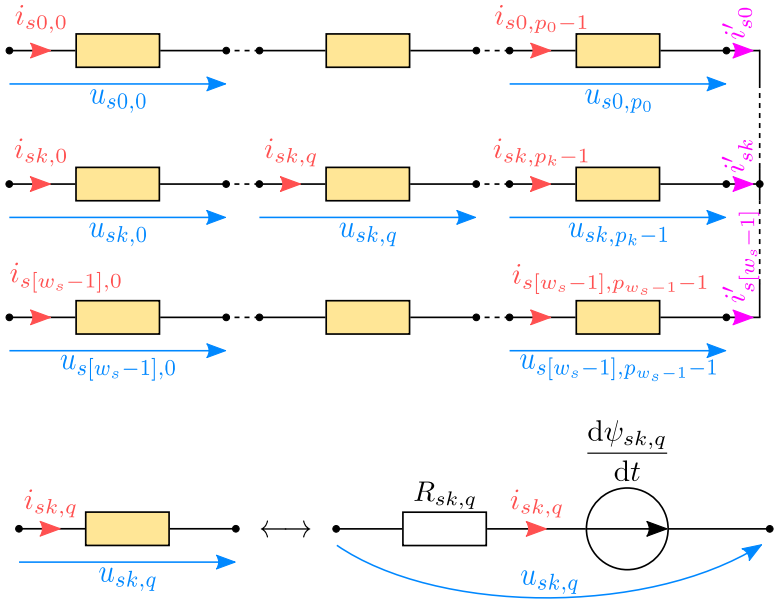

Figure 2.7: Star-connected windings modelled as a set of circuits connected in series

Fig. 2.7 illustrates the concept of modelling each of the w_s star-connected stator windings of a machine as a set of circuits. Let winding number $k \in [\![0,\, w_s - 1]\!]$ be the series connection of $p_k \in \mathbb{N}^\star$ circuits. The total number of circuits to be used in the model is therefore:

$$m_s = \sum_{k=0}^{w_s-1} p_k$$

The application of Kirchhoff's first law to the circuits of winding k yields:

$$\forall\, q \in [\![0,\, p_k - 1]\!],\, i_{sk,q} = i_{sk}$$

$$\iff \vec{i}_{sk} = \begin{bmatrix} i_{sk,0} & \dots & i_{sk,p_k-1} \end{bmatrix}^\top = \begin{bmatrix} 1 & \dots & 1 \end{bmatrix}^\top i_{sk} = \mathbf{C_{sk}} i'_{sk}$$

where i'_{sk} represents the current flowing through winding k and $\mathbf{C_{sk}}$ the related $p_k \times 1$ interconnection matrix.

Owing to relation (2.24), the voltage at the terminals of winding number k, u'_{sk} is

$$u'_{sk} = \mathbf{C_{sk}}^\top \begin{bmatrix} u_{sk,0} & \dots & u_{sk,p_k-1} \end{bmatrix}^\top$$

which is equivalent to the result provided by Kirchhoff's second law, i.e. the sum of the voltages at the terminals of the p_k circuits.

Kirchoff's current law applied to the star point again enables us to represent $i'_{s[w_s-1]}$ as a linear combination of the current flowing through the other windings:

$$i'_{s[w_s-1]} = -\sum_{k=0}^{w_s-2} i'_{sk}$$

$$\Longrightarrow \vec{i}_{s[w_s-1]} = -\mathbf{C_{s[w_s-1]}} \sum_{k=0}^{w_s-2} i'_{sk}$$

The vector $\vec{i}_s$, the components of which are the currents flowing through each single circuit, is expressed as follows:

$$\begin{aligned}
\vec{i}_s &= \begin{bmatrix} \vec{i}_{s0}^{\top} & \cdots & \vec{i}_{sk}^{\top} & \cdots & \vec{i}_{sw_s-1}^{\top} \end{bmatrix}^{\top} \\
&= \begin{bmatrix} \mathbf{C_{s0}^{\top}} i'_{s0} & \cdots & \mathbf{C_{sk}^{\top}} i'_{sk} & \cdots & \mathbf{C_{sw_s-1}^{\top}} \sum_{k=0}^{w_s-2} i'_{sk} \end{bmatrix}^{\top} \\
&= \begin{bmatrix} \mathbf{C_{s0}} & & & & \\ & \ddots & & & \mathbf{0} \\ & & \mathbf{C_{sk}} & & \\ & \mathbf{0} & & \ddots & \\ & & & & \mathbf{C_{s[w_s-2]}} \\ \mathbf{-C_{s[w_s-1]}} & \cdots & \cdots & \cdots & \mathbf{-C_{s[w_s-1]}} \end{bmatrix} \begin{bmatrix} i'_{s0} \\ \vdots \\ \\ \\ \\ i'_{s[w_s-2]} \end{bmatrix} = \mathbf{C_s} \vec{i}'_s
\end{aligned} \tag{2.27}$$

Hence, splitting the windings into several circuits increases the number of rows, m_s, of the interconnection matrix $\mathbf{C_s}$ while its number of columns, m'_s, remains unchanged and equal to $w_s - 1$ in case of a star connection.

The approach developed in this section can straightforwardly be applied to machines with wound rotors. It can also be easily extended to handle for instance winding configurations with multiple star points.

2.3.4 Modelling a squirrel cage as a set of interconnected circuits

As the two machines investigated in this thesis feature a squirrel cage rotor, a modelling scheme for the cage relying on the preceding considerations is to be discussed in detail.

A modelling strategy for rotor cages was proposed by Wallace and Wright in [57] and extensively used in models based on the winding function approach (see for instance [23, 42, 54, 58]). It consists in describing the cage as a set of magnetically coupled loops made of two consecutive bars and the end ring segments joining them (see fig. 2.8). The magnetic flux through such a loop exhibits a main as well as a leakage component. In order to take the latter into account, leakage inductances L_e and L_b are assigned to each segment of end ring and each rotor bar respectively. The resistance of an end ring segment is R_e, the one of a bar R_b.

Fig 2.9 presents the resulting electrical model of a cage with N_r bars as network of $3N_r$ circuits. Applying Kirchhoff's current law to each of the nodes A_k and B_k ($k \in [\![0, N_r - 1]\!]$) results in the subsequent $2N_r$ relations between the $3N_r$ currents:

- For $k = 0$:

$$i_{r1} - i_{r[2N_r-1]} - i_{r0} = 0 \quad \text{(node } A_0\text{)} \tag{2.28a}$$

$$i_{r[2N_r]} - i_{r[3N_r-1]} + i_{r0} = 0 \quad \text{(node } B_0\text{)} \tag{2.28b}$$

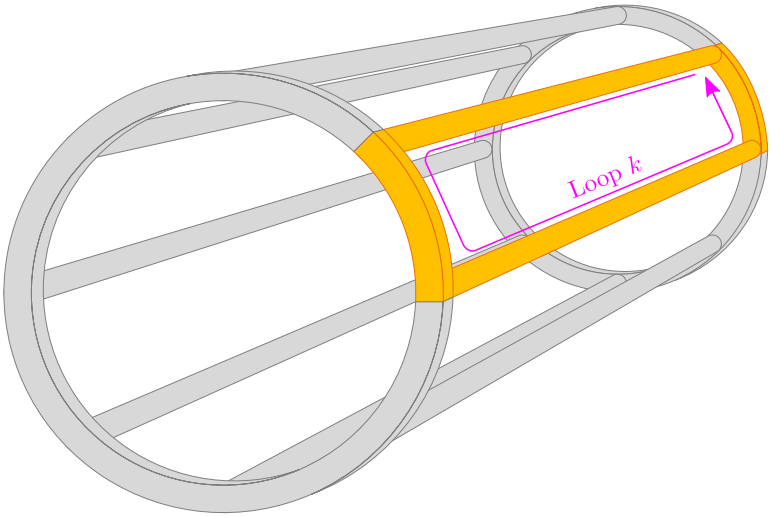

Figure 2.8: Schematic of the rotor cage visualizing the definition of the rotor loops

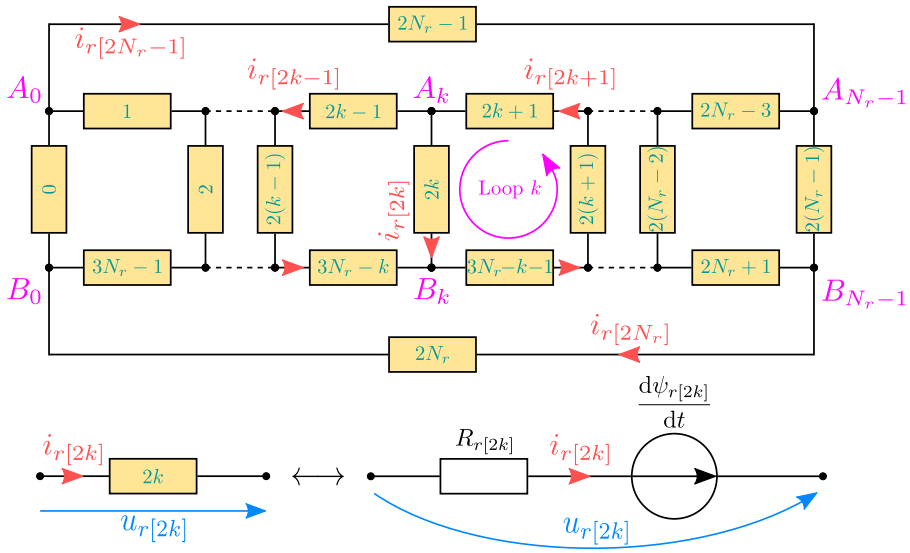

Figure 2.9: Model of the rotor cage as a set of $3N_r$ electrical circuits

- For $k \in [\![1,\ N_r - 2]\!]$:

$$i_{r[2k+1]} - i_{r[2k-1]} - i_{r[2k]} = 0 \quad \text{(node } A_k\text{)} \tag{2.28c}$$

$$i_{r[3N_r-k]} + i_{r[2k]} - i_{r[3N_r-k-1]} = 0 \quad \text{(node } B_k\text{)} \tag{2.28d}$$

- For $k = N_r - 1$:

$$i_{r[2N_r-1]} - i_{r[2(N_r-1)]} - i_{r[2N_r-3]} = 0 \quad \text{(node } A_{N_r-1}\text{)} \tag{2.28e}$$

$$i_{r[2N_r+1]} - i_{r[2N_r]} + i_{r[2(N_r-1)]} = 0 \quad \text{(node } B_{N_r-1}\text{)} \tag{2.28f}$$

The matrix associated with the above system of equations having rank $2N_r - 1$, the electric behaviour of the network represented in fig. 2.9 can be fully determined using $N_r + 1$ independent currents chosen among the $3N_r$. Thus, we introduce a vector of independent currents

$$\vec{i'_r} = \begin{bmatrix} i'_{r0} & \dots & i'_{rk} & \dots & i'_{rN_r} \end{bmatrix} \in \mathbb{R}^{N_r+1}$$

where for all $k \in [\![0,\, N_r - 1]\!]$, $i'_{rk} = i_{r[2k+1]}$ and $i'_{rN_r} = i_{r[2N_r]}$. Expressing the $3N_r$ currents in the network as linear combinations of the components of $\vec{i}'_r$ provides the relations:

$$\begin{cases} i_{r0} = i'_{r0} - i'_{r[N-1]} \\ i_{r1} = i'_{r0} \\ i_{r[2N_r]} = i'_{rN_r} \\ i_{r[2k]} = i'_{rk} - i'_{r[k-1]}, \quad \forall\, k \in [\![1,\, N_r - 1]\!] \\ i_{r[2k+1]} = i'_{rk} \\ i_{r[3N_r-k]} = i'_{rN_r} - i'_{r[N_r-1]} + i'_{r[k-1]} \end{cases} \tag{2.29}$$

which enable the definition of an interconnection matrix $\mathbf{C_r}$ such that:

$$\vec{i}_r = \mathbf{C_r}\vec{i}'_r \tag{2.30a}$$

To be consistent with (2.24), a vector of independent voltages,

$$\vec{u}'_r = \begin{bmatrix} u'_{r0} & \dots & u'_{rk} & \dots & u'_{rN_r} \end{bmatrix} \in \mathbb{R}^{N_r+1}$$

is defined as follows:

$$\vec{u}'_r = \mathbf{C}_\mathbf{r}^\top \vec{u}_r \tag{2.30b}$$

In order to understand the meaning of the components of $\vec{u}'_r$, we make use of eq. (2.29) to derive the form of the matrix $\mathbf{C_r}$ whose columns relate the voltage at the terminals of each circuit in fig. 2.9 to the components of $\vec{u}'_r$:

$$\mathbf{C_r} = \begin{array}{c} \\ 0 \\ 1 \\ \\ 2k \\ 2k{+}1 \\ \\ 2N_r \\ \\ 3N_r{-}k \end{array} \begin{array}{c} \begin{array}{ccccccccc} 0 & & & k{-}1 & k & & & N_r{-}1 & N_r \end{array} \\ \begin{bmatrix} 1 & 0 & \cdots & \cdots & \cdots & \cdots & 0 & -1 & 0 \\ 1 & 0 & \cdots & \cdots & \cdots & \cdots & \cdots & \cdots & 0 \\ & & & & & & & & \\ 0 & \cdots & 0 & -1 & 1 & 0 & \cdots & \cdots & 0 \\ 0 & \cdots & 0 & 0 & 1 & 0 & \cdots & \cdots & 0 \\ & & & & & & & & \\ 0 & \cdots & \cdots & \cdots & \cdots & \cdots & \cdots & 0 & 1 \\ & & & & & & & & \\ 0 & \cdots & 0 & 1 & 0 & \cdots & 0 & -1 & 1 \end{bmatrix} \end{array} \tag{2.31}$$

We can deduce from (2.31) that for $k \in [\![0,\, N_r - 2]\!]$, only four entries in column k of $\mathbf{C_r}$ will be different from 0, i.e. the entries in row $2k$, $2k+1$ and $3N_r - k - 1$ will be equal to 1 and the one in row $2k+2$ equal to -1. As the columns of $\mathbf{C_r}$ correspond to the rows of $\mathbf{C}_\mathbf{r}^\top$, for $k \in [\![0,\, N_r - 2]\!]$, the new voltage u'_k represents the sum of the voltages at the terminals of each circuit within loop k in anticlockwise direction (see fig. 2.9). As a result, for $k \in [\![0,\, N_r - 2]\!]$, $u'_k = 0$.

The coefficients of $\mathbf{C_r}$ in column $N_r - 1$ and row 0 as well as $2N_r + 1$ through $3Nr - 1$ are equal to -1 whereas the ones in row $2N_r - 2$ and $2N_r - 1$ are 1. Hence, the voltage $u'_{r[N-1]}$ is the sum of the voltages at the terminals of circuit number $2(N_r - 1)$, $2N_r$, 0 and $2N_r - 1$ added in anticlockwise direction. We have: $u'_{r[N_r-1]} = 0$.

The entries in column number N_r are 0 except for $k \in [\![2N_r,\, 3N_r - 1]\!]$. Thus, u'_{rN_r} is the sum of the voltages at the terminals of circuit number $2N_r$ through $3N_r - 1$ in anticlockwise direction and is also equal to 0. As we assume no axial magnetic field in the machine, there is no main flux across the loop formed by circuit $2N_r$ through $3N_r - 1$. Furthermore, each of these circuits having the same resistance

and the same leakage inductance, there will be no current flowing through this loop, i.e. $i'_{rN_r} = 0$.

In this context, N_r independent voltages and currents are sufficient to fully account for the electrical behaviour of the network in fig. 2.9. This observation is consistent with [54]. We will therefore substitute the squirrel cage for a set of N_r coils having one turn and a pitch equal to the rotor slot pitch. In all models considered from now on, each of these equivalent coils will be modelled as a separate circuit. We will therefore use $m_r = N_r$ rotor circuits, unless otherwise specified.

As our primary focus is on obtaining a model with a restricted number of parameters, we will assign a resistance R_r and a leakage inductance $L_{\sigma r}$ to each of the N_r equivalent coils instead of using distinct quantities for the cage bars on the one hand and end ring segments on the other. Although being less accurate, this approach offers the possibility of determining the parameters of the N_r rotor circuits more easily. Nonetheless, the previous considerations clearly demonstrate that interconnection matrices would make the use of bar and end ring segment quantities possible, if a more accurate cage model is required for a particular application.

2.3.5 Equations of the machine model including circuit interconnections

The equations of the general model built in section 2.2 can easily be adapted to match the winding configuration of a specific machine by means of an interconnection matrix $\mathbf{C}$. Multiplying both sides of the voltage equation (2.4) by the transpose of $\mathbf{C}$ and making use of relations (2.22) and (2.24), we obtain:

$$\mathbf{C}^\top \vec{u} = \mathbf{C}^\top \mathbf{R} \vec{i} + \mathbf{C}^\top \frac{\mathrm{d}\vec{\Psi}}{\mathrm{d}t}$$

$$\Longleftrightarrow \quad \vec{u}' = \mathbf{C}^\top \mathbf{R} \mathbf{C} \vec{i}' + \frac{\mathrm{d}\mathbf{C}^\top \vec{\Psi}}{\mathrm{d}t} \tag{2.32}$$

We introduce a new flux linkage vector $\vec{\Psi}'$ as well as a new resistance matrix $\mathbf{R}'$ for the model with circuit interconnections as follows:

$$\vec{\Psi}' = \mathbf{C}^\top \vec{\Psi} \tag{2.33}$$

$$\mathbf{R}' = \mathbf{C}^\top \mathbf{R} \mathbf{C} \tag{2.34}$$

Note that the relation between $\vec{\Psi}'$ and $\vec{\Psi}$ is of the same nature as the one linking $\vec{u}'$ to $\vec{u}$ and that $\mathbf{R}'$ is not diagonal. The dimension of $\mathbf{R}'$ is determined by the number of columns of $\mathbf{C}$ and is therefore $m' \times m'$.

Using the above notations, the voltage and torque equations holding for the model with interconnections are:

$$\vec{u}' = \mathbf{R}' \vec{i}' + \frac{\mathrm{d}\vec{\Psi}'}{\mathrm{d}t} \tag{2.35}$$

$$M_M = \frac{1}{2} \vec{i}^\top \frac{\partial \vec{\Psi}}{\partial \theta_r} = \frac{1}{2} \left[\mathbf{C} \vec{i}'\right]^\top \frac{\partial \vec{\Psi}}{\partial \theta_r} = \frac{1}{2} \vec{i}'^\top \mathbf{C}^\top \frac{\partial \vec{\Psi}}{\partial \theta_r}$$

$$= \frac{1}{2} \vec{i}'^\top \frac{\partial \vec{\Psi}'}{\partial \theta_r} \tag{2.36}$$

A comparison of (2.35) and (2.36) with (2.4) and (2.18) shows that the circuit interconnections do not affect the form of the voltage and torque expressions.

In the same manner, a relation between $\vec{\Psi}'$ and $\vec{i}'$ is derived from the one between $\vec{\Psi}$ and $\vec{i}$:

$$\vec{\Psi}'(\vec{i}', \theta_r) = \mathbf{C}^\top \vec{\Psi}(\mathbf{C}\vec{i}', \theta_r) \tag{2.37}$$

Assuming a linear magnetic behaviour for small variations around the operating point as in section 2.2.2, (2.37) becomes:

$$\vec{\Psi}'(\vec{i}', \theta_r) = \mathbf{C}^\top \mathbf{L}(\vec{i}, \theta_r)\mathbf{C}\vec{i}' = \mathbf{L}'(\vec{i}', \theta_r)\vec{i}' \tag{2.38}$$

The Jacobian matrix of $\vec{\Psi}'$ with respect to $\vec{i}'$, i.e. the differential inductance matrix in presence of circuit interconnections, is:

$$\frac{\partial \vec{\Psi}'}{\partial \vec{i}'} = \mathbf{C}^\top \frac{\partial \vec{\Psi}}{\partial \vec{i}} \mathbf{C} \tag{2.39}$$

The above results demonstrate that the process of interconnecting the electrical circuits in the model does not alter the general form of its equations. The *new* flux and voltage vectors resulting from the interconnection process are determined by pre-multiplying the corresponding *old* vectors in the model without interconnections by $\mathbf{C}^\top$. In contrast, the *old* current vector is computed by multiplying the *new* one by $\mathbf{C}$. The transformation of matrices involves a pre-multiplication by $\mathbf{C}^\top$ as well as a post-multiplication by $\mathbf{C}$.

2.4 Continuous-time state-space model with interconnections

2.4.1 Inverting the differential inductance matrix

Recalling section 2.2.4, the continuous-time machine model without circuit interconnections involves the inverse of the differential inductance matrix $\partial\vec{\Psi}/\partial\vec{i}$ which can be determined using a Cholesky decomposition, as in (2.21). Combining (2.39) and (2.21) provides the subsequent expression of the differential inductance matrix for the model including circuit interconnections:

$$\frac{\partial \vec{\Psi}'}{\partial \vec{i}'} = \mathbf{C}^\top \mathbf{\Delta}^\top \mathbf{\Delta} \mathbf{C} = (\mathbf{\Delta}\mathbf{C})^\top (\mathbf{\Delta}\mathbf{C}) \tag{2.40}$$

For all $\vec{x} \in \mathbb{R}^{m'}$,

$$\begin{aligned} \vec{x}^\top (\mathbf{\Delta}\mathbf{C})^\top (\mathbf{\Delta}\mathbf{C})\vec{x} &= [\mathbf{\Delta}\mathbf{C}\vec{x}]^\top [\mathbf{\Delta}\mathbf{C}\vec{x}] \\ &= \|\mathbf{\Delta}\mathbf{C}\vec{x}\|^2 \\ &\geqslant 0 \end{aligned}$$

which means that $\partial\vec{\Psi}'/\partial\vec{i}'$ is symmetric positive semidefinite. $\partial\vec{\Psi}'/\partial\vec{i}'$ is even positive definite as $\operatorname{rank}(\mathbf{C}) = m'$ implies that for all $\vec{x} \in \mathbb{R}^{m'} \setminus \{0\}$, $\mathbf{C}\vec{x} \neq 0$ and, $\mathbf{\Delta}$ being invertible, $\mathbf{\Delta}\mathbf{C}\vec{x} \neq 0$. Hence, the interconnection of the electric circuits does not alter the positive definiteness of the differential inductance matrix. Its remains invertible and its inverse and can still be calculated using a Cholesky decomposition.

2.4.2 State-space model with interconnected circuits

Under the assumptions formulated in section 2.1.1, the state-space model of the machine with interconnected circuits is described by the following set of equations:

$$\left[\begin{aligned} \frac{\mathrm{d}\vec{\Psi}'}{\mathrm{d}t} &= \vec{u}' - \mathbf{R}'\mathbf{L}'^{-1}(\vec{\Psi}',\, \theta_r)\vec{\Psi}' && \text{(2.41a)} \\ \frac{\mathrm{d}\omega_r}{\mathrm{d}t} &= \frac{1}{J_M}\left[\frac{1}{2}\left[\mathbf{L}'^{-1}(\vec{\Psi}',\, \theta_r)\vec{\Psi}'\right]^\top \frac{\partial \vec{\Psi}'}{\partial \theta_r} - C_W\omega_r - M_L\right] && \text{(2.41b)} \\ \frac{\mathrm{d}\theta_r}{\mathrm{d}t} &= \omega_r && \text{(2.41c)} \end{aligned}\right.$$

The components of the flux vector $\vec{\Psi}'$, the rotor angular velocity as well as the rotor angle are the state variables. The model has dimension $m'_s + m'_r + 2$ and forms the basis for all modelling considerations to come. We will refer to it as *geometric model*, since the computation of the relation between currents and flux linkages relies on geometric considerations.

2.5 Discussion

The procedure described in the present chapter was applied to the test machine IM1. Each of the three star-connected stator windings was modelled using a specific circuit, i.e. $m_s = w_s = 3$. This leads to the stator interconnection matrix, $\mathbf{C_{s,\,IM1}}$, having the form:

$$\mathbf{C_{s,\,IM1}} = \begin{bmatrix} 1 & 0 \\ 0 & 1 \\ -1 & -1 \end{bmatrix}$$

while in this particular case, $m'_s = 2$. Hence, the vector $\vec{u}'_s$ (or $\vec{i}'_s$) has two components, u'_{s0} and u'_{s1} (i'_{s0} and i'_{s1} respectively). The benefits resulting from an appropriate choice for the number of circuits in the model will be discussed in greater detail in section 3.7.

Owing to the considerations in section 2.3.4, $m_r = N_r = 16$ circuits are required to represent the rotor cage. The rotor interconnection matrix, $\mathbf{C_{r,\,IM1}}$, is thus the identity matrix of dimension m_r. Hence $m'_r = N_r = 16$.

Consequently, the model represented by (2.41) has order 20. Its implementation requires the discretization of the air-gap coordinates γ_s and γ_r to perform the flux computations (2.12) and (2.13).

Simulation results reported in [59] show that the model is principally able to generate the stator current components arising from winding distribution, slotting, eccentricity and saturation effects. However, the flux computations necessitate far too much time to be performed in real-time, even on a powerful computer. In addition, the many parameters needed to account for each type of flux density distribution harmonics and their difficult practical estimation make the model in its current form not suitable for the targeted applications. For this reason, we will focus on developing a strategy to avoid the discretization of the air-gap in the next chapter.

Summary

The considerations in the present chapter laid the foundation for an extended model of the induction machine taking into account the space harmonics present in the air-gap flux density distribution. The approach adopted is based on the winding function theory and consists of two distinct steps. First, the conductor arrangements on the stator and the rotor of the investigated machine are modelled as sets of *electrical circuits*. We then assign a *conductor distribution function* to each circuit which represents the geometric distribution of the conductors belonging to said circuit. This allows us to work out the relation between currents and flux linkages in the virtual case where no interconnection exists between the circuits.

In a second step, we connect the circuits to each other in order to correctly account for the actual conductor configuration of the machine. This process is accomplished by means of *interconnection matrices* and does not affect the positive definiteness of the inductance matrix which can be inverted efficiently using a Cholesky decomposition.

The resulting *geometric model* was investigated in the case of IM1. Simulation results show its ability to reproduce the additional stator current components arising from the flux density harmonics. However, the necessary discretization of the air-gap coordinates in order to calculate the flux linkages makes the model inappropriate for real-time applications. Hence, our next task consists in finding an alternative method to determine these quantities.

Chapter 3
Magnetically linear geometric model

Overview of chapter

The winding function based model introduced previously relies on the discretization of the air-gap coordinate to determine the magnetic flux through the electrical circuits. This time-consuming process makes a real-time computation of the model impossible. The considerations in the present chapter aim at overcoming this limitation by making use of the periodicity of air-gap quantities which can be expressed as Fourier series.

The expressions of the flux linkages are gained from the Fourier coefficients of the conductor distribution functions as well as the ones of the air-gap flux density distribution using Parseval's identity. As the corresponding Fourier coefficients decrease rapidly with the order, only a few of them have to be considered to achieve a fair approximation of the flux linkages.

Further simplification is obtained when assuming a linear magnetic behaviour and a constant air-gap length, since the flux density distribution can then be expressed as a linear combination of the conductor distribution functions. As a result, simple analytical approximations of the flux linkages can be found. In a first step, we consider a configuration in which no electrical interconnection is present. It is shown that, in this particular case, the resulting inductance matrix is symmetric positive definite.

Interconnections between electrical circuits on the stator as well as on the rotor side are taken into consideration by means of interconnection matrices. New electrical quantities are introduced for the system with interconnections. A continuous-time state-space model of the induction machine including the effect of space harmonics arising from the conductor distribution is gained.

Finally, two strategies for discretizing the state-space equations are examined. On the one hand, the continuous-time equations are solved using numerical methods. On the other, a zero-order hold is assumed and the exponential of the system matrix is approximated by means of a power series expansion. The two approaches are assessed experimentally with respect to their accuracy and computational performance.

3.1 Important results on Fourier series

This section provides a summary of results on Fourier series which will be instrumental in determining computationally efficient approximations of the flux linkages. For the sake of brevity, detailed proofs of theorems and propositions are omitted. The interested reader is invited to refer to the references provided.

3.1.1 Properties of Fourier coefficients

Let $E_{2\pi}$ be the set of 2π-periodic piecewise continuous functions from $\mathbb{R}$ to $\mathbb{C}$.

The transformation

$$\begin{aligned}\Gamma : E_{2\pi} \times E_{2\pi} &\longrightarrow \mathbb{C} \\ (f,\, g) &\longmapsto \frac{1}{2\pi}\int_0^{2\pi} \overline{f(\gamma)} g(\gamma)\,\mathrm{d}\gamma\end{aligned}$$

is a positive Hermitian form on the $\mathbb{C}$-vector space $E_{2\pi}$.

For $h \in \mathbb{Z}$, we define:

$$\begin{aligned}e_h : \mathbb{R} &\longrightarrow \mathbb{C} \\ \gamma &\longmapsto e^{jh\gamma}\end{aligned}$$

$\forall\, h \in \mathbb{Z}, e_h \in E_{2\pi}$ and $\Gamma(e_h,\, e_h) = 1$. For $(h_0,\, h_1) \in \mathbb{Z}^2$ such that $h_0 \neq h_1$, $\Gamma(e_{h_0},\, e_{h_1}) = 0$. As a result, the list $(e_h)_{h\in\mathbb{Z}}$ is orthonormal and linearly independent.

Definition 1: Fourier coefficients
For $f \in E_{2\pi}$ and $h \in \mathbb{Z}$, we denote

$$c_h(f) = \Gamma(e_h,\, f) = \frac{1}{2\pi}\int_0^{2\pi} f(\gamma) e^{-jh\gamma}\,\mathrm{d}\gamma$$

Definition 2: Fourier partial sum
For $f \in E_{2\pi}$ and $N \in \mathbb{N}$, we define

$$S_N(f) = \sum_{h=-N}^{N} c_h(f) e_h$$

Proposition 1: Results on Fourier coefficients
For $(f,\, g) \in E_{2\pi}^2$, for $h \in \mathbb{Z}$,

1. *Let $\lambda \in \mathbb{C}$. $c_h(f + \lambda g) = c_h(f) + \lambda c_h(g)$*
2. *$\forall\, \gamma \in \mathbb{R}$, $g(\gamma) = f(-\gamma) \Longrightarrow c_h(g) = c_{-h}(f)$*
   In particular, if f is even, $c_{-h}(f) = c_h(f)$. If f is odd, $c_{-h}(f) = -c_h(f)$
3. *Let $\gamma_0 \in \mathbb{R}$.*
   $[\forall\, \gamma \in \mathbb{R},\, g(\gamma) = f(\gamma + \gamma_0)] \Longrightarrow c_h(g) = e^{jh\gamma_0} c_h(f)$
4. *If f is real-valued, $c_{-h}(f) = \overline{c_h(f)}$*

Proof. The above results follow directly from definition 1. □

3.1.2 Convergence considerations

Theorem 2: Dirichlet conditions
If $f \in E_{2\pi}$ is piecewise continuously differentiable and 2π-periodic, then

$$\forall\, \gamma \in \mathbb{R}, \quad S_N(f)(\gamma) = \sum_{h=-N}^{N} c_h(f) e^{jh\gamma} \xrightarrow[N\to+\infty]{} \frac{1}{2}\left[\lim_{\Delta\gamma\to 0^+} [f(\gamma+\Delta\gamma) + f(\gamma-\Delta\gamma)]\right]$$

In particular, if f is continuous at a point $\gamma_0 \in \mathbb{R}$, $S_N(f)(\gamma_0) \xrightarrow[N\to+\infty]{} f(\gamma_0)$

A proof of the Dirichlet conditions of convergence of the Fourier partial sum can be found in [60].

The functions describing air-gap quantities satisfy the Dirichlet conditions. Their Fourier series representation therefore exists. Owing to the modelling assumptions made, the current density distribution is the only quantity exhibiting discontinuities. In contrast, conductor distribution and slot profile functions as well as MMF and flux density distributions are assumed to be continuous on the interval $[0,\, 2\pi]$. For this reason, we examine in the following section a few more instrumental properties applying to continuous 2π-periodic functions.

3.1.3 Parseval's identity

Let $C_{2\pi}$ be the set of 2π-periodic continuous functions from $\mathbb{R}$ to $\mathbb{C}$.

The map

$$\begin{aligned} \langle\cdot|\cdot\rangle : C_{2\pi} \times C_{2\pi} &\longrightarrow \mathbb{C} \\ (f,\, g) &\longmapsto \langle f|g\rangle = \frac{1}{2\pi}\int_0^{2\pi} \overline{f(\gamma)} g(\gamma)\, \mathrm{d}\gamma \end{aligned}$$

is a Hermitian inner product on $C_{2\pi}$. The norm associated to $\langle\cdot|\cdot\rangle$ is

$$\begin{aligned} \|\cdot\|_2 : C_{2\pi} &\longrightarrow \mathbb{R}^+ \\ f &\longmapsto \|f\|_2 = \sqrt{\langle f|f\rangle} = \sqrt{\frac{1}{2}\int_0^{2\pi} |f(\gamma)|^2\, \mathrm{d}\gamma} \end{aligned}$$

Let $\mathcal{F}$ be the vector subspace of $\mathbb{C}^{\mathbb{Z}}$ consisting of the sequences $(u_h)_{h\in\mathbb{Z}}$ such that the partial sum $\sum_{h=-N}^{N} |u_h|^2$ converges. The map

$$\begin{aligned} \chi : \mathcal{F} \times \mathcal{F} &\longrightarrow \mathbb{C} \\ ((u_h),\, (v_h)) &\longmapsto \chi((u_h),\, (v_h)) = \sum_{h=-\infty}^{+\infty} \overline{u_h} v_h \end{aligned}$$

is a Hermitian inner product on $\mathcal{F}$. The corresponding norm is denoted

$$\begin{aligned} \mathcal{N} : \mathcal{F} &\longrightarrow \mathbb{R}^+ \\ (u_h) &\longmapsto \mathcal{N}((u_h)) = \sqrt{\chi((u_h),\, (u_h))} = \sum_{h=-\infty}^{+\infty} |u_h|^2 \end{aligned}$$

We introduce the linear map

$$\zeta : (C_{2\pi},\, \|\cdot\|_2) \longrightarrow (\mathcal{F},\, \mathcal{N})$$

$$f \longmapsto \left(c_h(f) = \frac{1}{2\pi} \int_0^{2\pi} f(\gamma) e^{-jh\gamma} \, \mathrm{d}\gamma \right)_{h \in \mathbb{Z}}$$

Theorem 3: Parseval's identity

$$\forall f \in C_{2\pi}, \qquad \|f\|_2^2 = \mathcal{N}(\zeta(f))^2$$

$$\iff \frac{1}{2\pi} \int_0^{2\pi} |f(\gamma)|^2 \, \mathrm{d}\gamma = \sum_{h=-\infty}^{+\infty} |c_h(f)|^2 \tag{3.1}$$

Corollary: $\forall\, (f,\, g) \in C_{2\pi}^2$,

$$\langle f | g \rangle = \chi(\zeta(f), \zeta(g))$$

$$\frac{1}{2\pi} \int_0^{2\pi} \overline{f(\gamma)} g(\gamma) \, \mathrm{d}\gamma = \sum_{h=-\infty}^{+\infty} \overline{c_h(f)} c_h(g) \tag{3.2}$$

Proof. Use the polarization identity on the inner product space $(C_{2\pi},\, \|\cdot\|_2)$ and the fact that ζ is a norm-preserving map. □

From eq. (3.2) and Proposition 1.4 follows that if f is a real-valued function, i.e. $\overline{f} = f$,

$$\frac{1}{2\pi} \int_0^{2\pi} f(\gamma) g(\gamma) \, \mathrm{d}\gamma = \sum_{h=-\infty}^{+\infty} c_{-h}(f) c_h(g) \tag{3.3}$$

3.2 General expressions of flux linkages using Fourier coefficients

Owing to relation (2.12), the magnetic flux linking stator circuit $m \in [\![0,\, m_s - 1]\!]$ with the others (i.e. the main flux) is gained by integrating the product of the conductor distribution function W_{sm} and the air-gap flux density distribution over the whole air-gap circumference:

$$\widetilde{\psi}_{sm} = r \cdot l \cdot \int_0^{2\pi} W_{sm}(\gamma_s) B(\gamma_s) \, \mathrm{d}\gamma_s \tag{3.4}$$

W_{sm} and B being real-valued functions, relation (3.3) leads to:

$$\frac{1}{2\pi} \int_0^{2\pi} W_{sm}(\gamma_s) B(\gamma_s) \, \mathrm{d}\gamma_s = \sum_{h=-\infty}^{+\infty} c_{-h}(W_{sm}) c_h(B) \tag{3.5}$$

Hence, the main flux of circuit m can be rewritten involving the Fourier coefficients of W_{sm} and B rather than an integral with respect to the stator air-gap coordinate:

$$\widetilde{\psi}_{sm} = r \cdot l \cdot \int_0^{2\pi} W_{sm}(\gamma_s) B(\gamma_s) \, \mathrm{d}\gamma_s = 2\pi r l \sum_{h=-\infty}^{+\infty} c_{-h}(W_{sm}) c_h(B) \tag{3.6}$$

Since B does not have a DC component, $c_0(B) = 0$, which leads to:

$$\widetilde{\psi}_{sm} = 2\pi r l \left[\sum_{h=-\infty}^{-1} c_{-h}(W_{sm}) c_h(B) + \sum_{h=1}^{+\infty} c_{-h}(W_{sm}) c_h(B) \right]$$

$$= 2\pi r l \sum_{h=1}^{+\infty} [c_h(W_{sm}) c_{-h}(B) + c_{-h}(W_{sm}) c_h(B)]$$

$$= 2\pi r l \sum_{h=1}^{+\infty} \Big[c_h(W_{sm}) \overline{c_h(B)} + \overline{c_h(W_{sm})} c_h(B) \Big]$$

$$= 4\pi r l \sum_{h=1}^{+\infty} \mathfrak{Re}[c_h(W_{sm}) c_{-h}(B)] \tag{3.7}$$

Similarly, the magnetic flux linking rotor circuit $n \in [\![0,\, m_r - 1]\!]$ with the others is:

$$\widetilde{\psi}_{rn_0} = r\, l \int_0^{2\pi} W_{rn}(\gamma_r) B'(\gamma_r)\, \mathrm{d}\gamma_r = 2\pi r l \sum_{h=-\infty}^{+\infty} c_{-h}(W_{rn}) c_h(B')$$

$$= 4\pi r l \sum_{h=1}^{+\infty} \mathfrak{Re}\big[c_h(W_{rn}) c_{-h}(B')\big] \tag{3.8}$$

where B' represents the total main flux density distribution as a function of the rotor air-gap coordinate γ_r. Eq. (3.7) and (3.8) do not impose any particular restriction on the flux density distribution apart from the fact that the functions B and B' should not have discontinuities on the interval $[0,\, 2\pi]$.

The two equations show that a space harmonic of order h may have an effect on the flux linkage only if the considered conductor distribution function has a coefficient of order h. Thus, even if the air-gap flux density displays space harmonics other than the ones arising from the conductor distribution, for instance as a result of saturation or eccentricity, they will not have an impact on flux linkages. Eq. (3.7) and (3.8) are the mathematical justification of the fact that waves with different numbers of pole pairs do not interact with each other (see for instance the assumption of Kron's modelling approach in [1, chapt. 10]). In particular, the two above relations explain the existence of conditions for PSHs to appear in an induction machine (cf. section 1.2).

In order to avoid confusion with *time harmonics* which refer to the harmonics present in the waveforms of quantities such as currents, torque and angular velocity with respect to *time*, we will use the term *wavelengths* to denote the *space harmonics* which appear in the distribution of air-gap quantities. Hence, the *space harmonic* of order h will also be called *wavelength of order* h or simply *wavelength* h to emphasize the distributed character of the considered quantity.

3.3 Necessity of simplifying assumptions

Relations (3.7) and (3.8) are potentially interesting for the computation of the flux linkages if the Fourier coefficients of the conductor distribution functions and the ones of the flux density distribution are known.

Stator conductor distribution functions being time-invariant, their Fourier expansion can be determined without much effort during the model initialization procedure. The same applies to the conductor distribution functions of rotor circuits which can be precomputed for a specific rotor position when the model is being initialized. The phase-shift property (see Proposition 1.3) enables us to efficiently recover the Fourier coefficients for any rotor position.

The flux density distribution, however, not only depends on the conductor distribution functions but also on the stator and rotor slot profile as well as saturation distributions. As the latter change with the rotor angle, their Fourier coefficients cannot be precomputed and must be calculated during model execution. This time-consuming task does not offer any benefit in comparison to a direct integration with respect to the air-gap variables.

Bearing in mind that the fundamental objective of the modelling approach is the derivation of a real-time compliant model, we decide to focus exclusively on the influence of conductor distribution harmonics. For this reason, the following additional assumptions will apply to the rest of the document:

1.) The air-gap has a constant length. As a result, the influence of stator and rotor slots on magnetic paths is not taken into account. Neither is magnetic saturation;

2.) the winding arrangements on the stator and the rotor are symmetric over the air-gap circumference. This also applies to the conductors of rotor cages.

We will demonstrate in the following sections that these hypotheses are instrumental in finding computationally efficient approximations of the flux linkages which will allow the design of a real-time compliant model.

3.4 Flux linkage expressions including the effect of conductor distribution harmonics

3.4.1 Stator air-gap flux density

Assuming a current i_{s0} flowing through stator circuit number 0, the following relations hold between the conductor distribution function of stator circuit 0, W_{s0}, the resulting MMF, Θ_{s0}, and the radial flux density distribution, B_{s0}, when these quantities are expressed as functions of the geometric coordinate γ_s:

$$\Theta_{s0} = i_{s0} \cdot [W_{s0} - c_0(W_{s0})] \tag{3.9}$$

$$B_{s0} = \frac{\mu_0}{\delta_0}\Theta_{s0} = \frac{\mu_0}{\delta_0} \cdot i_{s0} \cdot [W_{s0} - c_0(W_{s0})] \tag{3.10}$$

As a result, for all $h \in \mathbb{Z}^\star$, the Fourier coefficients of Θ_{s0} and B_{s0} can be related to the ones of W_{s0}:

$$c_h(\Theta_{s0}) = i_{s0} \cdot c_h(W_{s0}) \tag{3.11}$$

$$c_h(B_{s0}) = \frac{\mu_0}{\delta_0} \cdot i_{s0} \cdot c_h(W_{s0}) \tag{3.12}$$

Making use of the symmetric arrangement of stator windings, we define stator circuit $m \in [\![0,\, m_s - 1]\!]$ so that its conductor distribution function, W_{sm}, is equal to the one of circuit 0 shifted by an angle $\gamma_{s0,m}$ (see fig. 3.1):

$$\forall\, \gamma_s \in \mathbb{R},\ W_{sm}(\gamma_s) = W_{s0}(\gamma_s + \gamma_{s0,m})$$

Following Prop. 1.3, the Fourier coefficients of the distributed quantities of a circuit $m \in [\![0,\, m_s - 1]\!]$ are given by the subsequent relations:

$$\forall\, h \in \mathbb{Z}, \quad c_h(W_{sm}) = e^{jh\gamma_{s0,m}} c_h(W_{s0}) \tag{3.13}$$

$$\forall\, h \in \mathbb{Z}^\star, \quad c_h(\Theta_{sm}) = i_{sm} \cdot c_h(W_{sm}) = i_{sm} e^{jh\gamma_{s0,m}} c_h(W_{s0}) \tag{3.14}$$

$$\text{and} \quad c_h(B_{sm}) = \frac{\mu_0}{\delta_0} \cdot i_{sm} e^{jh\gamma_{s0,m}} c_h(W_{s0}) \tag{3.15}$$

Owing to the hypothesis of magnetic linearity, the total radial air-gap flux density component originating from stator currents is the sum of the contributions of each stator circuit:

$$B_s(\gamma_s) = \sum_{m=0}^{m_s-1} B_{sm}(\gamma_s) \tag{3.16}$$

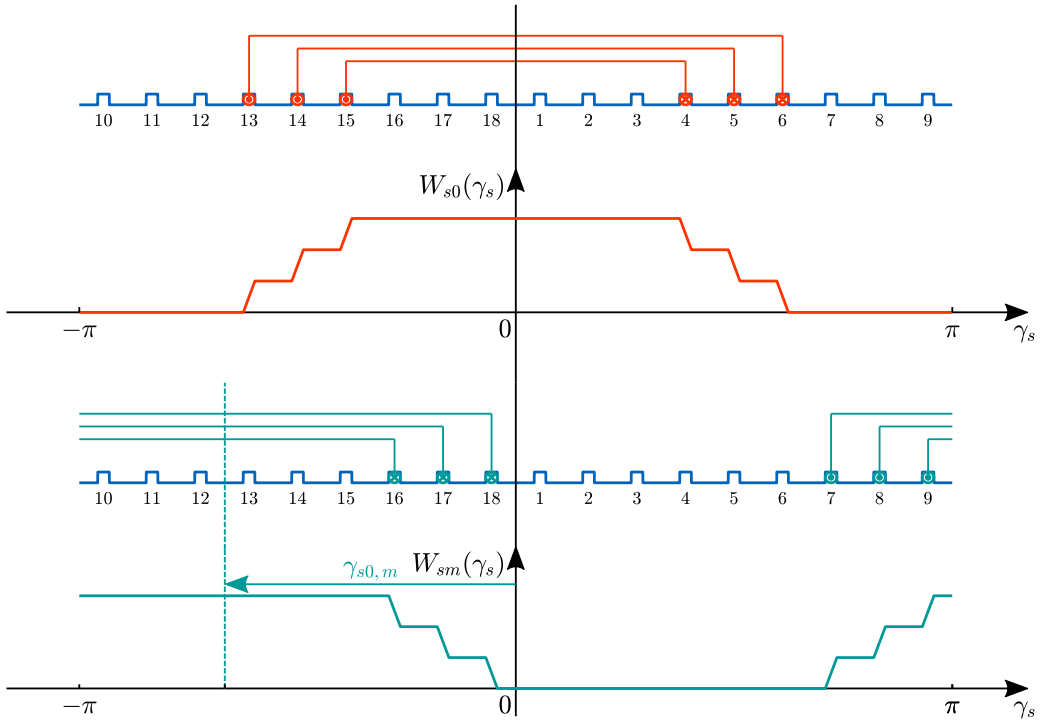

Figure 3.1: Definition of the phase shift angle between stator circuit m and 0, $\gamma_{s0,m}$

The Fourier coefficients of B_s result from Prop. 1.1 and can be related to the ones of W_{s0}:

$$c_h(B_s) = \sum_{m=0}^{m_s-1} c_h(B_{sm})$$

$$\forall\, h \in \mathbb{Z}^\star, \quad c_h(B_s) = \frac{\mu_0}{\delta_0} c_h(W_{s0}) \sum_{m=0}^{m_s-1} i_{sm} e^{jh\gamma_{s0,m}}$$

$$c_0(B_s) = 0$$

Consequently, the air-gap flux density wave produced by stator currents, expressed as a function of the stator air-gap coordinate γ_s, is described by the equation:

$$\begin{aligned} B_s(\gamma_s) &= \sum_{h=-\infty}^{+\infty} c_h(B_s) e^{jh\gamma_s} \\ &= \sum_{h=-\infty}^{+\infty} e^{jh\gamma_s} \frac{\mu_0}{\delta_0} \sum_{m=0}^{m_s-1} i_{sm} e^{jh\gamma_{s0,m}} c_h(W_{s0}) \end{aligned} \tag{3.17}$$

Considering the relationship between stator and rotor air-gap coordinates as illustrated in fig. 3.2,

$$\gamma_s = \gamma_r - \theta_r \tag{3.18}$$

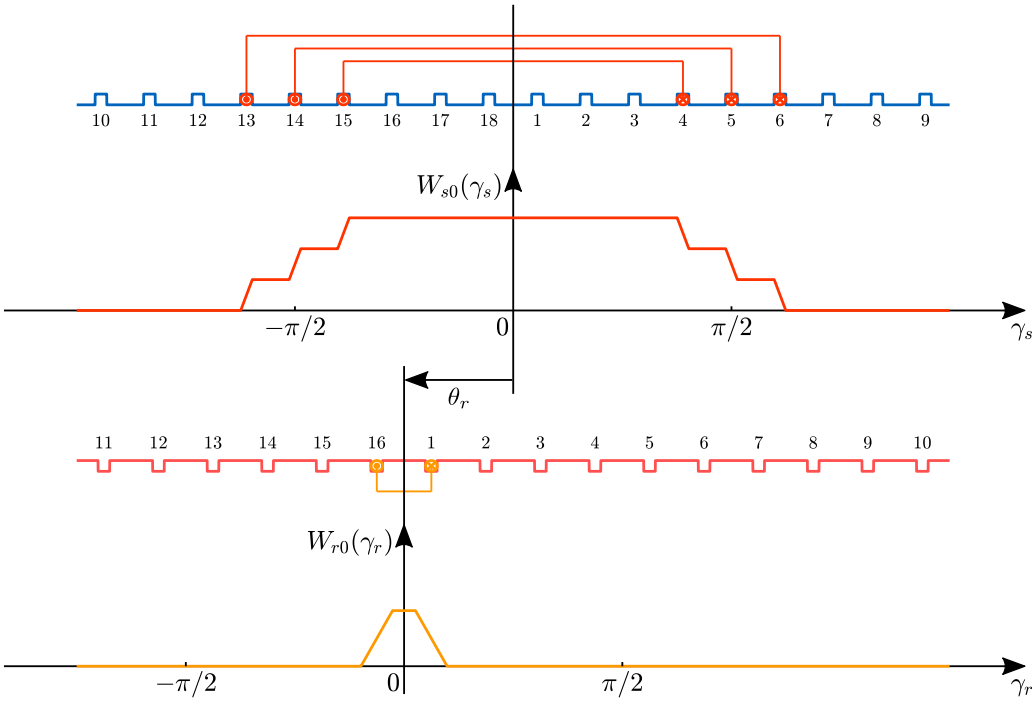

Figure 3.2: Definition of stator and rotor air-gap coordinates, exemplified for the case of IM1

the expression of the stator flux density wave as a function of the rotor air-gap coordinate γ_r, denoted B'_s, is:

$$\begin{aligned} B'_s(\gamma_r) &= B_s(\gamma_s) = B_s(\gamma_r - \theta_r) \\ &= \sum_{h=-\infty}^{+\infty} c_h(B_s) e^{jh(\gamma_r - \theta_r)} \\ &= \sum_{h=-\infty}^{+\infty} c_h(B_s) e^{-jh\theta_r} e^{jh\gamma_r} \\ &= \sum_{h\in\mathbb{Z}^\star} e^{jh\gamma_r} \frac{\mu_0}{\delta_0} \sum_{m=0}^{m_s-1} i_{sm} e^{jh(-\theta_r+\gamma_{s0,m})} c_h(W_{s0}) \end{aligned} \tag{3.19}$$

3.4.2 Rotor air-gap flux density

The Fourier coefficients related to the distributed quantities of rotor circuit $n \in [\![0,\, m_r - 1]\!]$ are derived similarly to section 3.4.1. In case the distributed quantities are expressed as functions of the air-gap coordinate γ_r, the following relations result:

$$\forall\, h \in \mathbb{Z}, \quad c_h(W_{rn}) = e^{jh\gamma_{r0,n}} c_h(W_{r0}) \tag{3.20}$$

$$\forall\, h \in \mathbb{Z}^\star, \quad c_h(\Theta_{rn}) = i_{rn} \cdot c_h(W_{rn}) = i_{rn} e^{jh\gamma_{r0,n}} c_h(W_{r0}) \tag{3.21}$$

$$\text{and} \quad c_h(B_{rn}) = \frac{\mu_0}{\delta_0} \cdot i_{rn} e^{jh\gamma_{r0,n}} c_h(W_{r0}) \tag{3.22}$$

where $\gamma_{r0,n}$ represents the shift angle between the conductor distribution functions W_{rn} and W_{r0}.

As a consequence of the superposition principle, the total radial air-gap flux density generated by currents flowing through rotor circuits is

$$B_r(\gamma_r) = \sum_{n=0}^{m_r-1} B_{rn}(\gamma_r) \tag{3.23}$$

and its Fourier coefficients are:

$$c_h(B_r) = \sum_{n=0}^{m_r-1} c_h(B_{rn}) = \frac{\mu_0}{\delta_0} c_h(W_{r0}) \sum_{n=0}^{m_r-1} i_{rn} e^{jh\gamma_{r0,n}} \tag{3.24}$$

Therefore, the air-gap flux density component resulting from rotor currents has the following Fourier representation:

$$\begin{aligned} B_r(\gamma_r) &= \sum_{h=-\infty}^{+\infty} c_h(B_r) e^{jh\gamma_r} \\ &= \sum_{h\in\mathbb{Z}^\star} e^{jh\gamma_r} \frac{\mu_0}{\delta_0} \sum_{n=0}^{m_r-1} i_{rn} e^{jh\gamma_{r0,n}} c_h(W_{r0}) \end{aligned} \tag{3.25}$$

The same quantity expressed as function of the stator air-gap coordinate is referred to as B'_r and satisfies the relation:

$$\begin{aligned} B'_r(\gamma_s) &= B_r(\gamma_r) = B_r(\gamma_s + \theta_r) \\ &= \sum_{h=-\infty}^{+\infty} c_h(B_r) e^{jh(\gamma_s+\theta_r)} \\ &= \sum_{h\in\mathbb{Z}^\star} e^{jh\gamma_s} \frac{\mu_0}{\delta_0} \sum_{n=0}^{m_r-1} i_{rn} e^{jh(\gamma_{r0,n}+\theta_r)} c_h(W_{r0}) \end{aligned} \tag{3.26}$$

3.4.3 Total air-gap flux density distribution

The assumption of magnetic linearity allows to sum the contributions of stator and rotor circuits to obtain the overall air-gap flux density distribution at a given time instant. These two contributions have to be expressed using the same coordinate, i.e. γ_s or γ_r.

Hence, the total air-gap flux density wave, B, has the following form in stator coordinates:

$$\begin{aligned} B(\gamma_s) &= B_s(\gamma_s) + B'_r(\gamma_s) = B_s(\gamma_s) + B_r(\gamma_s + \theta_r) \\ &= \sum_{m=0}^{m_s-1} B_{sm}(\gamma_s) + \sum_{n=0}^{m_r-1} B_{rn}(\gamma_s + \theta_r) \\ &= \sum_{m=0}^{m_s-1} \frac{\mu_0}{\delta_0} i_{sm} W_{sm}(\gamma_s) + \sum_{n=0}^{m_r-1} \frac{\mu_0}{\delta_0} i_{rn} W_{rn}(\gamma_s + \theta_r) \\ &= \sum_{m=0}^{m_s-1} \frac{\mu_0}{\delta_0} i_{sm} W_{s0}(\gamma_s + \gamma_{s0,m}) + \sum_{n=0}^{m_r-1} \frac{\mu_0}{\delta_0} i_{rn} W_{r0}(\gamma_s + \theta_r + \gamma_{r0,n}) \end{aligned}$$

The Fourier coefficients of B are computed using the ones of the conductor distribution functions W_{s0}

and W_{r0}:

$$\forall\, h \in \mathbb{Z}^\star,\; c_h(B) = \frac{\mu_0}{\delta_0} \sum_{m=0}^{m_s-1} i_{sm} e^{jh\gamma_{s0,m}} c_h(W_{s0}) + \frac{\mu_0}{\delta_0} e^{jh\theta_r} \sum_{n=0}^{m_r-1} i_{rn} e^{jh\gamma_{r0,n}} c_h(W_{r0}) \tag{3.27}$$

In the same manner, the results obtained in the previous section enable us to work out the expression of the total air-gap flux density distribution in rotor coordinates, B', based on the conductor distribution functions of stator and rotor circuit number 0:

$$\begin{aligned} B'(\gamma_r) &= B_r(\gamma_r) + B'_s(\gamma_r) = B_r(\gamma_r) + B_s(\gamma_r - \theta_r) \\ &= \sum_{n=0}^{m_r-1} B_{rn}(\gamma_r) + \sum_{m=0}^{m_s-1} B_{sm}(\gamma_r - \theta_r) \\ &= \sum_{n=0}^{m_r-1} \frac{\mu_0}{\delta_0} i_{rn} W_{rn}(\gamma_r) + \sum_{m=0}^{m_s-1} \frac{\mu_0}{\delta_0} i_{sm} W_{sm}(\gamma_r - \theta_r) \\ &= \sum_{n=0}^{m_r-1} \frac{\mu_0}{\delta_0} i_{rn} W_{r0}(\gamma_r + \gamma_{r0,n}) + \sum_{m=0}^{m_s-1} \frac{\mu_0}{\delta_0} i_{sm} W_{s0}(\gamma_r - \theta_r + \gamma_{s0,m}) \end{aligned}$$

Consequently, the Fourier coefficient of order $h \in \mathbb{Z}^\star$ of B' is:

$$c_h(B') = \frac{\mu_0}{\delta_0} \sum_{m=0}^{m_r-1} i_{rn} e^{jh\gamma_{r0,n}} c_h(W_{r0}) + \frac{\mu_0}{\delta_0} e^{-jh\theta_r} \sum_{m=0}^{m_s-1} i_{sm} e^{jh\gamma_{s0,m}} c_h(W_{s0}) \tag{3.28}$$

As we will see in the upcoming sections, relations (3.27) and (3.28) provide the information necessary to calculate flux linkages based on (3.7) and (3.8).

3.4.4 Contribution of a specific wavelength to the main flux

Flux through stator circuits

For $h \in \mathbb{N}^\star$, we consider the contribution of the wavelength of order h to the main flux through a specific stator circuit $m_0 \in [\![0,\, m_s - 1]\!]$, $\widetilde{\psi}_{sm_0,\,h}$, defined in accordance with relation (3.7):

$$\widetilde{\psi}_{sm_0,\,h} = 4\pi r l \mathfrak{Re}[c_h(W_{sm_0}) c_{-h}(B)] \tag{3.29}$$

The results listed in Prop. 2 in combination with eq. (3.27) allow us to express $\widetilde{\psi}_{sm_0,\,h}$ using the Fourier coefficients of W_{s0} and W_{r0} only:

$$\begin{aligned} c_h(W_{sm_0}) c_{-h}(B) &= e^{jh\gamma_{s0,m_0}} c_h(W_{s0}) c_{-h}(B) \\ &= \frac{\mu_0}{\delta_0} e^{jh\gamma_{s0,m_0}} c_h(W_{s0}) \Bigg[\sum_{m=0}^{m_s-1} i_{sm} e^{-jh\gamma_{s0,m}} c_{-h}(W_{s0}) \\ &\qquad + e^{-jh\theta_r} \sum_{n=0}^{m_r-1} i_{rn} e^{-jh\gamma_{r0,n}} c_{-h}(W_{r0}) \Bigg] \\ &= \frac{\mu_0}{\delta_0} |c_h(W_{s0})|^2 e^{jh\gamma_{s0,m_0}} \sum_{m=0}^{m_s-1} i_{sm} e^{-jh\gamma_{s0,m}} + \end{aligned}$$

$$\frac{\mu_0}{\delta_0} c_h(W_{s0}) c_{-h}(W_{r0}) e^{jh(\gamma_{s0,m_0}-\theta_r)} \sum_{n=0}^{m_r-1} i_{rn} e^{-jh\gamma_{r0,n}} \tag{3.30}$$

Let $\varphi_{s0,\,h} = \arg\left[c_h(W_{s0})\right]$, $\varphi_{r0,\,h} = \arg\left[c_h(W_{r0})\right]$ and $\varphi_h = \varphi_{s0,\,h} - \varphi_{r0,\,h}$.

$$c_h(W_{sm_0}) c_{-h}(B) = \frac{\mu_0}{\delta_0} |c_h(W_{s0})|^2 e^{jh\gamma_{s0,m_0}} \sum_{m=0}^{m_s-1} i_{sm} e^{-jh\gamma_{s0,m}}$$

$$+ \frac{\mu_0}{\delta_0} |c_h(W_{s0})||c_h(W_{r0})| e^{jh(\gamma_{s0,m_0}-\theta_r)} e^{j\varphi_h} \sum_{n=0}^{m_r-1} i_{rn} e^{-jh\gamma_{r0,n}}$$

As a consequence:

$$\mathfrak{Re}[c_h(W_{sm_0}) c_{-h}(B)] = \frac{\mu_0}{\delta_0} |c_h(W_{s0})|^2 \mathfrak{Re}\left[e^{jh\gamma_{s0,m_0}} \sum_{m=0}^{m_s-1} i_{sm} e^{-jh\gamma_{s0,m}}\right]$$

$$+ \frac{\mu_0}{\delta_0} |c_h(W_{s0})||c_h(W_{r0})| \mathfrak{Re}\left[e^{j\left[h(\gamma_{s0,m_0}-\theta_r)+\varphi_h\right]} \sum_{n=0}^{m_r-1} i_{rn} e^{-jh\gamma_{r0,n}}\right]$$

where

$$\mathfrak{Re}\left[e^{jh\gamma_{s0,m_0}} \sum_{m=0}^{m_s-1} i_{sm} e^{-jh\gamma_{s0,m}}\right] = \cos(h\gamma_{s0,m_0}) \sum_{m=0}^{m_s-1} i_{sm} \cos(h\gamma_{s0,m}) + \sin(h\gamma_{s0,m_0}) \sum_{m=0}^{m_s-1} i_{sm} \sin(h\gamma_{s0,m})$$

$$= \begin{bmatrix} \cos(h\gamma_{s0,m_0}) \\ \\ \sin(h\gamma_{s0,m_0}) \end{bmatrix}^\top \begin{bmatrix} \sum_{m=0}^{m_s-1} i_{sm} \cos(h\gamma_{s0,m}) \\ \sum_{m=0}^{m_s-1} i_{sm} \sin(h\gamma_{s0,m}) \end{bmatrix}$$

and

$$\mathfrak{Re}\left[e^{j\left[h(\gamma_{s0,m_0}-\theta_r)+\varphi_h\right]} \sum_{n=0}^{m_r-1} i_{rn} e^{-jh\gamma_{r0,n}}\right]$$

$$= \cos[h(\gamma_{s0,m_0} - \theta_r) + \varphi_h] \sum_{n=0}^{m_r-1} i_{rn} \cos(h\gamma_{r0,n}) + \sin[h(\gamma_{s0,m_0} - \theta_r) + \varphi_h] \sum_{n=0}^{m_r-1} i_{rn} \sin(h\gamma_{r0,n})$$

$$= \left[\begin{bmatrix} \cos(\varphi_h - h\theta_r) & \sin(\varphi_h - h\theta_r) \\ \\ \sin(\varphi_h - h\theta_r) & \cos(\varphi_h - h\theta_r) \end{bmatrix} \begin{bmatrix} \cos(h\gamma_{s0,m_0}) \\ \\ \sin(h\gamma_{s0,m_0}) \end{bmatrix}\right]^\top \begin{bmatrix} \sum_{n=0}^{m_r-1} i_{rn} \cos(h\gamma_{r0,n}) \\ \sum_{n=0}^{m_r-1} i_{rn} \sin(h\gamma_{r0,n}) \end{bmatrix}$$

We define the subsequent matrices:

$$\widetilde{\mathbf{T}}_{\mathbf{Cs\,h}} = \begin{bmatrix} 1 & \cdots & \cos(h\gamma_{s0,m}) & \cdots & \cos(h\gamma_{s0,m_s-1}) \\ 0 & \cdots & \sin(h\gamma_{s0,m}) & \cdots & \sin(h\gamma_{s0,m_s-1}) \end{bmatrix} \tag{3.31a}$$

$$\widetilde{\mathbf{T}}_{\mathbf{Cr\,h}} = \begin{bmatrix} 1 & \cdots & \cos(h\gamma_{r0,n}) & \cdots & \cos(h\gamma_{r0,m_r-1}) \\ 0 & \cdots & \sin(h\gamma_{r0,n}) & \cdots & \sin(h\gamma_{r0,m_r-1}) \end{bmatrix} \tag{3.31b}$$

$$\forall \varphi \in \mathbb{R},\ \mathbf{T}(\varphi) = \begin{bmatrix} \cos\varphi & -\sin\varphi \\ \sin\varphi & \cos\varphi \end{bmatrix} \tag{3.31c}$$

This enables us to express $\widetilde{\psi}_{sm_0,\,h}$ using the stator and rotor current vectors, $\vec{i}_s$ and $\vec{i}_r$:

$$\widetilde{\psi}_{sm_0,\,h} = 4\pi r l \frac{\mu_0}{\delta_0} |c_h(W_{s0})|^2 \begin{bmatrix} \cos(h\gamma_{s0,m_0}) \\ \\ \sin(h\gamma_{s0,m_0}) \end{bmatrix}^\top \widetilde{\mathbf{T}}_{\mathbf{Cs\,h}} \vec{i}_s$$

$$+ 4\pi r l \frac{\mu_0}{\delta_0} |c_h(W_{s0})||c_h(W_{r0})| \begin{bmatrix} \cos(h\gamma_{s0,m_0}) \\ \\ \sin(h\gamma_{s0,m_0}) \end{bmatrix}^\top \mathbf{T}(h\theta_r - \varphi_h) \widetilde{\mathbf{T}}_{\mathbf{Cr\,h}} \vec{i}_r \tag{3.32}$$

At this stage, it is convenient to introduce the stator and rotor main inductances as well as the coupling inductance between stator and rotor circuits for the wavelength of order h, $\widetilde{L}_{s,\,h}$, $\widetilde{L}_{r,\,h}$ and $L_{M,\,h}$:

$$\widetilde{L}_{s,\,h} = 4\pi r l \frac{\mu_0}{\delta_0} |c_h(W_{s0})|^2 \tag{3.33a}$$

$$\widetilde{L}_{r,\,h} = 4\pi r l \frac{\mu_0}{\delta_0} |c_h(W_{r0})|^2 \tag{3.33b}$$

$$L_{M,\,h} = 4\pi r l \frac{\mu_0}{\delta_0} |c_h(W_{s0})||c_h(W_{r0})| \tag{3.33c}$$

Using these notations, the expression of the main flux through stator circuit m_0 arising from the wavelength of order h becomes:

$$\widetilde{\psi}_{sm_0,\,h} = \begin{bmatrix} \cos(h\gamma_{s0,m_0}) \\ \\ \sin(h\gamma_{s0,m_0}) \end{bmatrix}^\top \left[\widetilde{L}_{s,\,h} \widetilde{\mathbf{T}}_{\mathbf{Cs\,h}} \vec{i}_s + L_{M,\,h} \mathbf{T}(h\theta_r - \varphi_h) \widetilde{\mathbf{T}}_{\mathbf{Cr\,h}} \vec{i}_r \right] \tag{3.34}$$

The vector of stator main flux linkage for wavelength of order h,

$$\vec{\widetilde{\psi}}_{s,\,h} = \begin{bmatrix} \widetilde{\psi}_{s0,\,h} & \cdots & \widetilde{\psi}_{sm,\,h} & \cdots & \widetilde{\psi}_{sm_s-1,\,h} \end{bmatrix}^\top$$

results directly from eq. (3.34):

$$\begin{aligned} \vec{\widetilde{\psi}}_{s,\,h} &= \widetilde{\mathbf{T}}^\top_{\mathbf{Cs\,h}} \left[\widetilde{L}_{s,\,h} \widetilde{\mathbf{T}}_{\mathbf{Cs\,h}} \vec{i}_s + L_{M,\,h} \mathbf{T}(h\theta_r - \varphi_h) \widetilde{\mathbf{T}}_{\mathbf{Cr\,h}} \vec{i}_r \right] \\ &= \widetilde{L}_{s,\,h} \widetilde{\mathbf{T}}^\top_{\mathbf{Cs\,h}} \widetilde{\mathbf{T}}_{\mathbf{Cs\,h}} \vec{i}_s + L_{M,\,h} \widetilde{\mathbf{T}}^\top_{\mathbf{Cs\,h}} \mathbf{T}(h\theta_r - \varphi_h) \widetilde{\mathbf{T}}_{\mathbf{Cr\,h}} \vec{i}_r \end{aligned} \tag{3.35}$$

The main inductance matrix of the stator circuits, $\widetilde{\mathbf{L}}_{\mathbf{s\,h}}$, and the coupling inductance matrix between rotor and stator circuits, $\widetilde{\mathbf{L}}_{\mathbf{rs\,h}}(\theta_r)$, both associated with wavelength h, are defined as follows:

$$\widetilde{\mathbf{L}}_{\mathbf{s\,h}} = \widetilde{L}_{s,\,h} \widetilde{\mathbf{T}}^\top_{\mathbf{Cs\,h}} \widetilde{\mathbf{T}}_{\mathbf{Cs\,h}} \tag{3.36}$$

$$\widetilde{\mathbf{L}}_{\mathbf{rs\,h}}(\theta_r) = L_{M,\,h} \widetilde{\mathbf{T}}^\top_{\mathbf{Cs\,h}} \mathbf{T}(h\theta_r - \varphi_h) \widetilde{\mathbf{T}}_{\mathbf{Cr\,h}} \tag{3.37}$$

Using these notations,

$$\vec{\widetilde{\psi}}_{s,\,h} = \widetilde{\mathbf{L}}_{\mathbf{s\,h}} \vec{i}_s + \widetilde{\mathbf{L}}_{\mathbf{rs\,h}}(\theta_r) \vec{i}_r \tag{3.38}$$

Note that since $\widetilde{\mathbf{L}}_{\mathbf{s\,h}}$ is square and $\widetilde{\mathbf{L}}^\top_{\mathbf{s\,h}} = \widetilde{\mathbf{L}}_{\mathbf{s\,h}}$, $\widetilde{\mathbf{L}}_{\mathbf{s\,h}}$ is symmetric.

Flux through rotor circuits

The space harmonic of order h of the flux density distribution generates a flux through rotor circuit $n_0 \in [\![0,\, m_r - 1]\!]$ denoted $\widetilde{\psi}_{rn_0,\,h}$ and defined according to (3.8) as follows:

$$\widetilde{\psi}_{rn_0,\,h} = 4\pi r l \mathfrak{Re}\big[c_h(W_{rn_0}) c_{-h}(B')\big] \tag{3.39}$$

Following the same considerations as for stator circuits,

$$\begin{aligned} c_h(W_{rn_0}) c_{-h}(B') = \frac{\mu_0}{\delta_0} e^{jh\gamma_{r0,n_0}} c_h(W_{r0}) \Bigg[& \sum_{n=0}^{m_r-1} i_{rn} e^{-jh\gamma_{r0,n}} c_{-h}(W_{r0}) \\ & + e^{jh\theta_r} \sum_{m=0}^{m_s-1} i_{sm} e^{-jh\gamma_{s0,m}} c_{-h}(W_{s0}) \Bigg] \\ = \frac{\mu_0}{\delta_0} |c_h(W_{r0})|^2 & \sum_{n=0}^{m_r-1} i_{rn} e^{-jh(\gamma_{r0,n} - \gamma_{r0,n_0})} \\ + \frac{\mu_0}{\delta_0} |c_h(W_{r0})| |c_h(W_{s0})| e^{j\left[h(\gamma_{r0,n_0} + \theta_r) - \varphi_h\right]} & \sum_{m=0}^{m_s-1} i_{sm} e^{-jh\gamma_{s0,m}} \end{aligned} \tag{3.40}$$

As a result,

$$\begin{aligned} \widetilde{\psi}_{rn_0,\,h} = 4\pi r l \frac{\mu_0}{\delta_0} |c_h(W_{r0})|^2 & \begin{bmatrix} \cos(h\gamma_{r0,n_0}) \\ \\ \sin(h\gamma_{r0,n_0}) \end{bmatrix}^\top \widetilde{\mathbf{T}}_{\mathbf{Cr\,h}} \vec{i}_r \\ + 4\pi r l \frac{\mu_0}{\delta_0} |c_h(W_{r0})| |c_h(W_{s0})| & \begin{bmatrix} \cos(h\gamma_{s0,m_0}) \\ \\ \sin(h\gamma_{s0,m_0}) \end{bmatrix}^\top \mathbf{T}^\top(h\theta_r - \varphi_h) \widetilde{\mathbf{T}}_{\mathbf{Cs\,h}} \vec{i}_s \end{aligned} \tag{3.41}$$

The vector of rotor main flux linkage for wavelength of order h,

$$\vec{\widetilde{\psi}}_{r,\,h} = \begin{bmatrix} \widetilde{\psi}_{r0,\,h} & \cdots & \widetilde{\psi}_{rn,\,h} & \cdots & \widetilde{\psi}_{rm_r-1,\,h} \end{bmatrix}^\top$$

follows directly from eq. (3.41) and the definitions (3.33):

$$\begin{aligned} \vec{\widetilde{\psi}}_{r,\,h} &= \widetilde{\mathbf{T}}^\top_{\mathbf{Cr\,h}} \Big[\widetilde{L}_{r,\,h} \widetilde{\mathbf{T}}_{\mathbf{Cr\,h}} \vec{i}_r + L_{M,\,h} \mathbf{T}^\top(h\theta_r - \varphi_h) \widetilde{\mathbf{T}}_{\mathbf{Cs\,h}} \vec{i}_s \Big] \\ &= \widetilde{L}_{r,\,h} \widetilde{\mathbf{T}}^\top_{\mathbf{Cr\,h}} \widetilde{\mathbf{T}}_{\mathbf{Cr\,h}} \vec{i}_r + \widetilde{\mathbf{L}}^\top_{\mathbf{rs,\,h}}(\theta_r) \vec{i}_s \end{aligned} \tag{3.42}$$

Introducing the notations

$$\widetilde{\mathbf{L}}_{\mathbf{r\,h}} = \widetilde{L}_{r,\,h} \widetilde{\mathbf{T}}^\top_{\mathbf{Cr\,h}} \widetilde{\mathbf{T}}_{\mathbf{Cr\,h}} \tag{3.43}$$

$$\widetilde{\mathbf{L}}_{\mathbf{sr\,h}}(\theta_r) = \widetilde{\mathbf{L}}^\top_{\mathbf{rs,\,h}}(\theta_r) \tag{3.44}$$

provides a compact expression for the vector of rotor main flux linkage arising from wavelength h:

$$\vec{\widetilde{\psi}}_{r,\,h} = \widetilde{\mathbf{L}}_{\mathbf{r\,h}} \vec{i}_r + \widetilde{\mathbf{L}}_{\mathbf{sr\,h}}(\theta_r) \vec{i}_s \tag{3.45}$$

Inductance matrix associated with a specific wavelength

Depending on the context, it might be useful to merge eq. (3.38) and (3.45) together and define the vector of main flux linkage associated with wavelength h,

$$\vec{\tilde{\Psi}}_h = \begin{bmatrix} \vec{\tilde{\psi}}_{s,h}^{\top} & \vec{\tilde{\psi}}_{r,h}^{\top} \end{bmatrix}^{\top}$$

$\vec{\tilde{\Psi}}_h$ is determined using the current vector $\vec{i} = \begin{bmatrix} \vec{i}_s^{\top} & \vec{i}_r^{\top} \end{bmatrix}^{\top}$ by means of the following relation:

$$\vec{\tilde{\Psi}}_h = \begin{bmatrix} \vec{\tilde{\psi}}_{s,h} \\ \vec{\tilde{\psi}}_{r,h} \end{bmatrix} = \begin{bmatrix} \widetilde{\mathbf{L}}_{\mathbf{s\,h}} & \widetilde{\mathbf{L}}_{\mathbf{rs\,h}}(\theta_r) \\ \widetilde{\mathbf{L}}_{\mathbf{sr\,h}}(\theta_r) & \widetilde{\mathbf{L}}_{\mathbf{r\,h}} \end{bmatrix} \begin{bmatrix} \vec{i}_s \\ \vec{i}_r \end{bmatrix} = \widetilde{\mathbf{L}}_{\mathbf{h}}(\theta_r)\vec{i} \tag{3.46}$$

The matrix $\widetilde{\mathbf{L}}_{\mathbf{h}}(\theta_r)$ introduced in eq. (3.46) links the currents with the main harmonic fluxes generated by wavelength h.

Proposition 4: Properties of the matrix $\widetilde{\mathbf{L}}_{\mathbf{h}}(\theta_r)$

1.) $\widetilde{\mathbf{L}}_{\mathbf{h}}(\theta_r)$ *is symmetric*

2.) $\widetilde{\mathbf{L}}_{\mathbf{h}}(\theta_r)$ *is positive semidefinite*

Refer to page 142 for the proof.

3.4.5 Total flux linkage

Using the relations gained in the previous sections, the vector of total *main* flux linkage

$$\vec{\tilde{\Psi}} = \begin{bmatrix} \widetilde{\psi}_{s0} & \cdots & \widetilde{\psi}_{sm} & \cdots & \widetilde{\psi}_{sm_s-1} & \widetilde{\psi}_{r0} & \cdots & \widetilde{\psi}_{rn} & \cdots & \widetilde{\psi}_{rm_r-1} \end{bmatrix}^{\top}$$

can be expressed as a function of the current vector $\vec{i}$ as follows:

$$\vec{\tilde{\Psi}} = \sum_{h\in\mathbb{N}^\star} \vec{\tilde{\Psi}}_h = \sum_{h\in\mathbb{N}^\star} \widetilde{\mathbf{L}}_{\mathbf{h}}(\theta_r)\vec{i} = \left[\sum_{h\in\mathbb{N}^\star} \widetilde{\mathbf{L}}_{\mathbf{h}}(\theta_r)\right]\vec{i} \tag{3.47}$$

Eq. (3.47) enables us to define a total *main* inductance matrix, $\widetilde{\mathbf{L}}(\theta_r)$:

$$\widetilde{\mathbf{L}}(\theta_r) = \begin{bmatrix} \widetilde{\mathbf{L}}_{\mathbf{s}} & \widetilde{\mathbf{L}}_{\mathbf{rs}}(\theta_r) \\ \widetilde{\mathbf{L}}_{\mathbf{sr}}(\theta_r) & \widetilde{\mathbf{L}}_{\mathbf{r}} \end{bmatrix} = \sum_{h\in\mathbb{N}^\star} \widetilde{\mathbf{L}}_{\mathbf{h}}(\theta_r) = \begin{bmatrix} \sum\limits_{h\in\mathbb{N}^\star} \widetilde{\mathbf{L}}_{\mathbf{s\,h}} & \sum\limits_{h\in\mathbb{N}^\star} \widetilde{\mathbf{L}}_{\mathbf{rs\,h}}(\theta_r) \\ \sum\limits_{h\in\mathbb{N}^\star} \widetilde{\mathbf{L}}_{\mathbf{sr\,h}}(\theta_r) & \sum\limits_{h\in\mathbb{N}^\star} \widetilde{\mathbf{L}}_{\mathbf{r\,h}} \end{bmatrix} \tag{3.48}$$

Proposition 5: Properties of the matrix $\widetilde{\mathbf{L}}(\theta_r)$

1.) $\widetilde{\mathbf{L}}(\theta_r)$ *is symmetric*

2.) $\widetilde{\mathbf{L}}(\theta_r)$ *is positive semidefinite*

The symmetry of $\widetilde{\mathbf{L}}(\theta_r)$ results from its definition. The positive semidefiniteness is gained from proposition 4 and the convergence of the sum in (3.48), while making use of the fact that the sum of positive semidefinite matrices is also positive semidefinite.

Eq. (3.47) and (3.48) include the contributions to the flux linkage of all wavelengths present in the flux density distribution but do not consider magnetic leakage occurring in the stator and rotor circuits.

The leakage flux through stator circuit m is accounted for by adding a further contribution $\psi_{\sigma sm}$ to the main flux $\widetilde{\psi}_{sm}$, depending exclusively on the current i_{sm}. In the same manner, the leakage flux through rotor circuit n is denoted by $\psi_{\sigma rn}$ and depends only on the current i_{rn}.

Owing to the assumptions made in section 3.3, neither the magnetic state of the machine nor the rotor angle have an influence on the leakage flux. For this reason, we will make use of a single leakage inductance value, $L_{\sigma s}$, for all stator circuits. The same applies to the rotor circuits, for which we introduce the leakage inductance $L_{\sigma r}$. Upon these considerations, the leakage flux vector $\vec{\Psi}_\sigma$ results in:

$$\vec{\Psi}_\sigma = \begin{bmatrix} \psi_{\sigma s0} \\ \vdots \\ \psi_{\sigma s m_s - 1} \\ \psi_{\sigma r0} \\ \vdots \\ \psi_{\sigma r m_r - 1} \end{bmatrix} = \begin{bmatrix} L_{\sigma s} & & & & \\ & \ddots & & \mathbf{0} & \\ & & L_{\sigma s} & & \\ & & & L_{\sigma r} & \\ & \mathbf{0} & & & \ddots \\ & & & & L_{\sigma r} \end{bmatrix} \begin{bmatrix} i_{s0} \\ \vdots \\ i_{s m_s - 1} \\ i_{r0} \\ \vdots \\ i_{r m_r - 1} \end{bmatrix} = \begin{bmatrix} \mathbf{L_{\sigma s}} & \mathbf{0} \\ \mathbf{0} & \mathbf{L_{\sigma r}} \end{bmatrix} \begin{bmatrix} \vec{i}_s \\ \vec{i}_r \end{bmatrix} = \mathbf{L}_\sigma \vec{i} \tag{3.49}$$

The expression of the total flux linkage follows from (3.47) and (3.49):

$$\vec{\Psi}(\vec{i},\, \theta_r) = \sum_{h \in \mathbb{N}^\star} \vec{\widetilde{\Psi}}_h + \vec{\Psi}_\sigma = \widetilde{\mathbf{L}}(\theta_r)\vec{i} + \mathbf{L}_\sigma \vec{i} = \left[\widetilde{\mathbf{L}}(\theta_r) + \mathbf{L}_\sigma\right]\vec{i} \tag{3.50}$$

The *total* inductance matrix, $\mathbf{L}(\theta_r)$, is computed as the sum of the *main* and the *leakage* inductance matrices:

$$\mathbf{L}(\theta_r) = \begin{bmatrix} \mathbf{L_s} & \mathbf{L_{rs}}(\theta_r) \\ \mathbf{L_{sr}}(\theta_r) & \mathbf{L_r} \end{bmatrix} = \begin{bmatrix} \widetilde{\mathbf{L}}_\mathbf{s} + \mathbf{L_{\sigma s}} & \widetilde{\mathbf{L}}_\mathbf{rs}(\theta_r) \\ \widetilde{\mathbf{L}}_\mathbf{sr}(\theta_r) & \widetilde{\mathbf{L}}_\mathbf{r} + \mathbf{L_{\sigma s}} \end{bmatrix} \tag{3.51}$$

We had already established in chapter 2 that $\mathbf{L}(\theta_r)$ must be symmetric positive definite for physical reasons. This property is verified in the present case as $\mathbf{L}(\theta_r)$ is the sum of a positive semidefinite main inductance matrix and a diagonal leakage inductance matrix with positive diagonal entries.

The expression of $\widetilde{\mathbf{L}}(\theta_r)$ according to (3.48) is of theoretical nature as it involves infinite sums and can therefore not be computed in real-time on a digital controller. For this reason, it is necessary to approximate $\widetilde{\mathbf{L}}(\theta_r)$ by means of a partial sum, i.e. to consider only a *finite* number of wavelengths in the conductor distribution functions and the air-gap field density distribution. This is generally not a limiting factor as the magnitude of the Fourier coefficients of W_{s0} and W_{r0} decreases rapidly with the wavelength order h [61]. As we will see for the machines IM1 and IM2, very few space harmonics need to be taken into consideration to fairly account for the time harmonics they give rise to in current and torque waveforms.

Based on these observations, we introduce the *finite* set of considered wavelength orders $\mathcal{H} \subset \mathbb{N}^\star$. In all simulations and test bench implementations, we will restrict the sums appearing in (3.48) and (3.50) to the subset $\mathcal{H}$ and compute the following approximation of $\vec{\Psi}$:

$$\vec{\Psi}_\mathcal{H}(\vec{i},\, \theta_r) = \sum_{h \in \mathcal{H}} \vec{\widetilde{\Psi}}_h + \vec{\Psi}_\sigma = \widetilde{\mathbf{L}}_\mathcal{H}(\theta_r)\vec{i} + \mathbf{L}_\sigma \vec{i} = \left[\widetilde{\mathbf{L}}_\mathcal{H}(\theta_r) + \mathbf{L}_\sigma\right]\vec{i} = \mathbf{L}_\mathcal{H}(\theta_r)\vec{i} \tag{3.52}$$

The approximation of the total inductance matrix used in (3.52), $\mathbf{L}_\mathcal{H}(\theta_r)$, remains symmetric positive definite.

We have worked out a simple relation between the current and flux linkage vectors accounting for the presence of conductor distribution harmonics under the assumption of a constant air-gap length and

linear magnetic behaviour. Together with the voltage and torque equations obtained in chapter 2, this will enable us to establish a real-time compliant state-space model of induction machines which includes the effect of conductor distribution harmonics.

3.5 Voltage and torque equations in presence of interconnected circuits

Combining the specific flux linkage expression (3.50) with the general relations set up in chapter 2, we obtain the following voltage equation for the model including conductor distribution harmonics and taking into account circuit interconnections:

$$\begin{aligned}\vec{u}' &= \mathbf{R}'\vec{i}' + \frac{\mathrm{d}\vec{\Psi}'}{\mathrm{d}t} = \mathbf{R}'\vec{i}' + \frac{\mathrm{d}\left[\mathbf{C}^\top\vec{\Psi}\right]}{\mathrm{d}t} = \mathbf{R}'\vec{i}' + \frac{\mathrm{d}\left[\mathbf{C}^\top\mathbf{L}(\theta_r)\mathbf{C}\vec{i}'\right]}{\mathrm{d}t} \\ &= \mathbf{R}'\vec{i}' + \mathbf{C}^\top\mathbf{L}(\theta_r)\mathbf{C}\frac{\mathrm{d}\vec{i}'}{\mathrm{d}t} + \omega_r\frac{\partial\left[\mathbf{C}^\top\mathbf{L}(\theta_r)\mathbf{C}\right]}{\partial\theta_r}\vec{i}'\end{aligned} \tag{3.53}$$

In accordance with definition (2.39), we introduce the *total* inductance matrix for the model with interconnections as:

$$\begin{aligned}\mathbf{L}'(\theta_r) &= \mathbf{C}^\top\mathbf{L}(\theta_r)\mathbf{C} \\ &= \begin{bmatrix}\mathbf{L}'_{\mathbf{s}} & \mathbf{L}'_{\mathbf{rs}}(\theta_r)\\ \mathbf{L}'_{\mathbf{sr}}(\theta_r) & \mathbf{L}'_{\mathbf{r}}\end{bmatrix} = \begin{bmatrix}\mathbf{C}_{\mathbf{s}}^\top\mathbf{L}_{\mathbf{s}}\mathbf{C}_{\mathbf{s}} & \mathbf{C}_{\mathbf{s}}^\top\mathbf{L}_{\mathbf{rs}}(\theta_r)\mathbf{C}_{\mathbf{r}}\\ \mathbf{C}_{\mathbf{r}}^\top\mathbf{L}_{\mathbf{sr}}(\theta_r)\mathbf{C}_{\mathbf{s}} & \mathbf{C}_{\mathbf{r}}^\top\mathbf{L}_{\mathbf{r}}\mathbf{C}_{\mathbf{r}}\end{bmatrix}\end{aligned} \tag{3.54}$$

The dimension of $\mathbf{L}'(\theta_r)$ is $m' \times m'$. The voltage equation (3.53) simplifies into:

$$\vec{u}' = \mathbf{R}'\vec{i}' + \mathbf{L}'(\theta_r)\frac{\mathrm{d}\vec{i}'}{\mathrm{d}t} + \omega_r\frac{\partial\mathbf{L}'(\theta_r)}{\partial\theta_r}\vec{i}' \tag{3.55}$$

Substituting the expression of the flux linkage (3.50) into the torque relation (2.36) results in:

$$M_M = \frac{1}{2}\vec{i}'^\top\frac{\partial\left[\mathbf{C}^\top\mathbf{L}(\theta_r)\mathbf{C}\vec{i}'\right]}{\partial\theta_r} = \frac{1}{2}\vec{i}'^\top\frac{\partial\mathbf{L}'(\theta_r)}{\partial\theta_r}\vec{i}' \tag{3.56}$$

Since the leakage flux is considered independent of the rotor angle, (3.56) is equivalent to:

$$M_M = \frac{1}{2}\vec{i}'^\top\frac{\partial\left[\mathbf{C}^\top\widetilde{\mathbf{L}}(\theta_r)\mathbf{C}\right]}{\partial\theta_r}\vec{i}' = \frac{1}{2}\vec{i}'^\top\frac{\partial\widetilde{\mathbf{L}}'(\theta_r)}{\partial\theta_r}\vec{i}' \tag{3.57}$$

where

$$\widetilde{\mathbf{L}}'(\theta_r) = \mathbf{C}^\top\widetilde{\mathbf{L}}(\theta_r)\mathbf{C} = \begin{bmatrix}\widetilde{\mathbf{L}}'_{\mathbf{s}} & \widetilde{\mathbf{L}}'_{\mathbf{rs}}(\theta_r)\\ \widetilde{\mathbf{L}}'_{\mathbf{sr}}(\theta_r) & \widetilde{\mathbf{L}}'_{\mathbf{r}}\end{bmatrix} = \begin{bmatrix}\mathbf{C}_{\mathbf{s}}^\top\widetilde{\mathbf{L}}'_{\mathbf{s}}\mathbf{C}_{\mathbf{s}} & \mathbf{C}_{\mathbf{s}}^\top\widetilde{\mathbf{L}}'_{\mathbf{rs}}(\theta_r)\mathbf{C}_{\mathbf{r}}\\ \mathbf{C}_{\mathbf{r}}^\top\widetilde{\mathbf{L}}'_{\mathbf{sr}}(\theta_r)\mathbf{C}_{\mathbf{s}} & \mathbf{C}_{\mathbf{r}}^\top\widetilde{\mathbf{L}}'_{\mathbf{r}}\mathbf{C}_{\mathbf{r}}\end{bmatrix} \tag{3.58}$$

is the *main* inductance matrix of the model with interconnected circuits.

Proposition 6:

1.) *For* $h \in \mathbb{N}^\star$, $\widetilde{\mathbf{L}}'_{\mathbf{h}}(\theta_r) = \mathbf{C}^\top\widetilde{\mathbf{L}}_{\mathbf{h}}(\theta_{\mathbf{r}})\mathbf{C}$ *is symmetric positive semidefinite.*

2.) $\widetilde{\mathbf{L}}'(\theta_r)$ *is positive semidefinite.*

3.) $\mathbf{L}'(\theta_r)$ *is positive definite.*

Refer to page 143 for the proof.

Depending on the context, it might be practical to use separate voltage equations for stator and rotor quantities as follows:

$$\begin{cases} \text{stator voltage:} & \vec{u}'_s = \mathbf{R}'_\mathbf{s}\vec{i}'_s + \mathbf{L}'_\mathbf{s}\dfrac{\mathrm{d}\vec{i}'_s}{\mathrm{d}t} + \mathbf{L}'_\mathbf{rs}(\theta_r)\dfrac{\mathrm{d}\vec{i}'_r}{\mathrm{d}t} + \dfrac{\partial \mathbf{L}'_\mathbf{rs}(\theta_r)}{\partial\theta_r}\vec{i}'_r & (3.59a) \\ \text{rotor voltage:} & \vec{u}'_r = \mathbf{R}'_\mathbf{r}\vec{i}'_r + \mathbf{L}'_\mathbf{r}\dfrac{\mathrm{d}\vec{i}'_r}{\mathrm{d}t} + \mathbf{L}'_\mathbf{sr}(\theta_r)\dfrac{\mathrm{d}\vec{i}'_s}{\mathrm{d}t} + \dfrac{\partial \mathbf{L}'_\mathbf{sr}(\theta_r)}{\partial\theta_r}\vec{i}'_s & (3.59b) \end{cases}$$

In this case, the torque relation becomes:

$$\begin{aligned} M_M &= \frac{1}{2}\begin{bmatrix}\vec{i}'^{\top}_s & \vec{i}'^{\top}_r\end{bmatrix}^{\top}\begin{bmatrix}\mathbf{0} & \dfrac{\partial\widetilde{\mathbf{L}}'_\mathbf{rs}(\theta_r)}{\partial\theta_r} \\ \dfrac{\partial\widetilde{\mathbf{L}}'_\mathbf{sr}(\theta_r)}{\partial\theta_r} & \mathbf{0}\end{bmatrix}\begin{bmatrix}\vec{i}'_s \\ \vec{i}'_r\end{bmatrix} \\ &= \frac{1}{2}\vec{i}'^{\top}_s\frac{\partial\widetilde{\mathbf{L}}'_\mathbf{rs}(\theta_r)}{\partial\theta_r}\vec{i}'_r + \frac{1}{2}\vec{i}'^{\top}_r\frac{\partial\widetilde{\mathbf{L}}'_\mathbf{sr}(\theta_r)}{\partial\theta_r}\vec{i}'_s = \frac{1}{2}\vec{i}'^{\top}_s\frac{\partial\widetilde{\mathbf{L}}'_\mathbf{rs}(\theta_r)}{\partial\theta_r}\vec{i}'_r + \frac{1}{2}\vec{i}'^{\top}_r\frac{\partial\widetilde{\mathbf{L}}'^{\top}_\mathbf{rs}(\theta_r)}{\partial\theta_r}\vec{i}'_s \\ &= \frac{1}{2}\vec{i}'^{\top}_s\frac{\partial\widetilde{\mathbf{L}}'_\mathbf{rs}(\theta_r)}{\partial\theta_r}\vec{i}'_r + \frac{1}{2}\left[\vec{i}'^{\top}_s\frac{\partial\widetilde{\mathbf{L}}'_\mathbf{rs}(\theta_r)}{\partial\theta_r}\vec{i}'_r\right]^{\top} \\ &= \vec{i}'^{\top}_s\frac{\partial\widetilde{\mathbf{L}}'_\mathbf{rs}(\theta_r)}{\partial\theta_r}\vec{i}'_r \end{aligned} \tag{3.60}$$

3.6 Continuous-time state-space machine model

Relations (3.55), (3.56) and (2.19) enable us to build a continuous-time state-space model of the induction machine which includes the effect of conductor distribution harmonics. Using the currents alongside the rotor angular velocity and the rotor angle as state variables leads to the subsequent set of equations:

$$\begin{cases} \dfrac{\mathrm{d}\vec{i}'}{\mathrm{d}t} = -\mathbf{L}'^{-1}(\theta_r)\left[\mathbf{R}' + \omega_r\dfrac{\partial\mathbf{L}'(\theta_r)}{\partial\theta_r}\right]\vec{i}' + \mathbf{L}'^{-1}(\theta_r)\vec{u}' & (3.61a) \\ \dfrac{\mathrm{d}\omega_r}{\mathrm{d}t} = \dfrac{1}{J_M}\left[\dfrac{1}{2}\vec{i}'^{\top}\dfrac{\partial\mathbf{L}'(\theta_r)}{\partial\theta_r}\vec{i}' - M_L - C_W\omega_r\right] & (3.61b) \\ \dfrac{\mathrm{d}\theta_r}{\mathrm{d}t} = \omega_r & (3.61c) \end{cases}$$

Introducing the notations

$$\mathbf{A}(\omega_r,\,\theta_r) = -\mathbf{L}'^{-1}(\theta_r)\left[\mathbf{R}' + \omega_r\frac{\partial\mathbf{L}'(\theta_r)}{\partial\theta_r}\right]; \qquad \mathbf{B}(\theta_r) = \mathbf{L}'^{-1}(\theta_r)$$

(3.61) becomes:

$$\begin{cases} \dfrac{\mathrm{d}\vec{i}'}{\mathrm{d}t} = \mathbf{A}(\omega_r,\, \theta_r)\vec{i}' + \mathbf{B}(\theta_r)\vec{u}' & \text{(3.62a)} \\ \dfrac{\mathrm{d}\omega_r}{\mathrm{d}t} = \dfrac{1}{J_M}\left[\dfrac{1}{2}\vec{i}'^{\top}\dfrac{\partial \mathbf{B}^{-1}(\theta_r)}{\partial \theta_r}\vec{i}' - M_L - C_W\omega_r\right] & \text{(3.62b)} \\ \dfrac{\mathrm{d}\theta_r}{\mathrm{d}t} = \omega_r & \text{(3.62c)} \end{cases}$$

The above equations are of theoretical nature. The implementation of (3.62) on a digital controller requires the following additional steps:

1.) computation of the Fourier coefficients of the conductor distribution functions;

2.) determination of the wavelength orders to be considered in the model;

3.) sampling of the state-space equations (3.62) to obtain a discrete-time model representation.

These aspects are best discussed with practical examples. We will therefore work out specific models for the machines under investigation, IM1 and IM2, next.

3.7 Case study

3.7.1 Deriving specific models for the investigated machines

Representation of the stator windings as sets of electrical circuits

To obtain the model equations of a particular machine, we first determine a representation of the stator windings and the rotor cage using the concepts of *electrical circuit* and *interconnection matrix* introduced in chapter 2. As both IM1 and IM2 feature three star-connected windings on the stator and a rotor cage (cf. appendix A.1), we will apply the general method for modelling a star-connection of windings presented in section 2.3.3.

A straightforward option is to introduce an electrical circuit for each of the windings. This is the choice we already made in chapter 2 for IM1. Using the notations of section 2.3, the number of circuits m_s is then identical to the number of windings $w_s = 3$, which results in the following stator interconnection matrix for IM1:

$$\mathbf{C}_{\mathbf{s},\,\mathbf{IM1}} = \begin{bmatrix} 1 & 0 \\ 0 & 1 \\ -1 & -1 \end{bmatrix}$$

Consequently, the vector $\vec{i}'_s$ has $m'_s = 2$ components, i'_{s0} and i'_{s1}, representing independent stator currents. Similarly, the components of $\vec{u}'$, u'_{s0} and u'_{s1}, are the two independent line-to-line voltages depicted in fig. 3.3(a).

Although the same strategy could be used with the stator windings of IM2, which would lead to an interconnection matrix identical to the above one, we adopt a slightly different perspective to illustrate the flexibility of the method. As IM2 features two pole pairs, half of the coils belonging to a stator winding lies within a pole pair pitch, the rest within the other. For this reason, each winding is modelled as a set of two circuits connected in series, a circuit being composed of the winding coils within a specific pole pair. Following the schematic in fig. 3.3(b), circuit 0 represents the coils of

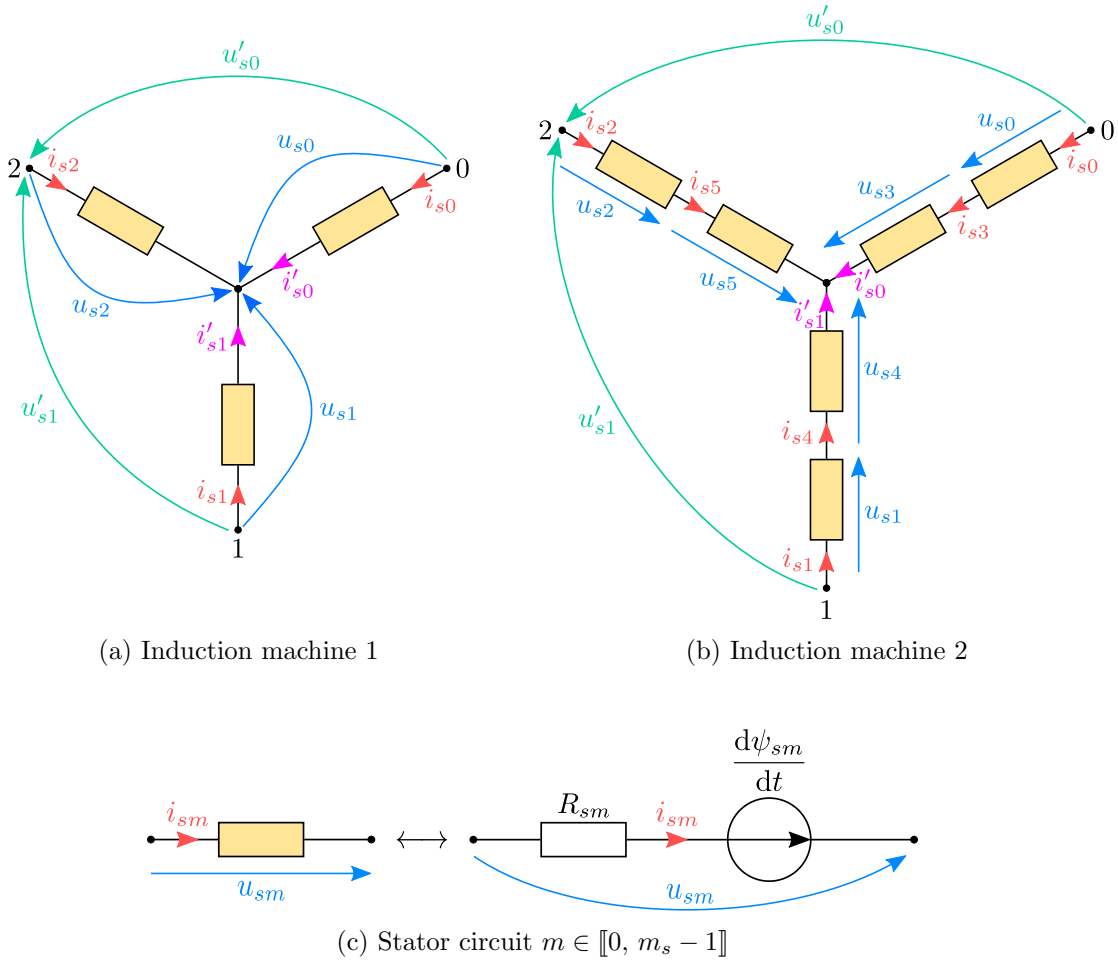

(a) Induction machine 1

(b) Induction machine 2

(c) Stator circuit $m \in [\![0,\, m_s - 1]\!]$

Figure 3.3: Schematics of the stator circuits used in the models of IM1 and IM2 and definition of corresponding electrical quantities

winding 0 within the first pole pair, circuit 3 the ones within the second. Hence, the series connection of circuit 0 and 3 in the model is equivalent to winding 0 in the real machine. The tremendous benefit resulting from the choice of the circuits according to fig. 3.3(b) will become apparent during the model optimization in chapter 4. Consequently, the model of IM2 includes $m_s = 6$ stator circuits and the stator interconnection matrix is defined as follows:

$$\mathbf{C_{s,\,IM2}} = \begin{bmatrix} 1 & 0 & -1 & 1 & 0 & -1 \\ 0 & 1 & -1 & 0 & 1 & -1 \end{bmatrix}^\top$$

Rotor circuits and rotor interconnection matrix

Owing to section 2.3.4, a rotor cage with N_r bars can be represented as a set of N_r coils, each of them having one turn and a pitch corresponding to the rotor slot pitch. In this context, it is convenient to introduce a specific circuit in the model for each rotor coil, the total number of rotor circuits being $m_r = N_r$. The currents flowing through the circuits and the voltages at their terminals constitute independent variables. Thus, the rotor interconnection matrix is simply the identity matrix of dimension m_r.

The underlying assumptions of the linear geometric model listed in section 3.3 imply that in fact only

$m_r - 1$ rotor currents are independent. Under these circumstances, the current in rotor circuit $m_r - 1$ can be expressed as a linear combination of the others. This leads to the rotor interconnection matrix becoming an $m_r \times (m_r - 1)$ matrix of the form:

$$\mathbf{C_r} = \begin{bmatrix} 1 & & 0 \\ & \ddots & \\ 0 & & 1 \\ -1 & \cdots & -1 \end{bmatrix}$$

The rotor interconnection matrix of IM1, $\mathbf{C_{r,IM1}}$, has $m_r = 16$ rows and $m'_r = 15$ columns while the one of IM2 possesses $m_r = 28$ rows and $m'_r = 27$ columns. The vector of independent rotor voltages $\vec{u}'_r$ (and the vector of independent rotor currents $\vec{i}'_r$) has therefore 15 components in the case IM1 and 27 in the case of IM2.

Order of the models

Following the above considerations, the total number of independent currents in the model of IM1, i.e. the components of the vector $\vec{i}'$, is $m'_s + m'_r = 17$. Taking into account the rotor angular velocity and angle, the number of state variables necessary to describe the dynamic behaviour of IM1 is 19. In contrast, 29 independent currents appear in the model of IM2, leading to 31 state variables in total.

These results show that the model complexity is directly impacted by the number of stator windings and rotor bars. Apart for machines with an integer number of bars per pole pair pitch, in which case it is common practice to use an equivalent model of reduced order by introducing an 'electrical angle', the model order cannot be further decreased.

Practical determination of the inductance matrix coefficients

Having chosen the electrical circuits in the model, their associated conductor distribution functions have to be derived from the winding configuration and rotor bar number of the machine. As explained in section 3.4, only the conductor distribution functions of stator and rotor circuit number 0, W_{s0} and W_{r0}, are necessary, since the remaining ones are shifted copies of W_{s0} and W_{r0} respectively. Note that the choice of the electrical circuits in the model has to ensure that this requirement is met (see section 3.4.1). The conductor distribution functions W_{s0} and W_{r0} of the machines IM1 and IM2 are provided in appendix A.1 alongside the related current density and MMF distribution functions.

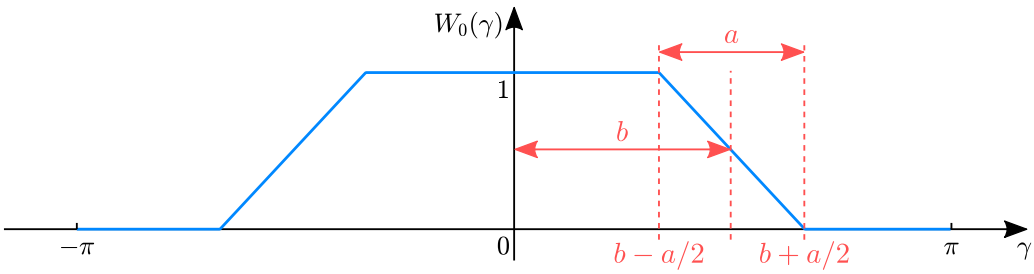

Figure 3.4: Basic function allowing for a straightforward computation of the Fourier coefficients of conductor distribution functions

The Fourier coefficients of W_{s0} and W_{r0} have to be calculated in order to determine the inductances associated with each wavelength order defined in (3.33). This potentially arduous task can be greatly simplified when considering W_{s0} and W_{r0} as linear combinations of shifted copies of the simple function W_0 depicted in fig. 3.4. The Fourier coefficients of W_0 are easily computed as functions of the

parameters a and b while the results in Proposition 1 enable us to infer the ones of W_{s0} and W_{r0} without difficulty. Note that this method provides general analytical expressions of the Fourier coefficients of W_{s0} and W_{r0} which can be adapted effortlessly to match a specific machine configuration. In addition, these expressions turn out to be instrumental when doing parameter tuning, as we will see in chapter 5.

The main inductance matrix for the wavelength of order $h \in \mathbb{N}^\star$ is calculated in accordance with (3.46) using the corresponding inductance values. This process involves the matrices $\widetilde{\mathbf{T}}_{\mathbf{Cs\,h}}$ and $\widetilde{\mathbf{T}}_{\mathbf{Cr\,h}}$ defined in (3.31a) and (3.31b) in which the angles $\gamma_{s0,m}$ and $\gamma_{r0,n}$ appear. $\gamma_{s0,m}$, $m \in [\![0,\, m_s - 1]\!]$ is the angle with which W_{s0} has to be shifted in order to obtain the conductor distribution function of stator circuit m. In the case of IM1, $\gamma_{s0,m} = m \cdot 2\pi/3$ while for IM2, $\gamma_{s0,m} = m \cdot \pi/3$. Similarly, $\gamma_{r0,n}$, $n \in [\![0,\, m_r - 1]\!]$, determines how W_{r0} has to be shifted to get the conductor distribution of rotor circuit n. $\gamma_{r0,n} = n \cdot 2\pi/16$ for IM1 and $\gamma_{r0,n} = n \cdot 2\pi/28$ for IM2.

The only remaining task to have all the information needed to calculate the coefficients of the total inductance matrix $\mathbf{L}_{\mathcal{H}}(\theta_r)$ is to select the wavelengths to consider in the model. This topic is discussed in the next section.

3.7.2 Selecting the wavelengths to be included in the model

An aspect of crucial practical importance which remains to be addressed concerns the choice of wavelengths accounted for in the model. A compromise must be found as a high number of terms in the flux linkage approximation (3.52) will result in a more accurate but slower model.

To gain insight into the matter, we will first examine the impact of the conductor distribution function spectral content on the stator current, torque and angular velocity waveforms obtained from the model. Fig. 3.5 shows the conductor distribution functions W_{s0} and W_{r0} of the two machines under investigation as well as their normalized Fourier spectra. The base wavelength order used for normalizing the Fourier coefficient amplitudes is selected according to the machine pole pair number, i.e. 1 for IM1 and 2 for IM2. As expected, the coefficient magnitude decreases rapidly with the wavelength order and drops below 1% of the base value for orders greater than 60.

The diagrams in fig. 3.6 illustrate the influence of the considered wavelengths on the shape of the conductor distribution functions W_{s0} and W_{r0}. The approximation including all wavelengths up to order 60 provides a fairly accurate representation of the actual conductor distribution functions. This observation is supported by the simulation results shown in Fig. 3.7, obtained with two variants of the state-space model (3.62) in the case of IM1: one with 60 wavelengths, the other with 500. The latter is considered as reference model given that the number of terms in the partial sum (3.52) is sufficiently high to correctly represent the actual conductor distribution function.

The simulations were performed using Heun's method and a step size $\delta t = 10^{-5}\,\mathrm{s}$. The two models were supplied with the same input quantities, i.e. balanced sinusoidal voltages and a rated load torque step applied at time $t = 0.5\,\mathrm{s}$. Hence, any discrepancy in the results generated by the two models can be regarded as approximation error originating from the neglect of wavelength orders. According to Fig. 3.7, the approximation error in the stator current, torque and angular velocity reaches its maximum in each case during the starting transient and slightly increases with the slip. This is likely to be linked to the increased weight of neglected space harmonics in the air-gap flux density distribution due to higher rotor currents. The steady-state error in all three quantities arises primarily from a small phase-lead while the amplitudes generated by the model with 60 wavelengths remain accurate. The overall error remains however rather insignificant, making the 60 wavelength model precise enough for most applications.

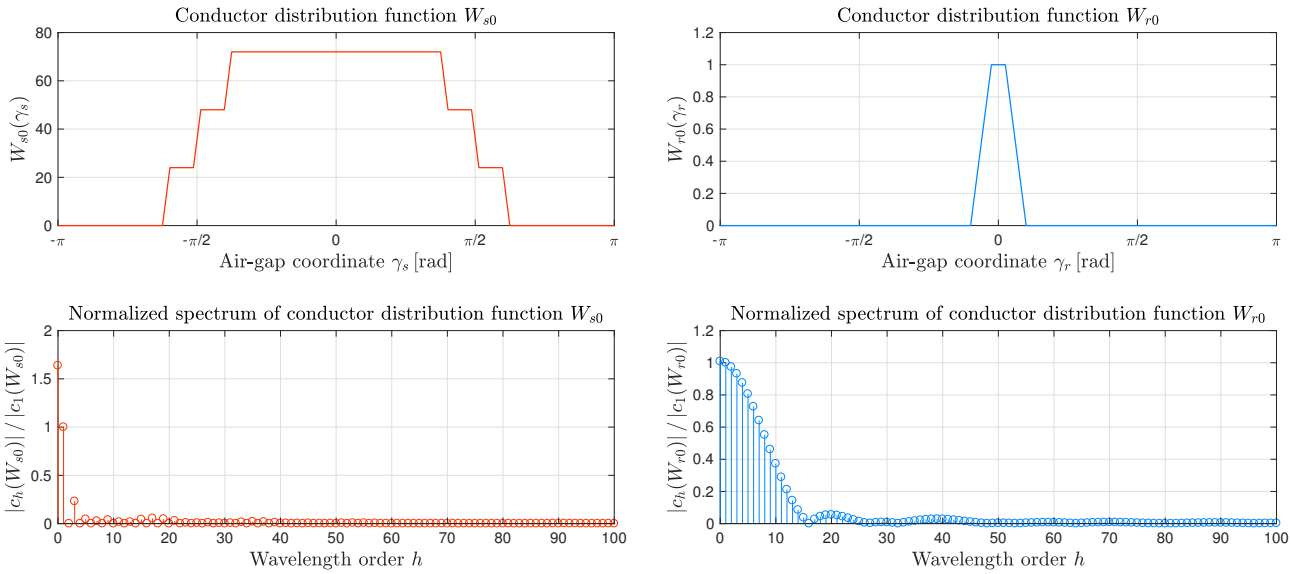

(a) Induction machine 1

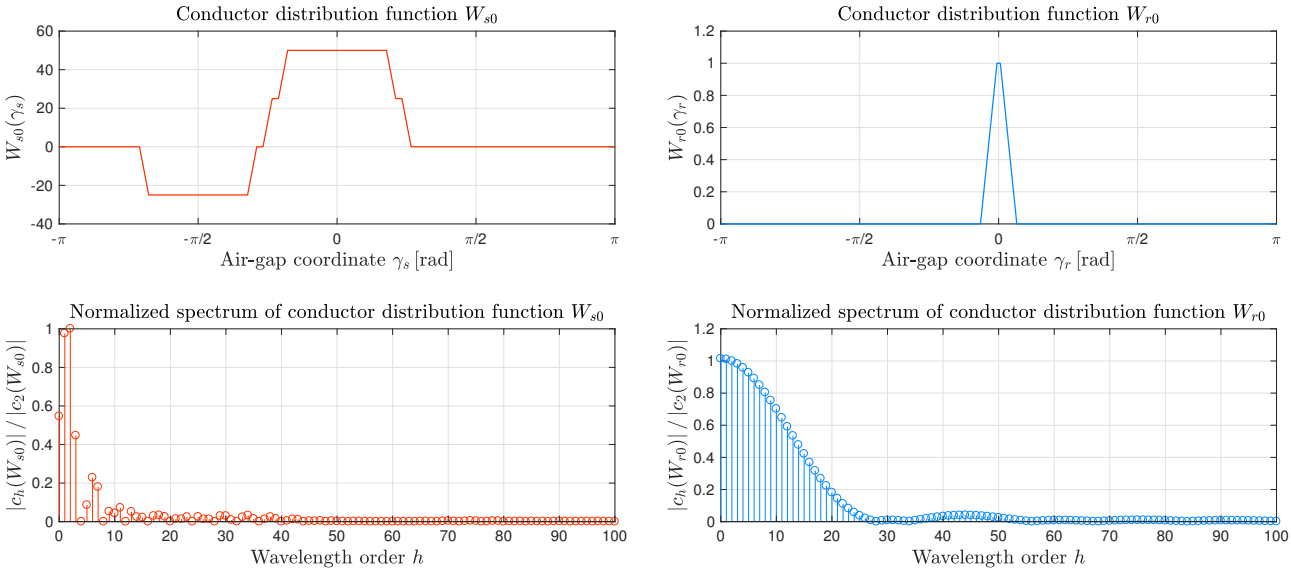

(b) Induction machine 2

Figure 3.5: Waveforms of conductor distribution functions W_{s0} and W_{r0} alongside their normalized spectra

Note that for both machines, W_{s0} does not exhibit even wavelength orders. Owing to the discussion in section 3.2, wavelengths of even order potentially present in other distributed quantities (e.g. W_{r0}) will not influence stator flux linkages and can therefore be ignored to lessen the computational effort.

We now examine a model with the minimal set of wavelength orders, $\mathcal{H}_m$, necessary to generate the principal slot harmonic (PSH) in the stator currents. In the case of IM1, $\mathcal{H}_m = \{1, 17\}$, while for IM2, $\mathcal{H}_m = \{2, 26\}$. The corresponding approximated conductor distribution functions are depicted in fig. 3.6.

A comparison of the stator current, torque and angular velocity waveforms with the 500 wavelength reference model under the conditions described above shows a notably larger error both during transi-

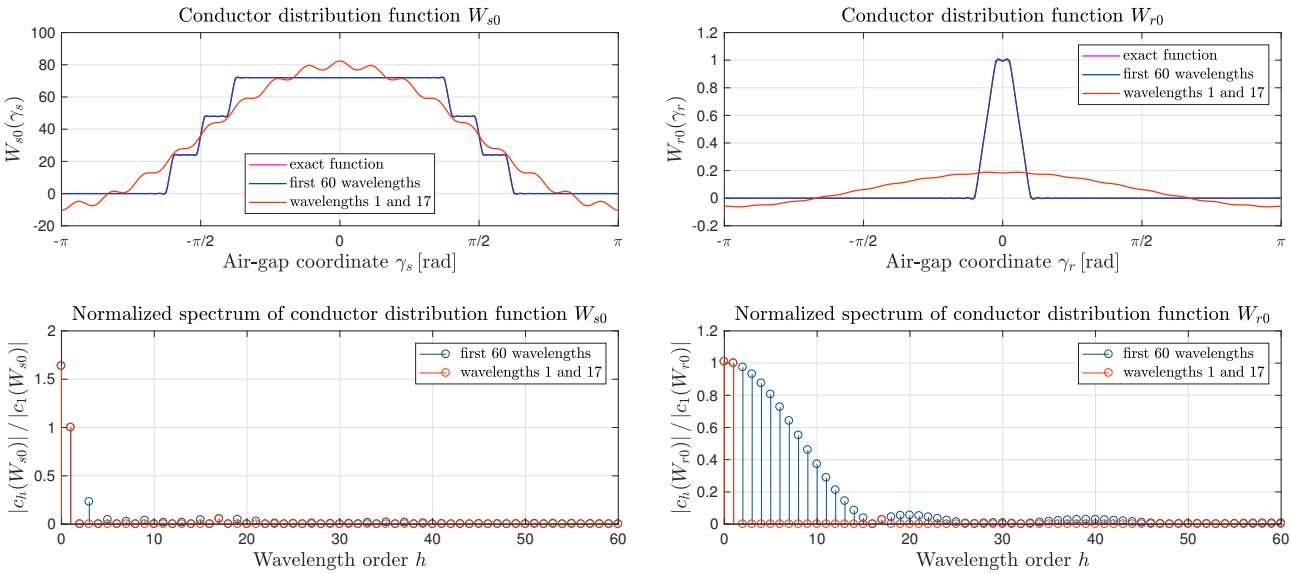

(a) Induction machine 1

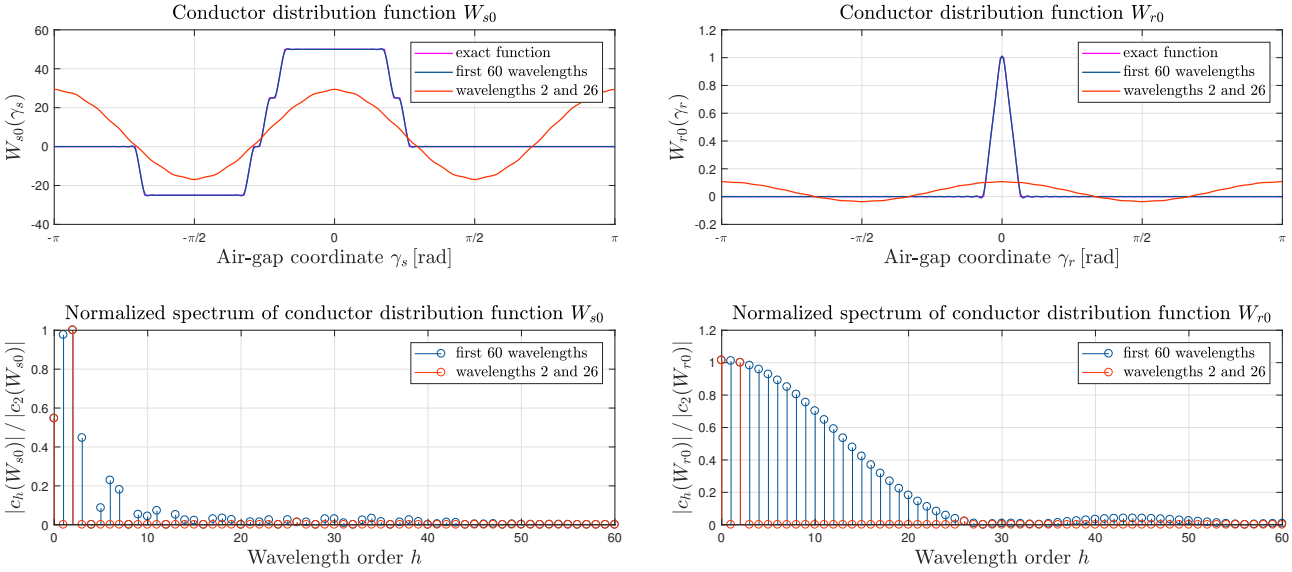

(b) Induction machine 2

Figure 3.6: Impact of the number of wavelength orders on the shape of the conductor distribution functions W_{s0} and W_{r0}

ents and in steady-state (see fig. 3.8). The steady-state error in current and torque is the combination of an incorrect estimation of phase and amplitude of the PSH, while the angular velocity error also shows the presence of an offset.

Notwithstanding these imprecisions, a model with only two space harmonics offers the advantage of being computationally particularly efficient and constitutes therefore the first choice for real-time applications, especially the ones involving model predictive control schemes. Depending on the context and requirements, additional wavelength orders can be added to improve the model accuracy. We will therefore narrow down our subsequent investigations to models with a handful of wavelength orders and examine the minimal models of IM1 and IM2 with two space harmonics extensively.

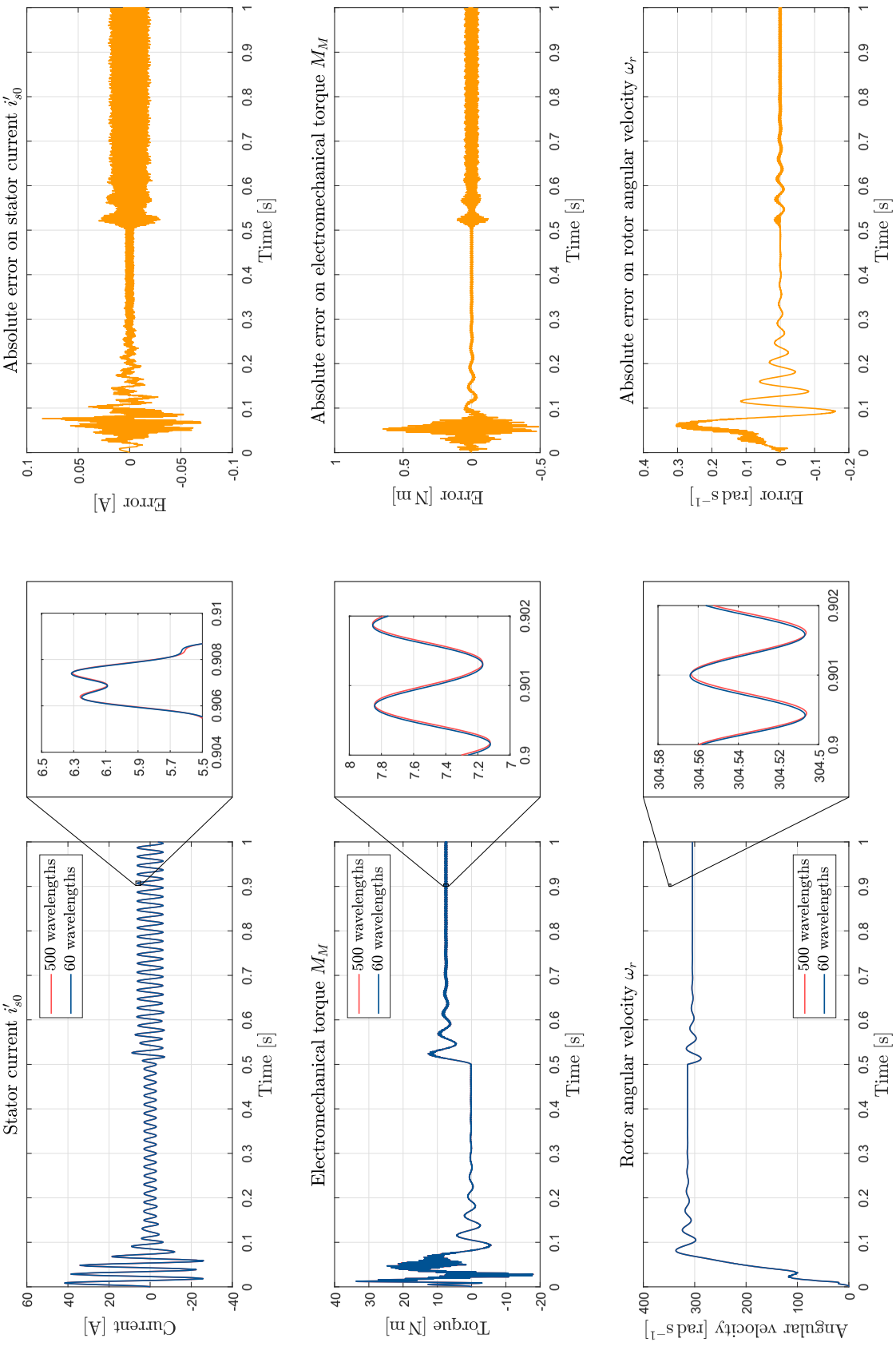

Figure 3.7: Comparison between two model variants of IM1, one including the first 60 wavelength orders, the other the first 500 (simulations with Heun's method, step size $\delta t = 10^{-5}$ s)

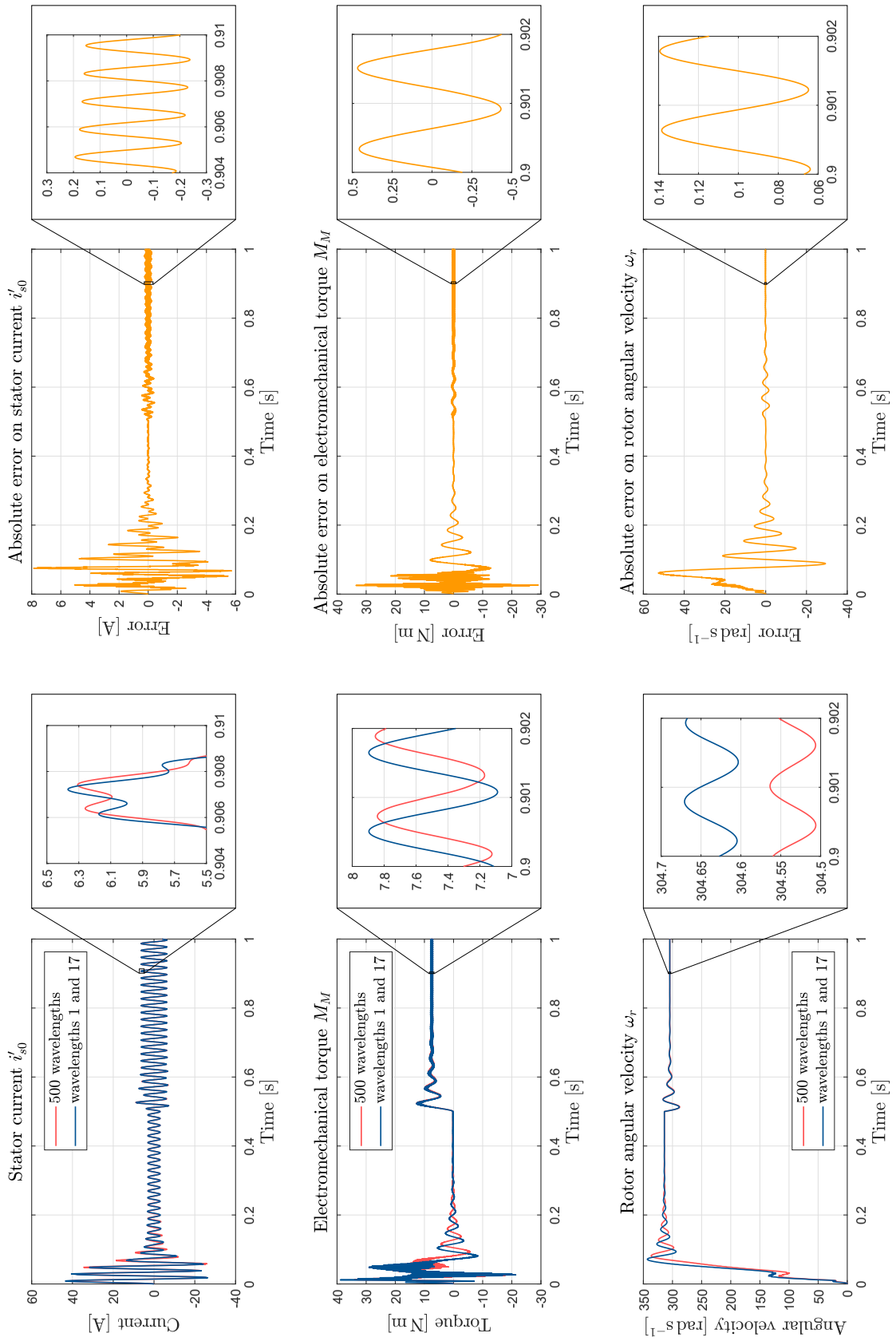

Figure 3.8: Comparison of the simulation waveforms generated by a model including wavelengths 1 and 17 with the ones of the 500 wavelength model

3.7.3 Determination of appropriate sampling methods

A discrete-time representation of the model (3.62), for which the total inductance matrix has been determined using a finite number of wavelength orders as explained previously, has to be found to enable its execution on a digital controller. The sampling process consists in estimating the state variables repetitively at time intervals T_s, a task for which diverse methods are available and which differ from each other in respect of their accuracy and complexity.

The easiest and for this reason in drive control applications most popular sampling technique relies on the explicit Euler method to work out an estimation of the state variables at the next sampling instant (see for example [62, 63]). The other side of the coin is the requirement for a sufficiently small sampling period T_s to ensure an acceptable state estimation. The sampling period is, however, often dictated by the inverter switching frequency or the controller performance. As a result, Euler's method may under certain practical conditions lack of precision.

Various strategies for drive control applications based on Park's model have been reported in the literature to overcome this limitation. These include solving the continuous-time model equations under the assumption of a zero-order hold and approximating the required exponential of the continuous-time system matrix (cf. [64–66]) or performing a Taylor expansion of the state vector [67]. In [68] a state feedback was used to achieve an exact model discretization. [69] proposes a discrete-time model based on variational integrators.

In any case, the choice of the sampling method constitutes a trade-off between the *estimation accuracy* and the *computational effort*. The performance of the following approaches in solving the system (3.62) is to be examined with respect to these two criteria:

- numerical methods for ordinary differential equations: forward Euler (order 1), Heun (order 2) and Bogacki-Shampine (order 3);
- zero-order hold assumption and solving of the resulting linear system of differential equations. The matrix exponential in the expression of the solution is approximated by means of a partial sum.

The interested reader may refer for instance to [70] to obtain detailed information about the mathematical background of above methods. The most appropriate strategy will be determined based on simulation and experimental results.

3.7.4 Computation of the state variables by means of numerical methods

Accuracy assessment of the selected methods

First insight into the performance of each preselected numerical method can be gained from offline simulations. Consequently, we simulate a model of IM1 with wavelength orders 1 and 17 ($\mathcal{H} = \mathcal{H}_m$) using Euler's, Heun's as well as the Bogacki-Shampine method and a step size $\delta t = 10^{-4}\,\mathrm{s}$, which corresponds to the sampling period of the real-time system used in the experiments. A further, more accurate simulation with the Runge-Kutta method of order 4 and a step size $\delta t = 10^{-6}\,\mathrm{s}$ is used as reference. The waveforms of the stator current i'_{s0}, the torque and the angular velocity delivered by each of the methods under test are compared to the ones of the reference model.

Fig. 3.9 presents the responses of the different model variants to a balanced sinusoidal voltage supply (frequency $f = 50\,\mathrm{Hz}$, line-to-line voltage $U = 400\,\mathrm{V}$) and a rated load torque step applied at time $t = 0.5\,\mathrm{s}$. The poor performance of Euler's scheme during transients as well as in steady-state even regarding the fundamental of the stator current is striking, which makes it unsuitable for the purpose.

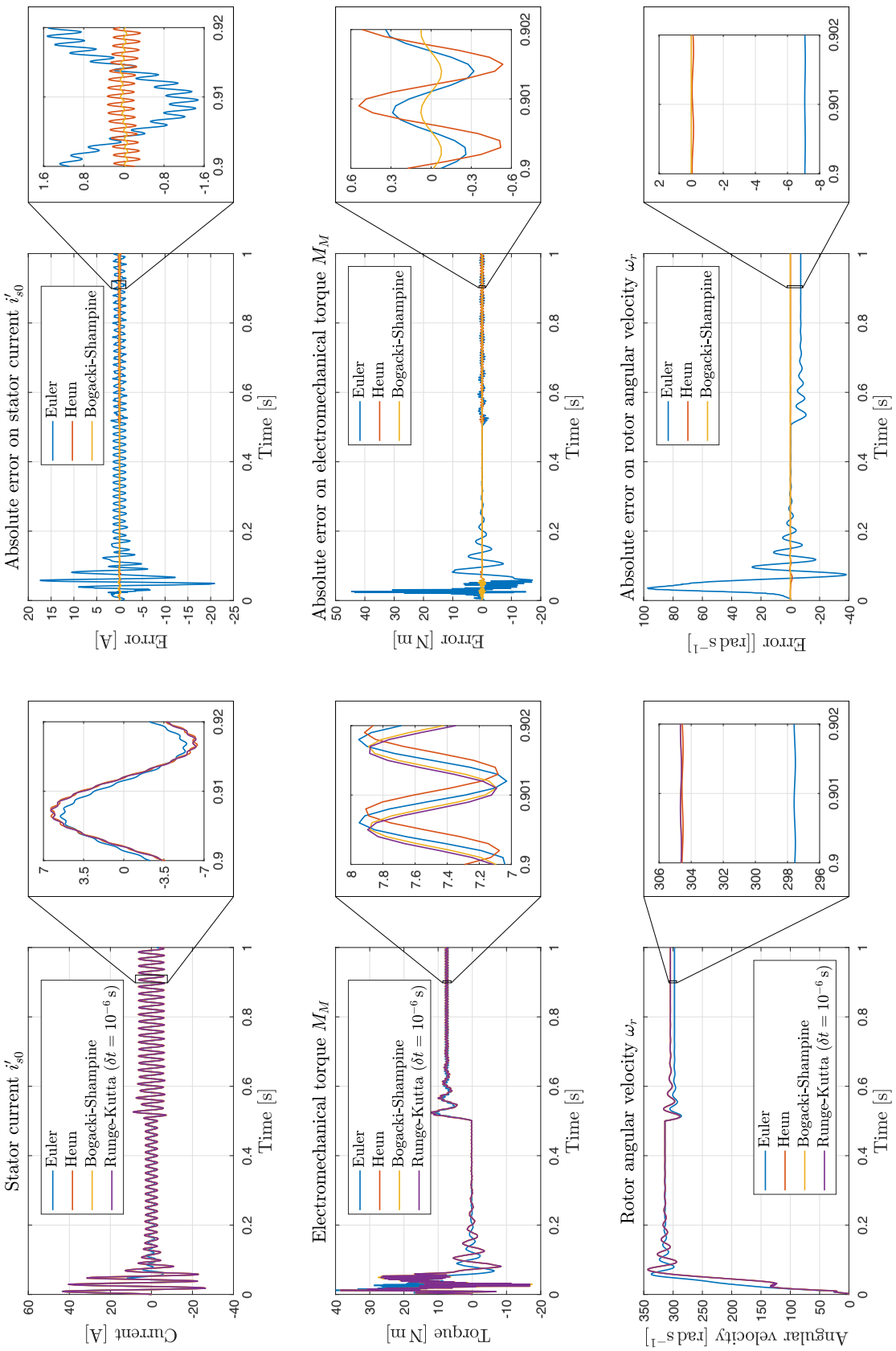

Figure 3.9: Simulation waveforms obtained with the numerical methods for a model of IM1 with $\mathcal{H} = \{1, 17\}$ and a balanced sinusoidal voltage excitation

Heun's method performs much more satisfactorily and provides decent waveforms overall. A closer look at the stator current and the torque under load shows that the scheme is however unable to correctly estimate the phase of high-frequency harmonic components, leading to an oscillating error. This error is still present in the results computed with the Bogacki-Shampine method, yet to a markedly lesser extent.

In order to validate these preliminary observations, the model with $\mathcal{H} = \{1, 17\}$ was implemented on the test rig using Euler's, Heun's and the Bogacki-Shampine method. A second model of IM1 including the additional wavelengths 5 and 11 and a model of IM2 with $\mathcal{H} = \{2, 26\}$ were examined experimentally as well (compare [71, 72]). The induction machines IM1 and IM2 were operated by means of a feedforward U/f control with balanced sinusoidal reference voltages of frequency $f = 40\,\mathrm{Hz}$. These reference voltages were also used as model inputs alongside the torque measured at the machine shaft. The mechanical topology of the test bench consisting of the two rotor masses and the one of the torque sensor constitutes a three spring-mass system. This results in complex torque waveforms with rich harmonic content. This aspect alongside noise impacting the signal transmission creates parasitic oscillations of the electromechanical torque and the rotor angular velocity computed by the machine models (see for example fig. 3.13). For this reason, in all steady-state investigations, the DC component of the torque signal was extracted using a moving average filter and fed into the model.

The steady-state comparison in fig. 3.10 of the calculated stator current, torque and rotor angular velocity waveforms with the corresponding measured quantities clearly highlights the insufficient accuracy of Euler's method. The amplitude of the fundamental stator current component is seriously underestimated as well as the DC component of the rotor angular velocity.

In contrast, Heun's and the Bogacki-Shampine methods provide similar, notably more realistic results in this regard. The erroneous phase estimation delivered by Heun for the stator current PSH in the simulation results depicted in fig. 3.9 appears to be much less serious in practice (see fig. 3.10 and 3.11). The no load current spectrum in fig. 3.11 shows a reasonable performance of Heun's method at estimating the amplitude of the PSH. A significant overestimation of the latter occurs however at rated load. As this phenomenon is also observed with the Bogacki-Shampine scheme, its origin is not related to the sampling process but likely to be found in the model assumptions, especially the hypothesis of magnetic linearity which has only limited physical validity. Note that this issue is less severe in the case of IM2 for which only a minimal increase of the discrepancy between predicted and measured PSH magnitudes is observed at rated load (compare fig. 3.12).

A consequence of the incorrect amplitude estimation of the PSH at rated load is the suspiciously high computed magnitude of the torque harmonic component associated with it in the case of IM1. This problem appears clearly in the traces in fig. 3.13 which were obtained by applying a rated load torque step. The amplitude of said torque harmonic drastically increases with the fundamental torque component, yet an experimental evidence of this phenomenon is nowhere to be found in the measured torque. Nonetheless, no hasty general conclusion should be drawn from this fact about the pertinence of the modelling approach as the results regarding the magnitude of the relevant torque harmonic look much more encouraging in the case of IM2 (cf. fig. 3.14, Heun's and Bogacki-Shampine methods).

Another important factor impacting on the electromagnetic torque and rotor angular velocity predictions is the use of the measured torque signal as load torque input of the model. In contrast to steady-state measurements, the signal had to be fed directly to the model as any filter delay would have been unacceptable. Thus, the parasitic oscillations present in the measured load torque generate additional frequency components in the model waveforms. Leaving aside this aspect, the traces in fig. 3.13 attest to an acceptable overall dynamic behaviour of the model variants based on Heun's or the Bogacki-Shampine method. Conversely, Euler's approach yields, yet again, poor results in the case of IM1 and even leads to the model of IM2 becoming unstable under no load conditions (see fig. 3.14).

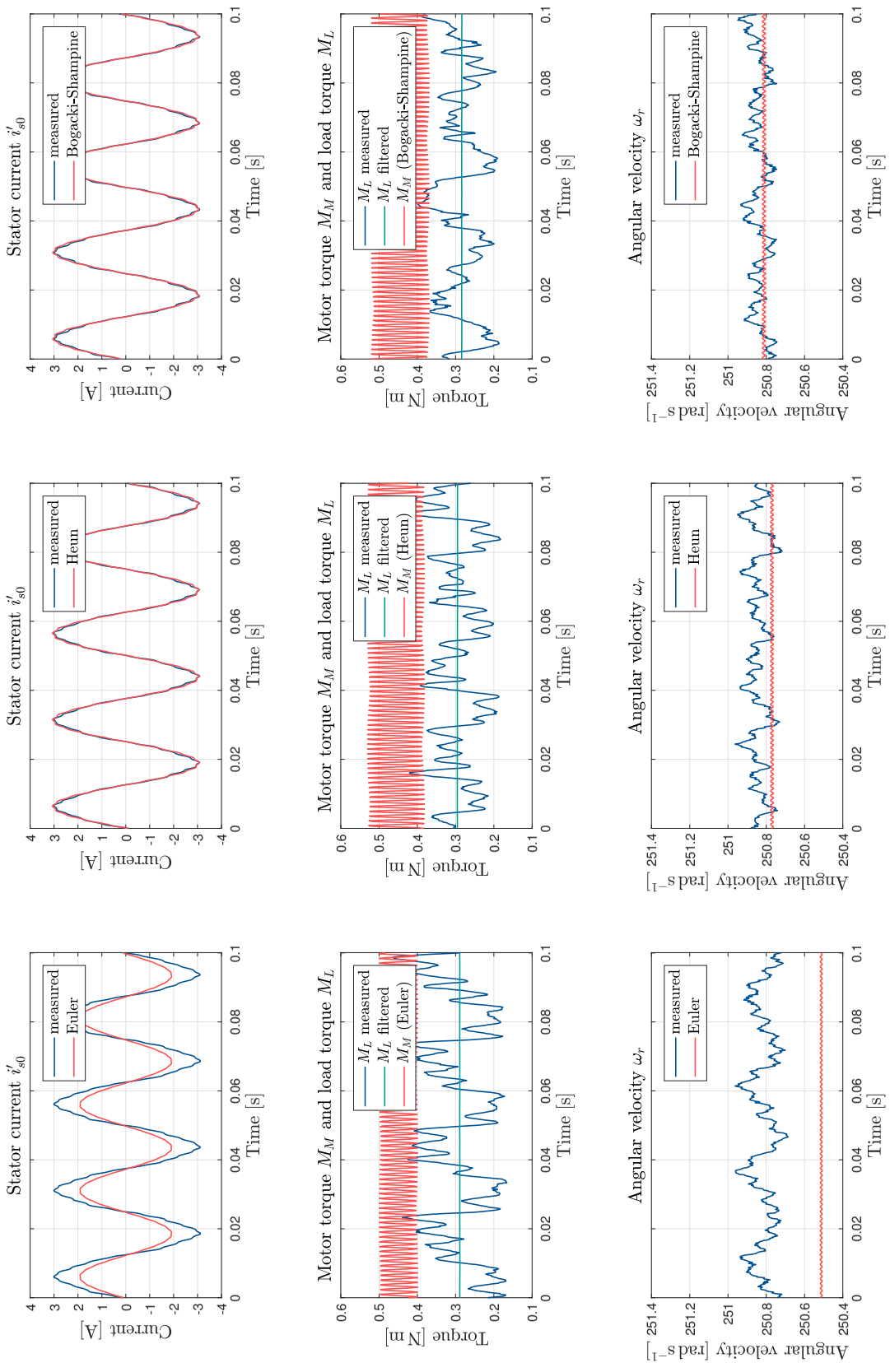

Figure 3.10: Steady-state performance assessment of the numerical methods with experimental results in the case of IM1 (model with $\mathcal{H} = \{1, 17\}$)

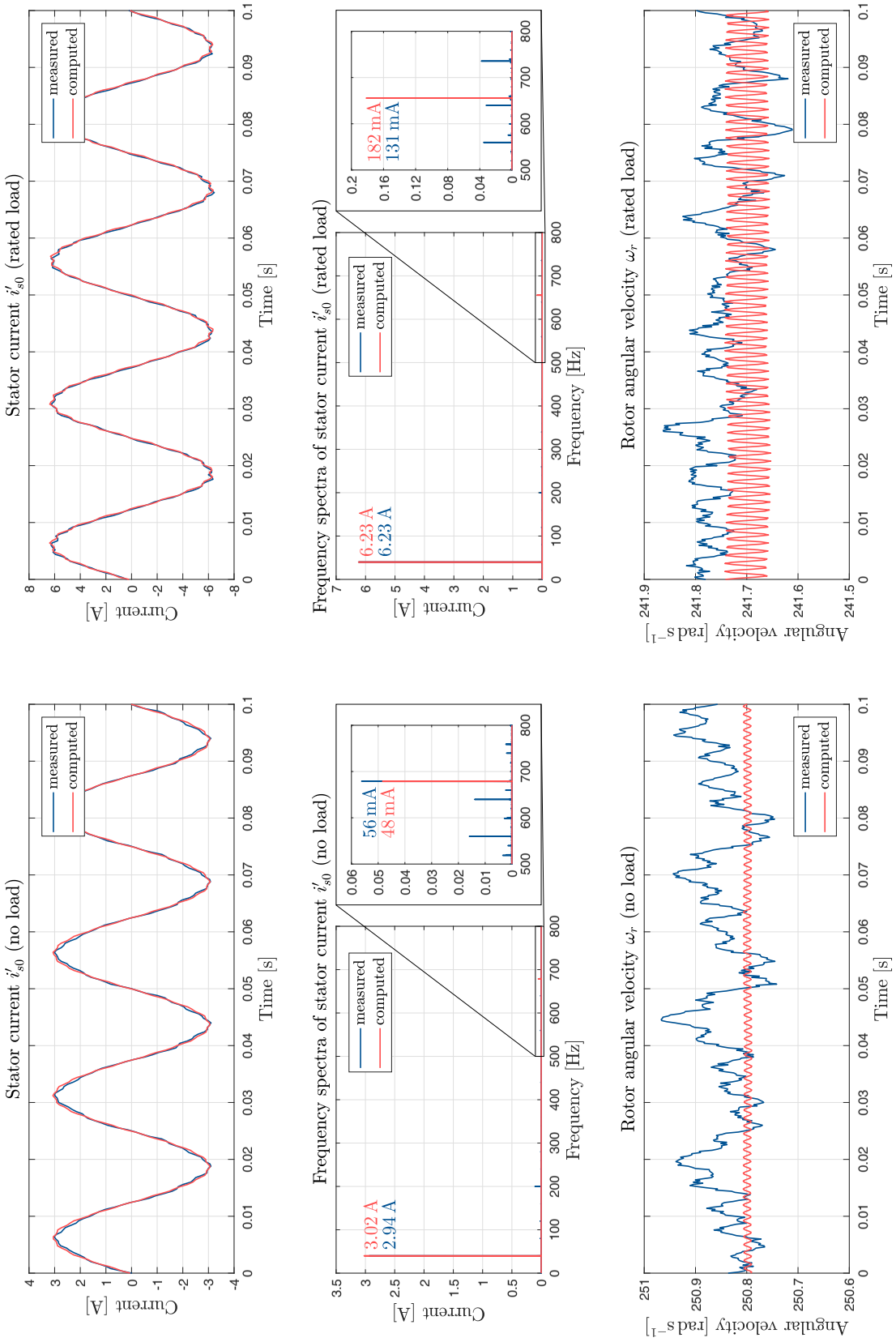

Figure 3.11: Comparison of stator current and rotor angular velocity waveforms as well as stator current spectra obtained using Heun's method with experimental results under no load and rated load conditions (model of IM1 with $\mathcal{H} = \{1, 17\}$)

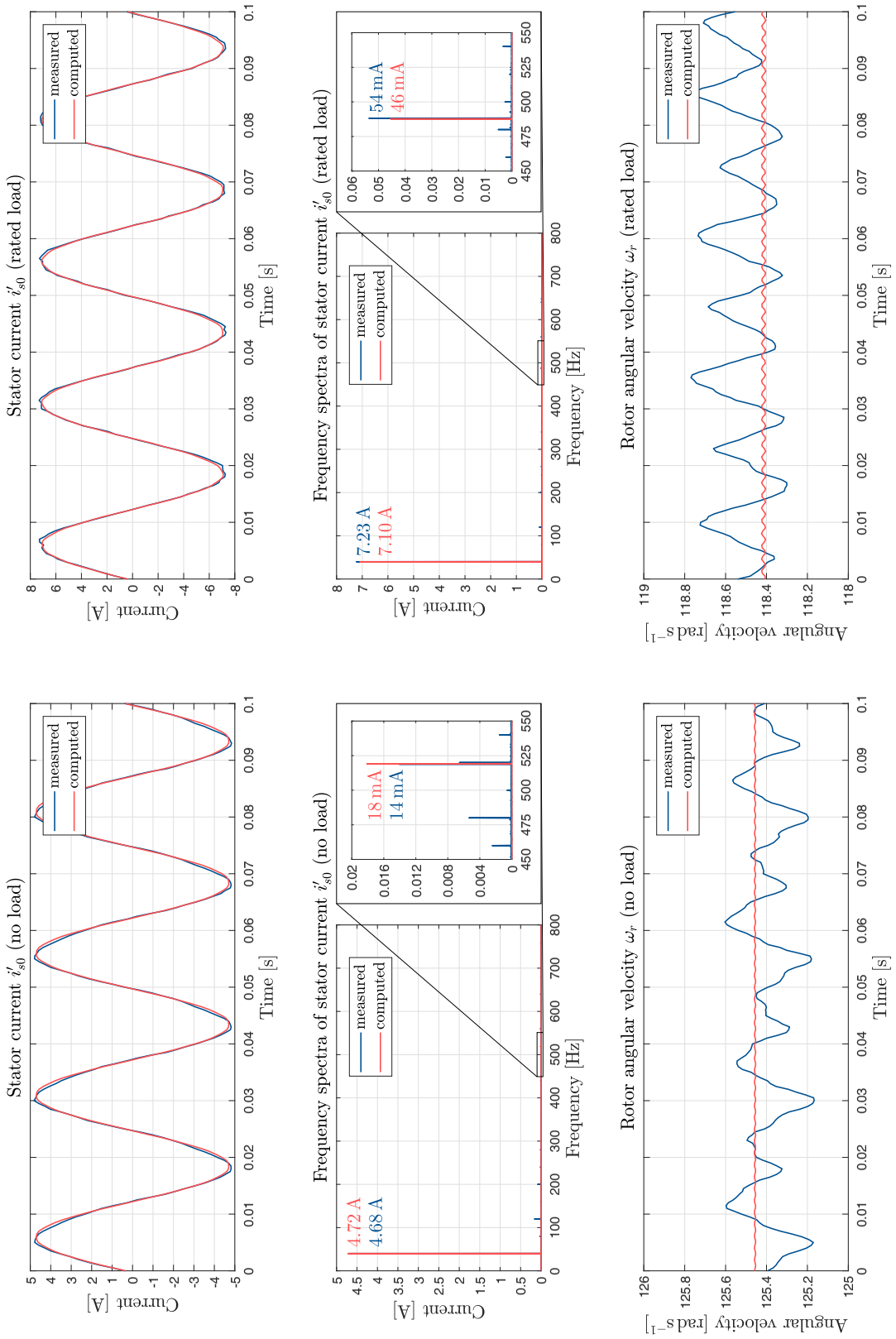

Figure 3.12: Measured and computed stator current waveforms and spectra as well as rotor angular velocity traces obtained under no load and rated load conditions (model of IM2 with $\mathcal{H} = \{2, 26\}$, Heun's method)

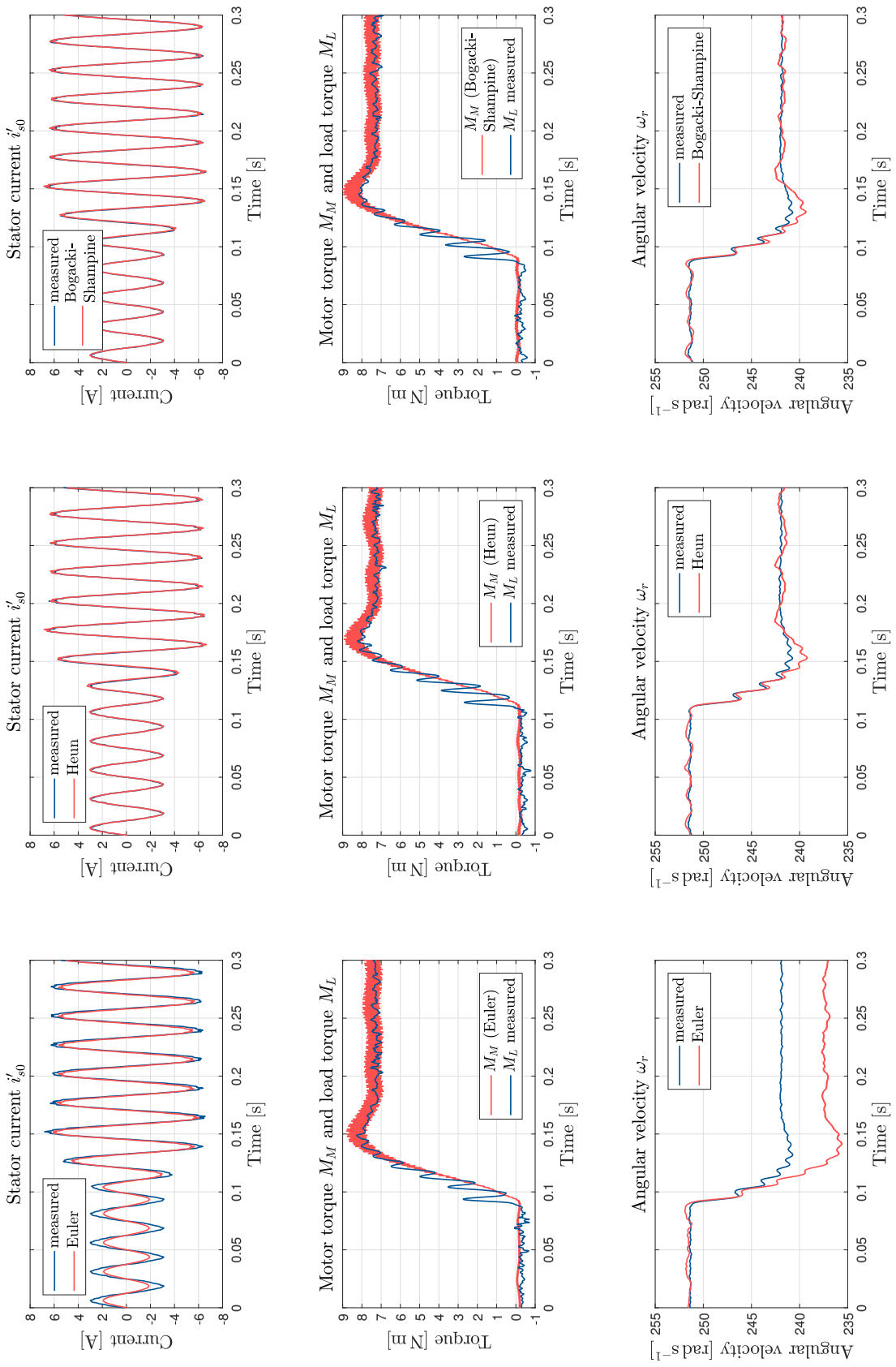

Figure 3.13: Response of each model variant to a rated load step compared to experimental data (IM1, model with $\mathcal{H} = \{1, 17\}$)

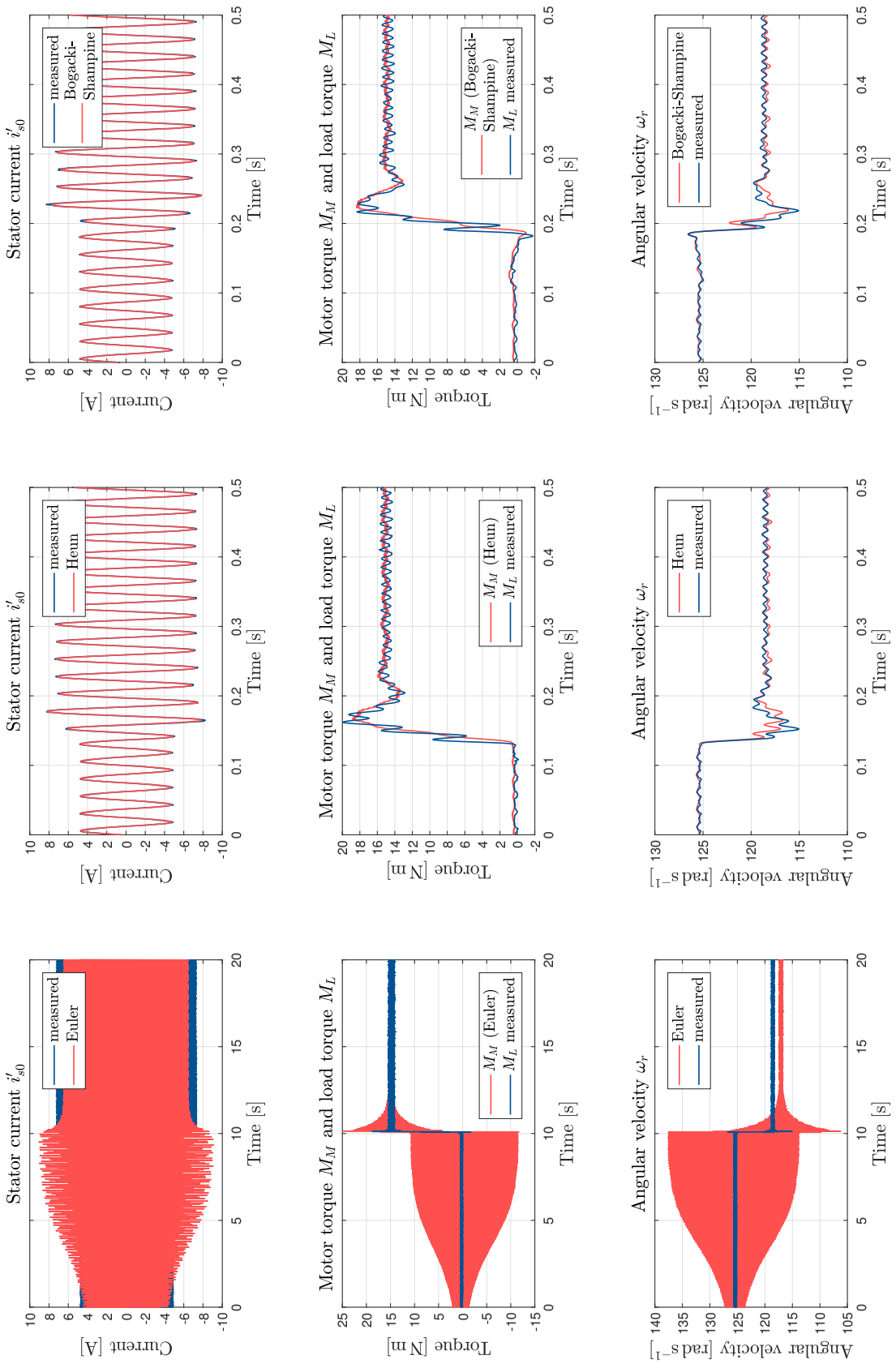

Figure 3.14: Response of each model variant to a rated load step in comparison with experiments (IM2, model with $\mathcal{H} = \{2, 26\}$)

The investigations so far examined the performance of the three numerical methods exclusively from an accuracy point of view. In this regard, Euler's method does not constitute a viable option which makes imperative the use of higher order schemes under the considered experimental conditions. Heun's and the Bogacki-Shampine methods appear to be promising candidates. However, careful considerations would have to be made for each specific application, as the simulation results presented in fig. 3.9 have shown inaccuracies with respect to the phase of current and torque harmonics.

Evaluation of the complexity of each model variant

The suitability of the models discussed above regarding practical applications highly depends on the time required to compute the state variables. Although it is in theory sufficient to ensure that the state variables can be calculated within a sampling period, target-specific implementation constraints such as interrupt latency require the model computation time to be less.

For this reason, we will on the one hand consider the time necessary to calculate the value of the state variables at the next sampling instant from their current value and the one of the inputs. We will refer to it as *model execution time*, as it represents a fair measure of the model complexity. The *model execution time* is easily determined by means of a processor timer. On the other hand, we will evaluate the model real-time capability based on the time needed for the execution of the complete interrupt service routine in which the model code is embedded. The latter includes for instance the interrupt latency as well as the servicing of data exchange processes and will be denoted *interrupt routine execution time*. It can vary considerably and must be less than the sampling period $T_s = 100\,\mu\text{s}$. The *interrupt routine execution time* is estimated using a timer on the FPGA generating the processor interrupt request signal. The latter is issued at the beginning of each inverter PWM period, as symmetric sampling is used.

We also introduce the *iteration time* describing the time necessary to evaluate the state derivatives in (3.62) for given state and input values. Heun's method requires two and the Bogacki-Shampine scheme three iterations to be carried out in order to gain the value of the state variables at the next sampling instant. As $\mathbf{L}'(\theta_r)$ is symmetric and its diagonal blocks $\mathbf{L}'_\mathbf{s}$ and $\mathbf{L}'_\mathbf{r}$ are constant, the *iteration time* primarily involves the computation of the submatrix $\widetilde{\mathbf{L}}'_\mathbf{sr}(\theta_r)$ (resp. $\widetilde{\mathbf{L}}'_\mathbf{rs}(\theta_r)$) and the Cholesky decomposition to obtain ${\mathbf{L}'}^{-1}(\theta_r)$. Thus, it is roughly independent of the numerical method selected.

Method	**Model** [μs]	**Interrupt routine** [μs]
Euler	14.9	34.5
Heun	29.4	49.3
Bogacki-Shampine	44.1	64.3

Table 3.1: Maximal execution times obtained on the real-time system for each numerical method (model of IM1 with $\mathcal{H} = \{1, 17\}$)

Table 3.1 provides an overview of the maximal model and interrupt routine execution times obtained on the real-time system with each numerical method and the model of IM1 including wavelengths of order 1 and 17. An iteration requires almost $15\,\mu$s, whereas the Cholesky decomposition alone takes around $8\,\mu$s ($\mathbf{L}'$ has dimension 17 and the model order is 19). Note the significantly higher maximal interrupt routine execution time, which is partly due to the data transfer processes used for acquiring the waveforms discussed previously.

Method	**Model** [μs]	**Interrupt routine** [μs]
Euler	18.9	37.5
Heun	37.2	56.5
Bogacki-Shampine	55.6	75.1

Table 3.2: Maximal execution times obtained on the real-time system for each numerical method (model of IM1 with $\mathcal{H} = \{1, 5, 11, 17\}$)

Table 3.2 gives an overview of the maximal execution times in the case of a model of IM1 for which $\mathcal{H} = \{1, 5, 11, 17\}$. It can be inferred from the data that an additional wavelength costs approximately $2\,\mu$s. Although the maximal model execution times are similar to the ones given in [71], the interrupt routine execution times are noticeably higher, attesting to the highly unpredictable character of this parameter. The value obtained with the Bogacki-Shampine scheme shows a processor utilization reaching already 75%.

Method	**Model** [μs]	**Interrupt routine** [μs]
Euler	46.9	66.8
Heun ($f_{sw} = 8\,\text{kHz}$)	93.7	113.5
Bogacki-Shampine ($f_{sw} = 5\,\text{kHz}$)	140.4	160.8

Table 3.3: Maximal execution times obtained on the real-time system for each numerical method (model of IM2 with $\mathcal{H} = \{2, 26\}$)

The time measurements carried out with the model of IM2 featuring the wavelengths of order 2 and 26 are listed in table 3.3. The model having order 31, its maximal execution time with Euler's method leaps to around $47\,\mu$s, i.e. more than three times the value obtained for the equivalent model of IM1. As a consequence of the model order increase compared to IM1, the model variants derived with Heun's and the Bogacki-Shampine methods are not real-time compliant at $f_{sw} = 10\,\text{kHz}$. Thus, the inverter switching frequency f_{sw} had to be reduced to 8 kHz (5 kHz respectively) to allow for execution on the real-time system. This issue shows the highly problematic dependence of the model order on the number of rotor bars.

The model of IM2 based on Euler's method is the only variant which complies with the real-time requirements. Since it does not yield acceptable results (see fig. 3.14), the strategy adopted so far fails to address the general goals set in section 1.5.

3.7.5 Zero-order hold assumption and discrete-time state-space model

Derivation of the discrete-time model

The comparatively high computation effort obtained with Heun's and the Bogacki-Shampine method primarily arises from the need for several iterations during which nearly all the model equations have to be evaluated. An attempt to alleviate the problem consists in assuming the rotor angular velocity ω_r and the rotor angle θ_r constant during a sampling period alongside the input voltage vector $\vec{u}'$ and the load torque M_L. This allows for eq. (3.62a) to be solved as a linear time-invariant differential system, independently of (3.62b) and (3.62c).

Under these circumstances, the knowledge of the state variables and the inputs at an instant $t_0 \geqslant 0$ enables the determination of the current vector $\vec{i}'(t_0+\nu)$, for all $\nu > 0$, as follows:

$$\vec{i}'(t_0+\nu) = e^{\nu \mathbf{A}(t_0)}\vec{i}'(t_0) + \int_0^{\nu} e^{(\nu-\tau)\mathbf{A}(t_0)}\,\mathrm{d}\tau \mathbf{B}\vec{u}'(t_0) \tag{3.63}$$

where $\mathbf{A}(t_0) = \mathbf{A}(\omega_r(t_0),\, \theta_r(t_0))$.

Solving eq. (3.62b) and (3.62c) yields:

$$\omega_r(t_0+\nu) = \left[\omega_r(t_0) - \frac{M_M - M_L}{C_W}\right] e^{-\frac{C_W}{J_M}\nu} + \frac{M_M - M_L}{C_W} \tag{3.64}$$

and

$$\theta_r(t_0+\nu) = \theta_r(t_0) + \frac{M_M - M_L}{C_W}\nu + \frac{J_M}{C_W}\left[\omega_r(t_0) - \frac{M_M - M_L}{C_W}\right]\left[1 - e^{-\frac{C_W}{J_M}\nu}\right] \tag{3.65}$$

In particular, for $k \in \mathbb{N}$, $t_0 = kT_s$ and $\nu = T_s$,

$$\vec{i}'((k+1)T_s) = e^{T_s\mathbf{A}(kT_s)}\vec{i}'(kT_s) + \int_0^{T_s} e^{(T_s-\tau)\mathbf{A}(kT_s)}\,\mathrm{d}\tau \mathbf{B}\vec{u}'(kT_s)$$

$$\omega_r((k+1)T_s) = \left[\omega_r(kT_s) - \frac{M_M - M_L}{C_W}\right] e^{-\frac{C_W}{J_M}T_s} + \frac{M_M - M_L}{C_W}$$

$$\theta_r((k+1)T_s) = \theta_r(kT_s) + \frac{M_M - M_L}{C_W}T_s + \frac{J_M}{C_W}\left[\omega_r(kT_s) - \frac{M_M - M_L}{C_W}\right]\left[1 - e^{-\frac{C_W}{J_M}T_s}\right]$$

Introducing the notations:

$$\vec{i}'[k] = \vec{i}'(kT_s); \quad \vec{u}'[k] = \vec{u}'(kT_s)$$

$$\omega_r[k] = \omega_r(kT_s); \quad \theta_r[k] = \theta_r(kT_s)$$

$$\mathbf{F}[k] = e^{T_s\mathbf{A}(kT_s)}; \quad \mathbf{G}[k] = \int_0^{T_s} e^{(T_s-\tau)\mathbf{A}(kT_s)}\,\mathrm{d}\tau\mathbf{B}$$

we obtain the subsequent discrete-time state-space representation of (3.62):

$$\begin{cases} \vec{i}'[k+1] = \mathbf{F}[k]\vec{i}'[k] + \mathbf{G}[k]\vec{u}'[k] & \text{(3.66a)} \\ \omega_r[k+1] = \left[\omega_r[k] - \dfrac{M_M - M_L}{C_W}\right] e^{-\frac{C_W}{J_M}T_s} + \dfrac{M_M - M_L}{C_W} & \text{(3.66b)} \\ \theta_r[k+1] = \theta_r[k] + \dfrac{M_M - M_L}{C_W}T_s + \dfrac{J_M}{C_W}\left[\omega_r[k] - \dfrac{M_M - M_L}{C_W}\right]\left[1 - e^{-\frac{C_W}{J_M}T_s}\right] & \text{(3.66c)} \end{cases}$$

The expressions of $\mathbf{F}$ and $\mathbf{G}$ involve a matrix exponential. Using the power series expansion of the exponential,

$$\forall\, t \in \mathbb{R}, \quad e^{t\mathbf{A}} = \sum_{n=0}^{+\infty} \frac{t^n \mathbf{A}^n}{n!} \tag{3.67}$$

$\mathbf{F}$ and $\mathbf{G}$ can be approximated by means of a partial sum of order $N \in \mathbb{N}$ to allow for an implementation of (3.66) on a digital controller, e.g.

$$\text{for } k \in \mathbb{N}, \quad \mathbf{F}[k] = \sum_{n=0}^{N} \frac{T_s^n \mathbf{A}^n[kT_s]}{n!} + \mathcal{O}(T_s^{N+1}) \tag{3.68}$$

Model assessment

We investigate variants of the model (3.66) obtained using approximations of the matrix exponential with partial sums of order 1 to 4. To do so, we repeat the simulation described in section 3.7.4 under the exact same conditions. Again, the stator current, torque and angular velocity waveforms obtained with the Runge-Kutta method of order 4 and a step size of 10^{-6} s are used as references.

The corresponding results are provided in fig. 3.15. The following remarks can be made:

- the approximation of order 1 substantially underestimates the amplitude of the stator fundamental current as well as the angular velocity under load. Since this approach is similar to Euler's method, the phenomenon is not surprising;
- the approximation of order 2 performs notably better from the perspective of the fundamental current. However, the phase error in the current and torque harmonics is appreciable;
- a comparison of the waveforms generated with approximations of order 3 and 4 shows no tangible reduction of the error. This suggests that increasing the number of terms in the partial sum beyond 3 is not beneficial;
- none of the model variants under test appears to be accurate during the initial transient until the machine has reached a nearly synchronous speed. This is a hint that the rotor angle variation and the one of its derivative become significant within a sampling period, making the zero-order hold assumption questionable.

A comparison of the model estimations with steady-state measurements carried out on the two machines under the same general conditions as with the numerical methods confirms the above observations (see fig. 3.16 and 3.17). Note that the approximation of order 1 is unstable in the case of IM2. A look at the stator current spectrum of IM1 under no load and rated load in fig. 3.18 shows that the approximation of order 3 delivers amplitude values for the PSH comparable to Heun's method. The DC component of the angular velocity is somewhat overestimated and the amplitude of the fundamental current slightly low under rated load. This is due to the fact that the model parameters were determined based on comparisons between estimations using Heun's method and measurements.

The dynamic responses of the models based on approximations of order 1 to 3 to a rated load torque step are compared to experiments in fig. 3.19 in the case of IM1. The third order approximation provides a fairly accurate representation of the current and angular velocity transient behaviour. As with numerical methods, the computed amplitude of the torque harmonic caused by the wavelength of order 17 is too high in all three cases. This confirms that the origin of this phenomena is not related to the discretization process but the result of somewhat restrictive modelling hypotheses made necessary by the need for a real-time compliant model (compare section 3.3).

Considering the model execution times given in table 3.4 and 3.5, an increase of the approximation order by 1 leads to an additional computation time of roughly 4.5 μs for IM1 and 13 μs for IM2. This is far less than the time required for a complete model iteration, since only a further power of the matrix $\mathbf{A}$ has to be calculated. Although all model variants are real-time compliant when sampling at 10 kHz, not enough time would remain within a sampling period to execute a control algorithm. Thus, the computational burden of the model implementations is still not satisfactory to consider their use in real-time control applications.

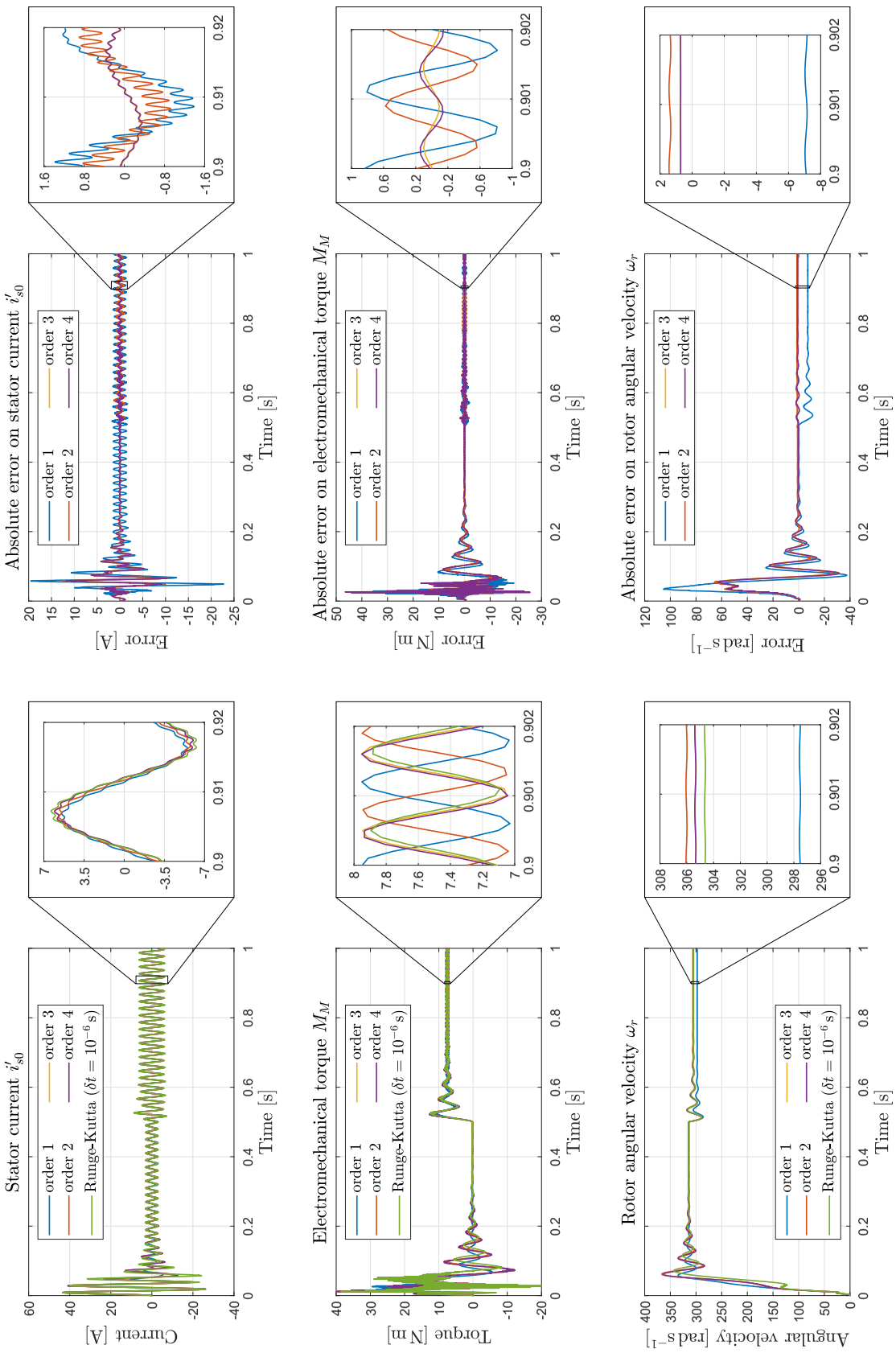

Figure 3.15: Simulation waveforms obtained with matrix exponential approximations of different orders (model with $\mathcal{H} = \{1, 17\}$, balanced sinusoidal voltage excitation)

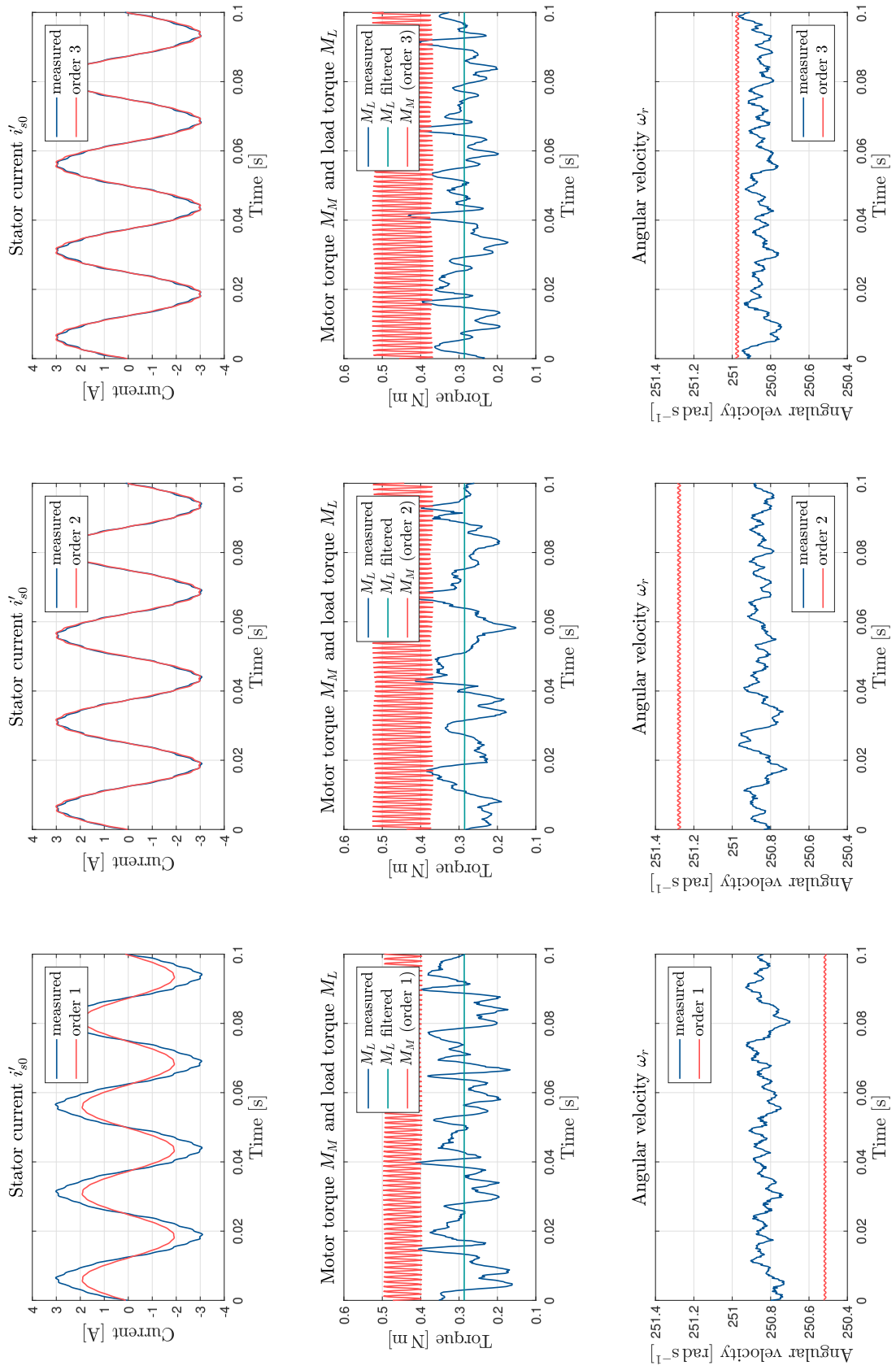

Figure 3.16: Steady-state performance assessment of the ZOH approximations with experimental results in the case of IM1 (model with $\mathcal{H} = \{1, 17\}$)

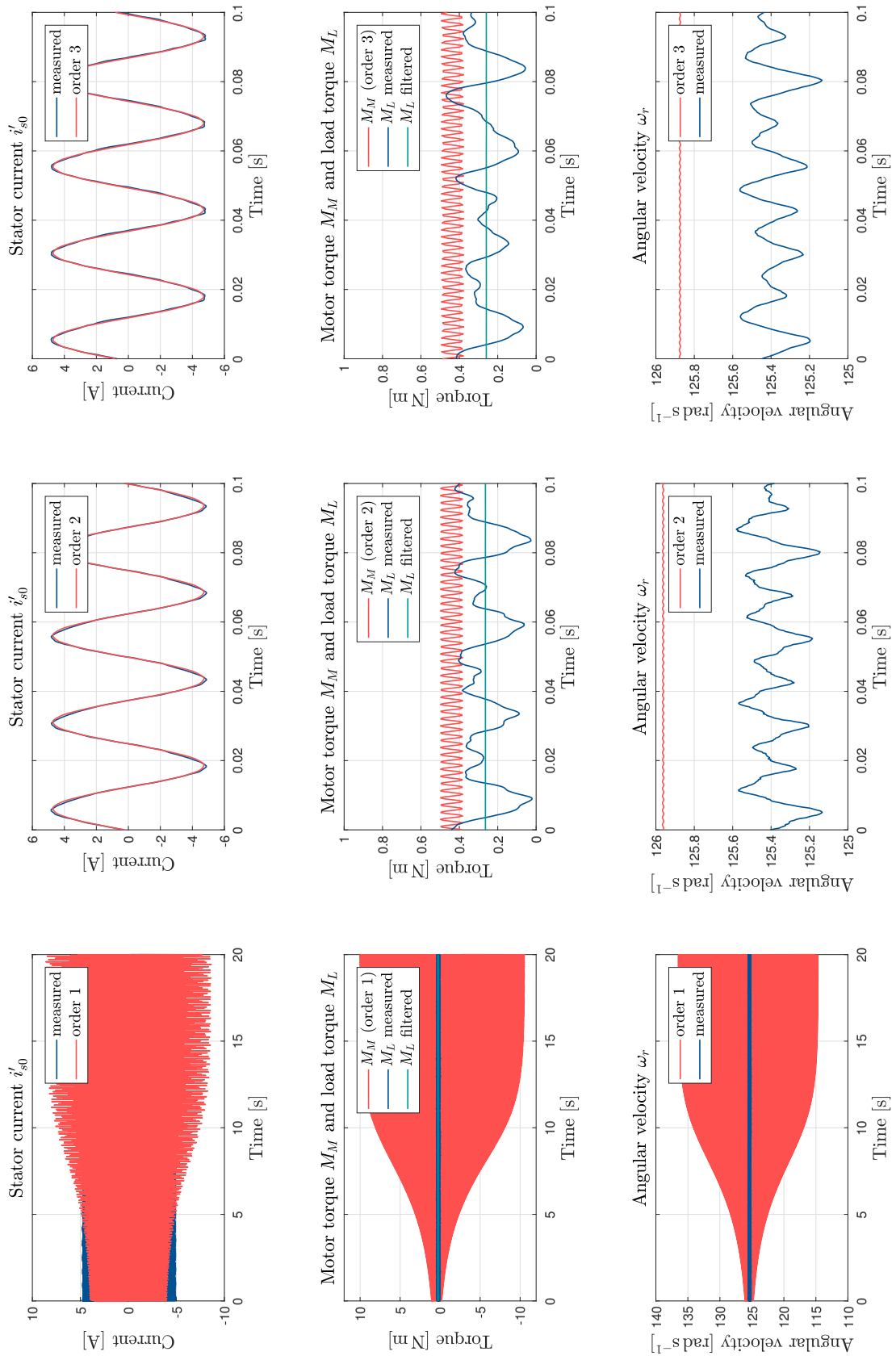

Figure 3.17: Steady-state performance assessment of the ZOH approximations with experimental results in the case of IM2 (model with $\mathcal{H} = \{2, 26\}$)

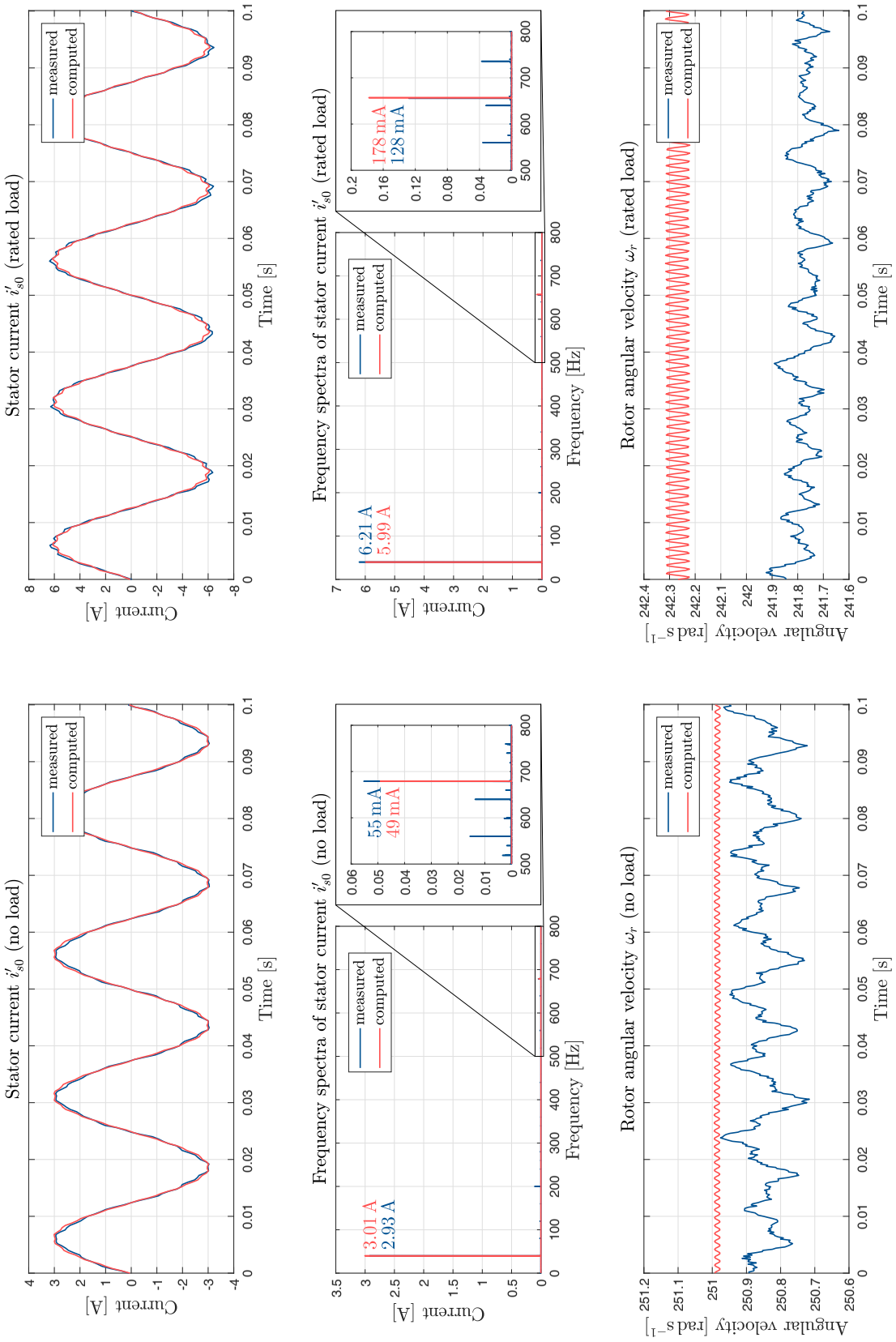

Figure 3.18: Comparison of stator current and rotor angular velocity waveforms as well as stator current spectra obtained using an order 3 approximation with experimental results under no load and rated load conditions (model of IM1 with $\mathcal{H} = \{1, 17\}$)

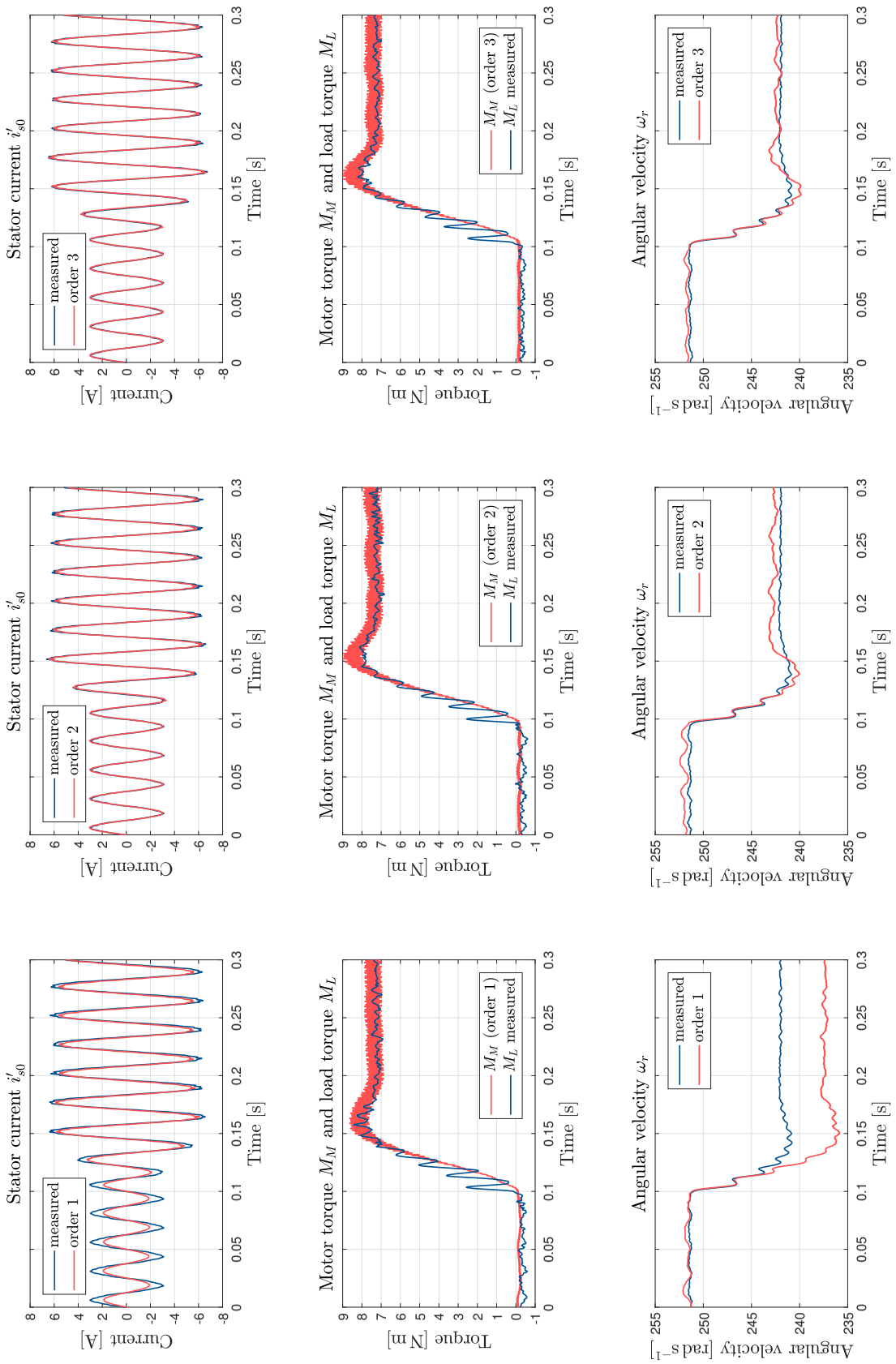

Figure 3.19: Response of the models with approximations of order 1 to 3 to a rated load step compared to experimental data (IM1, model with $\mathcal{H} = \{1, 17\}$)

Approximation order	Model [μs]	Interrupt routine [μs]
1	16.8	35.7
2	21.4	40.7
3	25.9	45.2

Table 3.4: Maximal execution times obtained on the real-time system with approximations of the matrix exponential of order 1 to 3 (model of IM1 with $\mathcal{H} = \{1, 17\}$)

Approximation order	Model [μs]	Interrupt routine [μs]
1	52.0	71.7
2	64.3	83.4
3	77.6	96.6

Table 3.5: Maximal execution times obtained on the real-time system with approximations of the matrix exponential of order 1 to 3 (model of IM2 with $\mathcal{H} = \{2, 26\}$)

3.7.6 Discussion

The results of the investigations presented in the foregoing sections lead to the following conclusions:

- the real-time execution of machine models including a few space harmonics is basically possible at a sampling frequency in the order of 10 kHz;
- Euler's method cannot be used in the considered context;
- Heun's scheme represents a fair compromise between accuracy and computation effort. So does an approximation of order 3 when discretizing the model based on the zero-order hold assumption;
- the dependence of the model order on the rotor bar number is a fundamental issue with respect to the computational burden. The real-time execution of the model, even on a powerful system, is challenging.

From the last observation follows that the proposed model in its current form has no prospect of practical use in drive control applications. Thus, our initial objectives are not yet fulfilled. The simplification of the model should become our main focus.

Summary

The periodicity of distributed air-gap quantities makes possible their representation as Fourier series. Taking advantage of this property, Parseval's identity enabled us to express the flux linkages using the Fourier coefficients of the conductor distribution functions and the air-gap flux density distribution.

Under the assumption of magnetic linearity and constant air-gap length, all air-gap quantities can be determined from the knowledge of the conductor distribution functions. Following the properties of Fourier series and the hypothesis of a symmetrical machine, only the conductor distribution function of a single stator circuit and the one of a single rotor circuit are required. In this context, the contribution of each space harmonic to the main flux is easily determined. This allowed us to establish the general form of a continuous-time state-space model including the effect of conductor distribution harmonics.

In a further step, specific models of the two investigated machines were derived. Two techniques for obtaining discrete-time representations were discussed from the perspective of accuracy and computational burden: numerical methods and the solving of the model equations assuming a zero-order hold. Heun's method and an order 3 approximation of the continuous-time system matrix exponential appear to provide fairly accurate results. A fundamental issue remains the unacceptably excessive computational effort with regard to the targeted applications.

Chapter 4
Transformed linear geometric model

Overview of chapter

In order to tackle the issue of computational effort encountered with the machine model developed in chapter 3, we aim at optimizing its mathematical description. The main drawback of the approach adopted so far is the dependence of the model order on the number of independent electrical variables. As a result, the model order is directly impacted by the number of rotor bars and stator windings.

In contrast, our goal is to gain a state-space representation equivalent to the one established in section 3.6 but in which the wavelength orders taken into account in the conductor distribution functions determines the model order. In other words, a model with only a handful wavelengths should be described with few state variables. We therefore focus our attention on the design of a state transformation following the same principles as the Clarke transformation in Park's model.

In a further step, we apply the proposed transformation to the state-space equations of the linear geometric model (3.62) to obtain a simple, yet general, model description. We will then customize the model equations to derive specific models for the investigated machines IM1 and IM2. These models will be assessed by means of simulations and experiments.

4.1 Preliminary considerations

4.1.1 Intuitive approach

A key step in the derivation of the linear geometric model developed in chapter 3 consisted in working out the contribution of a specific wavelength $h \in \mathbb{N}^\star$ to the main flux, which, as established in section 3.4.4, has the following form:

$$\vec{\tilde{\Psi}}_h = \begin{bmatrix} \vec{\tilde{\psi}}_{s,\,h} \\ \vec{\tilde{\psi}}_{r,\,h} \end{bmatrix} = \widetilde{\mathbf{L}}_{\mathbf{h}}(\theta_r)\vec{i} = \begin{bmatrix} \widetilde{\mathbf{L}}_{\mathbf{s\,h}} & \widetilde{\mathbf{L}}_{\mathbf{rs\,h}}(\theta_r) \\ \widetilde{\mathbf{L}}_{\mathbf{sr\,h}}(\theta_r) & \widetilde{\mathbf{L}}_{\mathbf{r\,h}} \end{bmatrix} \begin{bmatrix} \vec{i}_s \\ \vec{i}_r \end{bmatrix} = \begin{bmatrix} \widetilde{\mathbf{L}}_{\mathbf{s\,h}}\vec{i}_s + \widetilde{\mathbf{L}}_{\mathbf{rs\,h}}(\theta_r)\vec{i}_r \\ \widetilde{\mathbf{L}}_{\mathbf{sr\,h}}(\theta_r)\vec{i}_s + \widetilde{\mathbf{L}}_{\mathbf{r\,h}}\vec{i}_r \end{bmatrix} \tag{4.1}$$

The expressions of the submatrices appearing in (4.1) are summarized here:

$$\widetilde{\mathbf{L}}_{\mathbf{s\,h}} = \widetilde{L}_{s,\,h}\widetilde{\mathbf{T}}^{\top}_{\mathbf{Cs\,h}}\widetilde{\mathbf{T}}_{\mathbf{Cs\,h}} \tag{4.2}$$

$$\widetilde{\mathbf{L}}_{\mathbf{r\,h}} = \widetilde{L}_{r,\,h}\widetilde{\mathbf{T}}^{\top}_{\mathbf{Cr\,h}}\widetilde{\mathbf{T}}_{\mathbf{Cr\,h}} \tag{4.3}$$

$$\widetilde{\mathbf{L}}_{\mathbf{rs\,h}}(\theta_r) = L_{M,\,h}\widetilde{\mathbf{T}}^{\top}_{\mathbf{Cs\,h}}\mathbf{T}(h\theta_r - \varphi_h)\widetilde{\mathbf{T}}_{\mathbf{Cr\,h}} \tag{4.4}$$

$$\widetilde{\mathbf{L}}_{\mathbf{sr\,h}}(\theta_r) = L_{M,\,h}\widetilde{\mathbf{T}}^{\top}_{\mathbf{Cr\,h}}\mathbf{T}(-h\theta_r + \varphi_h)\widetilde{\mathbf{T}}_{\mathbf{Cs\,h}} = \widetilde{\mathbf{L}}^{\top}_{\mathbf{rs\,h}}(\theta_r) \tag{4.5}$$

The stator and rotor inductance submatrices associated with wavelength h, $\widetilde{\mathbf{L}}_{\mathbf{s\,h}}$ and $\widetilde{\mathbf{L}}_{\mathbf{r\,h}}$, have an interesting form, since they are the product of the matrix $\widetilde{\mathbf{T}}_{\mathbf{Cs\,h}}$ ($\widetilde{\mathbf{T}}_{\mathbf{Cr\,h}}$ resp.) and its transpose. This aspect might give us a hint on how a transformation could be designed. We therefore take a closer look at these matrices.

Recalling definitions (3.31a) and (3.31b), the general form of $\widetilde{\mathbf{T}}_{\mathbf{Cs\,h}}$ and $\widetilde{\mathbf{T}}_{\mathbf{Cr\,h}}$ is:

$$\widetilde{\mathbf{T}}_{\mathbf{Cs\,h}} = \begin{bmatrix} 1 & \cdots & \cos(h\gamma_{s0,m}) & \cdots & \cos(h\gamma_{s0,m_s-1}) \\ 0 & \cdots & \sin(h\gamma_{s0,m}) & \cdots & \sin(h\gamma_{s0,m_s-1}) \end{bmatrix} \tag{4.6a}$$

$$\widetilde{\mathbf{T}}_{\mathbf{Cr\,h}} = \begin{bmatrix} 1 & \cdots & \cos(h\gamma_{r0,n}) & \cdots & \cos(h\gamma_{r0,m_r-1}) \\ 0 & \cdots & \sin(h\gamma_{r0,n}) & \cdots & \sin(h\gamma_{r0,m_r-1}) \end{bmatrix} \tag{4.6b}$$

where $\gamma_{s0,m}$ (and $\gamma_{r0,n}$) represents the angle by which the conductor distribution of stator (resp. rotor) circuit 0 has to be shifted in order to obtain the one of stator circuit $m \in [\![0,\, m_s - 1]\!]$ (rotor circuit $n \in [\![0,\, m_r - 1]\!]$ resp.).

In section 3.7.1, we took advantage of the flexibility provided by the modelling approach with respect to the choice of the electrical circuits in the models of IM1 and IM2. In the case of IM1, we used a circuit for each of the $w_s = 3$ stator windings. Since IM1 has only one pole pair, this decision resulted in the angle $\gamma_{s0,m}$, $m \in [\![0,\, 2]\!]$ being a multiple of $2\pi/3$. Thus, the $m_s = 3$ stator shift angle values are equally spaced in the interval $[0,\, 2\pi]$. However, IM2 having two pole pairs, this condition would not have been satisfied if we had used a single circuit per winding. Modelling each winding as the series connection of two circuits enabled us to obtain $m_s = 6$ shift angle values equally spaced in the interval $[0,\, 2\pi]$.

In the considerations discussed in this chapter, we assume that the stator and rotor circuits in the model have been defined to meet the conditions:

$$\forall\, m \in [\![0,\, m_s - 1]\!],\ \gamma_{s0,m} = m\frac{2\pi}{m_s}$$

$$\forall\, n \in [\![0,\, m_r - 1]\!],\, \gamma_{r0,n} = n\frac{2\pi}{m_r}$$

In this situation, we obtain a more specific expression of $\widetilde{\mathbf{T}}_{\mathbf{Cs\,h}}$ and $\widetilde{\mathbf{T}}_{\mathbf{Cr\,h}}$ as follows:

$$\widetilde{\mathbf{T}}_{\mathbf{Cs\,h}} = \begin{bmatrix} 1 & \cdots & \cos\left(hm\dfrac{2\pi}{m_s}\right) & \cdots & \cos\left(h(m_s-1)\dfrac{2\pi}{m_s}\right) \\ 0 & \cdots & \sin\left(hm\dfrac{2\pi}{m_s}\right) & \cdots & \sin\left(h(m_s-1)\dfrac{2\pi}{m_s}\right) \end{bmatrix}, \quad m \in [\![0,\, m_s - 1]\!] \tag{4.7}$$

$$\widetilde{\mathbf{T}}_{\mathbf{Cr\,h}} = \begin{bmatrix} 1 & \cdots & \cos\left(hn\dfrac{2\pi}{m_r}\right) & \cdots & \cos\left(h(m_r-1)\dfrac{2\pi}{m_r}\right) \\ 0 & \cdots & \sin\left(hn\dfrac{2\pi}{m_r}\right) & \cdots & \sin\left(h(m_r-1)\dfrac{2\pi}{m_r}\right) \end{bmatrix}, \quad n \in [\![0,\, m_r - 1]\!] \tag{4.8}$$

For a given wavelength order $h \in \mathbb{N}^\star$,

$$\exists!\,(\lambda,\, k) \in \mathbb{N} \times [\![0,\, m_s - 1]\!],\, h = \lambda m_s + k$$

$$\exists!\,(\mu,\, l) \in \mathbb{N} \times [\![0,\, m_r - 1]\!],\, h = \mu m_r + l$$

As a result of the periodicity of sine and cosine functions,

$$\widetilde{\mathbf{T}}_{\mathbf{Cs\,h}} = \begin{bmatrix} 1 & \cdots & \cos\left(km\dfrac{2\pi}{m_s}\right) & \cdots & \cos\left(k(m_s-1)\dfrac{2\pi}{m_s}\right) \\ 0 & \cdots & \sin\left(km\dfrac{2\pi}{m_s}\right) & \cdots & \sin\left(k(m_s-1)\dfrac{2\pi}{m_s}\right) \end{bmatrix} = \widetilde{\mathbf{T}}_{\mathbf{Cs\,k}}, \quad m \in [\![0,\, m_s - 1]\!] \tag{4.9}$$

$$\widetilde{\mathbf{T}}_{\mathbf{Cr\,h}} = \begin{bmatrix} 1 & \cdots & \cos\left(ln\dfrac{2\pi}{m_r}\right) & \cdots & \cos\left(l(m_r-1)\dfrac{2\pi}{m_r}\right) \\ 0 & \cdots & \sin\left(ln\dfrac{2\pi}{m_r}\right) & \cdots & \sin\left(l(m_r-1)\dfrac{2\pi}{m_r}\right) \end{bmatrix} = \widetilde{\mathbf{T}}_{\mathbf{Cs\,l}}, \quad n \in [\![0,\, m_r - 1]\!] \tag{4.10}$$

Consequently, there exist only m_s different forms of the matrix $\widetilde{\mathbf{T}}_{\mathbf{Cs\,h}}$ and m_r variants of $\widetilde{\mathbf{T}}_{\mathbf{Cr\,h}}$, since $k \in [\![0,\, m_s - 1]\!]$ and $l \in [\![0,\, m_r - 1]\!]$. In addition, the two matrices can be represented by means of the following complex vectors:

$$\begin{bmatrix} 1 & \cdots & e^{jkm\frac{2\pi}{m_s}} & \cdots & e^{jk(m_s-1)\frac{2\pi}{m_s}} \end{bmatrix} \in \mathbb{C}^{m_s}, \quad (k,\, m) \in [\![0,\, m_s - 1]\!]^2 \tag{4.11a}$$

$$\begin{bmatrix} 1 & \cdots & e^{jln\frac{2\pi}{m_r}} & \cdots & e^{jl(m_r-1)\frac{2\pi}{m_r}} \end{bmatrix} \in \mathbb{C}^{m_r}, \quad (l,\, n) \in [\![0,\, m_r - 1]\!]^2 \tag{4.11b}$$

Considering all possible combinations of (4.11a) for $k \in [\![0,\, m_s - 1]\!]$ yields the matrix:

$$\mathbf{W_s} = \begin{bmatrix} 1 & 1 & \cdots & \cdots & \cdots & 1 \\ 1 & e^{j\frac{2\pi}{m_s}} & \cdots & e^{jm\frac{2\pi}{m_s}} & \cdots & e^{j(m_s-1)\frac{2\pi}{m_s}} \\ \vdots & \vdots & \vdots & \vdots & \vdots & \vdots \\ 1 & e^{jk\frac{2\pi}{m_s}} & \cdots & e^{jkm\frac{2\pi}{m_s}} & \cdots & e^{jk(m_s-1)\frac{2\pi}{m_s}} \\ \vdots & \vdots & \vdots & \vdots & \vdots & \vdots \\ 1 & e^{j(m_s-1)\frac{2\pi}{m_s}} & \cdots & e^{j(m_s-1)m\frac{2\pi}{m_s}} & \cdots & e^{j(m_s-1)^2\frac{2\pi}{m_s}} \end{bmatrix} \tag{4.12}$$

$\mathbf{W_s}$ is very similar to the $m_s \times m_s$ Fourier matrix.

Definition 3: Fourier matrix
For $m_s \in \mathbb{N}^\star$, the $m_s \times m_s$ Fourier matrix, denoted $\mathcal{W}_{\mathrm{m_s}}$, is defined as follows:

$$\mathcal{W}_{\mathrm{m_s}} = \frac{1}{\sqrt{m_s}} \begin{bmatrix} 1 & 1 & \cdots & \cdots & \cdots & 1 \\ 1 & W_{m_s} & \cdots & W_{m_s}^{m} & \cdots & W_{m_s}^{m_s-1} \\ \vdots & \vdots & \vdots & \vdots & \vdots & \vdots \\ 1 & W_{m_s}^{k} & \cdots & W_{m_s}^{mk} & \cdots & W_{m_s}^{(m_s-1)k} \\ \vdots & \vdots & \vdots & \vdots & \vdots & \vdots \\ 1 & W_{m_s}^{m_s-1} & \cdots & W_{m_s}^{m(m_s-1)} & \cdots & W_{m_s}^{(m_s-1)^2} \end{bmatrix} \tag{4.13}$$

where $W_{m_s} = e^{-j\frac{2\pi}{m_s}}$.

Remark 1:
The $m_s \times m_s$ Fourier matrix is the matrix of the m_s point Discrete Fourier Transform (DFT).

Remark 2:
In some sources such as [73], $W_{m_s} = e^{j\frac{2\pi}{m_s}}$ is used in the definition of the $m_s \times m_s$ Fourier matrix (and the one of the m_s point DFT matrix).

Due to the close similarity between $\mathbf{W_s}$ and $\mathcal{W}_{\mathrm{m_s}}$, the $m_s \times m_s$ Fourier matrix seems to be a prospective candidate for transforming vectors related to stator quantities. Using the same reasoning, vectors involving rotor quantities will be transformed by means of the m_r point DFT matrix.

4.1.2 Mathematical justification

Taking a closer look at the equations (4.2) and (4.7), the coefficient of $\widetilde{\mathbf{L}}_{\mathbf{s\,h}}$ in row k and column l, $(k,\, l) \in [\![0,\, m_s - 1]\!]^2$, is:

$$\widetilde{L}_{s\,h,\,kl} = \widetilde{L}_{s,\,h} \cos\left[(k-l)\frac{2\pi}{m_s}\right]$$

It can be readily observed from the above relation that the entry in row $k+1$ and column $l+1$ is equal to $\widetilde{L}_{s\,h,\,kl}$. It results from this property and the periodicity of the cosine function that the entries in each column of $\widetilde{\mathbf{L}}_{\mathbf{s\,h}}$ are shifted one position to the bottom compared to the column left of it with wraparound to the top, i.e. $\widetilde{\mathbf{L}}_{\mathbf{s\,h}}$ is *circulant*.

Proposition 7: Diagonalization of circulant matrices
For $m_s \in \mathbb{N}^\star$, an $m_s \times m_s$ circulant matrix is diagonalized by the $m_s \times m_s$ Fourier matrix.

See [74, p. 287] for the proof.

Proposition 7 justifies the use of Fourier matrices for the transformation to be designed, as they enable us to work with diagonal equivalents of $\widetilde{\mathbf{L}}_{\mathbf{s\,h}}$ and $\widetilde{\mathbf{L}}_{\mathbf{r\,h}}$ which are significantly easier to handle.

4.1.3 Other important properties of Fourier matrices

We mention here two additional properties of Fourier matrices which will turn out to be instrumental in the transformation of the linear geometric model.

Proposition 8: Important properties of Fourier matrices
For $m_s \in \mathbb{N}^\star$,

1.) $\mathcal{W}_{\mathrm{m_s}}$ is symmetric, i.e. $\mathcal{W}_{\mathrm{m_s}} = \mathcal{W}_{\mathrm{m_s}}^\top$

2.) $\mathcal{W}_{\mathrm{m_s}}$ is unitary: $\mathcal{W}_{\mathrm{m_s}}^{-1} = \overline{\mathcal{W}_{\mathrm{m_s}}}^\top$

Proof.

1.) The symmetry of $\mathcal{W}_{\mathrm{m_s}}$ results directly from its definition.

2.) For $(k,\, l) \in [\![0,\, m_s - 1]\!]^2$, the coefficient of $\mathcal{W}_{\mathrm{m_s}}\overline{\mathcal{W}_{\mathrm{m_s}}}^\top$ in row k and column l is:

$$\frac{1}{\sqrt{m_s}}\begin{bmatrix}1 & \cdots & W_{m_s}^{mk} & \cdots & W_{m_s}^{(m_s-1)k}\end{bmatrix}\frac{1}{\sqrt{m_s}}\begin{bmatrix}1\\ \vdots\\ W_{-m_s}^{ml}\\ \vdots\\ W_{-m_s}^{(m_s-1)l}\end{bmatrix}$$

$$=\frac{1}{m_s}\sum_{m=0}^{m_s-1} W_{m_s}^{mk}W_{-m_s}^{ml} = \sum_{m=0}^{m_s-1} e^{-jmk\frac{2\pi}{m_s}}e^{jml\frac{2\pi}{m_s}}$$

$$=\frac{1}{m_s}\sum_{m=0}^{m_s-1}\left[e^{j(l-k)\frac{2\pi}{m_s}}\right]^m$$

$$=\delta_{kl} = \frac{1}{\sqrt{m_s}}\begin{bmatrix}1 & \cdots & W_{-m_s}^{mk} & \cdots & W_{-m_s}^{(m_s-1)k}\end{bmatrix}\frac{1}{\sqrt{m_s}}\begin{bmatrix}1\\ \vdots\\ W_{m_s}^{ml}\\ \vdots\\ W_{m_s}^{(m_s-1)l}\end{bmatrix}$$

where δ_{kl} represents the Kronecker delta.
Consequently, $\mathcal{W}_{\mathrm{m_s}}\overline{\mathcal{W}_{\mathrm{m_s}}}^\top = \overline{\mathcal{W}_{\mathrm{m_s}}}^\top\mathcal{W}_{\mathrm{m_s}} = \mathbf{I_{m_s}}$, $\mathbf{I_{m_s}}$ being the $m_s \times m_s$ identity matrix.

□

4.1.4 Definition of transformed quantities

We introduce a transformation operator based on the Fourier matrix as follows:

Definition 4: Transformation operator
For $n \in \mathbb{N}^\star$, we define the following linear operator:

$$\begin{array}{rccc}\mathcal{T}_{\mathcal{W}n}: & \mathbb{C}^n & \longrightarrow & \mathbb{C}^n\\ \vec{x} = \begin{bmatrix}x_0 & \cdots & x_{n-1}\end{bmatrix}^\top & \longmapsto & \mathcal{T}_{\mathcal{W}n}(\vec{x}) & = \underline{x}^\natural = \begin{bmatrix}x_0^\natural & \cdots & x_{n-1}^\natural\end{bmatrix}^\top = \mathcal{W}_{\mathrm{n}}^{-1}\vec{x}\end{array} \tag{4.14}$$

The corresponding inverse operator, $\mathcal{T}_{\mathcal{W}n}^{-1}$, is:

$$\begin{aligned} \mathcal{T}_{\mathcal{W}n}^{-1}: \quad & \mathbb{C}^n \longrightarrow \mathbb{C}^n \\ \underline{x}^\natural = \begin{bmatrix} x_0^\natural & \cdots & x_{n-1}^\natural \end{bmatrix}^\top & \longmapsto \mathcal{T}_{\mathcal{W}n}^{-1}(\underline{x}^\natural) = \vec{x} = \begin{bmatrix} x_0 & \cdots & x_{n-1} \end{bmatrix}^\top = \mathcal{W}_{\mathrm{n}} \underline{x}^\natural \end{aligned} \tag{4.15}$$

Remark 3:
$\mathcal{T}_{\mathcal{W}n}$ is well-known in electrical engineering as 'symmetrical component transformation' for the analysis of unbalanced conditions in power systems (cf. for instance [5, p. 548]). We will adopt a perspective more common in signal processing and consider $\mathcal{T}_{\mathcal{W}n}$ as the Discrete Fourier Transform operator since this is likely to be beneficial to the understanding of the behaviour of space harmonics.

With $n = m_s$, the operator $\mathcal{T}_{\mathcal{W}m_s}$ enables us to introduce transformed stator quantities:

Definition 5: Transformed stator voltage and current vectors
The transformed stator voltage and current vectors, $\underline{u}_s^\natural \in \mathbb{C}^{m_s}$ and $\underline{i}_s^\natural \in \mathbb{C}^{m_s}$, are defined as follows:

$$\underline{u}_s^\natural = \mathcal{T}_{\mathcal{W}m_s}(\vec{u}_s) = \mathcal{W}_{\mathrm{m_s}}^{-1} \vec{u}_s \tag{4.16a}$$

$$\underline{i}_s^\natural = \mathcal{T}_{\mathcal{W}m_s}(\vec{i}_s) = \mathcal{W}_{\mathrm{m_s}}^{-1} \vec{i}_s \tag{4.16b}$$

Analogously, $\mathcal{T}_{\mathcal{W}m_r}$ allows for the definition of transformed rotor quantities:

Definition 6: Transformed rotor voltage and current vectors
The transformed rotor voltage and current vectors, $\underline{u}_r^\natural \in \mathbb{C}^{m_r}$ and $\underline{i}_r^\natural \in \mathbb{C}^{m_r}$, are defined as follows:

$$\underline{u}_r^\natural = \mathcal{T}_{\mathcal{W}m_r}(\vec{u}_r) = \mathcal{W}_{\mathrm{m_r}}^{-1} \vec{u}_r \tag{4.17a}$$

$$\underline{i}_r^\natural = \mathcal{T}_{\mathcal{W}m_r}(\vec{i}_r) = \mathcal{W}_{\mathrm{m_r}}^{-1} \vec{i}_r \tag{4.17b}$$

A comparable transformation was used in [5] and [61] to simplify the analysis of multiphase induction machines in presence of space harmonics, and in [75] in the specific case of three phase induction machines with rotor cage. However, in all these references no relation was established with the Discrete Fourier Transform.

4.2 Transforming the equations of the linear geometric model

4.2.1 Transformation of the voltage equations

We start with the transformation of the voltage equations assuming no interconnection between the electrical circuits of the model. An interconnection matrix will be introduced later on to account for the actual conductor configuration in the machine.

Combining relations (2.4) and (3.50), we obtain:

$$\begin{bmatrix} \vec{u}_s \\ \vec{u}_r \end{bmatrix} = \begin{bmatrix} \mathbf{R_s} & \mathbf{0} \\ \mathbf{0} & \mathbf{R_r} \end{bmatrix} \begin{bmatrix} \vec{i}_s \\ \vec{i}_r \end{bmatrix} + \begin{bmatrix} \widetilde{\mathbf{L}}_\mathbf{s} + \mathbf{L}_{\sigma\mathbf{s}} & \widetilde{\mathbf{L}}_\mathbf{rs}(\theta_r) \\ \widetilde{\mathbf{L}}_\mathbf{sr}(\theta_r) & \widetilde{\mathbf{L}}_\mathbf{r} + \mathbf{L}_{\sigma\mathbf{r}} \end{bmatrix} \begin{bmatrix} \frac{\mathrm{d}\vec{i}_s}{\mathrm{d}t} \\ \frac{\mathrm{d}\vec{i}_r}{\mathrm{d}t} \end{bmatrix} + \omega_r \begin{bmatrix} \mathbf{0} & \frac{\partial \widetilde{\mathbf{L}}_\mathbf{rs}(\theta_r)}{\partial \theta_r} \\ \frac{\partial \widetilde{\mathbf{L}}_\mathbf{sr}(\theta_r)}{\partial \theta_r} & \mathbf{0} \end{bmatrix} \begin{bmatrix} \vec{i}_s \\ \vec{i}_r \end{bmatrix} \tag{4.18}$$

Applying $\mathcal{T}_{\mathcal{W}m_s}$ to the first line of (4.18) provides the expression of the transformed voltage vector $\underline{u}_s^\natural$:

$$\underline{u}_s^\natural = \mathcal{W}_{\mathrm{m_s}}^{-1} \vec{u}_s = \mathcal{W}_{\mathrm{m_s}}^{-1} \mathbf{R_s} \vec{i}_s + \mathcal{W}_{\mathrm{m_s}}^{-1} \left(\widetilde{\mathbf{L}}_\mathbf{s} + \mathbf{L}_{\sigma\mathbf{s}} \right) \frac{\mathrm{d}\vec{i}_s}{\mathrm{d}t} + \mathcal{W}_{\mathrm{m_s}}^{-1} \widetilde{\mathbf{L}}_\mathbf{rs}(\theta_r) \frac{\mathrm{d}\vec{i}_r}{\mathrm{d}t} + \omega_r \mathcal{W}_{\mathrm{m_s}}^{-1} \frac{\partial \widetilde{\mathbf{L}}_\mathbf{rs}(\theta_r)}{\partial \theta_r} \vec{i}_r \tag{4.19}$$

The quantities $\vec{i}_s$ and $\vec{i}_r$ in (4.19) are eliminated by applying $\mathcal{T}_{\mathcal{W}m_s}^{-1}$ and $\mathcal{T}_{\mathcal{W}m_r}^{-1}$ respectively:

$$\begin{aligned}\underline{u}_s^\natural &= \mathcal{W}_{\mathrm{m_s}}^{-1}\mathbf{R_s}\mathcal{W}_{\mathrm{m_s}}\underline{i}_s^\natural + \mathcal{W}_{\mathrm{m_s}}^{-1}\Big(\widetilde{\mathbf{L}}_\mathbf{s} + \mathbf{L}_{\sigma\mathbf{s}}\Big)\frac{\mathrm{d}\mathcal{W}_{\mathrm{m_s}}\underline{i}_s^\natural}{\mathrm{d}t} + \mathcal{W}_{\mathrm{m_s}}^{-1}\widetilde{\mathbf{L}}_{\mathbf{rs}}(\theta_r)\frac{\mathrm{d}\mathcal{W}_{\mathrm{m_r}}\underline{i}_r^\natural}{\mathrm{d}t} + \omega_r\mathcal{W}_{\mathrm{m_s}}^{-1}\frac{\partial\widetilde{\mathbf{L}}_{\mathbf{rs}}(\theta_r)}{\partial\theta_r}\mathcal{W}_{\mathrm{m_r}}\underline{i}_r^\natural \\ &= \mathcal{W}_{\mathrm{m_s}}^{-1}\mathbf{R_s}\mathcal{W}_{\mathrm{m_s}}\underline{i}_s^\natural + \mathcal{W}_{\mathrm{m_s}}^{-1}\mathbf{L}_{\sigma\mathbf{s}}\mathcal{W}_{\mathrm{m_s}}\frac{\mathrm{d}\underline{i}_s^\natural}{\mathrm{d}t} + \mathcal{W}_{\mathrm{m_s}}^{-1}\widetilde{\mathbf{L}}_\mathbf{s}\mathcal{W}_{\mathrm{m_s}}\frac{\mathrm{d}\underline{i}_s^\natural}{\mathrm{d}t} \\ &\quad + \mathcal{W}_{\mathrm{m_s}}^{-1}\widetilde{\mathbf{L}}_{\mathbf{rs}}(\theta_r)\mathcal{W}_{\mathrm{m_r}}\frac{\mathrm{d}\underline{i}_r^\natural}{\mathrm{d}t} + \omega_r\frac{\partial\mathcal{W}_{\mathrm{m_s}}^{-1}\widetilde{\mathbf{L}}_{\mathbf{rs}}(\theta_r)\mathcal{W}_{\mathrm{m_r}}}{\partial\theta_r}\underline{i}_r^\natural\end{aligned} \tag{4.20}$$

Introducing the following matrices,

$$\mathbf{R}_\mathbf{s}^\natural = \mathcal{W}_{\mathrm{m_s}}^{-1}\mathbf{R_s}\mathcal{W}_{\mathrm{m_s}} \tag{4.21a}$$

$$\mathbf{L}_{\sigma\mathbf{s}}^\natural = \mathcal{W}_{\mathrm{m_s}}^{-1}\mathbf{L}_{\sigma\mathbf{s}}\mathcal{W}_{\mathrm{m_s}} \tag{4.21b}$$

$$\widetilde{\mathbf{L}}_\mathbf{s}^\natural = \mathcal{W}_{\mathrm{m_s}}^{-1}\widetilde{\mathbf{L}}_\mathbf{s}\mathcal{W}_{\mathrm{m_s}} \tag{4.21c}$$

$$\widetilde{\mathbf{L}}_{\mathbf{rs}}^\natural(\theta_r) = \mathcal{W}_{\mathrm{m_s}}^{-1}\widetilde{\mathbf{L}}_{\mathbf{rs}}(\theta_r)\mathcal{W}_{\mathrm{m_r}} \tag{4.21d}$$

the transformed stator voltage equation becomes:

$$\underline{u}_s^\natural = \mathbf{R}_\mathbf{s}^\natural\underline{i}_s^\natural + \Big(\mathbf{L}_{\sigma\mathbf{s}}^\natural + \widetilde{\mathbf{L}}_\mathbf{s}^\natural\Big)\frac{\mathrm{d}\underline{i}_s^\natural}{\mathrm{d}t} + \widetilde{\mathbf{L}}_{\mathbf{rs}}^\natural(\theta_r)\frac{\mathrm{d}\underline{i}_r^\natural}{\mathrm{d}t} + \omega_r\frac{\partial\widetilde{\mathbf{L}}_{\mathbf{rs}}^\natural(\theta_r)}{\partial\theta_r}\underline{i}_r^\natural \tag{4.22}$$

Similarly, the rotor voltage equation is gained from the second line of (4.18) by means of $\mathcal{T}_{\mathcal{W}m_r}$ and $\mathcal{T}_{\mathcal{W}m_r}^{-1}$:

$$\begin{aligned}\underline{u}_r^\natural = \mathcal{W}_{\mathrm{m_r}}^{-1}\vec{u}_r &= \mathcal{W}_{\mathrm{m_r}}^{-1}\mathbf{R_r}\vec{i}_r + \mathcal{W}_{\mathrm{m_r}}^{-1}\Big(\widetilde{\mathbf{L}}_\mathbf{r} + \mathbf{L}_{\sigma\mathbf{r}}\Big)\frac{\mathrm{d}\vec{i}_r}{\mathrm{d}t} + \mathcal{W}_{\mathrm{m_r}}^{-1}\widetilde{\mathbf{L}}_{\mathbf{sr}}(\theta_r)\frac{\mathrm{d}\vec{i}_s}{\mathrm{d}t} + \omega_r\mathcal{W}_{\mathrm{m_r}}^{-1}\frac{\partial\widetilde{\mathbf{L}}_{\mathbf{sr}}(\theta_r)}{\partial\theta_r}\vec{i}_s \\ &= \mathcal{W}_{\mathrm{m_r}}^{-1}\mathbf{R_r}\mathcal{W}_{\mathrm{m_r}}\underline{i}_r^\natural + \mathcal{W}_{\mathrm{m_r}}^{-1}\mathbf{L}_{\sigma\mathbf{r}}\mathcal{W}_{\mathrm{m_r}}\frac{\mathrm{d}\underline{i}_r^\natural}{\mathrm{d}t} + \mathcal{W}_{\mathrm{m_r}}^{-1}\widetilde{\mathbf{L}}_\mathbf{r}\mathcal{W}_{\mathrm{m_r}}\frac{\mathrm{d}\underline{i}_r^\natural}{\mathrm{d}t} \\ &\quad + \mathcal{W}_{\mathrm{m_r}}^{-1}\widetilde{\mathbf{L}}_{\mathbf{sr}}(\theta_r)\mathcal{W}_{\mathrm{m_s}}\frac{\mathrm{d}\underline{i}_s^\natural}{\mathrm{d}t} + \omega_r\frac{\partial\mathcal{W}_{\mathrm{m_r}}^{-1}\widetilde{\mathbf{L}}_{\mathbf{sr}}(\theta_r)\mathcal{W}_{\mathrm{m_s}}}{\partial\theta_r}\underline{i}_s^\natural \\ &= \mathbf{R}_\mathbf{r}^\natural\underline{i}_r^\natural + \Big(\mathbf{L}_{\sigma\mathbf{r}}^\natural + \widetilde{\mathbf{L}}_\mathbf{r}^\natural\Big)\frac{\mathrm{d}\underline{i}_r^\natural}{\mathrm{d}t} + \widetilde{\mathbf{L}}_{\mathbf{sr}}^\natural(\theta_r)\frac{\mathrm{d}\underline{i}_s^\natural}{\mathrm{d}t} + \omega_r\frac{\partial\widetilde{\mathbf{L}}_{\mathbf{sr}}^\natural(\theta_r)}{\partial\theta_r}\underline{i}_s^\natural\end{aligned} \tag{4.23}$$

where

$$\mathbf{R}_\mathbf{r}^\natural = \mathcal{W}_{\mathrm{m_r}}^{-1}\mathbf{R_r}\mathcal{W}_{\mathrm{m_r}} \tag{4.24a}$$

$$\mathbf{L}_{\sigma\mathbf{r}}^\natural = \mathcal{W}_{\mathrm{m_r}}^{-1}\mathbf{L}_{\sigma\mathbf{r}}\mathcal{W}_{\mathrm{m_r}} \tag{4.24b}$$

$$\widetilde{\mathbf{L}}_\mathbf{r}^\natural = \mathcal{W}_{\mathrm{m_r}}^{-1}\widetilde{\mathbf{L}}_\mathbf{r}\mathcal{W}_{\mathrm{m_r}} \tag{4.24c}$$

$$\widetilde{\mathbf{L}}_{\mathbf{sr}}^\natural(\theta_r) = \mathcal{W}_{\mathrm{m_r}}^{-1}\widetilde{\mathbf{L}}_{\mathbf{sr}}(\theta_r)\mathcal{W}_{\mathrm{m_s}} \tag{4.24d}$$

Combining stator and rotor quantities into a single vector, we obtain:

$$\begin{bmatrix}\underline{u}_s^\natural \\ \underline{u}_r^\natural\end{bmatrix} = \begin{bmatrix}\mathbf{R}_\mathbf{s}^\natural & \mathbf{0} \\ \mathbf{0} & \mathbf{R}_\mathbf{r}^\natural\end{bmatrix}\begin{bmatrix}\underline{i}_s^\natural \\ \underline{i}_r^\natural\end{bmatrix} + \begin{bmatrix}\widetilde{\mathbf{L}}_\mathbf{s}^\natural + \mathbf{L}_{\sigma\mathbf{s}}^\natural & \widetilde{\mathbf{L}}_{\mathbf{rs}}^\natural(\theta_r) \\ \widetilde{\mathbf{L}}_{\mathbf{sr}}^\natural(\theta_r) & \widetilde{\mathbf{L}}_\mathbf{r}^\natural + \mathbf{L}_{\sigma\mathbf{r}}^\natural\end{bmatrix}\frac{\mathrm{d}}{\mathrm{d}t}\begin{bmatrix}\underline{i}_s^\natural \\ \underline{i}_r^\natural\end{bmatrix} +$$

$$\omega_r \frac{\partial}{\partial \theta_r} \begin{bmatrix} \widetilde{\mathbf{L}}_{\mathbf{s}}^{\natural} + \mathbf{L}_{\sigma\mathbf{s}}^{\natural} & \widetilde{\mathbf{L}}_{\mathbf{rs}}^{\natural}(\theta_r) \\ \widetilde{\mathbf{L}}_{\mathbf{sr}}^{\natural}(\theta_r) & \widetilde{\mathbf{L}}_{\mathbf{r}}^{\natural} + \mathbf{L}_{\sigma\mathbf{r}}^{\natural} \end{bmatrix} \begin{bmatrix} \underline{i}_s^{\natural} \\ \underline{i}_r^{\natural} \end{bmatrix} \tag{4.25}$$

Introducing the definitions,

$$\underline{i}^{\natural} = \begin{bmatrix} \underline{i}_s^{\natural} \\ \underline{i}_r^{\natural} \end{bmatrix} \qquad \underline{u}^{\natural} = \begin{bmatrix} \underline{u}_s^{\natural} \\ \underline{u}_r^{\natural} \end{bmatrix} \qquad \mathbf{R}^{\natural} = \begin{bmatrix} \mathbf{R}_{\mathbf{s}}^{\natural} & \mathbf{0} \\ \mathbf{0} & \mathbf{R}_{\mathbf{r}}^{\natural} \end{bmatrix}$$

$$\mathbf{L}_{\sigma}^{\natural} = \begin{bmatrix} \mathbf{L}_{\sigma\mathbf{s}}^{\natural} & \mathbf{0} \\ \mathbf{0} & \mathbf{L}_{\sigma\mathbf{r}}^{\natural} \end{bmatrix} \quad \widetilde{\mathbf{L}}^{\natural}(\theta_r) = \begin{bmatrix} \widetilde{\mathbf{L}}_{\mathbf{s}}^{\natural} & \widetilde{\mathbf{L}}_{\mathbf{rs}}^{\natural}(\theta_r) \\ \widetilde{\mathbf{L}}_{\mathbf{sr}}^{\natural}(\theta_r) & \widetilde{\mathbf{L}}_{\mathbf{r}}^{\natural} \end{bmatrix} \quad \mathbf{L}^{\natural}(\theta_r) = \begin{bmatrix} \widetilde{\mathbf{L}}_{\mathbf{s}}^{\natural} + \mathbf{L}_{\sigma\mathbf{s}}^{\natural} & \widetilde{\mathbf{L}}_{\mathbf{rs}}^{\natural}(\theta_r) \\ \widetilde{\mathbf{L}}_{\mathbf{sr}}^{\natural}(\theta_r) & \widetilde{\mathbf{L}}_{\mathbf{r}}^{\natural} + \mathbf{L}_{\sigma\mathbf{r}}^{\natural} \end{bmatrix} = \widetilde{\mathbf{L}}^{\natural} + \mathbf{L}_{\sigma}^{\natural}$$

(4.25) becomes:

$$\underline{u}^{\natural} = \mathbf{R}^{\natural}\underline{i}^{\natural} + \mathbf{L}^{\natural}(\theta_r)\frac{\mathrm{d}\underline{i}^{\natural}}{\mathrm{d}t} + \omega_r \frac{\partial \mathbf{L}^{\natural}(\theta_r)}{\partial \theta_r}\underline{i}^{\natural} \tag{4.26}$$

Eq. (4.26) represents the voltage equation of the transformed linear geometric model.

4.2.2 Transformation of the torque equation

Using (2.18) and applying $\mathcal{T}_{\mathcal{W}m_s}^{-1}$ and $\mathcal{T}_{\mathcal{W}m_r}^{-1}$ while recalling that $\vec{i}_s \in \mathbb{R}^{m_s}$, we obtain an expression of the electromechanical torque depending on the stator and rotor transformed currents:

$$\begin{aligned} M_M &= \overrightarrow{i_s}^{\top} \frac{\partial \widetilde{\mathbf{L}}_{\mathbf{rs}}(\theta_r)}{\partial \theta_r} \vec{i}_r = \overline{\mathcal{W}_{\mathrm{m_s}} \underline{i}_s^{\natural}}^{\top} \frac{\partial \widetilde{\mathbf{L}}_{\mathbf{rs}}(\theta_r)}{\partial \theta_r} \mathcal{W}_{\mathrm{m_r}} \underline{i}_r^{\natural} \\ &= \overline{\underline{i}_s^{\natural}}^{\top} \frac{\partial}{\partial \theta_r} \left[\overline{\mathcal{W}_{\mathrm{m_s}}}^{\top} \widetilde{\mathbf{L}}_{\mathbf{rs}}(\theta_r) \mathcal{W}_{\mathrm{m_r}} \right] \underline{i}_r^{\natural} = \overline{\underline{i}_s^{\natural}}^{\top} \frac{\partial}{\partial \theta_r} \left[\mathcal{W}_{\mathrm{m_s}}^{-1} \widetilde{\mathbf{L}}_{\mathbf{rs}}(\theta_r) \mathcal{W}_{\mathrm{m_r}} \right] \underline{i}_r^{\natural} \\ &= \overline{\underline{i}_s^{\natural}}^{\top} \frac{\partial \widetilde{\mathbf{L}}_{\mathbf{rs}}^{\natural}(\theta_r)}{\partial \theta_r} \underline{i}_r^{\natural} \end{aligned} \tag{4.27}$$

The expression of the electromechanical torque given in (4.27) is consistent with [75].

In some situations, it may be preferable to express the torque as a function of $\underline{i}^{\natural}$ and $\mathbf{L}^{\natural}(\theta_r)$:

$$\begin{aligned} M_M &= \frac{1}{2}\left[\overline{\underline{i}_s^{\natural}}^{\top} \frac{\partial \widetilde{\mathbf{L}}_{\mathbf{rs}}^{\natural}(\theta_r)}{\partial \theta_r} \underline{i}_r^{\natural} + \overline{\underline{i}_s^{\natural}}^{\top} \frac{\partial \widetilde{\mathbf{L}}_{\mathbf{rs}}^{\natural}(\theta_r)}{\partial \theta_r} \underline{i}_r^{\natural} \right] = \frac{1}{2}\left[\overline{\underline{i}_s^{\natural}}^{\top} \frac{\partial \widetilde{\mathbf{L}}_{\mathbf{rs}}^{\natural}(\theta_r)}{\partial \theta_r} \underline{i}_r^{\natural} + \overline{\left(\overline{\underline{i}_s^{\natural}}^{\top} \frac{\partial \widetilde{\mathbf{L}}_{\mathbf{rs}}^{\natural}(\theta_r)}{\partial \theta_r} \underline{i}_r^{\natural} \right)}^{\top} \right] \\ &= \frac{1}{2}\left[\overline{\underline{i}_s^{\natural}}^{\top} \frac{\partial \widetilde{\mathbf{L}}_{\mathbf{rs}}^{\natural}(\theta_r)}{\partial \theta_r} \underline{i}_r^{\natural} + \overline{\underline{i}_r^{\natural}}^{\top} \overline{\frac{\partial \widetilde{\mathbf{L}}_{\mathbf{sr}}^{\natural}(\theta_r)}{\partial \theta_r}}^{\top} \underline{i}_s^{\natural} \right] = \frac{1}{2}\left[\overline{\underline{i}_s^{\natural}}^{\top} \frac{\partial \widetilde{\mathbf{L}}_{\mathbf{rs}}^{\natural}(\theta_r)}{\partial \theta_r} \underline{i}_r^{\natural} + \overline{\underline{i}_r^{\natural}}^{\top} \frac{\partial \widetilde{\mathbf{L}}_{\mathbf{rs}}^{\natural}(\theta_r)}{\partial \theta_r} \underline{i}_s^{\natural} \right] \\ &= \frac{1}{2}\begin{bmatrix} \overline{\underline{i}_s^{\natural}}^{\top} & \overline{\underline{i}_r^{\natural}}^{\top} \end{bmatrix} \begin{bmatrix} \mathbf{0} & \dfrac{\partial \widetilde{\mathbf{L}}_{\mathbf{rs}}^{\natural}(\theta_r)}{\partial \theta_r} \\ \dfrac{\partial \widetilde{\mathbf{L}}_{\mathbf{sr}}^{\natural}(\theta_r)}{\partial \theta_r} & \mathbf{0} \end{bmatrix} \begin{bmatrix} \underline{i}_s^{\natural} \\ \underline{i}_r^{\natural} \end{bmatrix} \\ &= \frac{1}{2}\overline{\underline{i}^{\natural}}^{\top} \frac{\partial \widetilde{\mathbf{L}}^{\natural}(\theta_r)}{\partial \theta_r} \underline{i}^{\natural} = \frac{1}{2}\overline{\underline{i}^{\natural}}^{\top} \frac{\partial \mathbf{L}^{\natural}(\theta_r)}{\partial \theta_r} \underline{i}^{\natural} \end{aligned} \tag{4.28}$$

4.2.3 Properties of the transformed resistance matrices $\mathbf{R_s^\natural}$ and $\mathbf{R_r^\natural}$

We now take a closer look at the structure of the transformed matrices introduced in section 4.2.1 and start with the resistance matrices $\mathbf{R_s^\natural}$ and $\mathbf{R_r^\natural}$. In the general case where each circuit has a different resistance, the matrices $\mathbf{R_s}$ and $\mathbf{R_r}$ have the following form:

$$\mathbf{R_s} = \operatorname{diag}\big[R_{s0}, \quad \dots \quad R_{sm}, \quad \dots \quad R_{sm_s-1}\big]$$

$$\mathbf{R_r} = \operatorname{diag}\big[R_{r0}, \quad \dots \quad R_{rn}, \quad \dots \quad R_{rm_r-1}\big]$$

Note that $\mathbf{R_s}$ and $\mathbf{R_r}$ are diagonal but not *circulant*. Applying the transformation to these matrices will not produce a diagonal matrix. The coefficient in row $k \in [\![0,\, m_s-1]\!]$ and column $l \in [\![0,\, m_s-1]\!]$ of $\mathbf{R_s^\natural}$ is given by:

$$R^\natural_{s,\,kl} = \frac{1}{m_s}\sum_{l'=0}^{m_s-1} W^{kl'}_{-m_s} R_{s\,l'} W^{l'l}_{m_s} = \frac{1}{m_s}\sum_{l'=0}^{m_s-1} R_{s\,l'} W^{l'(l-k)}_{m_s}$$

This expression cannot be further simplified without additional assumptions. When presuming that all stator (rotor) circuits have the same resistance R_s (R_r resp.), i.e.

$$\mathbf{R_s} = R_s\mathbf{I_{m_s}} \quad \text{and} \quad \mathbf{R_r} = R_r\mathbf{I_{m_r}}$$

$\mathbf{R_s^\natural}$ and $\mathbf{R_r^\natural}$ are diagonal as well:

$$\mathbf{R_s^\natural} = \mathcal{W}_{\mathrm{m_s}}^{-1} R_s \mathbf{I_{m_s}} \mathcal{W}_{\mathrm{m_s}} = R_s\mathbf{I_{m_s}} \tag{4.29}$$

$$\mathbf{R_r^\natural} = \mathcal{W}_{\mathrm{m_r}}^{-1} R_r \mathbf{I_{m_r}} \mathcal{W}_{\mathrm{m_r}} = R_r\mathbf{I_{m_r}} \tag{4.30}$$

4.2.4 Properties of the transformed leakage inductance matrices $\mathbf{L_{\sigma s}^\natural}$ and $\mathbf{L_{\sigma r}^\natural}$

If each circuit has a different leakage inductance, the matrices $\mathbf{L_{\sigma s}}$ and $\mathbf{L_{\sigma r}}$ are diagonal but not *circulant*:

$$\mathbf{L_{\sigma s}} = \operatorname{diag}\big[L_{\sigma s0}, \quad \dots \quad L_{\sigma sm}, \quad \dots \quad L_{\sigma sm_s-1}\big]$$

$$\mathbf{L_{\sigma r}} = \operatorname{diag}\big[L_{\sigma r0}, \quad \dots \quad L_{\sigma rn}, \quad \dots \quad L_{\sigma rm_r-1}\big]$$

The coefficient in row $k \in [\![0,\, m_s-1]\!]$ and column $l \in [\![0,\, m_s-1]\!]$ of $\mathbf{L_{\sigma s}^\natural}$ is:

$$L^\natural_{\sigma s,\,kl} = \frac{1}{m_s}\sum_{l'=0}^{m_s-1} L_{\sigma s\,l'} W^{l'(l-k)}_{m_s}$$

and cannot be simplified. Assuming that all stator (rotor) circuits have the same leakage inductance $L_{\sigma s}$ ($L_{\sigma r}$ resp.), i.e.:

$$\mathbf{L_{\sigma s}} = L_{\sigma s}\mathbf{I_{m_s}} \quad \text{and} \quad \mathbf{L_{\sigma r}} = L_{\sigma r}\mathbf{I_{m_r}}$$

results in $\mathbf{L_{\sigma s}^\natural}$ and $\mathbf{L_{\sigma r}^\natural}$ being diagonal:

$$\mathbf{L_{\sigma s}^\natural} = \mathcal{W}_{\mathrm{m_s}}^{-1} L_{\sigma s} \mathbf{I_{m_s}} \mathcal{W}_{\mathrm{m_s}} = L_{\sigma s}\mathbf{I_{m_s}} \tag{4.31}$$

$$\mathbf{L_{\sigma r}^\natural} = \mathcal{W}_{\mathrm{m_r}}^{-1} L_{\sigma r} \mathbf{I_{m_r}} \mathcal{W}_{\mathrm{m_r}} = L_{\sigma r}\mathbf{I_{m_r}} \tag{4.32}$$

4.2.5 Properties of the transformed main inductance matrices

In order to gain insight into the influence of each wavelength present in the air-gap quantities, the transformation will be carried out on the inductance submatrices associated with a single wavelength order $h \in \mathbb{N}^\star$, i.e. $\widetilde{\mathbf{L}}_{\mathbf{s\,h}}$ and $\widetilde{\mathbf{L}}_{\mathbf{rs\,h}}(\theta_r)$ on the stator side and $\widetilde{\mathbf{L}}_{\mathbf{r\,h}}$ and $\widetilde{\mathbf{L}}_{\mathbf{sr\,h}}(\theta_r)$ on the rotor side. As in

section 3.4.5, the expression of the transformed total main inductance matrix is obtained subsequently by adding the contributions of all wavelengths.

Transformed stator main inductance matrix of wavelength h, $\widetilde{\mathbf{L}}^{\natural}_{\mathbf{s\,h}}$

The transformed stator main inductance matrix of wavelength h is defined as follows:

$$\widetilde{\mathbf{L}}^{\natural}_{\mathbf{s\,h}} = \mathcal{W}_{\mathrm{m_s}}^{-1}\widetilde{\mathbf{L}}_{\mathbf{s\,h}}\mathcal{W}_{\mathrm{m_s}} \tag{4.33}$$

Owing to section 4.1 and, since the coefficients of $\widetilde{\mathbf{L}}_{\mathbf{s\,h}}$ are real numbers,

$$\begin{aligned}\widetilde{\mathbf{L}}^{\natural}_{\mathbf{s\,h}} &= \overline{\mathcal{W}_{\mathrm{m_s}}}^{\top}\widetilde{L}_{s,\,h}\widetilde{\mathbf{T}}^{\top}_{\mathbf{Cs\,h}}\widetilde{\mathbf{T}}_{\mathbf{Cs\,h}}\mathcal{W}_{\mathrm{m_s}} \\ &= \widetilde{L}_{s,\,h}\overline{\widetilde{\mathbf{T}}_{\mathbf{Cs\,h}}\mathcal{W}_{\mathrm{m_s}}}^{\top}\widetilde{\mathbf{T}}_{\mathbf{Cs\,h}}\mathcal{W}_{\mathrm{m_s}}\end{aligned} \tag{4.34}$$

Furthermore, there exists a unique $k_0 \in [\![0,\, m_s - 1]\!]$ such that

$$\widetilde{\mathbf{L}}^{\natural}_{\mathbf{s\,h}} = \widetilde{L}_{s,\,h}\overline{\widetilde{\mathbf{T}}_{\mathbf{Cs\,k_0}}\mathcal{W}_{\mathrm{m_s}}}^{\top}\widetilde{\mathbf{T}}_{\mathbf{Cs\,k_0}}\mathcal{W}_{\mathrm{m_s}} \tag{4.35}$$

Working out the matrix product in (4.35) leads to the following general expression of $\widetilde{\mathbf{L}}^{\natural}_{\mathbf{s\,h}}$ as a diagonal matrix with at most two non-zero eigenvalues (see details in appendix A.2.3):

$$\widetilde{\mathbf{L}}^{\natural}_{\mathbf{s\,h}} = \frac{m_s}{2}\widetilde{L}_{s,\,h}\begin{array}{c} \\ \\ \\ k{=}k_0 \\ \\ \\ k{=}m_s{-}k_0 \\ \\ \\ \end{array}\begin{array}{c} \begin{array}{ccccccccccc} & & & m{=}k_0 & & & & & m{=}m_s{-}k_0 & & \end{array} \\ \begin{bmatrix} & & & 0 & & & & 0 & & & \\ & 0 & & \vdots & & 0 & & \vdots & & 0 & \\ & & & 0 & & & & 0 & & & \\ 0 & \cdots & 0 & 1 & 0 & \cdots & 0 & 0 & 0 & \cdots & 0 \\ & & & 0 & & & & 0 & & & \\ & 0 & & \vdots & & 0 & & \vdots & & 0 & \\ & & & 0 & & & & 0 & & & \\ 0 & \cdots & 0 & 0 & 0 & \cdots & 0 & 1 & 0 & \cdots & 0 \\ & & & 0 & & & & 0 & & & \\ & 0 & & \vdots & & 0 & & \vdots & & 0 & \\ & & & 0 & & & & 0 & & & \end{bmatrix} \end{array} \tag{4.36}$$

Note that the position of the non-zero diagonal elements depends on the wavelength order considered.

Transformed rotor main inductance matrix of wavelength h, $\widetilde{\mathbf{L}}^{\natural}_{\mathbf{r\,h}}$

The transformation of the rotor main inductance matrix associated with wavelength h is performed analogously:

$$\begin{aligned}\widetilde{\mathbf{L}}^{\natural}_{\mathbf{r\,h}} &= \mathcal{W}_{\mathrm{m_r}}^{-1}\widetilde{\mathbf{L}}_{\mathbf{r\,h}}\mathcal{W}_{\mathrm{m_r}} \\ &= \overline{\mathcal{W}_{\mathrm{m_r}}}^{\top}\widetilde{L}_{r,\,h}\widetilde{\mathbf{T}}^{\top}_{\mathbf{Cr\,h}}\widetilde{\mathbf{T}}_{\mathbf{Cr\,h}}\mathcal{W}_{\mathrm{m_r}} \\ &= \widetilde{L}_{r,\,h}\overline{\widetilde{\mathbf{T}}_{\mathbf{Cr\,h}}\mathcal{W}_{\mathrm{m_r}}}^{\top}\widetilde{\mathbf{T}}_{\mathbf{Cr\,h}}\mathcal{W}_{\mathrm{m_r}}\end{aligned} \tag{4.37}$$

There exists a unique $l_0 \in [\![0,\, m_r - 1]\!]$ such that

$$\widetilde{\mathbf{L}}^{\natural}_{\mathbf{r\,h}} = \widetilde{L}_{r,\,h}\overline{\widetilde{\mathbf{T}}_{\mathbf{Cr\,l_0}}\mathcal{W}_{\mathrm{m_r}}}^{\top}\widetilde{\mathbf{T}}_{\mathbf{Cr\,l_0}}\mathcal{W}_{\mathrm{m_r}} \tag{4.38}$$

The computation of the matrix product in (4.38) yields a diagonal matrix with at most two non-zero eigenvalues as well (cf. appendix A.2.3):

$$\widetilde{\mathbf{L}}^{\natural}_{\mathbf{r\,h}} = \frac{m_r}{2}\widetilde{L}_{r,h} \begin{array}{c} \\ \\ \\ l{=}l_0 \\ \\ \\ \\ l{=}m_r{-}l_0 \\ \\ \\ \end{array} \begin{array}{c} \begin{array}{ccccccccccccc} & & & n{=}l_0 & & & & & & n{=}m_r{-}l_0 & & & \end{array} \\ \begin{bmatrix} & & & 0 & & & & & & 0 & & & \\ & 0 & & \vdots & & 0 & & & & \vdots & & 0 & \\ & & & 0 & & & & & & 0 & & & \\ 0 & \cdots & 0 & 1 & 0 & \cdots & 0 & & 0 & 0 & \cdots & 0 \\ & & & 0 & & & & & & 0 & & & \\ & 0 & & \vdots & & 0 & & & & \vdots & & 0 & \\ & & & 0 & & & & & & 0 & & & \\ 0 & \cdots & 0 & 0 & 0 & \cdots & 0 & & 1 & 0 & \cdots & 0 \\ & & & 0 & & & & & & 0 & & & \\ & 0 & & \vdots & & 0 & & & & \vdots & & 0 & \\ & & & 0 & & & & & & 0 & & & \end{bmatrix} \end{array} \tag{4.39}$$

The wavelength order determines the position of the non-zero entries on the diagonal.

Transformed mutual inductance matrix of wavelength h

The mutual inductance matrix for the wavelength of order h, $\widetilde{\mathbf{L}}_{\mathbf{rs\,h}}(\theta_r)$, is transformed as follows:

$$\begin{aligned} \widetilde{\mathbf{L}}^{\natural}_{\mathbf{rs\,h}} &= \mathcal{W}_{\mathrm{m_s}}^{-1}\widetilde{\mathbf{L}}_{\mathbf{rs\,h}}\mathcal{W}_{\mathrm{m_r}} \\ &= \overline{\mathcal{W}_{\mathrm{m_s}}}^{\top} L_{M,h}\widetilde{\mathbf{T}}^{\top}_{\mathbf{Cs\,h}}\mathbf{T}(\theta'_{r,h})\widetilde{\mathbf{T}}_{\mathbf{Cr\,h}}\mathcal{W}_{\mathrm{m_r}} \\ &= L_{M,h}\overline{\widetilde{\mathbf{T}}_{\mathbf{Cs\,h}}\mathcal{W}_{\mathrm{m_s}}}^{\top}\mathbf{T}(\theta'_{r,h})\widetilde{\mathbf{T}}_{\mathbf{Cr\,h}}\mathcal{W}_{\mathrm{m_r}} \end{aligned} \tag{4.40}$$

where $\theta'_{r,h} = h\theta_r - \varphi_h$.

A detailed analysis of above matrix product can be found in appendix A.2.3 and demonstrates that, in the general case, at most two entries of $\widetilde{\mathbf{L}}^{\natural}_{\mathbf{rs\,h}}$ are non-zero:

$$\widetilde{\mathbf{L}}^{\natural}_{\mathbf{rs\,h}} = L_{M,h}\frac{\sqrt{m_s m_r}}{2} \begin{array}{c} \\ \\ \\ k{=}k_0 \\ \\ \\ \\ k{=}m_s{-}k_0 \\ \\ \\ \end{array} \begin{array}{c} \begin{array}{ccccccccccccc} & & & n{=}l_0 & & & & & & n{=}m_r{-}l_0 & & & \end{array} \\ \begin{bmatrix} & & & 0 & & & & & & 0 & & & \\ & 0 & & \vdots & & 0 & & & & \vdots & & 0 & \\ & & & 0 & & & & & & 0 & & & \\ 0 & \cdots & 0 & e^{j\theta'_{r,h}} & 0 & \cdots & 0 & & 0 & 0 & \cdots & 0 \\ & & & 0 & & & & & & 0 & & & \\ & 0 & & \vdots & & 0 & & & & \vdots & & 0 & \\ & & & 0 & & & & & & 0 & & & \\ 0 & \cdots & 0 & 0 & 0 & \cdots & 0 & & e^{-j\theta'_{r,h}} & 0 & \cdots & 0 \\ & & & 0 & & & & & & 0 & & & \\ & 0 & & \vdots & & 0 & & & & \vdots & & 0 & \\ & & & 0 & & & & & & 0 & & & \end{bmatrix} \end{array} \tag{4.41}$$

As for the transformed stator and rotor inductance submatrices, the position of the non-zero elements results from the wavelength order under consideration.

The transformation of the matrix expressing the contribution of stator currents to rotor fluxes,

$\widetilde{\mathbf{L}}_{\mathbf{sr\,h}}(\theta_r)$, is straightforward:

$$\begin{aligned}\widetilde{\mathbf{L}}^{\natural}_{\mathbf{sr\,h}} &= \mathcal{W}_{\mathrm{m_r}}^{-1}\widetilde{\mathbf{L}}_{\mathbf{sr\,h}}\mathcal{W}_{\mathrm{m_s}} = \overline{\mathcal{W}_{\mathrm{m_r}}}^{\top}\widetilde{\mathbf{L}}^{\top}_{\mathbf{rs\,h}}\mathcal{W}_{\mathrm{m_s}} \\ &= \left[\mathcal{W}^{\top}_{\mathrm{m_s}}\widetilde{\mathbf{L}}_{\mathbf{rs\,h}}\overline{\mathcal{W}_{\mathrm{m_r}}}\right]^{\top}\end{aligned}$$

As the coefficients of $\widetilde{\mathbf{L}}_{\mathbf{rs\,h}}(\theta_r)$ are real, $\overline{\widetilde{\mathbf{L}}_{\mathbf{rs\,h}}}(\theta_r) = \widetilde{\mathbf{L}}_{\mathbf{rs\,h}}(\theta_r)$ and

$$\widetilde{\mathbf{L}}^{\natural}_{\mathbf{sr\,h}} = \overline{\left[\overline{\mathcal{W}_{\mathrm{m_s}}}^{\top}\widetilde{\mathbf{L}}_{\mathbf{rs\,h}}\mathcal{W}_{\mathrm{m_r}}\right]}^{\top} = \overline{\left[\mathcal{W}^{-1}_{\mathrm{m_s}}\widetilde{\mathbf{L}}_{\mathbf{rs\,h}}\mathcal{W}_{\mathrm{m_r}}\right]}^{\top} = \overline{\widetilde{\mathbf{L}}^{\natural}_{\mathbf{rs\,h}}}^{\top} \tag{4.42}$$

Transformed total main inductance matrix $\widetilde{\mathbf{L}}^{\natural}$

For a given wavelength h, the above results show that the transformation operators $\mathcal{T}_{\mathcal{W}m_s}$ and $\mathcal{T}_{\mathcal{W}m_r}$, besides diagonalizing the stator and rotor inductance submatrices, produce particularly simple transformed mutual inductance submatrices. In order to examine the consequences for the total main inductance matrix, we introduce the following linear map:

Definition 7:
For $(m,\, n) \in (\mathbb{N}^{\star})^2$, let $\Gamma_{(m,n)}$ be the linear map:

$$\begin{array}{rccc}\Gamma_{(m,n)}: & \mathcal{M}_{m,n}(\mathbb{C}) & \longrightarrow & \mathcal{M}_{m,n}(\mathbb{C}) \\ & \mathbf{M} & \longmapsto & \Gamma_{(m,n)}(\mathbf{M}) = \mathcal{W}_{\mathrm{m}}^{-1}\mathbf{M}\mathcal{W}_{\mathrm{n}}\end{array} \tag{4.43}$$

where $\mathcal{M}_{m,n}(\mathbb{C})$ is the set of $m \times n$ matrices with entries in $\mathbb{C}$.

The relations (4.33), (4.37) and (4.40), which relate an inductance submatrix to its transformed representation, can be rewritten as follows:

$$\widetilde{\mathbf{L}}^{\natural}_{\mathbf{s\,h}} = \Gamma_{(m_s,m_s)}(\widetilde{\mathbf{L}}_{\mathbf{s\,h}}) \tag{4.44}$$

$$\widetilde{\mathbf{L}}^{\natural}_{\mathbf{r\,h}} = \Gamma_{(m_r,m_r)}(\widetilde{\mathbf{L}}_{\mathbf{r\,h}}) \tag{4.45}$$

$$\widetilde{\mathbf{L}}^{\natural}_{\mathbf{rs\,h}} = \Gamma_{(m_s,m_r)}(\widetilde{\mathbf{L}}_{\mathbf{rs\,h}}) \tag{4.46}$$

Recalling the definition of $\widetilde{\mathbf{L}}_{\mathcal{H}}$, with $\mathcal{H} \subset \mathbb{N}^{\star}$,

$$\mathbf{L}_{\mathcal{H}} = \begin{bmatrix} \displaystyle\sum_{h\in\mathcal{H}} \widetilde{\mathbf{L}}_{\mathbf{s\,h}} & \displaystyle\sum_{h\in\mathcal{H}} \widetilde{\mathbf{L}}_{\mathbf{rs\,h}}(\theta_r) \\ \displaystyle\sum_{h\in\mathcal{H}} \widetilde{\mathbf{L}}_{\mathbf{sr\,h}}(\theta_r) & \displaystyle\sum_{h\in\mathcal{H}} \widetilde{\mathbf{L}}_{\mathbf{r\,h}} \end{bmatrix} \tag{4.47}$$

we introduce the transformed main inductance matrix for the set of wavelengths $\mathcal{H}$ in accordance with the rules set out in section 4.2.1:

$$\widetilde{\mathbf{L}}^{\natural}_{\mathcal{H}} = \begin{bmatrix} \Gamma_{(m_s,m_s)}\left(\displaystyle\sum_{h\in\mathcal{H}} \widetilde{\mathbf{L}}_{\mathbf{s\,h}}\right) & \Gamma_{(m_s,m_r)}\left(\displaystyle\sum_{h\in\mathcal{H}} \widetilde{\mathbf{L}}_{\mathbf{rs\,h}}(\theta_r)\right) \\ \Gamma_{(m_r,m_s)}\left(\displaystyle\sum_{h\in\mathcal{H}} \widetilde{\mathbf{L}}_{\mathbf{sr\,h}}(\theta_r)\right) & \Gamma_{(m_r,m_r)}\left(\displaystyle\sum_{h\in\mathcal{H}} \widetilde{\mathbf{L}}_{\mathbf{r\,h}}\right) \end{bmatrix} \tag{4.48}$$

Owing to the linearity of Γ,

$$\widetilde{\mathbf{L}}^{\natural}_{\mathcal{H}} = \begin{bmatrix} \sum\limits_{h\in\mathcal{H}} \widetilde{\mathbf{L}}^{\natural}_{\mathbf{s}\,\mathbf{h}} & \sum\limits_{h\in\mathcal{H}} \widetilde{\mathbf{L}}^{\natural}_{\mathbf{rs}\,\mathbf{h}}(\theta_r) \\ \sum\limits_{h\in\mathcal{H}} \widetilde{\mathbf{L}}^{\natural}_{\mathbf{sr}\,\mathbf{h}}(\theta_r) & \sum\limits_{h\in\mathcal{H}} \widetilde{\mathbf{L}}^{\natural}_{\mathbf{r}\,\mathbf{h}} \end{bmatrix} \tag{4.49}$$

Note also that Γ being a linear map in a finite dimensional vector space, it is continuous. For this reason, the partial sum

$$\begin{bmatrix} \sum\limits_{h=1}^{N} \widetilde{\mathbf{L}}^{\natural}_{\mathbf{s}\,\mathbf{h}} & \sum\limits_{h=1}^{N} \widetilde{\mathbf{L}}^{\natural}_{\mathbf{rs}\,\mathbf{h}}(\theta_r) \\ \sum\limits_{h=1}^{N} \widetilde{\mathbf{L}}^{\natural}_{\mathbf{sr}\,\mathbf{h}}(\theta_r) & \sum\limits_{h=1}^{N} \widetilde{\mathbf{L}}^{\natural}_{\mathbf{r}\,\mathbf{h}} \end{bmatrix}, \; N \in \mathbb{N}^{\star}$$

converges towards

$$\widetilde{\mathbf{L}}^{\natural}(\theta_r) = \begin{bmatrix} \sum\limits_{h\in\mathbb{N}^{\star}} \widetilde{\mathbf{L}}^{\natural}_{\mathbf{s}\,\mathbf{h}} & \sum\limits_{h\in\mathbb{N}^{\star}} \widetilde{\mathbf{L}}^{\natural}_{\mathbf{rs}\,\mathbf{h}}(\theta_r) \\ \sum\limits_{h\in\mathbb{N}^{\star}} \widetilde{\mathbf{L}}^{\natural}_{\mathbf{sr}\,\mathbf{h}}(\theta_r) & \sum\limits_{h\in\mathbb{N}^{\star}} \widetilde{\mathbf{L}}^{\natural}_{\mathbf{r}\,\mathbf{h}} \end{bmatrix} \tag{4.50}$$

when $N \longrightarrow \infty$ and

$$\begin{aligned} \widetilde{\mathbf{L}}^{\natural}(\theta_r) &= \begin{bmatrix} \mathcal{W}_{\mathrm{m_s}}^{-1}\left[\sum\limits_{h\in\mathbb{N}^{\star}} \widetilde{\mathbf{L}}_{\mathbf{s}\,\mathbf{h}}\right]\mathcal{W}_{\mathrm{m_s}} & \mathcal{W}_{\mathrm{m_s}}^{-1}\left[\sum\limits_{h\in\mathbb{N}^{\star}} \widetilde{\mathbf{L}}_{\mathbf{rs}\,\mathbf{h}}(\theta_r)\right]\mathcal{W}_{\mathrm{m_r}} \\ \mathcal{W}_{\mathrm{m_r}}^{-1}\left[\sum\limits_{h\in\mathbb{N}^{\star}} \widetilde{\mathbf{L}}_{\mathbf{sr}\,\mathbf{h}}(\theta_r)\right]\mathcal{W}_{\mathrm{m_s}} & \mathcal{W}_{\mathrm{m_r}}^{-1}\left[\sum\limits_{h\in\mathbb{N}^{\star}} \widetilde{\mathbf{L}}_{\mathbf{r}\,\mathbf{h}}\right]\mathcal{W}_{\mathrm{m_r}} \end{bmatrix} \\ &= \begin{bmatrix} \mathcal{W}_{\mathrm{m_s}}^{-1}\widetilde{\mathbf{L}}_{\mathbf{s}}\mathcal{W}_{\mathrm{m_s}} & \mathcal{W}_{\mathrm{m_s}}^{-1}\widetilde{\mathbf{L}}_{\mathbf{rs}}\mathcal{W}_{\mathrm{m_r}} \\ \mathcal{W}_{\mathrm{m_r}}^{-1}\widetilde{\mathbf{L}}_{\mathbf{sr}}\mathcal{W}_{\mathrm{m_s}} & \mathcal{W}_{\mathrm{m_r}}^{-1}\widetilde{\mathbf{L}}_{\mathbf{r}}\mathcal{W}_{\mathrm{m_r}} \end{bmatrix} = \begin{bmatrix} \mathcal{W}_{\mathrm{m_s}}^{-1} & \mathbf{0} \\ \mathbf{0} & \mathcal{W}_{\mathrm{m_r}}^{-1} \end{bmatrix} \widetilde{\mathbf{L}}(\theta_r) \begin{bmatrix} \mathcal{W}_{\mathrm{m_s}} & \mathbf{0} \\ \mathbf{0} & \mathcal{W}_{\mathrm{m_r}} \end{bmatrix} \end{aligned} \tag{4.51}$$

The results (4.49) and (4.51) justify our approach to first transform the inductance matrices of each single wavelength and, in a second step, add their contributions together to obtain the inductance matrices of the transformed model. This observation allows us to draw the following conclusions:

- the transformed total stator and rotor inductance submatrices are diagonal;
- the transformed mutual inductance matrices become dense when the number of considered wavelengths increases.

Moreover, these statements together with the position of the non-zero eigenvalues of the transformed stator main inductance submatrix $\widetilde{\mathbf{L}}^{\natural}_{\mathbf{s}}$ provide us with a means of segregating the wavelengths depending on their impact on the components of transformed stator quantities. Assuming a finite number of wavelengths is taken into account, if the greatest wavelength order considered is less than half the number of stator circuits, $m_s/2$, the effect of each wavelength will indeed be reflected in a separate component of the transformed stator current and flux linkage vectors. This is due to the fact that the non-zero eigenvalues of $\widetilde{\mathbf{L}}^{\natural}_{\mathbf{s}}$ appear at different positions on the diagonal.

In contrast, if the order of at least one wavelength is greater than $m_s/2$, some eigenvalues of $\widetilde{\mathbf{L}}^{\natural}_{\mathbf{s}}$ may be the sum of contributions arising from different wavelengths, the effect of which then appears in the same components of the transformed stator current and flux linkage vectors. A well-known analogy is the 'aliasing' phenomenon which occurs when a signal is sampled at a frequency less than twice

the maximal frequency present in its spectrum. Thus, using as many stator circuits in the model as possible may seem advantageous if the objective is to understand the influence of every single wavelength on the machine behaviour. However, we will see in the analysis of practical examples that the necessary process of interconnecting the circuits to account for the winding configuration of the real machine is a limiting factor in that respect.

4.2.6 Continuous-time transformed state-space model

The relations (4.26), (4.27) and (2.19) provide all the information required to set up a transformed state-space model of the induction machine which includes the effect of conductor distribution harmonics. We select the components of the transformed current vector $\underline{i}^\natural$, alongside the rotor angular velocity ω_r and the rotor angle θ_r as state variables. The components of the transformed voltage vector $\underline{u}^\natural$ and the load torque M_L will be the model inputs.

To do so, we need to ensure that the transformed total inductance matrix $\mathbf{L}^\natural$ is invertible, since the voltage equation (4.26) has to be solved for the current vector derivative. This is readily verified by taking a look at the relation between $\mathbf{L}^\natural(\theta_r)$ and $\mathbf{L}(\theta_r)$:

$$\mathbf{L}^\natural(\theta_r) = \begin{bmatrix} \mathcal{W}_{\mathrm{m_s}} & \mathbf{0} \\ \mathbf{0} & \mathcal{W}_{\mathrm{m_r}} \end{bmatrix}^{-1} \mathbf{L}(\theta_r) \begin{bmatrix} \mathcal{W}_{\mathrm{m_s}} & \mathbf{0} \\ \mathbf{0} & \mathcal{W}_{\mathrm{m_r}} \end{bmatrix}$$

Thus, $\mathbf{L}^\natural(\theta_r)$ and $\mathbf{L}(\theta_r)$ are similar and $\mathbf{L}(\theta_r)$ having full rank, so does $\mathbf{L}^\natural(\theta_r)$.

The continuous-time state-space model of the transformed linear geometric model follows:

$$\left[\begin{array}{l} \dfrac{\mathrm{d}\underline{i}^\natural}{\mathrm{d}t} = -\mathbf{L}^{\natural\,-1}(\theta_r)\left[\mathbf{R}^\natural + \omega_r \dfrac{\partial \mathbf{L}^\natural(\theta_r)}{\partial \theta_r}\right]\underline{i}^\natural + \mathbf{L}^{\natural\,-1}(\theta_r)\underline{u}^\natural \qquad (4.52a) \\ \dfrac{\mathrm{d}\omega_r}{\mathrm{d}t} = \dfrac{1}{J_M}\left[\dfrac{1}{2}\underline{i}^{\natural\top} \dfrac{\partial \mathbf{L}^\natural(\theta_r)}{\partial \theta_r}\underline{i}^\natural - M_L - C_W\omega_r\right] \qquad (4.52b) \\ \dfrac{\mathrm{d}\theta_r}{\mathrm{d}t} = \omega_r \qquad (4.52c) \end{array}\right.$$

Note that the general form of the equations describing the transformed model is the same as the one of the original (cf. (3.62)). This is to be expected since both models represent the same physical phenomena and confirms that the transformation is consistent.

Similarly to section 3.6, it is convenient to introduce the notations

$$\mathbf{A}^\natural(\omega_r,\, \theta_r) = -\mathbf{L}^{\natural\,-1}(\theta_r)\left[\mathbf{R}^\natural + \omega_r \frac{\partial \mathbf{L}^\natural(\theta_r)}{\partial \theta_r}\right]; \qquad \mathbf{B}^\natural(\theta_r) = \mathbf{L}^{\natural\,-1}(\theta_r)$$

which lead to the following compact model representation:

$$\left[\begin{array}{l} \dfrac{\mathrm{d}\underline{i}^\natural}{\mathrm{d}t} = \mathbf{A}^\natural(\omega_r,\, \theta_r)\underline{i}^\natural + \mathbf{B}^\natural(\theta_r)\underline{u}^\natural \qquad (4.53a) \\ \dfrac{\mathrm{d}\omega_r}{\mathrm{d}t} = \dfrac{1}{J_M}\left[\dfrac{1}{2}\underline{i}^{\natural\top} \dfrac{\partial \mathbf{B}^{\natural\,-1}(\theta_r)}{\partial \theta_r}\underline{i}^\natural - M_L - C_W\omega_r\right] \qquad (4.53b) \\ \dfrac{\mathrm{d}\theta_r}{\mathrm{d}t} = \omega_r \qquad (4.53c) \end{array}\right.$$

4.2.7 Transformation in presence of circuit interconnections

As described in the previous chapters, it is necessary to interconnect the electrical circuits present in the model in order to achieve a correct representation of the considered machine. This aspect has not been addressed in our approach so far, as potential constraints on the components of $\underline{u}^\natural$, i.e. the model inputs, have been ignored. In order to tackle this issue, we make use of the interconnection matrices $\mathbf{C_s}$ and $\mathbf{C_r}$ alongside the vectors of independent stator (rotor) voltages and currents, $\vec{u}'_s$ and $\vec{i}'_s$ ($\vec{u}'_r$ and $\vec{i}'_r$ resp.), as we did in chapter 3.

Combining relation (2.26a) and the definition of $\underline{i}^\natural_s$, we obtain:

$$\underline{i}^\natural_s = \mathcal{W}_{\mathrm{m_s}}^{-1}\mathbf{C_s}\vec{i}'_s = \left[\overline{\mathcal{W}_{\mathrm{m_s}}}^\top \mathbf{C_s}\right]\vec{i}'_s \tag{4.54a}$$

Definition 8: Transformation matrix for independent stator currents
We denote $\mathcal{Z}_\mathrm{s}$ *the matrix product* $\overline{\mathcal{W}_{\mathrm{m_s}}}^\top \mathbf{C_s}$. $\mathcal{Z}_\mathrm{s} \in \mathcal{M}_{m_s \times m'_s}(\mathbb{C})$

Therefore, $\mathcal{Z}_\mathrm{s}$ allows for the computation of the *transformed* stator currents from the *independent* stator currents.

Similarly, substituting the definition of $\underline{u}^\natural_s$ into (2.26b) and recalling that $\mathbf{C_s} = \overline{\mathbf{C_s}}$ yields:

$$\begin{aligned}\vec{u}'_s &= \mathbf{C_s}^\top \mathcal{W}_{\mathrm{m_s}} \underline{u}^\natural_s = \overline{\left[\overline{\mathcal{W}_{\mathrm{m_s}}}^\top \mathbf{C_s}\right]}^\top \underline{u}^\natural_s \\ &= \overline{\mathcal{Z}_\mathrm{s}}^\top \underline{u}^\natural_s \end{aligned} \tag{4.54b}$$

Thus, the complex conjugate transpose of $\mathcal{Z}_\mathrm{s}$ enables us to calculate the *independent* stator voltages from the *transformed* stator voltages.

Analogously, the relations for rotor quantities are:

$$\underline{i}^\natural_r = \mathcal{W}_{\mathrm{m_r}}^{-1}\mathbf{C_r}\vec{i}'_r = \left[\overline{\mathcal{W}_{\mathrm{m_r}}}^\top \mathbf{C_r}\right]\vec{i}'_r \tag{4.55a}$$

$$\vec{u}'_r = \overline{\left[\overline{\mathcal{W}_{\mathrm{m_r}}}^\top \mathbf{C_r}\right]}^\top \underline{u}^\natural_r \tag{4.55b}$$

Definition 9: Transformation matrix for independent rotor currents
The matrix product $\overline{\mathcal{W}_{\mathrm{m_r}}}^\top \mathbf{C_r}$ *is denoted* $\mathcal{Z}_\mathrm{r}$. $\mathcal{Z}_\mathrm{r} \in \mathcal{M}_{m_r \times m'_r}(\mathbb{C})$

Remark 4: Transformation of rotor voltages for squirrel-cage machines
Following the considerations in section 2.3.4, the interconnection matrix for the circuits of a rotor cage is the identity matrix. Since $\vec{u}'_r = \vec{u}_r = \vec{0}$, $\underline{u}^\natural_r = \underline{0}$ *as well.*

If necessary, stator and rotor equations can be combined together, which results in the subsequent relations:

$$\underline{i}^\natural = \begin{bmatrix}\underline{i}^\natural_s \\ \underline{i}^\natural_r\end{bmatrix} = \begin{bmatrix}\mathcal{Z}_\mathrm{s} & \mathbf{0} \\ \mathbf{0} & \mathcal{Z}_\mathrm{r}\end{bmatrix}\begin{bmatrix}\vec{i}'_s \\ \vec{i}'_r\end{bmatrix} = \mathcal{Z}\vec{i}' \qquad \text{where} \qquad \mathcal{Z} = \begin{bmatrix}\mathcal{Z}_\mathrm{s} & \mathbf{0} \\ \mathbf{0} & \mathcal{Z}_\mathrm{r}\end{bmatrix} \tag{4.56a}$$

$$\vec{u}' = \begin{bmatrix}\vec{u}'_s \\ \vec{u}'_r\end{bmatrix} = \begin{bmatrix}\overline{\mathcal{Z}_\mathrm{s}}^\top & \mathbf{0} \\ \mathbf{0} & \overline{\mathcal{Z}_\mathrm{r}}^\top\end{bmatrix}\begin{bmatrix}\underline{u}^\natural_s \\ \underline{u}^\natural_r\end{bmatrix} = \overline{\mathcal{Z}}^\top \underline{u}^\natural \tag{4.56b}$$

Substituting these expressions into the voltage equation (4.26) leads to:

$$\vec{u}' = \overline{\mathcal{Z}}^\top \underline{u}^\natural = \overline{\mathcal{Z}}^\top \mathbf{R}^\natural \underline{i}^\natural + \overline{\mathcal{Z}}^\top \mathbf{L}^\natural \frac{\mathrm{d}\underline{i}^\natural}{\mathrm{d}t} + \omega_r \overline{\mathcal{Z}}^\top \frac{\partial \mathbf{L}^\natural}{\partial \theta_r}\underline{i}^\natural$$

$$= \overline{\mathcal{Z}}^{\top}\mathbf{R}^{\natural}\mathcal{Z}\vec{i}' + \overline{\mathcal{Z}}^{\top}\mathbf{L}^{\natural}\mathcal{Z}\frac{\mathrm{d}\vec{i}'}{\mathrm{d}t} + \omega_r\frac{\partial\overline{\mathcal{Z}}^{\top}\mathbf{L}^{\natural}\mathcal{Z}}{\partial\theta_r}\vec{i}' \tag{4.57}$$

A comparison of this result with (3.55) yields the following relations:

$$\mathbf{R}' = \overline{\mathcal{Z}}^{\top}\mathbf{R}^{\natural}\mathcal{Z} \tag{4.58a}$$

$$\mathbf{L}' = \overline{\mathcal{Z}}^{\top}\mathbf{L}^{\natural}\mathcal{Z} \tag{4.58b}$$

Remark 5:
The fact that $\mathcal{Z}$ is not invertible hinders the determination of $\underline{u}^{\natural}$ from $\vec{u}'$ (or $\vec{i}'$ from $\underline{i}^{\natural}$). Although this may seem at first sight problematic, we will discuss workarounds while analysing practical examples.

4.3 Application to the investigated machines

4.3.1 Adopted approach

Discussing several examples involving the machines IM1 and IM2, we will see how the general form of the transformed model (4.53) evolves when a few wavelengths are considered. This will also provide the opportunity to illustrate the method for setting up the model equations. More specifically, we will focus on:

1.) the derivation of the fundamental model (i.e. the model with $\mathcal{H} = \{1\}$) for IM1, to show the consistency of the proposed approach;

2.) the extension of the fundamental model to the wavelength of order 17 ($\mathcal{H} = \{1;\ 17\}$);

3.) the derivation of the transformed model of IM2 with $\mathcal{H} = \{2;\ 26\}$.

The equations of each model will be derived step-by-step with detailed intermediate calculations to help the reader understand the methodology. The workflow includes the following tasks:

1.) work out the expressions of the transformed inductance matrices for each of the wavelengths taken into account;

2.) deduce the transformed total inductance matrix;

3.) set up the voltage and torque equations of the transformed model;

4.) eliminate the unnecessary voltage equations to determine the state-space representation of the transformed model.

The transformed model of IM1 with $\mathcal{H} = \{1;\ 17\}$ and the one of IM2 with $\mathcal{H} = \{2;\ 26\}$ will be compared to the original versions presented in chapter 3 by means of simulations and experiments. These two models are also discussed in [76].

In addition to the hypotheses made in section 3.3, we assume that all stator windings have the same resistance R_s and the same leakage inductance $L_{\sigma s}$. Likewise, all circuits modelling the rotor cage have the resistance R_r and the leakage inductance $L_{\sigma r}$. As explained in sections 4.2.3 and 4.2.4, this is necessary to ensure that the transformed resistance and leakage inductance matrices are diagonal.

4.3.2 Deriving the fundamental model of a squirrel cage induction machine

We illustrate the derivation of the well-known fundamental model of induction machines in the case of IM1. We therefore consider that the conductor distribution functions as well as the air-gap flux density distribution exhibit a single wavelength of order $h = 1$. Hence, the distributed quantities are sinusoidal functions of the air-gap coordinates, which corresponds to Park's modelling hypotheses.

We recall from section 3.7.1 that each of the $w_s = 3$ stator windings of IM1 is modelled using an electrical circuit, i.e. $m_s = 3$. The cage with $N_r = 16$ rotor bars is accounted for with $m_r = 16$ rotor circuits.

Transformed stator and rotor resistance matrices

As stator circuits are assumed to have the same resistance, following (4.29), the transformed stator resistance matrix results in:

$$\mathbf{R_s^\natural} = R_s \begin{array}{c} \\ k{=}0 \\ \\ k{=}2 \end{array} \begin{array}{c} \begin{array}{ccc} m{=}0 & & m{=}2 \end{array} \\ \begin{bmatrix} 1 & 0 & 0 \\ 0 & 1 & 0 \\ 0 & 0 & 1 \end{bmatrix} \end{array} \tag{4.59}$$

Similarly, (4.30) yields:

$$\mathbf{R_r^\natural} = R_r \begin{array}{c} \\ l{=}0 \\ \\ l{=}15 \end{array} \begin{array}{c} \begin{array}{ccc} n{=}0 & & n{=}15 \end{array} \\ \begin{bmatrix} 1 & & \\ & \ddots & \\ 0 & & 0 \\ & \ddots & \\ & & 1 \end{bmatrix} \end{array} \tag{4.60}$$

Transformed stator and rotor leakage inductance matrices

The leakage inductance of all stator circuits being the same, eq. (4.31) leads to the following expression for the transformed stator leakage inductance matrix:

$$\mathbf{L_{\sigma s}^\natural} = L_{\sigma s} \begin{array}{c} \\ k{=}0 \\ \\ k{=}2 \end{array} \begin{array}{c} \begin{array}{ccc} m{=}0 & & m{=}2 \end{array} \\ \begin{bmatrix} 1 & 0 & 0 \\ 0 & 1 & 0 \\ 0 & 0 & 1 \end{bmatrix} \end{array} \tag{4.61}$$

Likewise, from (4.32) follows:

$$\mathbf{L_{\sigma r}^\natural} = L_{\sigma r} \begin{array}{c} \\ l{=}0 \\ \\ l{=}15 \end{array} \begin{array}{c} \begin{array}{ccc} n{=}0 & & n{=}15 \end{array} \\ \begin{bmatrix} 1 & & \\ & \ddots & \\ 0 & & 0 \\ & \ddots & \\ & & 1 \end{bmatrix} \end{array} \tag{4.62}$$

Transformed main inductance matrices of the fundamental wave

The fundamental wave has the order $h = 1$. As $m_s = 3$ and $m_r = 16$,

$$\begin{bmatrix} h \equiv 1 \pmod{m_s} \\ h \equiv 1 \pmod{m_r} \end{bmatrix} \Longrightarrow \begin{bmatrix} k_0 = 1 \neq m_s - k_0 = 2 \\ l_0 = 1 \neq m_r - l_0 = 15 \end{bmatrix}$$

Consequently, the expressions of the transformed inductance matrices $\widetilde{\mathbf{L}}^{\natural}_{\mathbf{s\,1}}$, $\widetilde{\mathbf{L}}^{\natural}_{\mathbf{r\,1}}$, $\widetilde{\mathbf{L}}^{\natural}_{\mathbf{rs\,1}}$, given by (4.36), (4.39) and (4.41) respectively, are:

$$\widetilde{\mathbf{L}}^{\natural}_{\mathbf{s\,1}} = \frac{3}{2}\widetilde{L}_{s,1} \begin{array}{c} \\ k{=}0 \\ \\ k{=}2 \end{array} \overset{\begin{array}{ccc} m{=}0 & & m{=}2 \end{array}}{\begin{bmatrix} 0 & 0 & 0 \\ 0 & 1 & 0 \\ 0 & 0 & 1 \end{bmatrix}} \tag{4.63}$$

$$\widetilde{\mathbf{L}}^{\natural}_{\mathbf{r\,1}} = \frac{16}{2}\widetilde{L}_{r,1} \begin{array}{c} \\ l{=}0 \\ \\ \\ \\ l{=}15 \end{array} \overset{\begin{array}{ccc} n{=}0 & & n{=}15 \end{array}}{\begin{bmatrix} 0 & & & & \\ & 1 & & & \\ & & 0 & & \\ & & & \ddots & \\ & & & & 0 \\ 0 & & & & \\ & & & & 1 \end{bmatrix}} \tag{4.64}$$

$$\widetilde{\mathbf{L}}^{\natural}_{\mathbf{rs\,1}} = \frac{\sqrt{3 \times 16}}{2} L_{M,1} \begin{array}{c} \\ k{=}0 \\ \\ k{=}2 \end{array} \overset{\begin{array}{ccc} n{=}0 & & \end{array}}{\begin{bmatrix} 0 & 0 & 0 \\ 0 & e^{j\theta'_{r,1}} & 0 \\ 0 & 0 & 0 \end{bmatrix}} \quad 0 \quad \overset{\begin{array}{ccc} & & n{=}15 \end{array}}{\begin{bmatrix} 0 & 0 & 0 \\ 0 & 0 & 0 \\ 0 & 0 & e^{-j\theta'_{r,1}} \end{bmatrix}} \tag{4.65}$$

Transformed voltage equations

Substituting the expressions obtained above for the resistance and inductance matrices into the transformed stator voltage equation (4.22) yields:

$$\begin{aligned} \begin{bmatrix} u^{\natural}_{s,0} \\ u^{\natural}_{s,1} \\ u^{\natural}_{s,2} \end{bmatrix} &= \begin{bmatrix} R_s i^{\natural}_{s,0} \\ R_s i^{\natural}_{s,1} \\ R_s i^{\natural}_{s,2} \end{bmatrix} + \begin{bmatrix} L_{\sigma s} & 0 & 0 \\ 0 & L_{\sigma s} + \frac{3}{2}\widetilde{L}_{s,1} & 0 \\ 0 & 0 & L_{\sigma s} + \frac{3}{2}\widetilde{L}_{s,1} \end{bmatrix} \frac{\mathrm{d}}{\mathrm{d}t} \begin{bmatrix} i^{\natural}_{s,0} \\ i^{\natural}_{s,1} \\ i^{\natural}_{s,2} \end{bmatrix} \\ &+ 2\sqrt{3} L_{M,1} \left[\frac{\mathrm{d}i^{\natural}_{r,1}}{\mathrm{d}t} \begin{bmatrix} 0 \\ e^{j\theta'_{r,1}} \\ 0 \end{bmatrix} + \frac{\mathrm{d}i^{\natural}_{r,15}}{\mathrm{d}t} \begin{bmatrix} 0 \\ 0 \\ e^{-j\theta'_{r,1}} \end{bmatrix} \right] \\ &+ j\omega_r 2\sqrt{3} L_{M,1} \left[i^{\natural}_{r,1} \begin{bmatrix} 0 \\ e^{j\theta'_{r,1}} \\ 0 \end{bmatrix} + i^{\natural}_{r,15} \begin{bmatrix} 0 \\ 0 \\ -e^{-j\theta'_{r,1}} \end{bmatrix} \right] \end{aligned} \tag{4.66}$$

This leads to the following differential system:

$$\begin{cases} u_{s,0}^{\natural} = R_s i_{s,0}^{\natural} + L_{\sigma s}\dfrac{\mathrm{d}i_{s,0}^{\natural}}{\mathrm{d}t} \\ u_{s,1}^{\natural} = R_s i_{s,1}^{\natural} + \left(L_{\sigma s} + \dfrac{3}{2}\widetilde{L}_{s,1}\right)\dfrac{\mathrm{d}i_{s,1}^{\natural}}{\mathrm{d}t} + 2\sqrt{3}L_{M,1}e^{j\theta'_{r,1}}\dfrac{\mathrm{d}i_{r,1}^{\natural}}{\mathrm{d}t} + j\omega_r 2\sqrt{3}L_{M,1}e^{j\theta'_{r,1}}i_{r,1}^{\natural} \\ u_{s,2}^{\natural} = R_s i_{s,2}^{\natural} + \left(L_{\sigma s} + \dfrac{3}{2}\widetilde{L}_{s,1}\right)\dfrac{\mathrm{d}i_{s,2}^{\natural}}{\mathrm{d}t} + 2\sqrt{3}L_{M,1}e^{-j\theta'_{r,1}}\dfrac{\mathrm{d}i_{r,15}^{\natural}}{\mathrm{d}t} - j\omega_r 2\sqrt{3}L_{M,1}e^{-j\theta'_{r,1}}i_{r,15}^{\natural} \end{cases} \tag{4.67}$$

In the same way, the transformed rotor voltage equation (4.23) is rewritten using the previously determined resistance and inductance matrices:

$$\begin{bmatrix} u_{r,0}^{\natural} \\ u_{r,1}^{\natural} \\ u_{r,2}^{\natural} \\ \vdots \\ u_{r,14}^{\natural} \\ u_{r,15}^{\natural} \end{bmatrix} = \begin{bmatrix} R_r i_{r,0}^{\natural} \\ R_r i_{r,1}^{\natural} \\ R_r i_{r,2}^{\natural} \\ \vdots \\ R_r i_{r,14}^{\natural} \\ R_r i_{r,15}^{\natural} \end{bmatrix} + \begin{bmatrix} L_{\sigma r} & & & & & \\ & L_{\sigma r} + 8\widetilde{L}_{r,1} & & & 0 & \\ & & L_{\sigma r} & & & \\ & & & \ddots & & \\ & 0 & & & L_{\sigma r} & \\ & & & & & L_{\sigma r} + 8\widetilde{L}_{r,1} \end{bmatrix} \frac{\mathrm{d}}{\mathrm{d}t} \begin{bmatrix} i_{r,0}^{\natural} \\ i_{r,1}^{\natural} \\ i_{r,2}^{\natural} \\ \vdots \\ i_{r,14}^{\natural} \\ i_{r,15}^{\natural} \end{bmatrix}$$

$$+ 2\sqrt{3}L_{M,1}\left[\frac{\mathrm{d}i_{s,1}^{\natural}}{\mathrm{d}t}\begin{bmatrix} 0 \\ e^{-j\theta'_{r,1}} \\ 0 \\ \vdots \\ 0 \end{bmatrix} + \frac{\mathrm{d}i_{s,2}^{\natural}}{\mathrm{d}t}\begin{bmatrix} 0 \\ \vdots \\ 0 \\ e^{j\theta'_{r,1}} \end{bmatrix}\right]$$

$$+ j\omega_r 2\sqrt{3}L_{M,1}\left[i_{s,1}^{\natural}\begin{bmatrix} 0 \\ -e^{-j\theta'_{r,1}} \\ 0 \\ \vdots \\ 0 \end{bmatrix} + i_{s,2}^{\natural}\begin{bmatrix} 0 \\ \vdots \\ 0 \\ e^{j\theta'_{r,1}} \end{bmatrix}\right] \tag{4.68}$$

The foregoing relations result in the subsequent system of differential equations:

$$\begin{cases} 0 = R_r i_{r,0}^{\natural} + L_{\sigma r}\dfrac{\mathrm{d}i_{r,0}^{\natural}}{\mathrm{d}t} \\ 0 = R_r i_{r,1}^{\natural} + \left(L_{\sigma r} + 8\widetilde{L}_{r,1}\right)\dfrac{\mathrm{d}i_{r,1}^{\natural}}{\mathrm{d}t} + 2\sqrt{3}L_{M,1}e^{-j\theta'_{r,1}}\dfrac{\mathrm{d}i_{s,1}^{\natural}}{\mathrm{d}t} - j\omega_r 2\sqrt{3}L_{M,1}e^{-j\theta'_{r,1}}i_{s,1}^{\natural} \\ 0 = R_r i_{r,2}^{\natural} + L_{\sigma r}\dfrac{\mathrm{d}i_{r,2}^{\natural}}{\mathrm{d}t} \\ \vdots \qquad\qquad \vdots \\ 0 = R_r i_{r,14}^{\natural} + L_{\sigma r}\dfrac{\mathrm{d}i_{r,14}^{\natural}}{\mathrm{d}t} \\ 0 = R_r i_{r,15}^{\natural} + \left(L_{\sigma r} + 8\widetilde{L}_{r,1}\right)\dfrac{\mathrm{d}i_{r,15}^{\natural}}{\mathrm{d}t} + 2\sqrt{3}L_{M,1}e^{j\theta'_{r,1}}\dfrac{\mathrm{d}i_{s,2}^{\natural}}{\mathrm{d}t} + j\omega_r 2\sqrt{3}L_{M,1}e^{j\theta'_{r,1}}i_{s,2}^{\natural} \end{cases} \tag{4.69}$$

Simplifying the voltage equations

Assuming that all rotor currents are initially zero, i.e. $\forall\, n \in [\![0,\, m_r - 1]\!]$, $i_{r,n}^{\natural}(0) = 0$, (4.69) ensures that $\forall\, n \in [\![0,\, m_r - 1]\!] \setminus \{1,\, 15\}$, $\forall\, t \in \mathbb{R}^+$, $i_{r,n}^{\natural}(t) = 0$.

Hence, (4.69) can be reduced to a system of two differential equations:

$$\begin{cases} 0 = R_r i_{r,1}^{\natural} + \left[L_{\sigma r} + 8\widetilde{L}_{r,1}\right]\dfrac{\mathrm{d}i_{r,1}^{\natural}}{\mathrm{d}t} + 2\sqrt{3}L_{M,1}e^{-j\theta'_{r,1}}\dfrac{\mathrm{d}i_{s,1}^{\natural}}{\mathrm{d}t} - j\omega_r 2\sqrt{3}L_{M,1}e^{-j\theta'_{r,1}}i_{s,1}^{\natural} \\ 0 = R_r i_{r,15}^{\natural} + \left[L_{\sigma r} + 8\widetilde{L}_{r,1}\right]\dfrac{\mathrm{d}i_{r,15}^{\natural}}{\mathrm{d}t} + 2\sqrt{3}L_{M,1}e^{j\theta'_{r,1}}\dfrac{\mathrm{d}i_{s,2}^{\natural}}{\mathrm{d}t} + j\omega_r 2\sqrt{3}L_{M,1}e^{j\theta'_{r,1}}i_{s,2}^{\natural} \end{cases} \tag{4.70}$$

At this stage, it is interesting to examine the case of delta and star connections of stator windings separately:

• **Case 1:** delta connection
The delta connection does not introduce any restriction regarding the currents flowing through the stator windings. However, the following constraint applies to the voltages at their terminals:

$$u_{s0} + u_{s1} + u_{s2} = 0$$

$$\iff \quad \vec{u}_s = \begin{bmatrix} u_{s0} & u_{s1} & u_{s2} \end{bmatrix}^\top \in \mathrm{span}\left(\begin{bmatrix} 1 & 1 & 1 \end{bmatrix}^\top\right)^\perp$$

Since

$$\mathcal{T}_{\mathcal{W}3}\left(\begin{bmatrix} 1 \\ 1 \\ 1 \end{bmatrix}\right) = \begin{bmatrix} \sqrt{3} \\ 0 \\ 0 \end{bmatrix} \in \mathrm{span}\left(\begin{bmatrix} 1 & 0 & 0 \end{bmatrix}^\top\right)$$

$$\vec{u}_s \in \mathrm{span}\left(\begin{bmatrix} 1 \\ 1 \\ 1 \end{bmatrix}\right)^\perp \iff \quad \underline{u}_s^{\natural} = \mathcal{T}_{\mathcal{W}3}(\vec{u}_s) \in \mathrm{span}\left(\begin{bmatrix} 0 \\ 1 \\ 0 \end{bmatrix},\, \begin{bmatrix} 0 \\ 0 \\ 1 \end{bmatrix}\right)$$

$$\iff \quad \forall\, t \in \mathbb{R}^+,\, u_{s,0}^{\natural}(t) = 0$$

Stator currents being initially equal to zero, the above relations imply that: $\forall\, t \in \mathbb{R}^+,\ i^\natural_{s,\,0}(t) = 0$.

• **Case 2:** star connection

The interconnection matrix for stator circuits takes the form

$$\mathbf{C_{s,\,IM1}} = \begin{bmatrix} 1 & 0 \\ 0 & 1 \\ -1 & -1 \end{bmatrix}$$

leading to the transformation matrix between $\vec{i}'_s \in \mathbb{R}^2$ and $\underline{i}^\natural_s \in \mathbb{C}^3$:

$$\mathcal{Z}_{\mathrm{s,\,IM1}} = \overline{\mathcal{W}_3}^{\top}\,\mathbf{C_{s,\,IM1}} = \frac{1}{\sqrt{3}} \begin{bmatrix} 0 & 0 \\ 1 - e^{j4\pi/3} & e^{j2\pi/3} - e^{j4\pi/3} \\ 1 - e^{j2\pi/3} & e^{j4\pi/3} - e^{j2\pi/3} \end{bmatrix}$$

$$= -j \begin{bmatrix} 0 & 0 \\ e^{j2\pi/3} & -1 \\ e^{j\pi/3} & 1 \end{bmatrix} \tag{4.71}$$

This results in $\underline{i}^\natural_s \in \mathrm{span}\left(\begin{bmatrix} 0 \\ 1 \\ 0 \end{bmatrix}, \begin{bmatrix} 0 \\ 0 \\ 1 \end{bmatrix} \right)$. Hence, $\forall\, t \in \mathbb{R}^+,\ i^\natural_{s,\,0}(t) = 0$.

Consequently, in both cases, (4.67) can be simplified as follows:

$$\begin{cases} u^\natural_{s,\,1} = R_s i^\natural_{s,\,1} + \left(L_{\sigma s} + \dfrac{3}{2}\widetilde{L}_{s,\,1} \right) \dfrac{\mathrm{d}i^\natural_{s,\,1}}{\mathrm{d}t} + 2\sqrt{3} L_{M,\,1} e^{j\theta'_{r,\,1}} \dfrac{\mathrm{d}i^\natural_{r,\,1}}{\mathrm{d}t} + j\omega_r 2\sqrt{3} L_{M,\,1} e^{j\theta'_{r,\,1}} i^\natural_{r,\,1} \\ u^\natural_{s,\,2} = R_s i^\natural_{s,\,2} + \left(L_{\sigma s} + \dfrac{3}{2}\widetilde{L}_{s,\,1} \right) \dfrac{\mathrm{d}i^\natural_{s,\,2}}{\mathrm{d}t} + 2\sqrt{3} L_{M,\,1} e^{-j\theta'_{r,\,1}} \dfrac{\mathrm{d}i^\natural_{r,\,15}}{\mathrm{d}t} - j\omega_r 2\sqrt{3} L_{M,\,1} e^{-j\theta'_{r,\,1}} i^\natural_{r,\,15} \end{cases} \tag{4.72}$$

The components of the vector $\vec{i}_s$ being real, for all $m \in [\![0,\, m_s - 1]\!]$,

$$i^\natural_{s,\,m_s - m} = \sum_{k=0}^{m_s-1} i_{sk} e^{j\frac{2\pi}{m_s} k(m_s - m)} = \sum_{k=0}^{m_s-1} i_{sk} e^{-j\frac{2\pi}{m_s} km} = \overline{i^\natural_{s,\,m}} \tag{4.73}$$

For this reason, $i^\natural_{s,\,2} = \overline{i^\natural_{s,\,1}}$. Likewise, $i^\natural_{r,\,15} = \overline{i^\natural_{r,\,1}}$.

In consequence, the evolution of stator and rotor currents can be described by the two differential equations below:

$$\begin{cases} u^\natural_{s,\,1} = R_s i^\natural_{s,\,1} + \left(L_{\sigma s} + \dfrac{3}{2}\widetilde{L}_{s,\,1} \right) \dfrac{\mathrm{d}i^\natural_{s,\,1}}{\mathrm{d}t} + 2\sqrt{3} L_{M,\,1} e^{j\theta'_{r,\,1}} \dfrac{\mathrm{d}i^\natural_{r,\,1}}{\mathrm{d}t} + j\omega_r 2\sqrt{3} L_{M,\,1} e^{j\theta'_{r,\,1}} i^\natural_{r,\,1} \\ 0 = R_r i^\natural_{r,\,1} + \left(L_{\sigma r} + 8\widetilde{L}_{r,\,1} \right) \dfrac{\mathrm{d}i^\natural_{r,\,1}}{\mathrm{d}t} + 2\sqrt{3} L_{M,\,1} e^{-j\theta'_{r,\,1}} \dfrac{\mathrm{d}i^\natural_{s,\,1}}{\mathrm{d}t} - j\omega_r 2\sqrt{3} L_{M,\,1} e^{-j\theta'_{r,\,1}} i^\natural_{s,\,1} \end{cases} \tag{4.74}$$

Owing to the previous considerations, (4.74) completely describes the electrical behaviour of the machine and therefore carries the same amount of information as (4.67) and (4.69) together. It becomes apparent that only two complex components of the transformed voltage vector, $u^\natural_{s,\,1}$ and $u^\natural_{r,\,1}$, as well as two of the transformed current vector, $i^\natural_{s,\,1}$ and $i^\natural_{r,\,1}$, are required. This property explains the drastic reduction of model order achieved with the well-known Clarke transformation.

Rewriting (4.74) as:

$$\begin{cases} u_{s,1}^{\natural} = R_s i_{s,1}^{\natural} + \left(L_{\sigma s} + \frac{3}{2}\widetilde{L}_{s,1}\right)\frac{\mathrm{d}i_{s,1}^{\natural}}{\mathrm{d}t} + 2\sqrt{3}L_{M,1}\frac{\mathrm{d}e^{j\theta'_{r,1}}i_{r,1}^{\natural}}{\mathrm{d}t} \\ 0 = R_r i_{r,1}^{\natural} + \left(L_{\sigma r} + 8\widetilde{L}_{r,1}\right)\frac{\mathrm{d}i_{r,1}^{\natural}}{\mathrm{d}t} + 2\sqrt{3}L_{M,1}\frac{\mathrm{d}e^{-j\theta'_{r,1}}i_{s,1}^{\natural}}{\mathrm{d}t} \end{cases} \tag{4.75}$$

and introducing the notations

$$i_{s,1}^{\flat} = i_{s,1}^{\natural} e^{-j\theta'_{r,1}} \tag{4.76a}$$

$$i_{r,1}^{\sharp} = i_{r,1}^{\natural} e^{j\theta'_{r,1}} \tag{4.76b}$$

yields:

$$\begin{cases} u_{s,1}^{\natural} = R_s i_{s,1}^{\natural} + \left(L_{\sigma s} + \frac{3}{2}\widetilde{L}_{s,1}\right)\frac{\mathrm{d}i_{s,1}^{\natural}}{\mathrm{d}t} + 2\sqrt{3}L_{M,1}\frac{\mathrm{d}i_{r,1}^{\sharp}}{\mathrm{d}t} \\ 0 = R_r i_{r,1}^{\natural} + \left(L_{\sigma r} + 8\widetilde{L}_{r,1}\right)\frac{\mathrm{d}i_{r,1}^{\natural}}{\mathrm{d}t} + 2\sqrt{3}L_{M,1}\frac{\mathrm{d}i_{s,1}^{\flat}}{\mathrm{d}t} \end{cases} \tag{4.77}$$

The above change of variable leading to (4.77) corresponds to the familiar Park transformation and results in electrical equations independent of the rotor angle.

Referring rotor quantities to the stator side

In order to allow for comparisons with the usual modelling approach of induction machines, it is insightful to refer the second equation in (4.77) to the stator side. Recalling the expressions of the inductances $\widetilde{L}_{s,1}$, $\widetilde{L}_{r,1}$ and $L_{M,1}$ from (3.33):

$$\widetilde{L}_{s,1} = 4\pi r l \frac{\mu_0}{\delta_0}|c_1(W_{s0})|^2$$

$$\widetilde{L}_{r,1} = 4\pi r l \frac{\mu_0}{\delta_0}|c_1(W_{r0})|^2$$

$$L_{M,1} = 4\pi r l \frac{\mu_0}{\delta_0}|c_1(W_{r0})||c_1(W_{s0})|$$

and defining $M_1 = \frac{3}{2}\widetilde{L}_{s,1}$, we then express $\widetilde{L}_{r,1}$ and $L_{M,1}$ as functions of M_1:

$$\widetilde{L}_{r,1} = \widetilde{L}_{s,1}\frac{|c_1(W_{r0})|^2}{|c_1(W_{s0})|^2} = \frac{2}{3}M_1\frac{|c_1(W_{r0})|^2}{|c_1(W_{s0})|^2}$$

$$L_{M,1} = \widetilde{L}_{s,1}\frac{|c_1(W_{r0})|}{|c_1(W_{s0})|} = \frac{2}{3}M_1\frac{|c_1(W_{r0})|}{|c_1(W_{s0})|}$$

This results in:

$$u_{s,1}^{\natural} = R_s i_{s,1}^{\natural} + (L_{\sigma s} + M_1)\frac{\mathrm{d}i_{s,1}^{\natural}}{\mathrm{d}t} + \frac{4\sqrt{3}}{3}M_1\frac{|c_1(W_{r0})|}{|c_1(W_{s0})|}\frac{\mathrm{d}i_{r,1}^{\sharp}}{\mathrm{d}t} \tag{4.78a}$$

$$0 = R_r i_{r,1}^{\natural} + \left(L_{\sigma r} + \frac{16}{3}M_1\frac{|c_1(W_{r0})|^2}{|c_1(W_{s0})|^2}\right)\frac{\mathrm{d}i_{r,1}^{\natural}}{\mathrm{d}t} + \frac{4\sqrt{3}}{3}M_1\frac{|c_1(W_{r0})|}{|c_1(W_{s0})|}\frac{\mathrm{d}i_{s,1}^{\flat}}{\mathrm{d}t} \tag{4.78b}$$

(4.78b) is rewritten as follows:

$$0 = R_r i^{\natural}_{r,1} + \frac{16}{3}\frac{|c_1(W_{r0})|^2}{|c_1(W_{s0})|^2}\left(\frac{3}{16}\frac{|c_1(W_{s0})|^2}{|c_1(W_{r0})|^2}L_{\sigma r} + M_1\right)\frac{\mathrm{d}i^{\natural}_{r,1}}{\mathrm{d}t} + \frac{4\sqrt{3}}{3}M_1\frac{|c_1(W_{r0})|}{|c_1(W_{s0})|}\frac{\mathrm{d}i^{\flat}_{s,1}}{\mathrm{d}t} \tag{4.79}$$

Multiplying both sides by $\sqrt{\frac{3}{16}}\frac{|c_1(W_{s0})|}{|c_1(W_{r0})|}$ then leads to:

$$0 = \sqrt{\frac{3}{16}}\frac{|c_1(W_{s0})|}{|c_1(W_{r0})|}R_r i^{\natural}_{r,1} + \sqrt{\frac{16}{3}}\frac{|c_1(W_{r0})|}{|c_1(W_{s0})|}\left(\frac{3}{16}\frac{|c_1(W_{s0})|^2}{|c_1(W_{r0})|^2}L_{\sigma r} + M_1\right)\frac{\mathrm{d}i^{\natural}_{r,1}}{\mathrm{d}t} + M_1\frac{\mathrm{d}i^{\flat}_{s,1}}{\mathrm{d}t} \tag{4.80}$$

Introducing the definitions

$$\underline{i}^r_r = \sqrt{\frac{16}{3}}\frac{|c_1(W_{r0})|}{|c_1(W_{s0})|}i^{\natural}_{r,1} \qquad \underline{i}^r_s = i^{\flat}_{s,1} \qquad L'_{\sigma r} = \frac{3}{16}\frac{|c_1(W_{s0})|^2}{|c_1(W_{r0})|^2}L_{\sigma r}$$

subsequently provides:

$$0 = \frac{3}{16}\frac{|c_1(W_{s0})|^2}{|c_1(W_{r0})|^2}R_r\underline{i}^r_r + \left(\frac{3}{16}\frac{|c_1(W_{s0})|^2}{|c_1(W_{r0})|^2}L_{\sigma r} + M_1\right)\frac{\mathrm{d}\underline{i}^r_r}{\mathrm{d}t} + M_1\frac{\mathrm{d}\underline{i}^r_s}{\mathrm{d}t} \tag{4.81}$$

The notations

$$R'_r = \frac{3}{16}\frac{|c_1(W_{s0})|^2}{|c_1(W_{r0})|^2}R_r \qquad L'_{\sigma r} = \frac{3}{16}\frac{|c_1(W_{s0})|^2}{|c_1(W_{r0})|^2}L_{\sigma r}$$

allow for further simplification which results in a compact expression of (4.78b):

$$0 = R'_r\underline{i}^r_r + \left(L'_{\sigma r} + M_1\right)\frac{\mathrm{d}\underline{i}^r_r}{\mathrm{d}t} + M_1\frac{\mathrm{d}\underline{i}^r_s}{\mathrm{d}t} \tag{4.82}$$

Finally, using the following definitions

$$\underline{u}^s_s = u^{\natural}_{s,1} \qquad \underline{i}^s_s = i^{\natural}_{s,1} \qquad \underline{i}^s_r = \sqrt{\frac{16}{3}}\frac{|c_1(W_{r0})|}{|c_1(W_{s0})|}i^{\sharp}_{r,1} = \underline{i}^r_r e^{j\theta'_{r,1}}$$

one obtains the well-known differential equations of Park's model expressed in their respective coordinate systems:

$$\begin{cases} \underline{u}^s_s = R_s\underline{i}^s_s + (L_{\sigma s} + M_1)\dfrac{\mathrm{d}\underline{i}^s_s}{\mathrm{d}t} + M_1\dfrac{\mathrm{d}\underline{i}^s_r}{\mathrm{d}t} & \text{(4.83a)} \\ 0 = R'_r\underline{i}^r_r + \left(L'_{\sigma r} + M_1\right)\dfrac{\mathrm{d}\underline{i}^r_r}{\mathrm{d}t} + M_1\dfrac{\mathrm{d}\underline{i}^r_s}{\mathrm{d}t} & \text{(4.83b)} \end{cases}$$

Torque equation

We now examine the expression of the electromechanical torque which is computed from the transformed quantities using eq. (4.27):

$$M_M = \overline{\underline{i}^{\natural}_s}^{\top}\frac{\partial\widetilde{\mathbf{L}}^{\natural}_{\mathbf{rs\,1}}(\theta_r)}{\partial\theta_r}\underline{i}^{\natural}_r = \overline{\underline{i}^{\natural}_s}^{\top} j2\sqrt{3}L_{M,1}\begin{bmatrix} 0 & 0 & 0 & & 0 & 0 \\ 0 & e^{j\theta'_{r,1}} & 0 & 0 & 0 & 0 \\ 0 & 0 & 0 & & 0 & -e^{-j\theta'_{r,1}} \end{bmatrix}\underline{i}^{\natural}_r$$

$$= \overline{\underline{i}_s^\natural}^\top j2\sqrt{3}L_{M,1}\begin{bmatrix} 0 \\ e^{j\theta'_{r,1}} i_{r,1}^\natural \\ -e^{-j\theta'_{r,1}} i_{r,15}^\natural \end{bmatrix} = 2\sqrt{3}L_{M,1}\left(\overline{i_{s,1}^\natural} j e^{j\theta'_{r,1}} i_{r,1}^\natural - \overline{i_{s,2}^\natural} j e^{-j\theta'_{r,1}} i_{r,15}^\natural\right)$$

As $i_{s,2}^\natural = \overline{i_{s,1}^\natural}$ and $i_{r,15}^\natural = \overline{i_{r,1}^\natural}$,

$$M_M = 2\sqrt{3}L_{M,1}\left(\overline{i_{s,1}^\natural} j e^{j\theta'_{r,1}} i_{r,1}^\natural + i_{s,1}^\natural \overline{j e^{j\theta'_{r,1}} i_{r,1}^\natural}\right) = 4\sqrt{3}L_{M,1}\mathfrak{Re}\left[\overline{i_{s,1}^\natural} j e^{j\theta'_{r,1}} i_{r,1}^\natural\right]$$

$$= 4\sqrt{3}L_{M,1}\mathfrak{Re}\left[\overline{i_{s,1}^\natural} j i_{r,1}^\sharp\right] \tag{4.84}$$

The notations introduced in the previous section allow for a further simplification of the torque equation as follows:

$$M_M = 4\sqrt{3}\frac{2}{3}M_1\frac{|c_1(W_{r0})|}{|c_1(W_{s0})|}\mathfrak{Re}\left[\overline{\underline{i}_s^s} j \sqrt{\frac{3}{16}}\frac{|c_1(W_{s0})|}{|c_1(W_{r0})|}\underline{i}_r^s\right]$$

$$= 2M_1\mathfrak{Re}\left[\overline{\underline{i}_s^s} j \underline{i}_r^s\right] \tag{4.85}$$

(4.85) differs from the usual expression of the electromagnetic torque of an induction machine obtained using Clarke's transformation by a scaling factor. This is not surprising as $\mathcal{T}_{\mathcal{W}3}$ introduces a factor $1/\sqrt{3}$ instead of $2/3$, which means that the quantities $\underline{i}_s^s$ and $\underline{i}_s^r$ each have to be multiplied by $\sqrt{3}/2$ to get back to the standard definition of space vectors. In this case, (4.85) would be multiplied by $3/4$, leading to the typical factor $3/2$.

The results (4.83) and (4.85) demonstrate that the proposed approach is consistent and generalizes the common modelling method for induction machines.

4.3.3 Model of IM1 with wavelengths of order $h = 1$ and $h = 17$

We extend the model derived previously and add a wavelength of order 17 on top of the fundamental. The resistance and leakage inductance matrices remain unchanged. Consequently, only the main inductance matrices as well as the voltage and torque equations need to be determined.

Expressions of the transformed inductance matrices

The subsequent relations hold for the wavelength of order $h = 17$ in the case of $m_s = 3$ and $m_r = 16$:

$$\begin{bmatrix} h \equiv 2 \pmod{m_s} \\ h \equiv 1 \pmod{m_r} \end{bmatrix} \Longrightarrow \begin{bmatrix} k_0 = 2 \neq m_s - k_0 = 1 \\ l_0 = 1 \neq m_r - l_0 = 15 \end{bmatrix}$$

Following (4.36), (4.39) and (4.41), the transformed inductance matrices associated with the wavelength of order 17, $\widetilde{\mathbf{L}}_{\mathbf{s\,17}}^\natural$, $\widetilde{\mathbf{L}}_{\mathbf{r\,17}}^\natural$ and $\widetilde{\mathbf{L}}_{\mathbf{rs\,17}}^\natural$, are:

$$\widetilde{\mathbf{L}}_{\mathbf{s\,17}}^\natural = \frac{3}{2}\widetilde{L}_{s,17} \begin{matrix} \\ k{=}0 \\ \\ k{=}2 \end{matrix} \begin{matrix} \begin{matrix} m{=}0 & & m{=}2 \end{matrix} \\ \begin{bmatrix} 0 & 0 & 0 \\ 0 & 1 & 0 \\ 0 & 0 & 1 \end{bmatrix} \end{matrix}$$

$$\widetilde{\mathbf{L}}^{\natural}_{\mathbf{r\,17}} = 8\widetilde{L}_{r,17} \begin{array}{c} \\ l{=}0 \\ \\ \\ \\ l{=}15 \end{array} \begin{array}{c} \begin{array}{cccccc} n{=}0 & & & & & n{=}15 \end{array} \\ \begin{bmatrix} 0 & & & & & \\ & 1 & & & & \\ & & 0 & & & \\ & & & \ddots & & \\ & & & & 0 & \\ & & & & & 1 \end{bmatrix} \end{array}$$

$$\widetilde{\mathbf{L}}^{\natural}_{\mathbf{rs\,17}} = 2\sqrt{3}L_{M,17} \begin{array}{c} \\ k{=}0 \\ \\ k{=}2 \end{array} \begin{array}{c} \begin{array}{cccccc} n{=}0 & & & & & n{=}15 \end{array} \\ \begin{bmatrix} 0 & 0 & 0 & \dots & 0 & 0 \\ 0 & 0 & 0 & \dots & 0 & e^{-j\theta'_{r,17}} \\ 0 & e^{j\theta'_{r,17}} & 0 & \dots & 0 & 0 \end{bmatrix} \end{array}$$

Thus, the transformed total stator and rotor inductance matrices are given by:

$$\mathbf{L}^{\natural}_{\mathbf{s}} = \mathbf{L}^{\natural}_{\sigma\mathbf{s}} + \widetilde{\mathbf{L}}^{\natural}_{\mathbf{s\,1}} + \widetilde{\mathbf{L}}^{\natural}_{\mathbf{s\,17}} = \begin{bmatrix} L_{\sigma s} & 0 & 0 \\ 0 & L_{\sigma s} + \frac{3}{2}\left[\widetilde{L}_{s,1} + \widetilde{L}_{s,17}\right] & 0 \\ 0 & 0 & L_{\sigma s} + \frac{3}{2}\left[\widetilde{L}_{s,1} + \widetilde{L}_{s,17}\right] \end{bmatrix} \tag{4.86}$$

$$\mathbf{L}^{\natural}_{\mathbf{r}} = \mathbf{L}^{\natural}_{\sigma\mathbf{r}} + \widetilde{\mathbf{L}}^{\natural}_{\mathbf{r\,1}} + \widetilde{\mathbf{L}}^{\natural}_{\mathbf{r\,17}} = \begin{bmatrix} L_{\sigma r} & & & & \\ & L_{\sigma r} + 8\left[\widetilde{L}_{r,1} + \widetilde{L}_{r,17}\right] & & 0 & \\ & & L_{\sigma r} & & \\ & 0 & & \ddots & \\ & & & & L_{\sigma r} \\ & & & & & L_{\sigma r} + 8\left[\widetilde{L}_{r,1} + \widetilde{L}_{r,17}\right] \end{bmatrix} \tag{4.87}$$

The submatrix $\widetilde{\mathbf{L}}^{\natural}_{\mathbf{rs}}$ which describes the effect of transformed rotor currents on transformed stator flux linkages has the following expression:

$$\widetilde{\mathbf{L}}^{\natural}_{\mathbf{rs}} = 2\sqrt{3}\begin{bmatrix} 0 & 0 & 0 & \dots & 0 & 0 \\ 0 & L_{M,1}e^{j\theta'_{r,1}} & 0 & \dots & 0 & L_{M,17}e^{-j\theta'_{r,17}} \\ 0 & L_{M,17}e^{j\theta'_{r,17}} & 0 & \dots & 0 & L_{M,1}e^{-j\theta'_{r,1}} \end{bmatrix} \tag{4.88}$$

We notice the presence of two additional non-zero entries compared to the expression of $\widetilde{\mathbf{L}}^{\natural}_{\mathbf{rs}}$ obtained for the model with $\mathcal{H} = \{1\}$.

Simplified transformed voltage and torque equations

Upon simplification of the stator and rotor voltage relations similarly to section 4.3.2, we obtain:

$$\begin{aligned}
u^{\natural}_{s,1} &= R_s i^{\natural}_{s,1} + \left[L_{\sigma s} + \frac{3}{2}(\widetilde{L}_{s,1} + \widetilde{L}_{s,17})\right]\frac{\mathrm{d}i^{\natural}_{s,1}}{\mathrm{d}t} + 2\sqrt{3}\left[L_{M,1}e^{j\theta'_{r,1}}\frac{\mathrm{d}i^{\natural}_{r,1}}{\mathrm{d}t} + L_{M,17}e^{-j\theta'_{r,17}}\frac{\mathrm{d}\overline{i^{\natural}_{r,1}}}{\mathrm{d}t}\right] \\
&\quad + j\omega_r 2\sqrt{3}\left[L_{M,1}e^{j\theta'_{r,1}}i^{\natural}_{r,1} - 17L_{M,17}e^{-j\theta'_{r,17}}\overline{i^{\natural}_{r,1}}\right] \\
0 &= R_r i^{\natural}_{r,1} + \left[L_{\sigma r} + 8(\widetilde{L}_{r,1} + \widetilde{L}_{r,17})\right]\frac{\mathrm{d}i^{\natural}_{r,1}}{\mathrm{d}t} + 2\sqrt{3}\left[L_{M,1}e^{-j\theta'_{r,1}}\frac{\mathrm{d}i^{\natural}_{s,1}}{\mathrm{d}t} + L_{M,17}e^{-j\theta'_{r,17}}\frac{\mathrm{d}\overline{i^{\natural}_{s,1}}}{\mathrm{d}t}\right] \\
&\quad - j\omega_r 2\sqrt{3}\left[L_{M,1}e^{-j\theta'_{r,1}}i^{\natural}_{s,1} + 17L_{M,17}e^{-j\theta'_{r,17}}\overline{i^{\natural}_{s,1}}\right]
\end{aligned} \tag{4.89}$$

The fact that the systems (4.74) and (4.89) have the same order results from the form of the submatrices $\widetilde{\mathbf{L}}^{\natural}_{\mathbf{rs}}$ and $\widetilde{\mathbf{L}}^{\natural}_{\mathbf{sr}}$ and the properties of the discrete Fourier transform with respect to *real-valued* vectors (see (4.73)). The latter impose $i^{\natural}_{s,1} = \overline{i^{\natural}_{s,2}}$ and $i^{\natural}_{r,15} = \overline{i^{\natural}_{r,1}}$. Thus the order of the transformed system of voltage equations including the effect of wavelengths 1 and 17 remains 4. However, wavelength 17 introduces additional complex exponentials in (4.89) which depend on the rotor angle.

The torque expression taking into account wavelength 17 is derived from (4.27) as follows:

$$\begin{aligned}
M_M &= \overline{\underline{i}^{\natural}_{s}}^{\top}\frac{\partial\widetilde{\mathbf{L}}^{\natural}_{\mathbf{rs}}(\theta_r)}{\partial\theta_r}\underline{i}^{\natural}_{r} = \overline{\underline{i}^{\natural}_{s}}^{\top} j2\sqrt{3}\begin{bmatrix} 0 & 0 & 0 & \dots & 0 & 0 \\ 0 & L_{M,1}e^{j\theta'_{r,1}} & 0 & \dots & 0 & -17L_{M,17}e^{-j\theta'_{r,17}} \\ 0 & 17L_{M,17}e^{j\theta'_{r,17}} & 0 & \dots & 0 & -L_{M,1}e^{-j\theta'_{r,1}} \end{bmatrix}\underline{i}^{\natural}_{r} \\
&= \begin{bmatrix}\overline{i^{\natural}_{s,0}} & \overline{i^{\natural}_{s,1}} & \overline{i^{\natural}_{s,2}}\end{bmatrix}^{\top} j2\sqrt{3}\left[i^{\natural}_{r,1}\begin{bmatrix}0\\ L_{M,1}e^{j\theta'_{r,1}}\\ 17L_{M,17}e^{j\theta'_{r,17}}\end{bmatrix} - i^{\natural}_{r,15}\begin{bmatrix}0\\ 17L_{M,17}e^{-j\theta'_{r,17}}\\ L_{M,1}e^{-j\theta'_{r,1}}\end{bmatrix}\right] \\
&= j2\sqrt{3}\begin{bmatrix}\overline{i^{\natural}_{s,0}} & \overline{i^{\natural}_{s,1}} & \overline{i^{\natural}_{s,2}}\end{bmatrix}^{\top}\begin{bmatrix}0\\ L_{M,1}e^{j\theta'_{r,1}}i^{\natural}_{r,1} - 17L_{M,17}e^{-j\theta'_{r,17}}\overline{i^{\natural}_{r,1}}\\ 17L_{M,17}e^{-j\theta'_{r,17}}i^{\natural}_{r,1} - L_{M,1}e^{-j\theta'_{r,1}}\overline{i^{\natural}_{r,1}}\end{bmatrix} \\
&= 4\sqrt{3}L_{M,1}\mathfrak{Re}\left[\overline{i^{\natural}_{s,1}}je^{j\theta'_{r,1}}i^{\natural}_{r,1}\right] + 4\sqrt{3}\cdot 17L_{M,17}\mathfrak{Re}\left[i^{\natural}_{s,1}je^{j\theta'_{r,17}}i^{\natural}_{r,1}\right]
\end{aligned} \tag{4.90}$$

In comparison to (4.84), an extra term representing the influence of the wavelength of order 17 appears in the torque relation.

Continuous-time state-space model using real state variables

The model equations so far involve complex numbers. From a practical perspective, it appears more suitable to work out a state-space representation of the model with wavelengths 1 and 17 using real state variables. Such a model description is gained from eq. (4.89) and (4.90) by splitting the transformed voltage and current components into their real and imaginary parts.

We therefore make use of the notations:

$$u^{\natural}_{s,1} = u_{s,1\alpha} + j u_{s,1\beta} \qquad (u_{s,1\alpha},\, u_{s,1\beta}) \in \mathbb{R}^2; \qquad u^{\natural}_{r,1} = u_{r,1d} + j u_{r,1q} \qquad (u_{r,1d},\, u_{r,1q}) \in \mathbb{R}^2$$

$$i^{\natural}_{s,1} = i_{s,1\alpha} + j i_{s,1\beta} \qquad (i_{s,1\alpha},\, i_{s,1\beta}) \in \mathbb{R}^2; \qquad i^{\natural}_{r,1} = i_{r,1d} + j i_{r,1q} \qquad (i_{r,1d},\, i_{r,1q}) \in \mathbb{R}^2$$

Introducing the definitions

$$L_s = L_{\sigma s} + \frac{3}{2}(\widetilde{L}_{s,1} + \widetilde{L}_{s,17}); \qquad L_r = L_{\sigma r} + 8(\widetilde{L}_{r,1} + \widetilde{L}_{r,17})$$

$$\mathbf{I_2} = \begin{bmatrix} 1 & 0 \\ 0 & 1 \end{bmatrix}; \qquad \mathbf{J} = \begin{bmatrix} 0 & -1 \\ 1 & 0 \end{bmatrix}; \qquad \mathbf{S} = \begin{bmatrix} 1 & 0 \\ 0 & -1 \end{bmatrix}$$

leads to the following relations for the components of the transformed stator voltage:

$$\begin{bmatrix} u_{s,1\alpha} \\ u_{s,1\beta} \end{bmatrix} = R_s \begin{bmatrix} i_{s,1\alpha} \\ i_{s,1\beta} \end{bmatrix} + L_s \frac{\mathrm{d}}{\mathrm{d}t} \begin{bmatrix} i_{s,1\alpha} \\ i_{s,1\beta} \end{bmatrix} + 2\sqrt{3} \left[L_{M,1} \mathbf{T}(\theta'_{r,1}) \frac{\mathrm{d}}{\mathrm{d}t} \begin{bmatrix} i_{r,1d} \\ i_{r,1q} \end{bmatrix} + L_{M,17} \mathbf{T}(-\theta'_{r,17}) \mathbf{S} \frac{\mathrm{d}}{\mathrm{d}t} \begin{bmatrix} i_{r,1d} \\ i_{r,1q} \end{bmatrix} \right]$$

$$+ 2\omega_r \sqrt{3} \mathbf{J} \left[L_{M,1} \mathbf{T}(\theta'_{r,1}) \begin{bmatrix} i_{r,1d} \\ i_{r,1q} \end{bmatrix} - 17 L_{M,17} \mathbf{T}(-\theta'_{r,17}) \mathbf{S} \begin{bmatrix} i_{r,1d} \\ i_{r,1q} \end{bmatrix} \right] \tag{4.91}$$

The components of the rotor voltage are obtained in the same manner:

$$\begin{bmatrix} 0 \\ 0 \end{bmatrix} = R_r \begin{bmatrix} i_{r,1d} \\ i_{r,1q} \end{bmatrix} + L_r \frac{\mathrm{d}}{\mathrm{d}t} \begin{bmatrix} i_{r,1d} \\ i_{r,1q} \end{bmatrix} + 2\sqrt{3} \left[L_{M,1} \mathbf{T}(-\theta'_{r,1}) \frac{\mathrm{d}}{\mathrm{d}t} \begin{bmatrix} i_{s,1\alpha} \\ i_{s,1\beta} \end{bmatrix} + L_{M,17} \mathbf{T}(-\theta'_{r,17}) \mathbf{S} \frac{\mathrm{d}}{\mathrm{d}t} \begin{bmatrix} i_{s,1\alpha} \\ i_{s,1\beta} \end{bmatrix} \right]$$

$$- 2\sqrt{3} \omega_r \mathbf{J} \left[L_{M,1} \mathbf{T}(-\theta'_{r,1}) \begin{bmatrix} i_{s,1\alpha} \\ i_{s,1\beta} \end{bmatrix} + 17 L_{M,17} \mathbf{T}(-\theta'_{r,17}) \mathbf{S} \begin{bmatrix} i_{s,1\alpha} \\ i_{s,1\beta} \end{bmatrix} \right] \tag{4.92}$$

Eq. (4.91) and (4.92) are merged together to express the model in the form:

$$\vec{u}_{\circ} = \mathbf{L}_{\circ}(\theta_r) \frac{\mathrm{d}\vec{i}_{\circ}}{\mathrm{d}t} + \mathbf{P}_{\circ}(\theta_r, \omega_r) \vec{i}_{\circ} \tag{4.93}$$

which involves the following quantities:

$$\vec{u}_{\circ} = \begin{bmatrix} u_{s,1\alpha} & u_{s,1\beta} & u_{r,1d} & u_{r,1q} \end{bmatrix}^{\top}; \qquad \vec{i}_{\circ} = \begin{bmatrix} i_{s,1\alpha} & i_{s,1\beta} & i_{r,1d} & i_{r,1q} \end{bmatrix}^{\top}$$

$$\mathbf{L}_{\circ} = \begin{bmatrix} L_s \mathbf{I_2} & 2\sqrt{3} \left[L_{M,1} \mathbf{T}(\theta'_{r,1}) + L_{M,17} \mathbf{T}(-\theta'_{r,17}) \mathbf{S} \right] \\ 2\sqrt{3} \left[L_{M,1} \mathbf{T}(-\theta'_{r,1}) + L_{M,17} \mathbf{T}(-\theta'_{r,17}) \mathbf{S} \right] & L_r \mathbf{I_2} \end{bmatrix}$$

$$\mathbf{P}_{\circ} = \begin{bmatrix} R_s \mathbf{I_2} & 2\sqrt{3} \omega_r \mathbf{J} \left[L_{M,1} \mathbf{T}(\theta'_{r,1}) - 17 L_{M,17} \mathbf{T}(-\theta'_{r,17}) \mathbf{S} \right] \\ -2\sqrt{3} \omega_r \mathbf{J} \left[L_{M,1} \mathbf{T}(-\theta'_{r,1}) + 17 L_{M,17} \mathbf{T}(-\theta'_{r,17}) \mathbf{S} \right] & R_r \mathbf{I_2} \end{bmatrix}$$

Remark:
The definitions of the conductor distribution functions W_{s0} and W_{r0} according to fig. A.4 and A.5 impose $\varphi_1 = 0$ and $\varphi_{17} = \pi$, which leads to $\theta'_{r,1} = \theta_r$ and $\theta'_{r,17} = 17\theta_r - \pi$.

We select the components of the vector $\vec{i}_{\circ}$ as model states alongside ω_r and θ_r. We need therefore to make sure that $\mathbf{L}_{\circ}$ has full rank to calculate its inverse. In the above relation, $\mathbf{L}_{\circ}$ appears as 2×2 block matrix, each block having dimension 2×2. Since the diagonal blocks are nonsingular, it is sufficient to verify that the corresponding Schur complement is invertible [77]. This condition is satisfied for the values of the considered machine parameters.

Transforming the torque relation (4.90) in order to express it as a function of the state variables results in:

$$M_M = 4\sqrt{3}\begin{bmatrix} i_{s,\,1\alpha} & i_{s,\,1\beta} \end{bmatrix} \mathbf{J} \left[L_{M,\,1}\mathbf{T}(\theta'_{r,\,1}) - 17 L_{M,\,17}\mathbf{ST}(\theta'_{r,\,17}) \right] \begin{bmatrix} i_{r,\,1d} \\ i_{r,\,1q} \end{bmatrix} \tag{4.94}$$

where the term $-17L_{M,\,17}\mathbf{ST}(\theta'_{r,\,17})$ describes the influence of wavelength 17.

Finally, the continuous-time state-space representation of the transformed model is gained by combining the equations (4.93), (4.94) and (2.19):

$$\left[\begin{array}{l} \dfrac{\mathrm{d}\vec{i}_{\circ}}{\mathrm{d}t} = -\mathbf{L}_{\circ}^{-1}(\theta_r)\mathbf{P}_{\circ}(\theta_r, \omega_r)\vec{i}_{\circ} + \mathbf{L}_{\circ}^{-1}(\theta_r)\vec{u}_{\circ} & \text{(4.95a)} \\ \dfrac{\mathrm{d}\omega_r}{\mathrm{d}t} = \dfrac{1}{J_M}(M_M - C_W\omega_r - M_L) & \text{(4.95b)} \\ \dfrac{\mathrm{d}\theta_r}{\mathrm{d}t} = \omega_r & \text{(4.95c)} \\ M_M = 4\sqrt{3}\begin{bmatrix} i_{s,\,1\alpha} & i_{s,\,1\beta} \end{bmatrix} \mathbf{J} [L_{M,\,1}\mathbf{T}(\theta_r) + 17 L_{M,\,17}\mathbf{ST}(17\theta_r)] \begin{bmatrix} i_{r,\,1d} \\ i_{r,\,1q} \end{bmatrix} \end{array}\right.$$

We notice the tremendous order reduction, which is now 6, compared to the original version of the model discussed in section 3.7, which had order 19.

Computation of the transformed stator voltages and the original stator currents

For the model (4.95) to be of practical interest, there must exist a simple way of determining the transformed voltages $u_{s,\,1\alpha}$ and $u_{s,\,1\beta}$ from the impressed line-to-line voltages u'_{s0} and u'_{s1} depicted in fig. 3.3(a). Another condition is that the computation of the currents i'_{s0} and i'_{s1} must be possible to allow for comparisons with the measured ones.

Recalling the general transformation relations (4.54a) and (4.54b), these requirements do not seem to be met, since $\mathcal{Z}_{\mathrm{s}}$ is not square and therefore not invertible. However, in the case of IM1, eq. (4.54a) has the following specific form:

$$\begin{bmatrix} i^{\natural}_{s,\,0} \\ i^{\natural}_{s,\,1} \\ i^{\natural}_{s,\,2} \end{bmatrix} = \mathcal{Z}_{\mathrm{s,\,IM1}} \begin{bmatrix} i'_{s0} \\ i'_{s1} \end{bmatrix} = -j \begin{bmatrix} 0 & 0 \\ e^{j2\pi/3} & -1 \\ e^{j\pi/3} & 1 \end{bmatrix} \begin{bmatrix} i'_{s0} \\ i'_{s1} \end{bmatrix} \tag{4.96}$$

The first row of $\mathcal{Z}_{\mathrm{s,\,IM1}}$ does not carry any relevant information with respect to the simplified model (4.95) and we can focus on the square submatrix:

$$\mathcal{Z}'_{\mathrm{s,\,IM1}} = -j \begin{bmatrix} e^{j2\pi/3} & -1 \\ e^{j\pi/3} & 1 \end{bmatrix} \tag{4.97}$$

The determinant of $\mathcal{Z}'_{\mathrm{s,\,IM1}}$ is non-zero and its inverse is:

$$\mathcal{Z}'^{-1}_{\mathrm{s,\,IM1}} = \frac{\sqrt{3}}{3} \begin{bmatrix} 1 & 1 \\ -e^{j\pi/3} & e^{j2\pi/3} \end{bmatrix} \tag{4.98}$$

Owing to (4.73), $i^{\natural}_{s,\,2} = \overline{i^{\natural}_{s,\,1}}$ and

$$\begin{bmatrix} i'_{s0} \\ i'_{s1} \end{bmatrix} = \mathcal{Z}'^{-1}_{\mathrm{s,\,IM1}} \begin{bmatrix} i^{\natural}_{s,\,1} \\ \overline{i^{\natural}_{s,\,1}} \end{bmatrix} \tag{4.99}$$

which leads to:

$$\begin{bmatrix} i'_{s0} \\ i'_{s1} \end{bmatrix} = \begin{bmatrix} 2/\sqrt{3} & 0 \\ -1/\sqrt{3} & 1 \end{bmatrix} \begin{bmatrix} i_{s,\,1\alpha} \\ i_{s,\,1\beta} \end{bmatrix} \tag{4.100}$$

(4.100) enables us to calculate the required currents i'_{s0} and i'_{s1} from the state variables $i_{s,\,1\alpha}$ and $i_{s,\,1\beta}$. Similarly, by substituting $\mathcal{Z}_{\mathrm{s,\,IM1}}$ into (4.54b), we deduce the subsequent relation for the voltages:

$$\begin{bmatrix} u_{s,\,1\alpha} \\ u_{s,\,1\beta} \end{bmatrix} = \begin{bmatrix} \frac{\sqrt{3}}{3} & -\frac{1}{2\sqrt{3}} \\ 0 & \frac{1}{2} \end{bmatrix} \begin{bmatrix} u'_{s0} \\ u'_{s1} \end{bmatrix} \tag{4.101}$$

The relations (4.100) and (4.101) allow us to determine the inputs and process the outputs of the simplified model as required. (4.95) can now be discretized and tested in simulation as well as on the test bench.

Model validation

We first verify the consistency of the simplified transformed model of IM1 with its original counterpart used in section 3.7 in offline simulations. More specifically, we compare the stator current, torque and angular velocity waveforms generated by the two models while feeding them with the same inputs. Fig. 4.1 shows the simulated traces of the relevant quantities when using a balanced sinusoidal voltage excitation (frequency $f = 50\,\mathrm{Hz}$, line-to-line voltage $U = 400\,\mathrm{V}$) and applying a rated load torque step at $t = 0.5\,\mathrm{s}$. Heun's method and a step size $\delta t = 10^{-5}\,\mathrm{s}$ were used. The outputs of the original model are considered as reference and any discrepancy between the waveforms in fig. 4.1 is interpreted as error of the transformed model.

Owing to the results in fig. 4.1, the current and torque error is in the order of $10^{-3}\,\mathrm{N\,m}$ which is negligible. With a discrepancy less than $10^{-10}\,\mathrm{rad\,s^{-1}}$, the angular velocity waveforms are almost perfectly correlated. Reducing the step size by a power of ten decreases the current and torque error by a factor 100. This suggests that the apparent differences observed between the two models are caused by numerical errors.

Euler's, Heun's and the Bogacki-Shampine method were examined alongside the zero-order hold assumption to obtain a discrete-time representation of the transformed model. Tests were conducted on the real-time system under the same conditions as for the original model (cf. sections 3.7.4 and 3.7.5). Fig. 4.2 compares the steady-state stator current and its spectrum as well as the angular velocity predicted using Heun's method with the corresponding measured quantities at no load and rated load. The results are in line with the ones presented in fig. 3.11. Fig. 4.3 shows the dynamic responses of the quantities computed with Euler's, Heun's and the Bogacki-Shampine method to a rated load torque step alongside the measured waveforms. The results are consistent with the ones shown in fig. 3.13.

Table 4.1 provides an overview of the maximal model and interrupt routine execution times obtained with the three numerical methods. The substantial decrease of the model execution time resulting from the order reduction achieved by means of the transformation is striking (cf. table 3.1). No tangible difference in computational effort can be detected in comparison to Park's model.

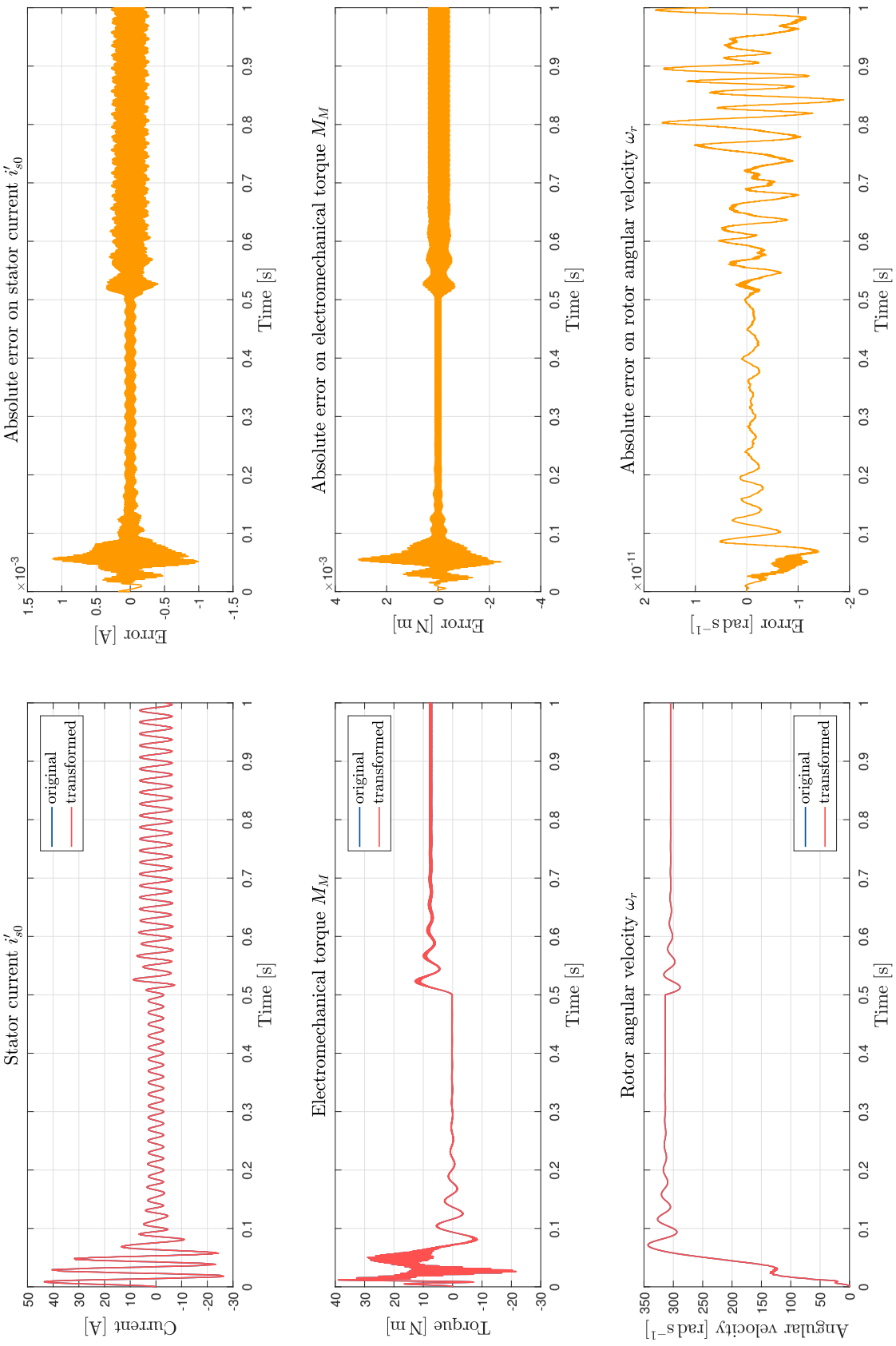

Figure 4.1: Comparison of the transformed and the original model in simulation (models of IM1 with $\mathcal{H} = \{1, 17\}$, Heun's method with step size $\delta t = 10^{-5}$ s)

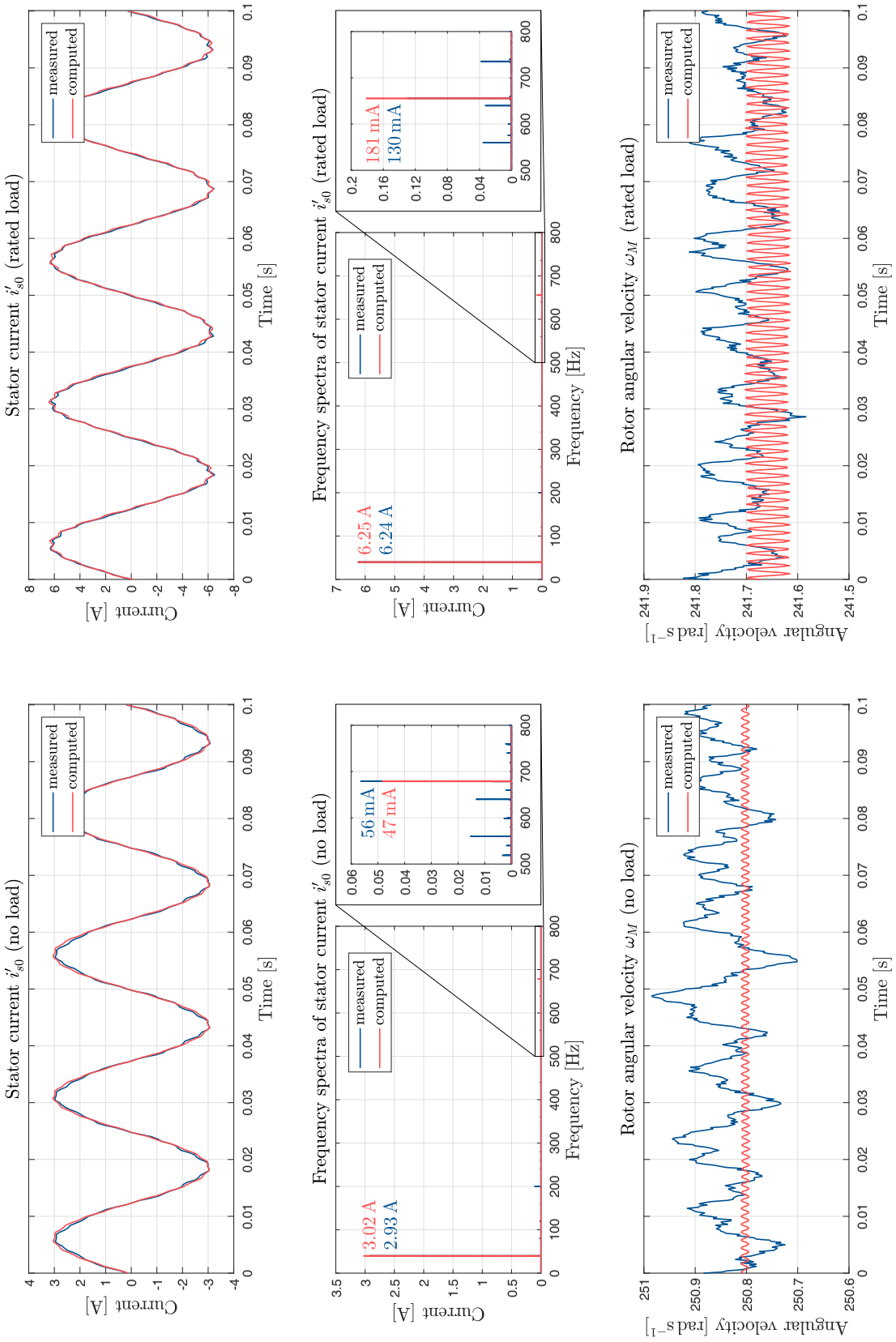

Figure 4.2: Comparison of stator current and rotor angular velocity waveforms as well as stator current spectra obtained using Heun's method with experimental results under no load and rated load conditions (transformed model of IM1 with $\mathcal{H} = \{1, 17\}$)

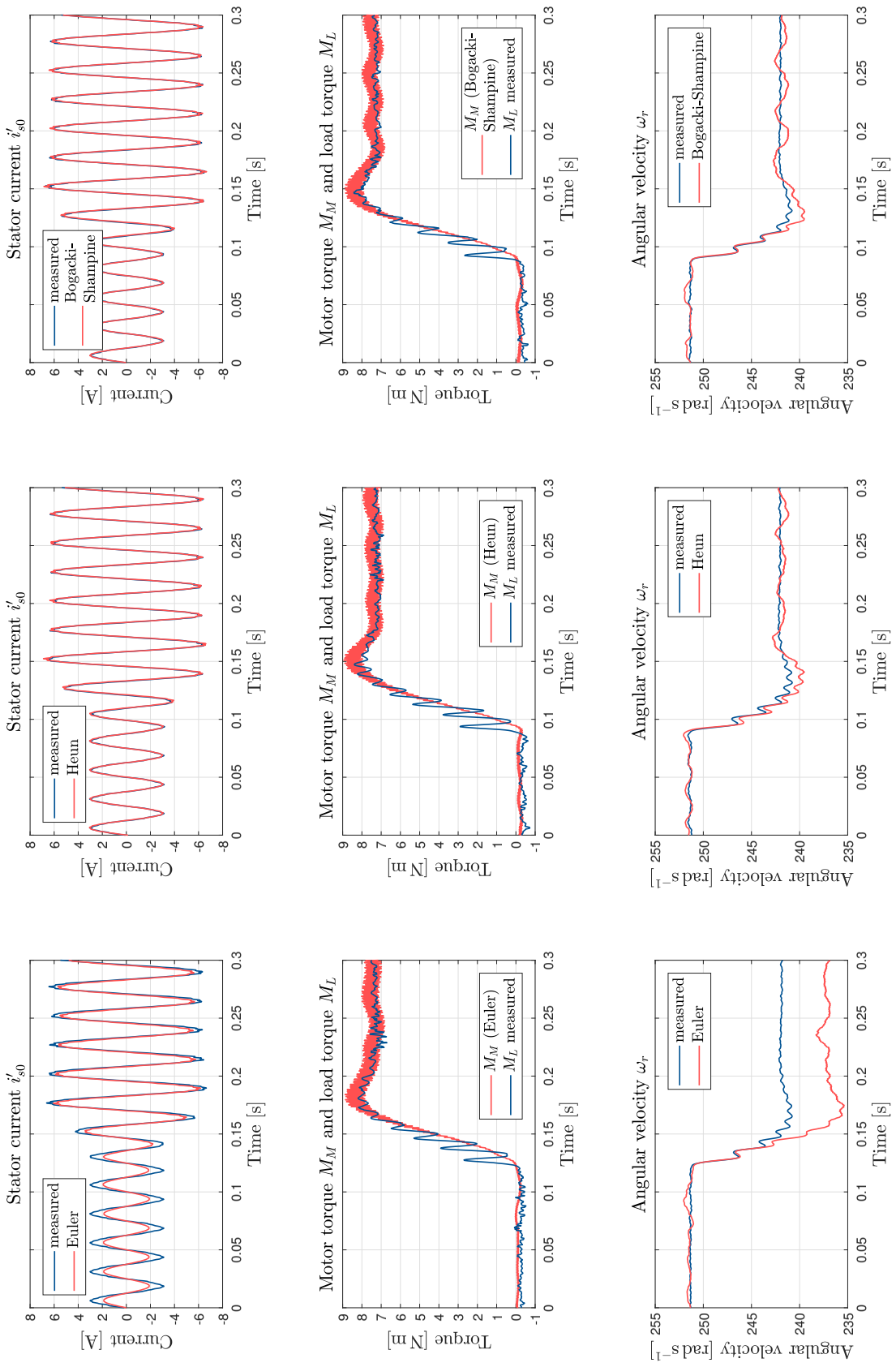

Figure 4.3: Response of each model variant to a rated load step compared to experimental data (IM1, transformed model with $\mathcal{H} = \{1, 17\}$)

Method	**Model** [μs]	**Interrupt routine** [μs]
Euler	3.4	23.6
Heun	5.3	25.8
Bogacki-Shampine	7.5	27.8

Table 4.1: Maximal execution times obtained on the real-time system for each numerical method (transformed model of IM1 with $\mathcal{H} = \{1, 17\}$)

The computation times resulting from the zero-order hold assumption and the approximations of the matrix exponential as partial sum of order 1 to 3 are summarized in table 4.2. An increase of the order from 1 to 3 has imperceptible consequences on the execution times. For this reason, order 3 should be used as it provides better accuracy.

Approximation order	**Model** [μs]	**Interrupt routine** [μs]
1	3.4	23.5
2	3.5	23.5
3	3.5	23.3

Table 4.2: Maximal execution times obtained on the real-time system with approximations of the matrix exponential of order 1 to 3 (transformed model of IM1 with $\mathcal{H} = \{1, 17\}$)

4.3.4 Model of IM2 with wavelengths of order $h = 2$ and $h = 26$

Following the particularly encouraging results delivered by the transformed model of IM1, we apply the same methodology to build a model of IM2 taking into account the space harmonics of order 2 and 26.

Expressions of the transformed inductance matrices

We recall that each of the $w_s = 3$ stator windings was modelled as a series connection of two circuits and therefore $m_s = 6$ (see section 3.7.1). This choice enables us to apply the transformation theory developed in this chapter, since it ensures that the stator and rotor main inductance matrices are *circulant*. The rotor cage having $N_r = 28$ bars, $m_r = 28$ rotor circuits are used. We also remember that the wavelength of order 2 represents the 'fundamental' in respect of Park's approach, since the machine has $Z_p = 2$ pole pairs.

The subsequent relations apply to the wavelength of order 2:

$$\begin{cases} h \equiv 2 \pmod{m_s} \\ h \equiv 2 \pmod{m_r} \end{cases} \implies \begin{cases} k_0 = 2 \neq m_s - k_0 = 4 \\ l_0 = 2 \neq m_r - l_0 = 26 \end{cases}$$

The expressions of the transformed inductance matrices for the space harmonic of order 2, $\widetilde{\mathbf{L}}^{\natural}_{\mathbf{s\,2}}$, $\widetilde{\mathbf{L}}^{\natural}_{\mathbf{r\,2}}$ and $\widetilde{\mathbf{L}}^{\natural}_{\mathbf{rs\,2}}$, are:

$$\widetilde{\mathbf{L}}^{\natural}_{\mathbf{s\,2}} = 3\widetilde{L}_{s,\,2}\,\mathrm{diag}[0,\,0,\,1,\,0,\,1,\,0]$$

$$\widetilde{\mathbf{L}}^{\natural}_{\mathbf{r\,2}} = 14\widetilde{L}_{r,\,2}\,\mathrm{diag}[0,\,0,\,1,\,0 \quad \ldots \quad 0,\,1,\,0]$$

$$\widetilde{\mathbf{L}}^{\natural}_{\mathbf{rs\,2}} = \sqrt{42} L_{M,2} \begin{array}{c} \\ k{=}0 \\ \\ \\ \\ \\ k{=}5 \end{array} \overset{\begin{matrix} n{=}0 & & & & & & & n{=}27 \end{matrix}}{\begin{bmatrix} 0 & 0 & 0 & 0 & \dots & 0 & 0 & 0 \\ 0 & 0 & 0 & 0 & \dots & 0 & 0 & 0 \\ 0 & 0 & e^{j\theta'_{r,2}} & 0 & \dots & 0 & 0 & 0 \\ 0 & 0 & 0 & 0 & \dots & 0 & 0 & 0 \\ 0 & 0 & 0 & 0 & \dots & 0 & e^{-j\theta'_{r,2}} & 0 \\ 0 & 0 & 0 & 0 & \dots & 0 & 0 & 0 \end{bmatrix}}$$

Now considering the contribution of wavelength 26,

$$\begin{cases} h \equiv 2 \pmod{m_s} \\ h \equiv 26 \pmod{m_r} \end{cases} \Longrightarrow \begin{cases} k_0 = 2 \neq m_s - k_0 = 4 \\ l_0 = 26 \neq m_r - l_0 = 2 \end{cases}$$

the corresponding transformed inductance matrices, $\widetilde{\mathbf{L}}^{\natural}_{\mathbf{s\,26}}$, $\widetilde{\mathbf{L}}^{\natural}_{\mathbf{r\,26}}$ and $\widetilde{\mathbf{L}}^{\natural}_{\mathbf{rs\,26}}$ are:

$$\widetilde{\mathbf{L}}^{\natural}_{\mathbf{s\,26}} = 3\widetilde{L}_{s,26}\,\mathrm{diag}[0,\ 0,\ 1,\ 0,\ 1,\ 0]$$

$$\widetilde{\mathbf{L}}^{\natural}_{\mathbf{r\,26}} = 14\widetilde{L}_{r,26}\,\mathrm{diag}[0,\ 0,\ 1,\ 0 \quad \dots \quad 0,\ 1,\ 0]$$

$$\widetilde{\mathbf{L}}^{\natural}_{\mathbf{rs\,26}} = \sqrt{42} L_{M,26} \begin{array}{c} \\ k{=}0 \\ \\ \\ \\ \\ k{=}5 \end{array} \overset{\begin{matrix} n{=}0 & & & & & & & n{=}27 \end{matrix}}{\begin{bmatrix} 0 & 0 & 0 & 0 & \dots & 0 & 0 & 0 \\ 0 & 0 & 0 & 0 & \dots & 0 & 0 & 0 \\ 0 & 0 & 0 & 0 & \dots & 0 & e^{j\theta'_{r,26}} & 0 \\ 0 & 0 & 0 & 0 & \dots & 0 & 0 & 0 \\ 0 & 0 & e^{-j\theta'_{r,26}} & 0 & \dots & 0 & 0 & 0 \\ 0 & 0 & 0 & 0 & \dots & 0 & 0 & 0 \end{bmatrix}}$$

The transformed total stator and rotor inductance matrices follow as:

$$\begin{aligned} \mathbf{L}^{\natural}_{\mathbf{s}} &= \mathbf{L}^{\natural}_{\sigma\mathbf{s}} + \widetilde{\mathbf{L}}^{\natural}_{\mathbf{s\,2}} + \widetilde{\mathbf{L}}^{\natural}_{\mathbf{s\,26}} \\ &= \mathrm{diag}\Big[L_{\sigma s},\ L_{\sigma s},\ L_{\sigma s} + 3\Big(\widetilde{L}_{s,2} + \widetilde{L}_{s,26}\Big),\ L_{\sigma s},\ L_{\sigma s} + 3\Big(\widetilde{L}_{s,2} + \widetilde{L}_{s,26}\Big),\ L_{\sigma s}\Big] \end{aligned} \tag{4.102}$$

$$\begin{aligned} \mathbf{L}^{\natural}_{\mathbf{r}} &= \mathbf{L}^{\natural}_{\sigma\mathbf{r}} + \widetilde{\mathbf{L}}^{\natural}_{\mathbf{r\,2}} + \widetilde{\mathbf{L}}^{\natural}_{\mathbf{r\,26}} \\ &= \mathrm{diag}\Big[L_{\sigma r},\ L_{\sigma r},\ L_{\sigma r} + 14\Big(\widetilde{L}_{r,2} + \widetilde{L}_{r,26}\Big),\ L_{\sigma r} \quad \dots \quad L_{\sigma r},\ L_{\sigma r} + 14\Big(\widetilde{L}_{r,2} + \widetilde{L}_{r,26}\Big),\ L_{\sigma r}\Big] \end{aligned} \tag{4.103}$$

The submatrix $\widetilde{\mathbf{L}}^{\natural}_{\mathbf{rs}}$, accounting for the effect of transformed rotor currents on transformed stator flux linkages, has the following expression:

$$\widetilde{\mathbf{L}}^{\natural}_{\mathbf{rs}} = \sqrt{42} \begin{bmatrix} 0 & 0 & 0 & 0 & \dots & 0 & 0 & 0 \\ 0 & 0 & 0 & 0 & \dots & 0 & 0 & 0 \\ 0 & 0 & L_{M,2} e^{j\theta'_{r,2}} & 0 & \dots & 0 & L_{M,26} e^{j\theta'_{r,26}} & 0 \\ 0 & 0 & 0 & 0 & \dots & 0 & 0 & 0 \\ 0 & 0 & L_{M,26} e^{-j\theta'_{r,26}} & 0 & \dots & 0 & L_{M,2} e^{-j\theta'_{r,2}} & 0 \\ 0 & 0 & 0 & 0 & \dots & 0 & 0 & 0 \end{bmatrix} \tag{4.104}$$

Simplified transformed voltage and torque equations

As for the model of IM1, a single voltage equation is needed on the stator and the rotor side respectively to fully describe the electromagnetic relations in the model with $\mathcal{H} = \{2,\, 26\}$. This fact follows from the position of the non-zero entries in the transformed inductance submatrices.

Bearing in mind that $u^{\natural}_{s,\,4} = \overline{u^{\natural}_{s,\,2}}$, $i^{\natural}_{s,\,4} = \overline{i^{\natural}_{s,\,2}}$ and $i^{\natural}_{r,\,26} = \overline{i^{\natural}_{r,\,2}}$, we obtain:

$$\begin{aligned}
u^{\natural}_{s,\,2} &= R_s i^{\natural}_{s,\,2} + L_s \frac{\mathrm{d}i^{\natural}_{s,\,2}}{\mathrm{d}t} + \sqrt{42}\left[L_{M,\,2} e^{j\theta'_{r,\,2}} \frac{\mathrm{d}i^{\natural}_{r,\,2}}{\mathrm{d}t} + L_{M,\,26} e^{j\theta'_{r,\,26}} \frac{\mathrm{d}\overline{i^{\natural}_{r,\,2}}}{\mathrm{d}t}\right] \\
&\quad + j\omega_r \sqrt{42}\left[2L_{M,\,2} e^{j\theta'_{r,\,2}} i^{\natural}_{r,\,2} + 26 L_{M,\,26} e^{j\theta'_{r,\,26}} \overline{i^{\natural}_{r,\,2}}\right] \\
0 &= R_r i^{\natural}_{r,\,2} + L_r \frac{\mathrm{d}i^{\natural}_{r,\,2}}{\mathrm{d}t} + \sqrt{42}\left[L_{M,\,2} e^{-j\theta'_{r,\,2}} \frac{\mathrm{d}i^{\natural}_{s,\,2}}{\mathrm{d}t} + L_{M,\,26} e^{j\theta'_{r,\,26}} \frac{\mathrm{d}\overline{i^{\natural}_{s,\,2}}}{\mathrm{d}t}\right] \\
&\quad + j\omega_r \sqrt{42}\left[-2L_{M,\,2} e^{-j\theta'_{r,\,2}} i^{\natural}_{s,\,2} + 26 L_{M,\,26} e^{j\theta'_{r,\,26}} \overline{i^{\natural}_{s,\,2}}\right]
\end{aligned} \tag{4.105}$$

where $L_s = L_{\sigma s} + 3\left[\widetilde{L}_{s,\,2} + \widetilde{L}_{s,\,26}\right]$ and $L_r = L_{\sigma r} + 14\left[\widetilde{L}_{r,\,2} + \widetilde{L}_{r,\,26}\right]$.

The expression of the electromechanical torque including the influence of wavelengths 2 and 26 results from (4.27):

$$\begin{aligned}
M_M &= \overline{\underline{i}^{\natural}_{s}}^{\top} \frac{\partial \widetilde{\mathbf{L}}^{\natural}_{\mathbf{rs}}(\theta_r)}{\partial \theta_r} \underline{i}^{\natural}_{r} \\
&= \left[\overline{i^{\natural}_{s,\,0}} \quad \overline{i^{\natural}_{s,\,1}} \quad \overline{i^{\natural}_{s,\,2}} \quad \overline{i^{\natural}_{s,\,3}} \quad \overline{i^{\natural}_{s,\,4}} \quad \overline{i^{\natural}_{s,\,5}}\right]^{\top} j\sqrt{42} \left[i^{\natural}_{r,\,2} \begin{bmatrix} 0 \\ 0 \\ 2L_{M,\,2} e^{j\theta'_{r,\,2}} \\ 0 \\ -26 L_{M,\,26} e^{-j\theta'_{r,\,26}} \\ 0 \end{bmatrix} + i^{\natural}_{r,\,26} \begin{bmatrix} 0 \\ 0 \\ 26 L_{M,\,26} e^{j\theta'_{r,\,26}} \\ 0 \\ -2L_{M,\,2} e^{-j\theta'_{r,\,2}} \\ 0 \end{bmatrix} \right] \\
&= \sqrt{42}\left[\overline{i^{\natural}_{s,\,2}} \quad i^{\natural}_{s,\,2}\right]^{\top} \begin{bmatrix} j2L_{M,\,2} e^{j\theta'_{r,\,2}} i^{\natural}_{r,\,2} + j26 L_{M,\,26} e^{j\theta'_{r,\,26}} \overline{i^{\natural}_{r,\,2}} \\ -j2L_{M,\,2} e^{-j\theta'_{r,\,2}} i^{\natural}_{r,\,2} - j26 L_{M,\,26} e^{-j\theta'_{r,\,26}} \overline{i^{\natural}_{r,\,2}} \end{bmatrix} \\
&= 4\sqrt{42}\left[L_{M,\,2} \mathfrak{Re}\left[\overline{i^{\natural}_{s,\,2}} j e^{j\theta'_{r,\,2}} i^{\natural}_{r,\,2}\right] + 13 L_{M,\,26} \mathfrak{Re}\left[\overline{i^{\natural}_{s,\,2}} j e^{j\theta'_{r,\,26}} \overline{i^{\natural}_{r,\,2}}\right]\right]
\end{aligned} \tag{4.106}$$

Continuous-time state-space model with real state variables

In order to obtain a model representation with real variables, we define:

$$u^{\natural}_{s,\,2} = u_{s,\,2\alpha} + j u_{s,\,2\beta} \qquad (u_{s,\,2\alpha},\, u_{s,\,2\beta}) \in \mathbb{R}^2; \qquad u^{\natural}_{r,\,2} = u_{r,\,2d} + j u_{r,\,2q} \qquad (u_{r,\,2d},\, u_{r,\,2q}) \in \mathbb{R}^2$$

$$i^{\natural}_{s,\,2} = i_{s,\,2\alpha} + j i_{s,\,2\beta} \qquad (i_{s,\,2\alpha},\, i_{s,\,2\beta}) \in \mathbb{R}^2; \qquad i^{\natural}_{r,\,2} = i_{r,\,2d} + j i_{r,\,2q} \qquad (i_{r,\,2d},\, i_{r,\,2q}) \in \mathbb{R}^2$$

and bring the voltage equation in the form:

$$\vec{\underset{\circ}{u}} = \underset{\circ}{\mathbf{L}}(\theta_r)\frac{\mathrm{d}\vec{\underset{\circ}{i}}}{\mathrm{d}t} + \underset{\circ}{\mathbf{P}}(\theta_r, \omega_r)\vec{\underset{\circ}{i}} \tag{4.107}$$

where

$$\vec{\underset{\circ}{u}} = \begin{bmatrix} u_{s,\,2\alpha} & u_{s,\,2\beta} & u_{r,\,2d} & u_{r,\,2q} \end{bmatrix}^\top; \qquad \vec{\underset{\circ}{i}} = \begin{bmatrix} i_{s,\,2\alpha} & i_{s,\,2\beta} & i_{r,\,2d} & i_{r,\,2q} \end{bmatrix}^\top$$

$$\underset{\circ}{\mathbf{L}} = \begin{bmatrix} L_s\mathbf{I_2} & \sqrt{42}\left[L_{M,\,2}\mathbf{T}(\theta'_{r,\,2}) + L_{M,\,26}\mathbf{T}(\theta'_{r,\,26})\mathbf{S}\right] \\ \sqrt{42}\left[L_{M,\,2}\mathbf{T}(-\theta'_{r,\,2}) + L_{M,\,26}\mathbf{T}(\theta'_{r,\,26})\mathbf{S}\right] & L_r\mathbf{I_2} \end{bmatrix}$$

and

$$\underset{\circ}{\mathbf{P}} = \begin{bmatrix} R_s\mathbf{I_2} & \sqrt{42}\omega_r\mathbf{J}\left[2L_{M,\,2}\mathbf{T}(\theta'_{r,\,2}) + 26L_{M,\,26}\mathbf{T}(\theta'_{r,\,26})\mathbf{S}\right] \\ \sqrt{42}\omega_r\mathbf{J}\left[-2L_{M,\,2}\mathbf{T}(-\theta'_{r,\,2}) + 26L_{M,\,26}\mathbf{T}(\theta'_{r,\,26})\mathbf{S}\right] & R_r\mathbf{I_2} \end{bmatrix}$$

The torque is given by the relation:

$$M_M = 4\sqrt{42}\begin{bmatrix} i_{s,\,2\alpha} & i_{s,\,2\beta} \end{bmatrix}\mathbf{J}\left[L_{M,\,2}\mathbf{T}(\theta'_{r,\,2}) + 13L_{M,\,26}\mathbf{S}\mathbf{T}(-\theta'_{r,\,26})\right]\begin{bmatrix} i_{r,\,2d} \\ i_{r,\,2q} \end{bmatrix} \tag{4.108}$$

Remark:
For the conductor distribution functions W_{s0} and W_{r0} shown in fig. A.8 and A.9, $\varphi_2 = 0$ and $\varphi_{26} = 0$. Hence, $\theta'_{r,\,2} = 2\theta_r$ and $\theta'_{r,\,26} = 26\theta_r$.

For the same reasons as in section 4.3.3, $\underset{\circ}{\mathbf{L}}$ has full rank. This allows for the components of $\vec{\underset{\circ}{i}}$ to be chosen as state variables alongside the rotor angular velocity ω_r and the rotor angle θ_r. The subsequent continuous-time state-space representation of the model with wavelengths 2 and 26 results from this choice:

$$\begin{cases} \dfrac{\mathrm{d}\vec{\underset{\circ}{i}}}{\mathrm{d}t} = -\underset{\circ}{\mathbf{L}}^{-1}(\theta_r)\underset{\circ}{\mathbf{P}}(\theta_r, \omega_r)\vec{\underset{\circ}{i}} + \underset{\circ}{\mathbf{L}}^{-1}(\theta_r)\vec{\underset{\circ}{u}} & \text{(4.109a)} \\ \dfrac{\mathrm{d}\omega_r}{\mathrm{d}t} = \dfrac{1}{J_M}(M_M - C_W\omega_r - M_L) & \text{(4.109b)} \\ \dfrac{\mathrm{d}\theta_r}{\mathrm{d}t} = \omega_r & \text{(4.109c)} \\ M_M = 4\sqrt{42}\begin{bmatrix} i_{s,\,2\alpha} & i_{s,\,2\beta} \end{bmatrix}\mathbf{J}[L_{M,\,2}\mathbf{T}(2\theta_r) + 13L_{M,\,26}\mathbf{S}\mathbf{T}(-26\theta_r)]\begin{bmatrix} i_{r,\,2d} \\ i_{r,\,2q} \end{bmatrix} \end{cases}$$

Setting up the transformation matrix

Substituting the expression of the stator interconnection matrix introduced in section 3.7.1 into Definition 8 yields the transformation matrix $\mathcal{Z}_{\mathrm{s,\,IM2}}$:

$$\mathcal{Z}_{\mathrm{s,\,IM2}} = \overline{\mathcal{W}_6}^{\top}\mathbf{C_{s,\,IM2}} = \frac{1}{\sqrt{6}}\begin{bmatrix} 1 & 1 & 1 & 1 & 1 & 1 \\ 1 & e^{j\pi/3} & e^{j2\pi/3} & -1 & e^{j4\pi/3} & e^{j5\pi/3} \\ 1 & e^{j2\pi/3} & e^{j4\pi/3} & 1 & e^{j2\pi/3} & e^{j4\pi/3} \\ 1 & -1 & 1 & -1 & 1 & -1 \\ 1 & e^{j4\pi/3} & e^{j2\pi/3} & 1 & e^{j4\pi/3} & e^{j2\pi/3} \\ 1 & e^{j5\pi/3} & e^{j4\pi/3} & -1 & e^{j2\pi/3} & e^{j\pi/3} \end{bmatrix}\begin{bmatrix} 1 & 0 \\ 0 & 1 \\ -1 & -1 \\ 1 & 0 \\ 0 & 1 \\ -1 & -1 \end{bmatrix}$$

$$= \sqrt{2}j\begin{bmatrix} 0 & 0 \\ 0 & 0 \\ -e^{j2\pi/3} & 1 \\ 0 & 0 \\ e^{-j2\pi/3} & -1 \\ 0 & 0 \end{bmatrix} \tag{4.110}$$

Thus, in the present case, (4.54a) becomes:

$$\underline{i}_s^{\natural} = \begin{bmatrix} i_{s,\,0}^{\natural} \\ i_{s,\,1}^{\natural} \\ i_{s,\,2}^{\natural} \\ i_{s,\,3}^{\natural} \\ i_{s,\,4}^{\natural} \\ i_{s,\,5}^{\natural} \end{bmatrix} = \sqrt{2}j\begin{bmatrix} 0 & 0 \\ 0 & 0 \\ -e^{j2\pi/3} & 1 \\ 0 & 0 \\ e^{-j2\pi/3} & -1 \\ 0 & 0 \end{bmatrix}\begin{bmatrix} i'_{s0} \\ i'_{s1} \end{bmatrix} \tag{4.111}$$

In other words, the process of interconnecting the stator circuits imposes $i_{s,\,0}^{\natural} = 0$, $i_{s,\,1}^{\natural} = 0$, $i_{s,\,3}^{\natural} = 0$ and $i_{s,\,5}^{\natural} = 0$. Owing to relation (4.73), $i_{s,\,4}^{\natural} = \overline{i_{s,\,2}^{\natural}}$.

Consequently, defining the matrix

$$\mathcal{Z}'_{\mathrm{s,\,IM2}} = \sqrt{2}j\begin{bmatrix} -e^{j2\pi/3} & 1 \\ e^{-j2\pi/3} & -1 \end{bmatrix} \tag{4.112}$$

(4.111) can be simplified as follows:

$$\begin{bmatrix} i_{s,\,2}^{\natural} \\ \overline{i_{s,\,2}^{\natural}} \end{bmatrix} = \mathcal{Z}'_{\mathrm{s,\,IM2}}\begin{bmatrix} i'_{s0} \\ i'_{s1} \end{bmatrix} \tag{4.113}$$

Remark:
As the $w_s = 3$ stator windings are modelled with $m_s = 6$ circuits, the transformation of stator quantities involves a 6 point DFT. Theoretically, the 6 point DFT allows for the distinction between three classes of wavelengths depending on which of the following condition holds for the order h:

1.) $h \equiv 0 \pmod 3$: the wavelength will directly influence component number 0 of the stator quantities

(e.g. $i^{\natural}_{s,0}$*);*

2.) $h \equiv 1 \pmod 3$*: the wavelength will impact on component no. 1;*

3.) $h \equiv 2 \pmod 3$*: the wavelength will have a direct effect on component no. 2.*

We see, however, that these benefits are lost when the circuits are interconnected and we obtain a situation similar to IM1. Thus, not the number of circuits but the number of windings is decisive with respect to the segregation of wavelengths.

As $\det\left(\mathcal{Z}'_{\mathrm{s,\,IM2}}\right) = -j2\sqrt{3}$, $\mathcal{Z}'_{\mathrm{s,\,IM2}}$ is nonsingular and

$$\mathcal{Z}'^{-1}_{\mathrm{s,\,IM2}} = \frac{1}{\sqrt{6}} \begin{bmatrix} 1 & 1 \\ e^{-j2\pi/3} & e^{j2\pi/3} \end{bmatrix} \tag{4.114}$$

Consequently, the following relation can be deduced, which enables us to determine the original stator currents from the transformed ones:

$$\begin{bmatrix} i'_{s0} \\ i'_{s1} \end{bmatrix} = \frac{2}{\sqrt{6}} \begin{bmatrix} 1 & 0 \\ -1/2 & \sqrt{3}/2 \end{bmatrix} \begin{bmatrix} i_{s,\,2\alpha} \\ i_{s,\,2\beta} \end{bmatrix} \tag{4.115}$$

Similarly, using (4.54b), the subsequent relation is derived for the voltages

$$\begin{bmatrix} u_{s,\,2\alpha} \\ u_{s,\,2\beta} \end{bmatrix} = \begin{bmatrix} \frac{1}{\sqrt{6}} & -\frac{1}{2\sqrt{6}} \\ 0 & \frac{1}{2\sqrt{2}} \end{bmatrix} \begin{bmatrix} u'_{s0} \\ u'_{s1} \end{bmatrix} \tag{4.116}$$

which allows the computation of the model inputs from the impressed stator voltages.

Simulation and experimental results

As for IM1, the simulated response of the transformed model to a set of balanced sinusoidal voltages (frequency $f = 50\,\mathrm{Hz}$, line-to-line voltage $U = 400\,\mathrm{V}$) and a rated load torque step is consistent with the original (see fig. 4.4). Again, a decrease of the step size by a factor 10 reduces the error by a factor 100, which makes numerical issues the likely cause of the discrepancies between the two model versions.

Fig. 4.5 provides a steady-state comparison of the computed and measured stator current and rotor angular velocity. The results are in line with the ones of the original model (cf. fig. 3.12). This is also the case for the dynamic responses of the discrete-time model variants derived from Euler's, Heun's and the Bogacki-Shampine method to a rated load torque step (compare fig. 4.6 and 3.14). We note that Euler's method remains unstable with the reduced-order transformed model.

Method	**Model** [μs]	**Interrupt routine** [μs]
Euler	3.8	24.1
Heun	6.0	26.5
Bogacki-Shampine	8.2	28.7

Table 4.3: Maximal execution times obtained on the real-time system with numerical methods (transformed model of IM2 with $\mathcal{H} = \{2, 26\}$)

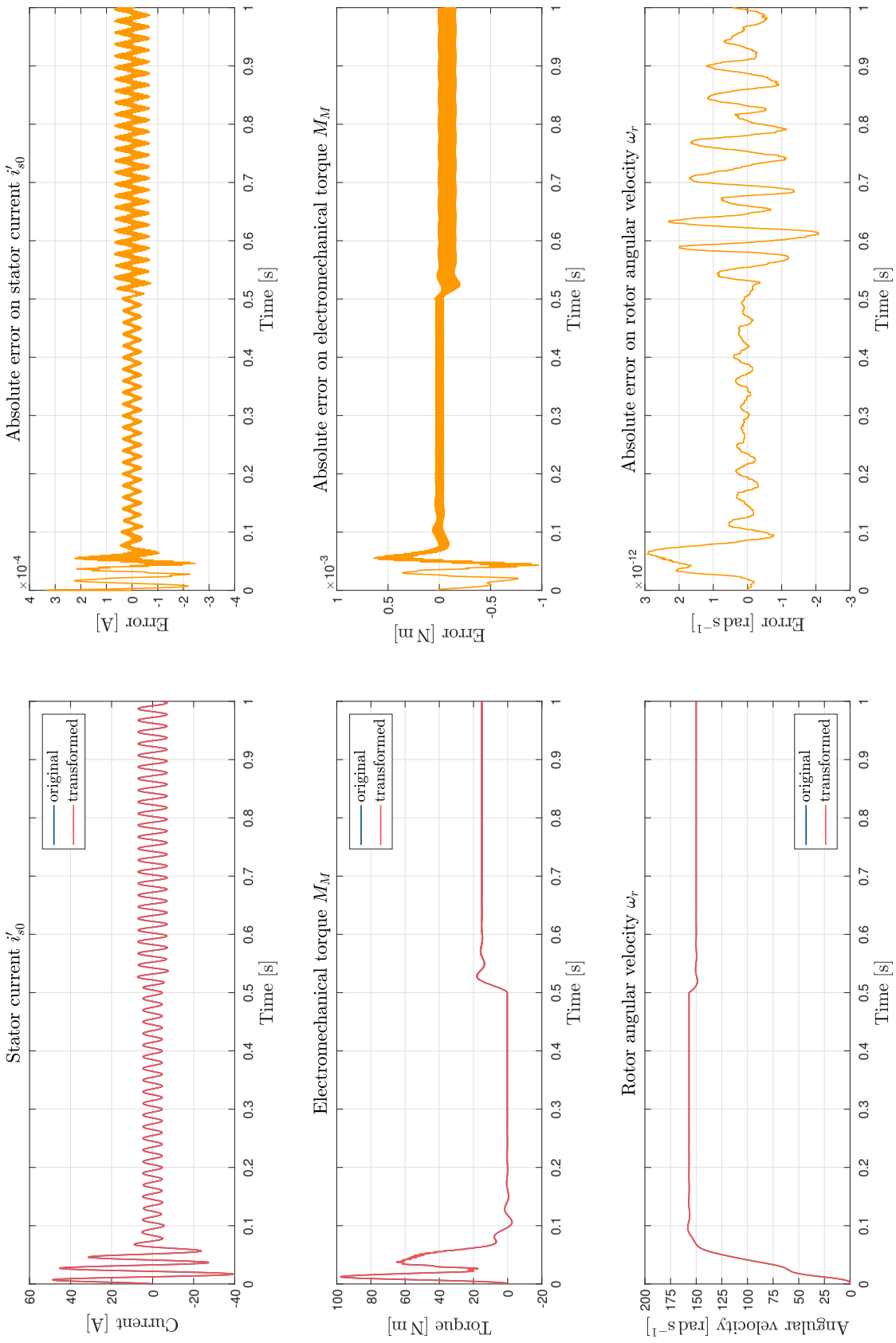

Figure 4.4: Comparison of the transformed and the original model in simulation (models of IM2 with $\mathcal{H} = \{2, 26\}$, Heun's method with step size $\delta t = 10^{-5}$ s)

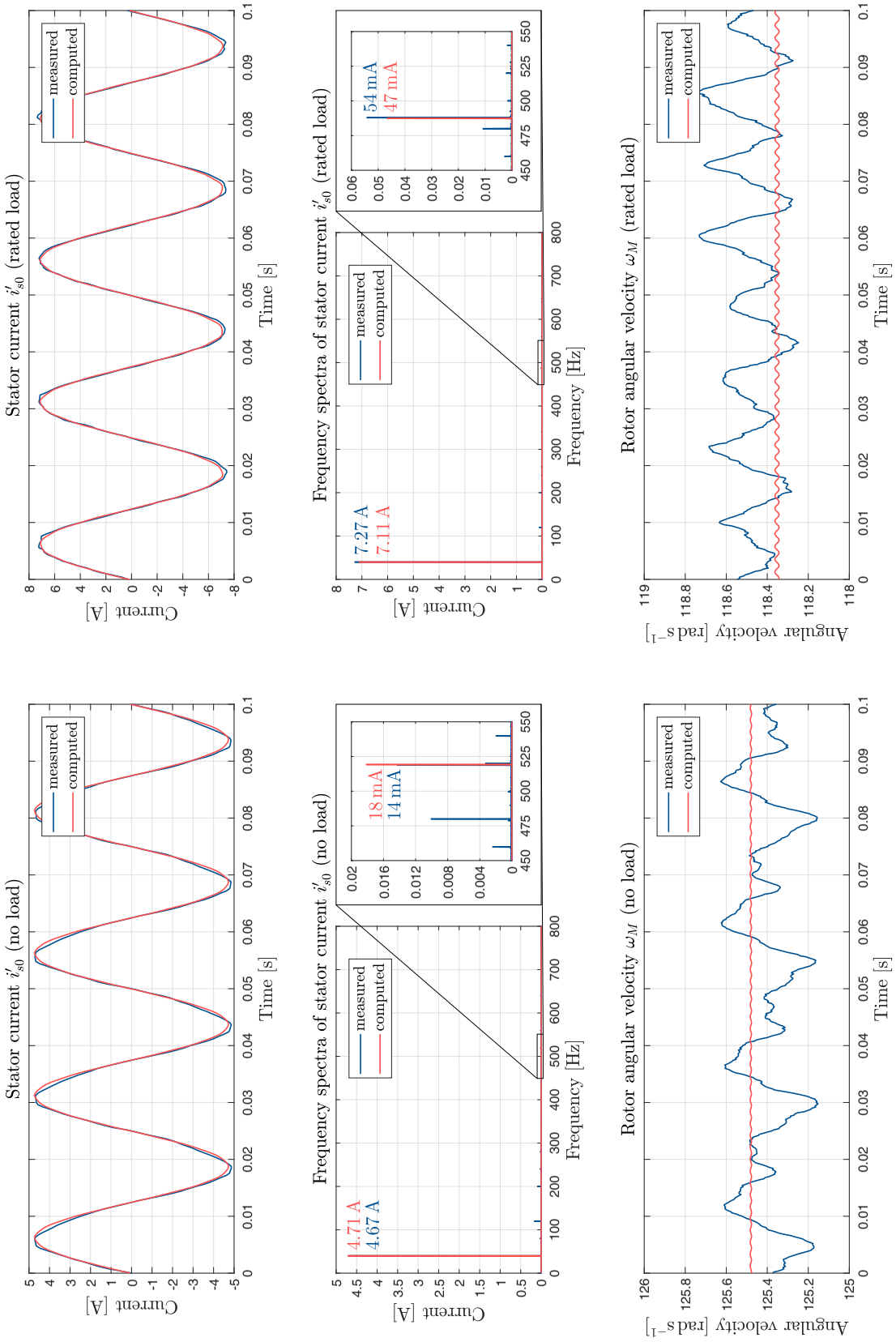

Figure 4.5: Comparison of stator current and rotor angular velocity waveforms as well as stator current spectra obtained using Heun's method with experimental results under no load and rated load conditions (transformed model of IM2 with $\mathcal{H} = \{2, 26\}$)

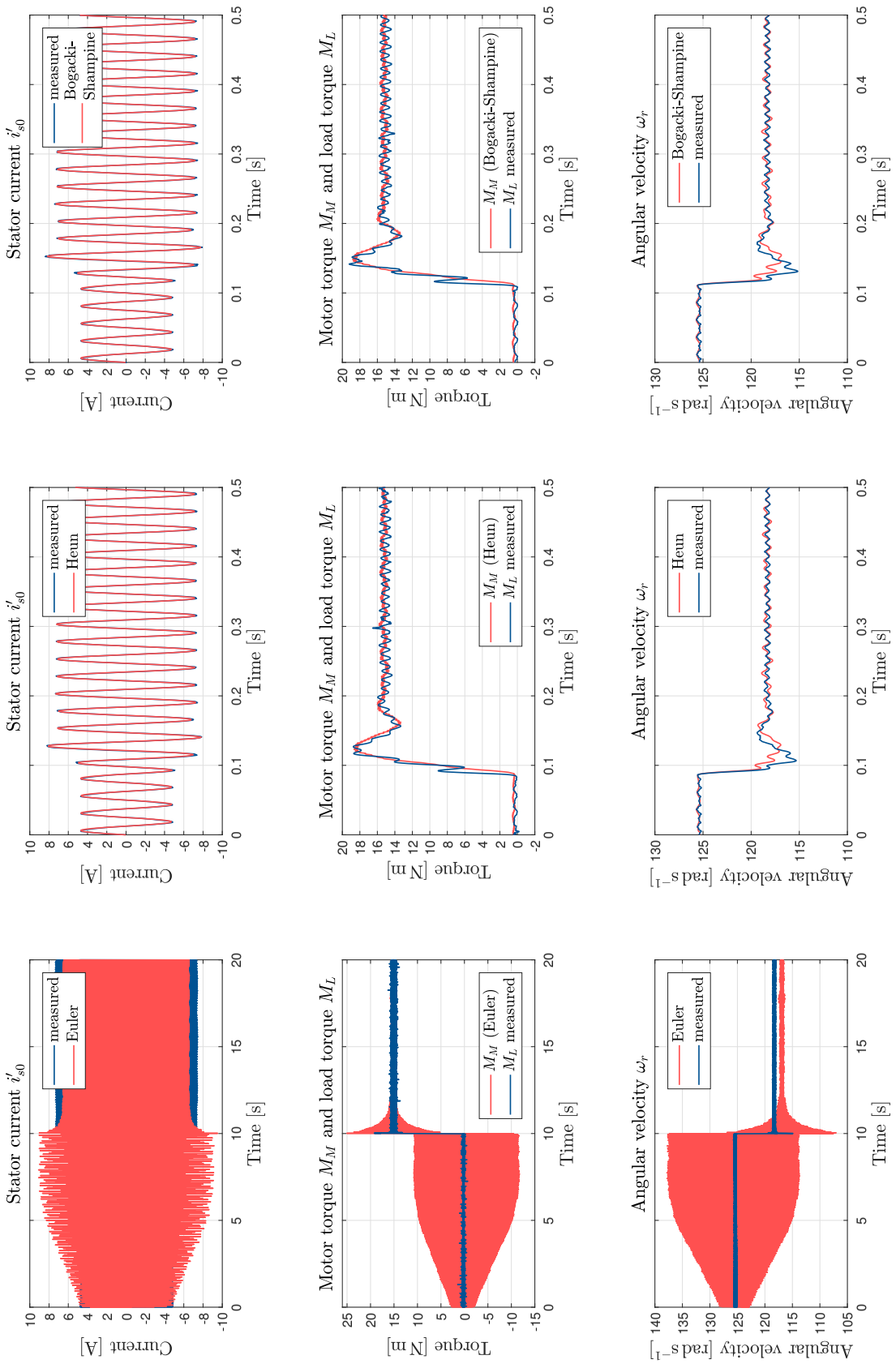

Figure 4.6: Response of each model variant to a rated load step compared to experimental data (IM2, transformed model with $\mathcal{H} = \{2, 26\}$)

Approximation order	**Model** [μs]	**Interrupt routine** [μs]
1	4.1	24.2
2	4.1	24.2
3	4.2	24.4

Table 4.4: Maximal execution times obtained on the real-time system with the zero-order hold assumption (transformed model of IM2 with $\mathcal{H} = \{2, 26\}$)

Table 4.3 provides an overview of the execution times achieved with the numerical methods, while the times obtained with the zero-order hold assumption are given in table 4.4. The model order being 6 as well, the computational effort is comparable to the one of the transformed model of IM1. The order reduction from 31 to 6 resulting from the transformation makes possible the use of Heun's and the Bogacki-Shampine methods at $f_{sw} = 10\,\text{kHz}$, which was unfeasible with the original model (see table 3.3).

4.4 Comments on the proposed transformation

The strategy applied in this chapter to simplify the linear geometric model relies on a coordinate transformation (in mathematical terms, a change of vector basis) which allows for the diagonalization of the stator and rotor main inductance submatrices. As the latter are *circulant*, their diagonalization is carried out using Fourier matrices. In the new vector basis, the main stator and rotor inductance submatrices associated with each space harmonic have at most two non-zero entries. This is also the case for the corresponding mutual inductance matrices. These particular characteristics are at the very heart of the order reduction achieved through the basis transformation.

The method leading to the transformed state-space model presented in section 4.2.6 is essentially the same as the one developed by White and Woodson in [5] and Nasar in [61] for multi-winding induction machines. Fudeh followed a similar technique to model the effect of MMF harmonics in multi-winding machines in [78] and examined the specific case of three-phase squirrel cage machines in [79] as well as the impact of space harmonics in steady-state operation in [80]. In the latter case, the computation efficiency of the model was considered as well. Drozdowski in [75] and Munõz in [54] followed comparable approaches to derive efficient models of the three-phase squirrel-cage induction machine accounting for space harmonics. However, none of these references mentions the relationship with the discrete Fourier transform, although Nasar points out the fundamental role of circulant inductance matrices in the derivation of a simplified model.

The DFT allows us to consider space harmonics from a signal processing point of view and thus helps us gain a broader understanding of their impact on the model behaviour. The fact that the contributions of different wavelengths may appear in the same component of the transformed voltage and current vectors is a direct consequence of the aliasing phenomenon. The number of stator and rotor circuits in the model determines the size of the Fourier matrices involved in the coordinate transformation and therefore the number of points of the corresponding DFTs.

For this reason, it might seem judicious to use as many circuits as possible to describe a given winding configuration, since a DFT with more points would provide a better means of separating the space harmonics arising from this winding configuration. This property is comparable to sampling a time signal at a higher rate, which enables higher frequencies to be detected. The example of IM2, however, has shown that the necessary process of circuit interconnection will cause wavelengths seemingly distinguishable to affect the same components of the transformed voltage and current vectors.

Hence, increasing the number of stator phases is the only effective option allowing for a more accurate segregation between wavelengths.

From a broader perspective, the combination of Fourier and interconnection matrices provides a systematic method for transforming the model equations of all categories of induction machines. This is especially the case for multiphase machines and generalizes previous definitions of coordinate transformations (compare for instance [81] and [82, p. 493]).

Summary

Owing to the modelling hypotheses of the linear geometric model (cf. section 3.3, p. 37), the stator and rotor inductance submatrices are *circulant* and can therefore be diagonalized using Fourier matrices. Assuming that the circuits representing stator windings all have the same resistance and leakage inductance and this property also applies to the circuits modelling the rotor cage, the transformation of the original equations by means of Fourier matrices results in a much simpler model representation. In addition, the relation between Fourier matrices and the discrete Fourier transform provides a deeper understanding of the influence of space harmonics.

Combining Fourier and interconnection matrices, we introduced a systematic transformation for modelling multi-winding induction machines. This is one of the main contributions of the present work.

From a practical perspective, the transformation allows for a substantial decrease of computational requirements in comparison to the original model presented in chapter 3. The transformed state-space models of the machines IM1 and IM2 including two space harmonics appear interesting for real-time applications, since their complexity is comparable to Park's.

As we intend to use these models in control applications, we will take a closer look at their structural properties in the following chapter. This will allow us to make a few important observations about the controllability and the observability of the state variables.

Chapter 5
Potential of the transformed geometric model in control applications

Overview of chapter

The coordinate transformation introduced previously provides us with an extended model of induction machines promising for real-time control applications such as current or torque harmonic reduction. We now examine its practical potential more closely from two perspectives.

First, as we intend to make use of the model in closed-loop control strategies, the controllability and the observability of its states (e.g. the transformed stator and rotor currents or the rotor angular velocity) should be investigated. This is a particularly challenging task, even in the case for which only two wavelengths are considered, since the model is non-linear due to the presence of the rotor angle and speed in the inductance matrix. As a thorough analysis would go far beyond the scope of the present thesis, we focus on the structural properties of the model with $\mathcal{H} = \{1, 17\}$ and show that it is substantially similar to the one of the well-known fundamental model. For this reason, no major problem is to be expected in respect of the controllability and the observability of the currents. In addition, preliminary investigations suggest that the extended model may be appropriate for speed estimation around standstill.

Second, we discuss the issue of parameter determination. Despite the model having a very limited number of parameters, some basic information about the internal structure of the machine is necessary, e.g. the number of turns of the winding coils. This might be problematic in field applications and further work should be carried out to estimate these parameters rather than open the machine.

5.1 Controllability and observability of the transformed model

5.1.1 Adopted approach

Following the considerations in chapter 4, the order of the differential system (4.53) directly depends on the wavelengths taken into account in the model. Given the variety of possible cases, a general conclusion about the controllability and observability of the state variables is thus not possible.

In addition, the dependence of the system matrix $\mathbf{A}^\natural$ and input matrix $\mathbf{B}^\natural$ on the rotor angle can, in general, not be eliminated as in the equations of Park's model (see conclusion of [78], for instance). This is especially the case for the models of IM1 (resp. IM2) with $\mathcal{H} = \{1, 17\}$ (resp. $\mathcal{H} = \{2, 26\}$), for which the contributions of the two wavelengths appear at the same positions on the diagonal of the transformed stator and rotor inductance submatrices (see section 4.3.3). As a result, methods of non-linear control theory would have to be used to investigate properties such as controllability and observability (cf. for example [83]).

Since such analyses goes way beyond the scope of the present work, we will examine the structure of the model with $\mathcal{H} = \{1, 17\}$ and show its striking similarity to Park's. This will enable us to make a few preliminary observations with respect to controllability and observability.

5.1.2 Structural analysis of the model with wavelengths $h = 1$ and $h = 17$

We consider the model of IM1 with $\mathcal{H} = \{1, 17\}$ derived in section 4.3.3. The following continuous-time state-space representation was obtained (see (4.95)):

$$\begin{cases} \dfrac{\mathrm{d}\vec{\underset{\circ}{i}}}{\mathrm{d}t} = -\underset{\circ}{\mathbf{L}}^{-1}(\theta_r)\underset{\circ}{\mathbf{P}}(\theta_r, \omega_r)\vec{\underset{\circ}{i}} + \underset{\circ}{\mathbf{L}}^{-1}(\theta_r)\vec{\underset{\circ}{u}} & \text{(5.1a)} \\ \dfrac{\mathrm{d}\omega_r}{\mathrm{d}t} = \dfrac{1}{J_M}(M_M - M_L) & \text{(5.1b)} \\ \dfrac{\mathrm{d}\theta_r}{\mathrm{d}t} = \omega_r & \text{(5.1c)} \\ M_M = 4\sqrt{3}\begin{bmatrix} i_{s,1\alpha} & i_{s,1\beta} \end{bmatrix}\mathbf{J}[L_{M,1}\mathbf{T}(\theta_r) + 17L_{M,17}\mathbf{ST}(17\theta_r)]\begin{bmatrix} i_{r,1d} \\ i_{r,1q} \end{bmatrix} \end{cases}$$

with $i_{s,1\alpha}$, $i_{s,1\beta}$, $i_{r,1d}$, $i_{r,1q}$ as well as ω_r and θ_r as state variables.

As the matrix product $-\underset{\circ}{\mathbf{L}}^{-1}(\theta_r)\underset{\circ}{\mathbf{P}}(\theta_r, \omega_r)$ involves many trigonometric expressions depending on the rotor angle, it is preferable to use an alternative model representation to allow for better comparison with Park's. To do so, we go back to the complex voltage equations (4.89), which are rewritten in a slightly more compact form:

$$\begin{cases} u^\natural_{s,1} = R_s i^\natural_{s,1} + L_s \dfrac{\mathrm{d}i^\natural_{s,1}}{\mathrm{d}t} + 2\sqrt{3}\left[L_{M,1}\dfrac{\mathrm{d}}{\mathrm{d}t}\left[e^{j\theta'_{r,1}} i^\natural_{r,1}\right] + L_{M,17}\dfrac{\mathrm{d}}{\mathrm{d}t}\left[e^{-j\theta'_{r,17}}\overline{i^\natural_{r,1}}\right]\right] \\ u^\natural_{r,1} = R_r i^\natural_{r,1} + L_r \dfrac{\mathrm{d}i^\natural_{r,1}}{\mathrm{d}t} + 2\sqrt{3}\left[L_{M,1}\dfrac{\mathrm{d}}{\mathrm{d}t}\left[e^{-j\theta'_{r,1}} i^\natural_{s,1}\right] + L_{M,17}\dfrac{\mathrm{d}}{\mathrm{d}t}\left[e^{-j\theta'_{r,17}}\overline{i^\natural_{s,1}}\right]\right] \end{cases} \quad (5.2)$$

where $L_s = L_{\sigma s} + \dfrac{3}{2}(\widetilde{L}_{s,1} + \widetilde{L}_{s,17})$, $L_r = L_{\sigma r} + 8(\widetilde{L}_{r,1} + \widetilde{L}_{r,17})$ and $u^\natural_{r,1} = 0$.

As for the derivation of Park's model in section 4.3.2, we make the following change of variable:

$$i^{\sharp}_{r,1} = i^{\natural}_{r,1} e^{j\theta'_{r,1}} \tag{5.3}$$

and multiply the second equation in (5.2) by $e^{j\theta'_{r,1}}$, which yields:

$$\begin{cases} u^{\natural}_{s,1} = R_s i^{\natural}_{s,1} + L_s \dfrac{\mathrm{d}i^{\natural}_{s,1}}{\mathrm{d}t} + 2\sqrt{3}\left[L_{M,1} \dfrac{\mathrm{d}i^{\sharp}_{r,1}}{\mathrm{d}t} + L_{M,17} e^{-j(\theta'_{r,17} - \theta'_{r,1})} \dfrac{\mathrm{d}\overline{i^{\sharp}_{r,1}}}{\mathrm{d}t} \right] \\ \qquad - 16 j\omega_r 2\sqrt{3} L_{M,17} e^{-j(\theta'_{r,17} - \theta'_{r,1})} i^{\sharp}_{r,1} \\ u^{\sharp}_{r,1} = R_r i^{\sharp}_{r,1} + L_r \dfrac{\mathrm{d}i^{\sharp}_{r,1}}{\mathrm{d}t} + 2\sqrt{3}\left[L_{M,1} \dfrac{\mathrm{d}i^{\natural}_{s,1}}{\mathrm{d}t} + L_{M,17} e^{-j(\theta'_{r,17} - \theta'_{r,1})} \dfrac{\mathrm{d}\overline{i^{\natural}_{s,1}}}{\mathrm{d}t} \right] \\ \qquad - j\omega_r \left[L_r i^{\sharp}_{r,1} + 2\sqrt{3} L_{M,1} i^{\natural}_{s,1} + 17 L_{M,17} 2\sqrt{3} e^{-j(\theta'_{r,17} - \theta'_{r,1})} \overline{i^{\natural}_{s,1}} \right] \end{cases} \tag{5.4}$$

The torque equation becomes

$$M_M = 4\sqrt{3} L_{M,1} \mathfrak{Re}\left[\overline{i^{\natural}_{s,1}} j i^{\sharp}_{r,1} \right] + 4\sqrt{3} \cdot 17 L_{M,17} \mathfrak{Re}\left[i^{\natural}_{s,1} j e^{j(\theta'_{r,17} - \theta'_{r,1})} i^{\sharp}_{r,1} \right] \tag{5.5}$$

Introducing the notations

$$u^{\sharp}_{r,1} = u_{r,1\alpha} + j u_{r,1\beta} \qquad (u_{r,1\alpha},\, u_{r,1\beta}) \in \mathbb{R}^2 \tag{5.6}$$

$$i^{\sharp}_{r,1} = i_{r,1\alpha} + j i_{r,1\beta} \qquad (i_{r,1\alpha},\, i_{r,1\beta}) \in \mathbb{R}^2 \tag{5.7}$$

the voltage equations (5.4) are brought in a form similar to (4.93):

$$\vec{\underset{\wedge}{u}} = \underset{\wedge}{\mathbf{L}}(\theta_r) \frac{\mathrm{d}\vec{\underset{\wedge}{i}}}{\mathrm{d}t} + \underset{\wedge}{\mathbf{P}}(\theta_r, \omega_r) \vec{\underset{\wedge}{i}} \tag{5.8}$$

where

$$\vec{\underset{\wedge}{u}} = \begin{bmatrix} u_{s,1\alpha} & u_{s,1\beta} & u_{r,1\alpha} & u_{r,1\beta} \end{bmatrix}^\top; \qquad \vec{\underset{\wedge}{i}} = \begin{bmatrix} i_{s,1\alpha} & i_{s,1\beta} & i_{r,1\alpha} & i_{r,1\beta} \end{bmatrix}^\top$$

$$\underset{\wedge}{\mathbf{L}} = \begin{bmatrix} L_s \mathbf{I_2} & 2\sqrt{3}\left[L_{M,1} \mathbf{I_2} + L_{M,17} \mathbf{ST}(\theta'_{r,17} - \theta'_{r,1}) \right] \\ 2\sqrt{3}\left[L_{M,1} \mathbf{I_2} + L_{M,17} \mathbf{ST}(\theta'_{r,17} - \theta'_{r,1}) \right] & L_r \mathbf{I_2} \end{bmatrix}$$

$$\underset{\wedge}{\mathbf{P}} = \begin{bmatrix} R_s \mathbf{I_2} & -16\omega_r \cdot 2\sqrt{3} L_{M,17} \mathbf{JST}(\theta'_{r,17} - \theta'_{r,1}) \\ -2\sqrt{3}\omega_r \mathbf{J}\left[L_{M,1} \mathbf{I_2} + 17 L_{M,17} \mathbf{ST}(\theta'_{r,17} - \theta'_{r,1}) \right] & R_r \mathbf{I_2} - \omega_r L_r \mathbf{J} \end{bmatrix}$$

Note that, as $\theta'_{r,1} = \theta_r$ and $\theta'_{r,17} = 17\theta_r - \pi$, the above expressions can be simplified as follows:

$$\underset{\wedge}{\mathbf{L}} = \begin{bmatrix} L_s \mathbf{I_2} & 2\sqrt{3}[L_{M,1} \mathbf{I_2} - L_{M,17} \mathbf{ST}(16\theta_r)] \\ 2\sqrt{3}[L_{M,1} \mathbf{I_2} - L_{M,17} \mathbf{ST}(16\theta_r)] & L_r \mathbf{I_2} \end{bmatrix}$$

$$\underset{\wedge}{\mathbf{P}} = \begin{bmatrix} R_s \mathbf{I_2} & 16\omega_r \cdot 2\sqrt{3} L_{M,17} \mathbf{JST}(16\theta_r) \\ -2\sqrt{3}\omega_r \mathbf{J}[L_{M,1} \mathbf{I_2} - 17 L_{M,17} \mathbf{ST}(16\theta_r)] & R_r \mathbf{I_2} - \omega_r L_r \mathbf{J} \end{bmatrix}$$

while the subsequent relation holds for the torque:

$$M_M = 4\sqrt{3} \begin{bmatrix} i_{s,1\alpha} & i_{s,1\beta} \end{bmatrix} \mathbf{J} [L_{M,1} \mathbf{I_2} + 17 L_{M,17} \mathbf{ST}(16\theta_r)] \begin{bmatrix} i_{r,1\alpha} \\ i_{r,1\beta} \end{bmatrix} \tag{5.9}$$

$\underset{\hat{}}{\mathbf{L}}$ is invertible since the Schur complement of $L_r\mathbf{I_2}$ has full rank. We can therefore solve (5.8) for the current vector and build a state-space model with the components of $\vec{\underset{\hat{}}{i}}$, ω_r and θ_r as state variables:

$$\begin{cases} \dfrac{\mathrm{d}\vec{\underset{\hat{}}{i}}}{\mathrm{d}t} = -\underset{\hat{}}{\mathbf{L}}^{-1}(\theta_r)\underset{\hat{}}{\mathbf{P}}(\theta_r,\omega_r)\vec{\underset{\hat{}}{i}} + \underset{\hat{}}{\mathbf{L}}^{-1}(\theta_r)\vec{\underset{\hat{}}{u}} & \text{(5.10a)} \\ \dfrac{\mathrm{d}\omega_r}{\mathrm{d}t} = \dfrac{1}{J_M}(M_M - M_L) & \text{(5.10b)} \\ \dfrac{\mathrm{d}\theta_r}{\mathrm{d}t} = \omega_r & \text{(5.10c)} \\ M_M = 4\sqrt{3}\begin{bmatrix} i_{s,1\alpha} & i_{s,1\beta} \end{bmatrix}\mathbf{J}[L_{M,1}\mathbf{I_2} + 17L_{M,17}\mathbf{ST}(16\theta_r)]\begin{bmatrix} i_{r,1\alpha} \\ i_{r,1\beta} \end{bmatrix} \end{cases}$$

In order to gain insight into the model structure, we now take a closer look at the form of $\underset{\hat{}}{\mathbf{L}}^{-1}(\theta_r)$, which can be calculated using block matrix algebra (cf. [77]). We introduce the subsequent set of parameters to obtain manageable expressions:

$$\lambda_1 = 2\sqrt{3}L_{M,1} \qquad \mu_1 = 2\sqrt{3}L_{M,17}$$

$$\lambda_2 = L_s - \frac{1}{L_r}\left[\lambda_1^2 + \mu_1^2\right] \qquad \mu_2 = -\frac{2}{L_r}\lambda_1\mu_1$$

$$\lambda_3 = \frac{\lambda_2}{\lambda_2^2 - \mu_2^2}, \quad \lambda_2 \neq \mu_2 \qquad \mu_3 = -\frac{\mu_2}{\lambda_2^2 - \mu_2^2}, \quad \lambda_2 \neq \mu_2$$

$$\lambda_4 = \lambda_3\lambda_1 + \mu_3\mu_1 \qquad \mu_4 = \lambda_3\mu_1 + \mu_3\lambda_1$$

$$\lambda_5 = \frac{1}{L_r} + \frac{1}{L_r^2}[\lambda_1\lambda_4 + \mu_1\mu_4] \qquad \mu_5 = \frac{1}{L_r^2}[\lambda_1\mu_4 + \mu_1\lambda_4]$$

$$\lambda_6 = -\frac{\lambda_4}{L_r} \qquad \mu_6 = -\frac{\mu_4}{L_r}$$

From these definitions follows:

$$\underset{\hat{}}{\mathbf{L}} = \begin{bmatrix} L_s\mathbf{I_2} & \lambda_1\mathbf{I_2} - \mu_1\mathbf{ST}(16\theta_r) \\ \lambda_1\mathbf{I_2} - \mu_1\mathbf{ST}(16\theta_r) & L_r\mathbf{I_2} \end{bmatrix} \tag{5.11}$$

$$\underset{\hat{}}{\mathbf{L}}^{-1} = \begin{bmatrix} \lambda_3\mathbf{I_2} - \mu_3\mathbf{ST}(16\theta_r) & \lambda_6\mathbf{I_2} - \mu_6\mathbf{ST}(16\theta_r) \\ \lambda_6\mathbf{I_2} - \mu_6\mathbf{ST}(16\theta_r) & \lambda_5\mathbf{I_2} - \mu_5\mathbf{ST}(16\theta_r) \end{bmatrix} \tag{5.12}$$

$$\underset{\hat{}}{\mathbf{P}} = \begin{bmatrix} R_s\mathbf{I_2} & 16\mu_1\omega_r\mathbf{JST}(16\theta_r) \\ -\lambda_1\omega_r\mathbf{J} + 17\mu_1\omega_r\mathbf{JST}(16\theta_r) & R_r\mathbf{I_2} - \omega_r L_r\mathbf{J} \end{bmatrix} \tag{5.13}$$

We now take a closer look at the matrix:

$$\underset{\hat{}}{\mathbf{A}}(\theta_r,\omega_r) = -\underset{\hat{}}{\mathbf{L}}^{-1}(\theta_r)\underset{\hat{}}{\mathbf{P}}(\theta_r,\omega_r) \tag{5.14}$$

Defining the following additional constants

$$\lambda_7 = \lambda_6\lambda_1 - 17\mu_6\mu_1 \qquad \mu_7 = \mu_6\lambda_1 - 17\lambda_6\mu_1$$

$$\lambda_8 = \lambda_1\lambda_5 - 17\mu_1\mu_5 \qquad \mu_8 = \mu_5\lambda_1 - 17\mu_1\lambda_5$$

leads to the expression of $\underset{\wedge}{\mathbf{A}}$ as block matrix:

$$\underset{\wedge}{\mathbf{A}} = \begin{bmatrix} \underset{\wedge}{\mathbf{A}}_{11} & \underset{\wedge}{\mathbf{A}}_{12} \\ \underset{\wedge}{\mathbf{A}}_{21} & \underset{\wedge}{\mathbf{A}}_{22} \end{bmatrix} \tag{5.15}$$

where

$$\underset{\wedge}{\mathbf{A}}_{11} = -R_s\lambda_3\mathbf{I_2} + \lambda_7\omega_r\mathbf{J} + [R_s\mu_3\mathbf{I_2} + \mu_7\omega_r\mathbf{J}]\mathbf{ST}(16\theta_r) \tag{5.16a}$$

$$\underset{\wedge}{\mathbf{A}}_{21} = -R_s\lambda_6\mathbf{I_2} + \lambda_8\omega_r\mathbf{J} + [R_s\mu_6\mathbf{I_2} + \mu_8\omega_r\mathbf{J}]\mathbf{ST}(16\theta_r) \tag{5.16b}$$

$$\underset{\wedge}{\mathbf{A}}_{12} = -R_r\lambda_6\mathbf{I_2} + [\lambda_6 L_r - 16\mu_1\mu_3]\omega_r\mathbf{J} + [R_r\mu_6\mathbf{I_2} + (\mu_6 L_r - 16\lambda_3\mu_1)\omega_r\mathbf{J}]\mathbf{ST}(16\theta_r) \tag{5.16c}$$

$$\underset{\wedge}{\mathbf{A}}_{22} = -R_r\lambda_5\mathbf{I_2} + [\lambda_5 L_r - 16\mu_1\mu_6]\omega_r\mathbf{J} + [R_r\mu_5\mathbf{I_2} + (\mu_5 L_r - 16\lambda_6\mu_1)\omega_r\mathbf{J}]\mathbf{ST}(16\theta_r) \tag{5.16d}$$

Using the notations

$$\lambda_9 = \lambda_6 L_r - 16\mu_1\mu_3 \qquad \mu_9 = \mu_6 L_r - 16\lambda_3\mu_1$$

$$\lambda_{10} = \lambda_5 L_r - 16\mu_1\mu_6 \qquad \mu_{10} = \mu_5 L_r - 16\mu_1\lambda_6$$

the blocks of $\underset{\wedge}{\mathbf{A}}$ are rewritten in a slightly more convenient form:

$$\underset{\wedge}{\mathbf{A}}_{11} = -R_s\lambda_3\mathbf{I_2} + R_s\mu_3\mathbf{ST}(16\theta_r) + \omega_r\mathbf{J}[\lambda_7\mathbf{I_2} + \mu_7\mathbf{ST}(16\theta_r)] \tag{5.17a}$$

$$\underset{\wedge}{\mathbf{A}}_{21} = -R_s\lambda_6\mathbf{I_2} + R_s\mu_6\mathbf{ST}(16\theta_r) + \omega_r\mathbf{J}[\lambda_8\mathbf{I_2} + \mu_8\mathbf{ST}(16\theta_r)] \tag{5.17b}$$

$$\underset{\wedge}{\mathbf{A}}_{12} = -R_r\lambda_6\mathbf{I_2} + R_r\mu_6\mathbf{ST}(16\theta_r) + \omega_r\mathbf{J}[\lambda_9\mathbf{I_2} + \mu_9\mathbf{ST}(16\theta_r)] \tag{5.17c}$$

$$\underset{\wedge}{\mathbf{A}}_{22} = -R_r\lambda_5\mathbf{I_2} + R_r\mu_5\mathbf{ST}(16\theta_r) + \omega_r\mathbf{J}[\lambda_{10}\mathbf{I_2} + \mu_{10}\mathbf{ST}(16\theta_r)] \tag{5.17d}$$

Considering the above relations, it becomes apparent that all four blocks of $\underset{\wedge}{\mathbf{A}}$ have the same structure. The state-space model can now be brought in its final form. To do so, we define:

- the state vector $\vec{x} \in \mathbb{R}^6$:

$$\begin{aligned} \vec{X} &= \begin{bmatrix} x_0 & x_1 & x_2 & x_3 & x_4 & x_5 \end{bmatrix}^\top \\ &= \begin{bmatrix} i_{s,\,1\alpha} & i_{s,\,2\alpha} & i_{r,\,1\alpha} & i_{r,\,1\beta} & \omega_r & \theta_r \end{bmatrix}^\top \end{aligned}$$

- the input vector $\vec{U} \in \mathbb{R}^3$:

$$\vec{U} = \begin{bmatrix} u_0 & u_1 & u_2 \end{bmatrix}^\top = \begin{bmatrix} u_{s,\,1\alpha} & u_{s,\,2\beta} & M_L \end{bmatrix}^\top$$

  Note that the load torque is an unknown input.

- the input matrix $\underset{\wedge}{\mathbf{B}}(x_5) \in \mathcal{M}_{4\times 2}(\mathbb{R})$ which consists of the first two columns of $\underset{\wedge}{\mathbf{L}}^{-1}(x_5)$:

$$\underset{\wedge}{\mathbf{B}}(x_5) = \begin{bmatrix} \lambda_3\mathbf{I_2} - \mu_3\mathbf{ST}(16x_5) \\ \lambda_6\mathbf{I_2} - \mu_6\mathbf{ST}(16x_5) \end{bmatrix} = \begin{bmatrix} \underset{\wedge}{\mathbf{B}}_1(x_5) \\ \underset{\wedge}{\mathbf{B}}_2(x_5) \end{bmatrix} \tag{5.18}$$

- the output vector $\vec{Y} \in \mathbb{R}^3$:

$$\vec{Y} = \begin{bmatrix} y_0 & y_1 & y_2 \end{bmatrix}^\top = \begin{bmatrix} i_{s,\,1\alpha} & i_{s,\,2\beta} & \theta_r \end{bmatrix}^\top$$

The rotor angle is assumed to be known.

- the output matrix $\underset{\wedge}{\mathbf{C}} \in \mathcal{M}_{3\times 6}(\mathbb{R})$:

$$\underset{\wedge}{\mathbf{C}} = \begin{bmatrix} 1 & 0 & 0 & 0 & 0 & 0 \\ 0 & 1 & 0 & 0 & 0 & 0 \\ 0 & 0 & 0 & 0 & 0 & 1 \end{bmatrix}$$

Owing to the above definitions, the state-space equations of the transformed model with wavelengths 1 and 17 are rewritten as follows:

$$\begin{cases} \dfrac{\mathrm{d}}{\mathrm{d}t}\begin{bmatrix} x_0 \\ x_1 \\ x_2 \\ x_3 \end{bmatrix} = \underset{\wedge}{\mathbf{A}}(x_4, x_5)\begin{bmatrix} x_0 \\ x_1 \\ x_2 \\ x_3 \end{bmatrix} + \underset{\wedge}{\mathbf{B}}(x_5)\begin{bmatrix} u_0 \\ u_1 \end{bmatrix} \\ \dfrac{\mathrm{d}x_4}{\mathrm{d}t} = \dfrac{1}{J_M}\left[4\sqrt{3}\begin{bmatrix} x_0 & x_1 \end{bmatrix}\mathbf{J}[L_{M,1}\mathbf{I_2} + 17L_{M,17}\mathbf{ST}(16x_5)]\begin{bmatrix} x_2 \\ x_3 \end{bmatrix} - u_2\right] \\ \dfrac{\mathrm{d}x_5}{\mathrm{d}t} = x_4 \\ \vec{Y} = \underset{\wedge}{\mathbf{C}}\vec{X} \end{cases} \tag{5.19}$$

In order to understand to which extend the consideration of wavelength 17 modifies the structure of the model equations, we take a look at the numerical values of the parameters λ_p and μ_p, $p \in [\![1,\, 10]\!]$. The latter are summarized in table 5.1 for the model with $\mathcal{H} = \{1, 17\}$ and table 5.2 in case of the fundamental model, i.e. $\mathcal{H} = \{1\}$ and thus, $L_{M,17} = 0$.

Symbol and value (SI)				**Symbol and value (SI)**			
λ_1	=	2.153×10^{-3}	H	μ_1	=	3.111×10^{-6}	H
λ_2	=	2.861×10^{-2}	H	μ_2	=	-9.167×10^{-4}	H
λ_3	=	3.498×10^{1}	H^{-1}	μ_3	=	1.121×10^{0}	H^{-1}
λ_4	=	7.532×10^{-2}		μ_4	=	2.521×10^{-3}	
λ_5	=	8.281×10^{5}	H^{-1}	μ_5	=	2.653×10^{4}	H^{-1}
λ_6	=	-5.155×10^{3}	H^{-1}	μ_6	=	-1.726×10^{2}	H^{-1}
λ_7	=	-1.109×10^{1}		μ_7	=	-9.899×10^{-2}	
λ_8	=	1.781×10^{3}		μ_8	=	1.333×10^{1}	
λ_9	=	-7.538×10^{-2}		μ_9	=	-4.263×10^{-3}	
λ_{10}	=	1.211×10^{1}		μ_{10}	=	6.442×10^{-1}	

Table 5.1: Numerical values of the constants in the state-space model with $\mathcal{H} = \{1, 17\}$

We notice that the value of all μ_p, $p \in [\![1,\, 10]\!]$, is zero for the fundamental model, as $L_{M,17} = 0$. As a result, the dependence of the matrices $\underset{\wedge}{\mathbf{A}}$ and $\underset{\wedge}{\mathbf{B}}$ on the rotor angle disappears. The general structure of the state-space model, however, remains the same. In addition, the value of the parameters λ_p, $p \in [\![1,\, 10]\!]$, is only marginally affected by the presence of wavelength 17.

Symbol and value (SI)				Symbol and value (SI)			
λ_1	=	2.153×10^{-3}	H	μ_1	=	0	H
λ_2	=	2.743×10^{-2}	H	μ_2	=	0	H
λ_3	=	3.645×10^{1}	H^{-1}	μ_3	=	0	H^{-1}
λ_4	=	7.849×10^{-2}		μ_4	=	0	
λ_5	=	8.611×10^{5}	H^{-1}	μ_5	=	0	H^{-1}
λ_6	=	-5.375×10^{3}	H^{-1}	μ_6	=	0	H^{-1}
λ_7	=	-1.157×10^{1}		μ_7	=	0	
λ_8	=	1.854×10^{3}		μ_8	=	0	
λ_9	=	-7.849×10^{-2}		μ_9	=	0	
λ_{10}	=	1.257×10^{1}		μ_{10}	=	0	

Table 5.2: Numerical values of the constants in the state-space model with $\mathcal{H} = \{1\}$

5.1.3 Comments on the controllability and the observability of the state variables

Rotor currents

Since extending the fundamental model to wavelength 17 does not affect the elementary structure of the state-space equations, we expect the two models to share similar behaviour regarding the properties of controllability and observability. In particular, rotor currents should remain controllable and observable in the model with $\mathcal{H} = \{1, 17\}$, even though the input and system matrices depend on the rotor angle.

In order to support this conjecture, we examine whether there exist values of θ_r for which the impressed stator voltages have no effect on stator and rotor currents. The influence of the voltages on the derivative of the stator currents is described by the submatrix $\underset{\wedge}{\mathbf{B}}_1$ which was introduced in relation (5.18). We observe that its determinant is non-zero and independent of the rotor angle:

$$\det \underset{\wedge}{\mathbf{B}}_1 = \det[\lambda_3 \mathbf{I_2} - \mu_3 \mathbf{ST}(16x_5)] = \det \begin{bmatrix} \lambda_3 - \mu_3 \cos(16x_5) & \mu_3 \sin(16x_5) \\ \mu_3 \sin(16x_5) & \lambda_3 + \mu_3 \cos(16x_5) \end{bmatrix}$$

$$= \lambda_3^2 - \mu_3^2 \cos^2(16x_5) - \mu_3^2 \sin^2(16x_5) = \lambda_3^2 - \mu_3^2 \neq 0$$

This means that any non-zero input voltage vector $[u_0 \; u_1]^\top$ will have an effect on the derivative of the stator currents. Similarly,

$$\det \underset{\wedge}{\mathbf{B}}_2 = \det[\lambda_6 \mathbf{I_2} - \mu_6 \mathbf{ST}(16x_5)] = \lambda_6^2 - \mu_6^2 \neq 0$$

and any non-zero input voltage vector will also influence the derivatives of rotor currents. In other words, the impressed voltages can be used to command stator as well as rotor currents and thus the electromechanical torque.

We now investigate the observability of rotor currents in the model with wavelengths 1 and 17. In order to be observable at the model outputs, rotor currents must have an impact on stator currents regardless the value of the rotor angle. To check whether this is the case, we work out the determinant of the submatrix $\underset{\wedge}{\mathbf{A}}_{12}$ which describes the influence of rotor currents on the derivative of stator currents.

To draw more general conclusions, as all four blocks in the system matrix $\underset{\wedge}{\mathbf{A}}$ have the same form, we compute the determinant of the following general expression:

$$\det[\alpha_1 \mathbf{I_2} + \alpha_2 \mathbf{ST}(16\theta_r) + \omega_r \mathbf{J}[\beta_1 \mathbf{I_2} + \beta_2 \mathbf{ST}(16\theta_r)]] \quad \text{for} \quad (\alpha_1, \, \alpha_2, \, \beta_1, \, \beta_2) \in \mathbb{R}^4$$

$$
\begin{aligned}
&= \det \begin{bmatrix} \alpha_1 + \alpha_2 \cos(16x_5) + \beta_2 \omega_r \sin(16x_5) & -\omega_r[\beta_1 - \beta_2 \cos(16x_5)] - \alpha_2 \sin(16x_5) \\ [\beta_1 + \beta_2 \cos(16x_5)]\omega_r - \alpha_2 \sin(16x_5) & \alpha_1 - \alpha_2 \cos(16x_5) - \beta_2 \omega_r \sin(16x_5) \end{bmatrix} \\
&= \alpha_1^2 - [\alpha_2 \cos(16x_5) + \beta_2 \omega_r \sin(16x_5)]^2 + \beta_1^2 \omega_r^2 - [\beta_2 \omega_r \cos(16x_5) - \alpha_2 \sin(16x_5)]^2 \\
&= \alpha_1^2 - \alpha_2^2 + \omega_r^2(\beta_1^2 - \beta_2^2)
\end{aligned}
$$

We notice that the determinant of the four blocks of $\hat{\mathbf{A}}$ depends on the rotor angular velocity but not on the rotor angle, as for the fundamental model. In particular,

$$
\begin{aligned}
\det \hat{\mathbf{A}}_{12} &= R_r^2(\lambda_6^2 - \mu_6^2) + \omega_r^2(\lambda_9^2 - \mu_9^2) \\
&= 1.375 \times 10^{-1} + 5.663 \times 10^{-3} \omega_r^2 \\
&> 0 \quad \forall\, \omega_r \in \mathbb{R}
\end{aligned}
$$

This result demonstrates that the rotor angle does not impose any restriction regarding the influence of rotor currents on stator current derivatives.

We can deduce from the considerations in this section that the extended model of IM1 with $\mathcal{H} = \{1, 17\}$ is fundamentally suitable for use in torque ripple reduction applications, as the dependence of the system and input matrices on the rotor angle does not impose limitations on the controllability and observability of rotor currents.

The same conclusions can be drawn for the model of IM2 with wavelengths 2 and 26, since it has the very same structure. In general, however, the number of states in the model may increase depending on the wavelengths considered (see chapter 4). For this reason, a thorough model analysis should be carried out in each specific case.

Observability of the rotor speed

The structure of the state equations (5.19) shows that for a constant rotor angle, i.e. $\omega_r = 0$, the differential system describing the behaviour of the currents is linear. Under these circumstances, if the model is excited with input voltages at a given frequency, the output currents will exhibit only this frequency. Owing to the expressions given in (5.17), the coefficients of the system matrix will change depending on the value of θ_r. This is a major difference with the fundamental model, for which the rotor angle has no impact on the system matrix at zero-speed.

Fig. 5.1 compares the stator current response of the model with wavelengths 1 and 17 to the one obtained with the fundamental model for $\theta_r = \pi/12$ and $\theta_r = \pi/16$. As expected, the current trajectory computed with the fundamental model is circular and does not change when the rotor is moved from one position to the other. This contrasts with the elliptic trajectory generated by the model with $\mathcal{H} = \{1, 17\}$ whose main axis is directly impacted by the change in rotor position.

This characteristic makes the extended model potentially interesting for encoderless control applications. An extensive theoretical analysis of the rotor speed observability, similar to the ones reported by Wit in [84] or Vaclavek in [85] in the case of Park's model, would be valuable as well as experimental investigations.

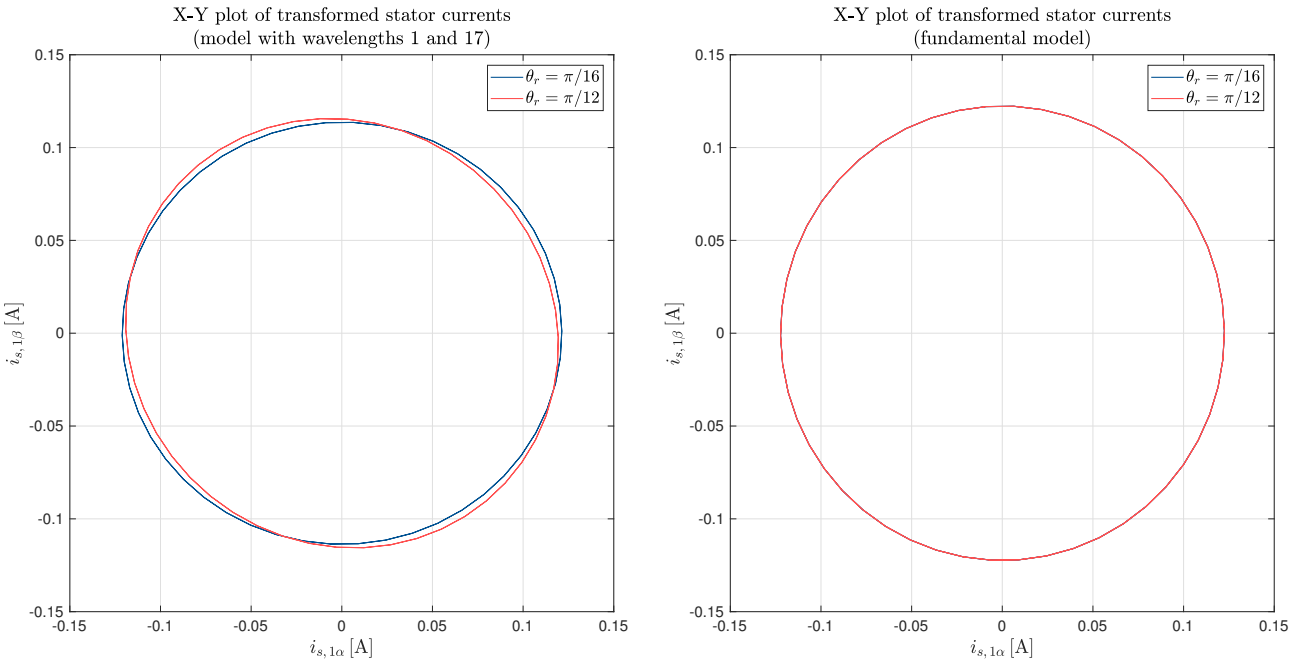

Figure 5.1: Simulated current responses of the transformed models with $\mathcal{H} = \{1, 17\}$ and $\mathcal{H} = \{1\}$ to balanced sinusoidal voltages ($U = 0.15\,U_{NY}$, $f = 2\,\mathrm{kHz}$) for two different rotor angles

5.2 Practical determination of the model parameters

Besides the controllability and the observability of the model states, a straightforward determination of its parameters is crucial for its practical suitability. As described in chapter 3, the linear geometric model requires a few additional parameters in comparison with Park's. They describe the machine internal geometry and are summarized in table 5.3.

Parameter	**Symbol**
Mean air-gap length	δ_0
Mean air-gap radius	r
Lamination stack length	l
Number of stator slots	N_s
Stator slot width	–
Number of rotor slots	N_r
Rotor slot width	–
Number of turns of the stator winding coils	W_S

Table 5.3: Additional parameters required in the linear geometric model

For the purpose of the investigations, the test machines IM1 and IM2 were opened to simplify the parameter estimation. This is usually not acceptable in practice. Thus, estimation methods should be developed to allow for the determination of the geometry related parameters from the stator current response of the machine.

The number of rotor slots could, for instance, be deduced from the time-harmonics present in the stator currents under balanced voltage excitation. An alternative would be the injection of a high-frequency test voltage and the processing of the current response (see fig. 5.1).

While the lamination stack length might be available in the documentation provided by the machine manufacturer, the determination of the other parameters is more complicated. The machine size and number of pole pairs may provide valuable hints on the stator winding configuration and thus help determine the shape of the corresponding conductor distribution functions.

An approach adopted in the context of this thesis consists in using Park's model parameters as reference and perform simulations with the linear geometric model (cf. chapter 3) to find suitable values for the unknown parameters. This method requires a systematic means of computing the Fourier coefficients of the conductor distribution functions. A particularly effective technique for tackling this problem is to understand the conductor distribution functions as linear combinations of shifted copies of a basic function, such as the one shown in fig. 3.4 on page 52. The shape of this basic function is determined for instance by two parameters and parametric expressions of its Fourier coefficients are found straightforwardly. The properties listed in section 3.1 allow to deduce the Fourier coefficients of the conductor distribution functions, which then depend on the geometric parameters. The influence of the latter on the inductances can easily be determined in simulations.

Nonetheless, finding appropriate values of the parameters remains arduous. Further work should therefore be carried out to optimize this process.

Summary

Controllability and observability of the rotor currents and the rotor angular velocity have been empirically assessed for the model of IM1 with wavelengths 1 and 17. For this particular model, the dependence of the system and input matrices on the rotor angle caused by the presence of wavelength 17 turns out to be unproblematic in respect of the controllability and the observability of rotor currents. This property makes the model suitable for use in applications aiming at reducing current and torque oscillations caused by space harmonics.

By contrast, the influence of the rotor angle on the coefficients of the system matrix could be useful for encoderless control applications. This aspect, however, necessitates comprehensive investigations from a theoretical as well as experimental perspective.

A further point needing additional research is the efficient determination of the model parameters describing the machine geometry, since no optimal solution has yet been found.

Conclusion and outlook

The investigations reported in this thesis started with a general model of induction machines including the effect of different categories of space harmonics. In order to meet our first objective of achieving real-time compliance, we then focused on space harmonics caused by the discrete distribution of electric conductors in the machine. We therefore assumed a linear magnetic behaviour as well as a uniform air-gap. Taking advantage of the mathematical properties of Fourier series, we proposed a simplified machine representation. Corresponding models of the two machines under test including a handful of space harmonics were analysed in simulation and experimentally. Although acceptable from the perspective of accuracy, they turn out to be computationally too demanding with respect to the targeted applications. This observation led us to develop a coordinate transformation to reduce the model order. Transformed models of the investigated machines with two space harmonics were derived and assessed. The transformation proves to drastically reduce the computational burden and provides execution times similar to Park's model. Our first goal is therefore met.

The considerations in chapter 5 showed that the transformed models with two space harmonics have essentially the same structure as Park's. The dependence of the system and input matrices on the rotor angle does not appear to have any detrimental consequence. On the contrary, the rotor angle seems to be observable at zero speed. As the currents are controllable and observable, the model is suitable for use in current and torque harmonic reduction applications. Thus, our second objective is achieved.

The extended model requires some additional information about the machine structure, which, in the frame of the study, was determined by looking inside the machine. As this method is not acceptable in practice, we proposed alternatives in chapter 5. Our third objective is fulfilled although further research would be needed to simplify the parameter determination.

Beyond the initial goals, the main contribution of the work presented is the derivation of a general coordinate transformation for multiphase machines taking into account the effect of winding interconnections. The transformation is based on the discrete Fourier transform and the concept of interconnection matrices. Besides diagonalizing the stator and rotor inductance submatrices of the model, it sheds new light on space harmonics and enables to consider them from the insightful perspective of signal processing.

More generally, the present work demonstrated the fundamental role played by the mathematical properties of the model:

- the symmetric positive definiteness of the inductance matrix as a result of physical phenomena;
- the careful choice of the interconnection matrix such that the inductance matrix remains symmetric positive definite after interconnection and therefore invertible using a efficient Cholesky decomposition;
- the interpretation of the inductance matrix diagonalization as a discrete Fourier transform;
- the combination of Fourier and interconnection matrices to obtain a general coordinate trans-

formation for multiphase machines.

These observations should always motivate the engineer to consider a given problem from different perspectives to propose original solutions.

Finally, the investigation of the following potentially promising aspects would be beneficial:

- the practical implementation and assessment of the transformed linear geometric model to reduce current and torque harmonics. Its complexity is comparable to Park's model and makes it suitable for use in predictive control schemes;
- the potential of the transformed model for encoderless control purposes should be determined, especially in the case of multiphase machines;
- we have only discussed transformed models including two space harmonics. The possible benefits of selecting different combinations of space harmonics for a given machine should be examined. In the case of IM1, this includes the orders 1, 5 and 11, which also generate a principal slot harmonic, instead of 1 and 17;
- an extensive comparison with Kron's method would be of interest. The advantage of Kron's approach is the possibility of assigning state variables to each space harmonic, which may provide more possibilities to influence the corresponding current components. The original geometric model, however, allows to examine the influence of specific space harmonics without difficulty, as no further parameter is needed;
- an extension of the linear geometric model to account for the effect of slotting or non-uniform air-gap, as in synchronous reluctance machines, might also be interesting. The geometric model might be extended to other types of machines as well.

Appendix

A.1 Characteristics and parameters of the investigated machines

A.1.1 Induction machine 1 (IM1)

Figure A.1: Induction machine 1 on the test rig

Physical quantity	**Symbol and value (SI)**			
Rated power	P_N	=	2.2	kW
Rated rotor speed	N_N	=	2 890	min^{-1}
Rated torque	M_{MN}	=	7.3	N m
Rated voltage (star, line-to-line)	U_{NY}	=	400	V
Rated current (star)	I_{NY}	=	4.5	A
Rated frequency	f_N	=	50	Hz
Power factor	$\cos\varphi$	=	0.85	

Table A.1: Nameplate specifications of induction machine 1

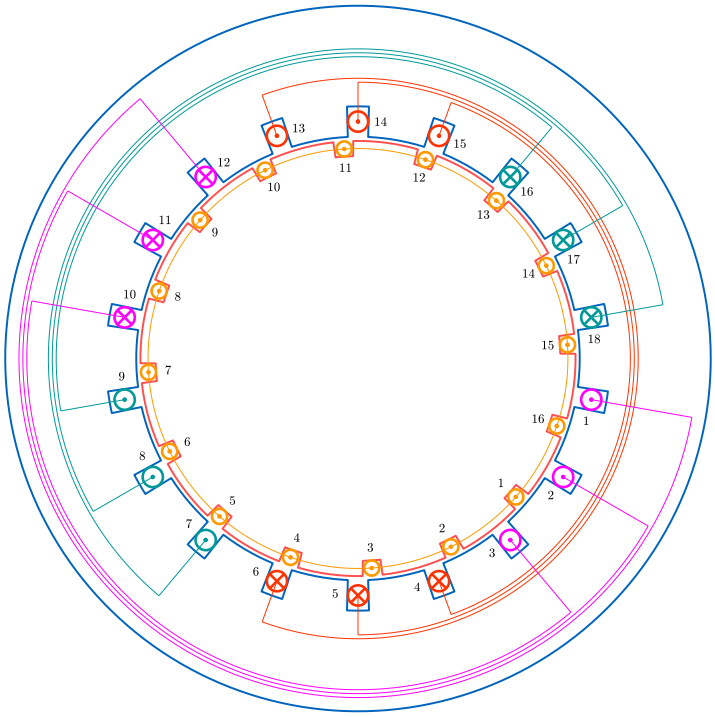

(a) Model showing the rotor cage

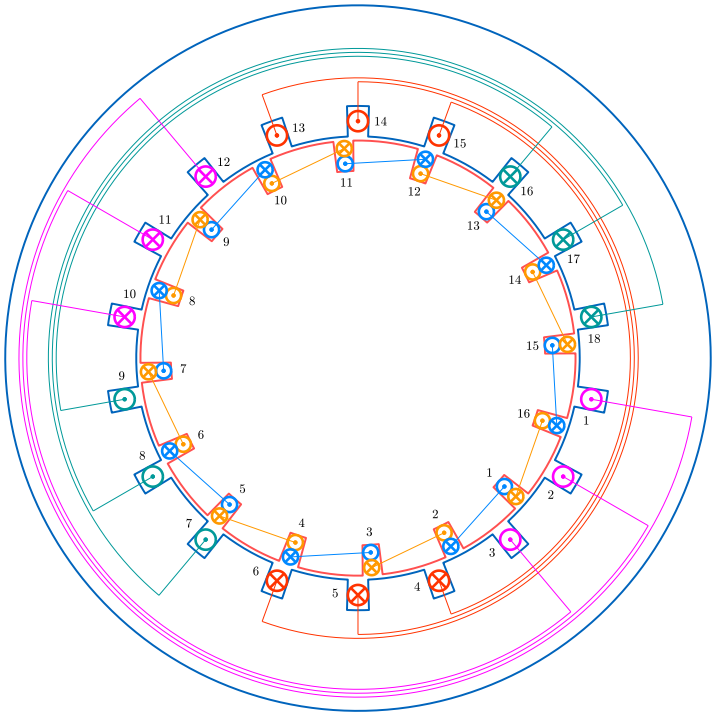

(b) Cross section of IM1 with rotor cage modelled as a set of N_r circuits

Figure A.2: Schematics of a cross section of IM1

Physical quantity	**Symbol and value (SI)**			
Number of stator slots	N_s	=	18	
Number of rotor slots	N_r	=	16	
Number of stator circuits	m_s	=	3	
Number of rotor circuits	m_r	=	$N_r = 16$	
Moment of inertia	J_M	=	2.2×10^{-3}	$\mathrm{kg\,m^2}$
Coefficient of friction	C_W	=	6.4×10^{-4}	$\mathrm{N\,m\,s}$

Table A.2: Geometric data of induction machine 1

Physical quantity	**Symbol and value (SI)**			
Number of pole pairs	Z_p	=	1	
Stator resistance	R_s	=	2.2	Ω
Main inductance	M	=	326	mH
Stator leakage inductance	$L_{\sigma s}$	=	14	mH
Rotor leakage inductance	$L_{\sigma r}$	=	14	mH
Rotor resistance	R_r	=	1.7	Ω

Table A.3: Park's model parameters of induction machine 1

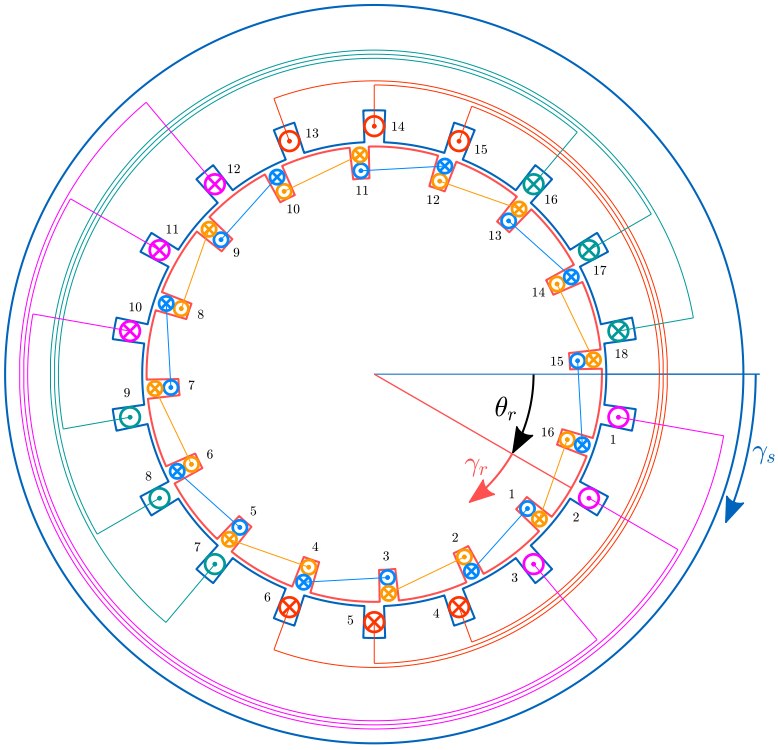

Figure A.3: Definition of normalized stator and rotor air-gap coordinates (IM1)

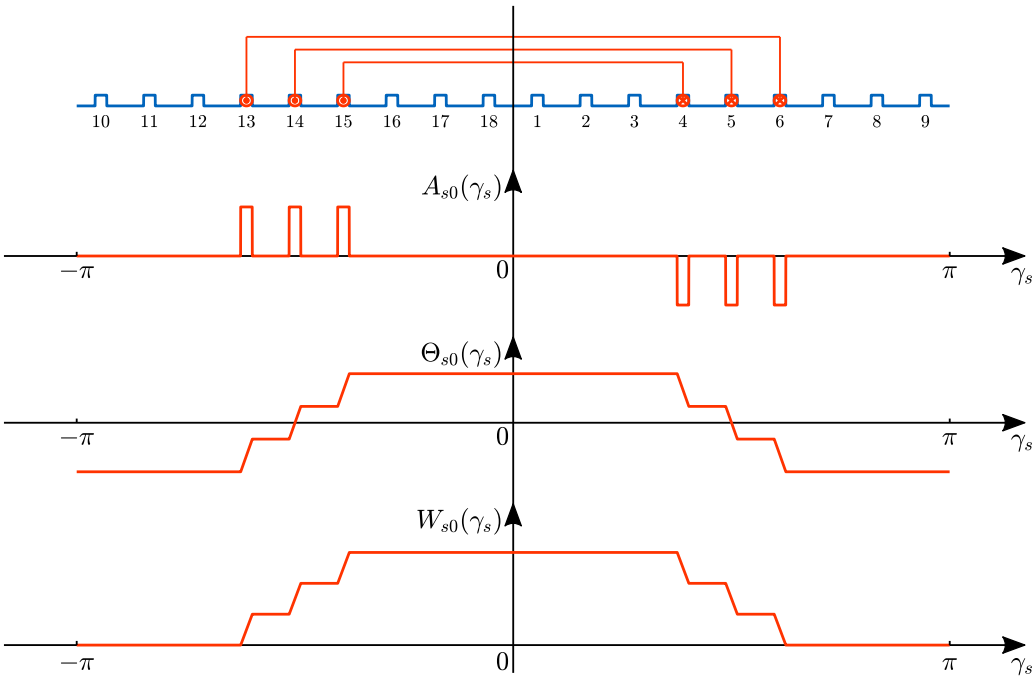

Figure A.4: Distributed quantities of stator circuit 0 (IM1)

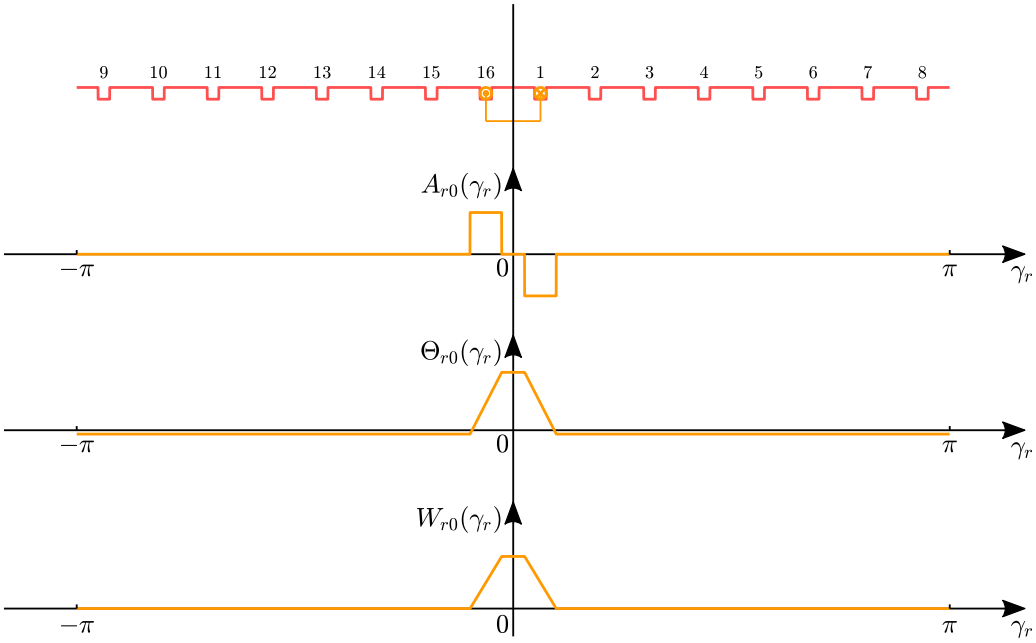

Figure A.5: Distributed quantities of rotor circuit 0 (IM1)

A.1.2 Induction machine 2 (IM2)

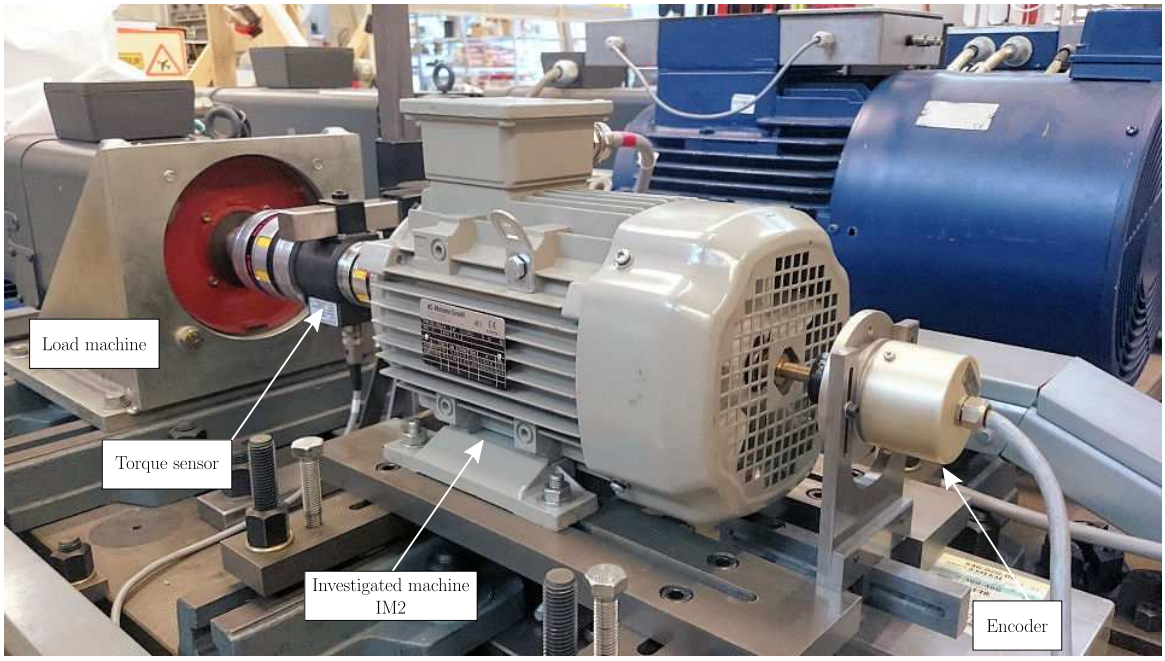

Figure A.6: Induction machine 2 on the test rig

Physical quantity	**Symbol and value (SI)**			
Rated power	P_N	=	2.2	kW
Rated rotor speed	N_N	=	1 410	min^{-1}
Rated torque	M_{MN}	=	14.9	N m
Rated voltage (star, line-to-line)	U_{NY}	=	400	V
Rated current (star)	I_{NY}	=	4.9	A
Rated frequency	f_N	=	50	Hz
Power factor	$\cos\varphi$	=	0.81	1

Table A.4: Nameplate specifications of induction machine 2

Physical quantity	**Symbol and value (SI)**			
Number of stator slots	N_s	=	36	
Number of rotor slots	N_r	=	28	
Number of stator circuits	m_s	=	6	
Number of rotor circuits	m_r	=	$N_r = 28$	
Moment of inertia	J_M	=	6.0×10^{-3}	$\mathrm{kg\,m^2}$
Coefficient of friction	C_W	=	1.3×10^{-3}	N m s

Table A.5: Geometric data of induction machine 2

Physical quantity	**Symbol and value (SI)**			
Number of pole pairs	Z_p	=	2	
Stator resistance	R_s	=	3.0	Ω
Main inductance	M	=	214	mH
Stator leakage inductance	$L_{\sigma s}$	=	7	mH
Rotor leakage inductance	$L_{\sigma r}$	=	7	mH
Rotor resistance	R_r	=	2.7	Ω

Table A.6: Park's model parameters of induction machine 2

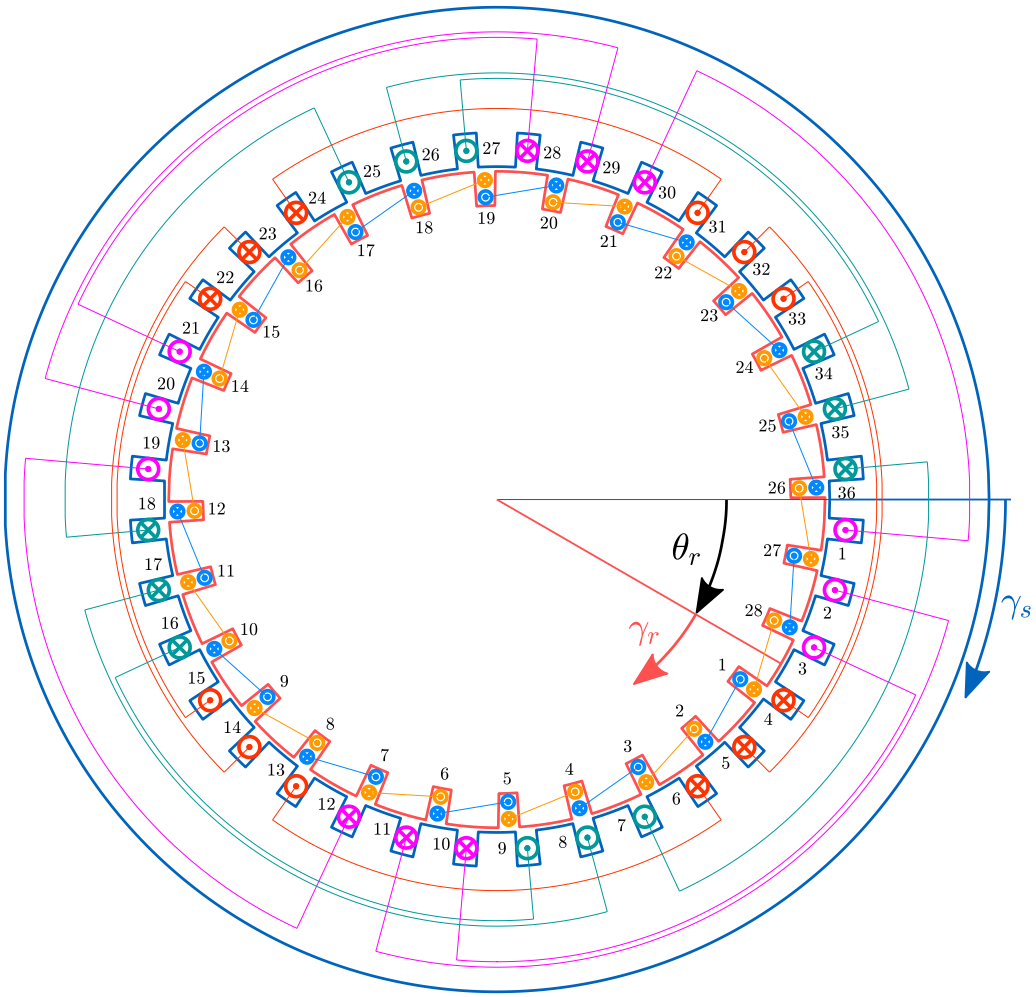

Figure A.7: Cross section of IM2 with normalized stator and rotor air-gap coordinates

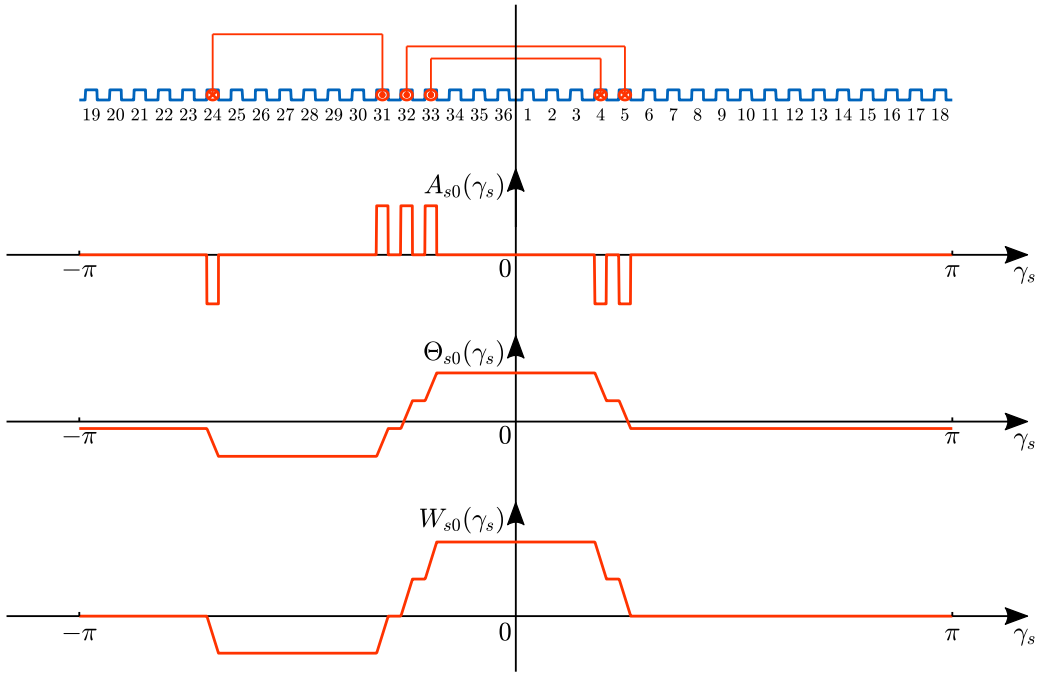

Figure A.8: Distributed quantities of stator circuit 0 (IM2)

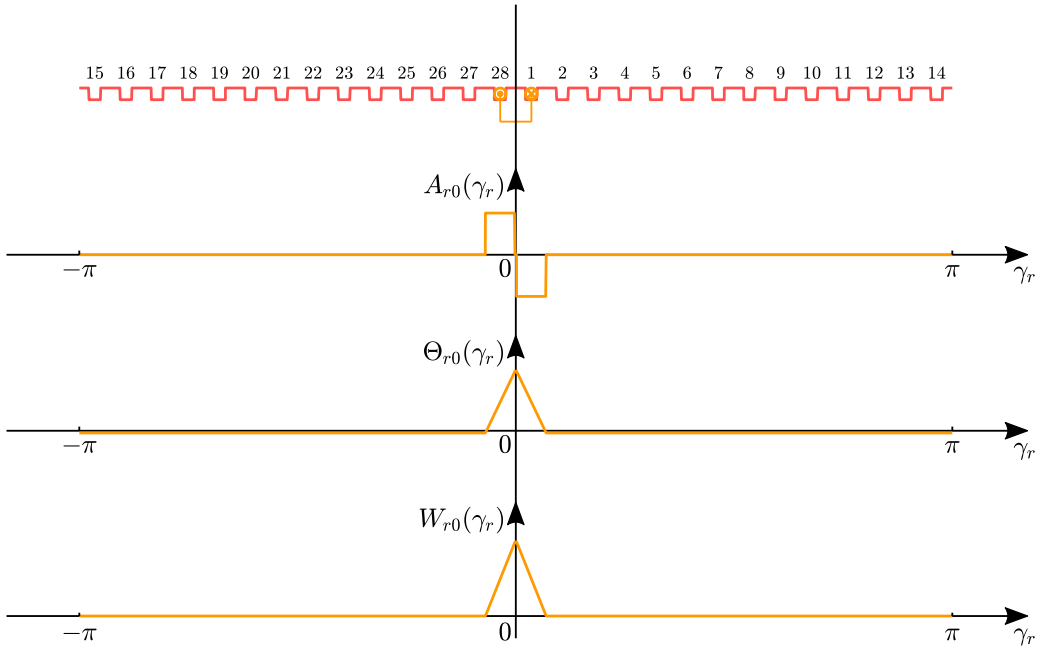

Figure A.9: Distributed quantities of rotor circuit 0 (IM2)

A.2 Mathematical proofs

A.2.1 Winding function based model (chapter 2)

Expression of the electromagnetic torque (p. 20)

The derivation of the torque expression (2.18) proposed below is based on [51].

During the infinitesimal time interval $\mathrm{d}t$, the energy of the coupling field, W_f, experiences a variation $\mathrm{d}E_{el}$ which is linked to the exchanged electrical and mechanical energy $\mathrm{d}W_e$ and $\mathrm{d}W_m$:

$$\begin{aligned}\mathrm{d}W_f &= \mathrm{d}W_e - \mathrm{d}W_m \\ &= \sum_{k=0}^{m_s+m_r-1} i_k \frac{\mathrm{d}\widetilde{\psi}_k}{\mathrm{d}t}\,\mathrm{d}t - M_M\,\mathrm{d}\theta_r \\ &= \sum_{k=0}^{m_s+m_r-1} i_k\,\mathrm{d}\widetilde{\psi}_k - M_M\,\mathrm{d}\theta_r \end{aligned} \tag{A.1}$$

In order to use the currents and the rotor angle as system variables, the coenergy W_c is introduced:

$$W_c = \sum_{k=0}^{m_s+m_r-1} i_k\widetilde{\psi}_k - W_f \tag{A.2}$$

The differential form of (A.2) is:

$$\mathrm{d}W_c = \sum_{k=0}^{m_s+m_r-1} \widetilde{\psi}_k\,\mathrm{d}i_k + \sum_{k=0}^{m_s+m_r-1} i_k\,\mathrm{d}\widetilde{\psi}_k - \mathrm{d}W_f \tag{A.3}$$

Appropriate substitution of (A.1) into (A.3) gives:

$$\begin{aligned}\mathrm{d}W_c &= \sum_{k=0}^{m_s+m_r-1} \widetilde{\psi}_k\,\mathrm{d}i_k + \sum_{k=0}^{m_s+m_r-1} i_k\,\mathrm{d}\widetilde{\psi}_k - \sum_{k=0}^{m_s+m_r-1} i_k\,\mathrm{d}\widetilde{\psi}_k + M_M\,\mathrm{d}\theta_r \\ &= \sum_{k=0}^{m_s+m_r-1} \widetilde{\psi}_k\,\mathrm{d}i_k + M_M\,\mathrm{d}\theta_r \end{aligned} \tag{A.4}$$

As W_c is depends exclusively on the currents and the rotor angle, $\mathrm{d}W_c$ is a total differential. The following relationship holds:

$$\mathrm{d}W_c = \sum_{k=0}^{m_s+m_r-1} \frac{\partial W_c}{\partial i_k}\,\mathrm{d}i_k + \frac{\partial W_c}{\partial \theta_r}\,\mathrm{d}\theta_r \tag{A.5}$$

Equations (A.4) and (A.5) lead to the expressions:

$$\widetilde{\psi}_k = \frac{\partial W_c(i_0, \cdots, i_{m_s+m_r-1}, \theta_r)}{\partial i_k} \tag{A.6}$$

$$M_M = \frac{\partial W_c(i_0, \cdots, i_{m_s+m_r-1}, \theta_r)}{\partial \theta_r} \tag{A.7}$$

Having neglected hysteresis and eddy current losses, the coupling field is conservative. Thus, the energy stored in this field at a certain time instant only depends on the value of the state variables at this time instant. As a result:

$$\oint \mathrm{d}W_f = 0 \qquad \text{and} \qquad \oint \mathrm{d}W_c = 0$$

This property makes possible to freely choose the path of integration to compute the value of W_f and W_c. It appears opportune to select a path along which the rotor is first moved to its position θ_r while the currents remain zero and then bring each current successively to its final value i_k. This results in:

$$W_c(\vec{i},\,\theta_r) = \int_{(\vec{0},\,0)}^{(\vec{i},\,\theta_r)} \mathrm{d}W_c = \int_{(\vec{0},\,0)}^{(\vec{0},\,\theta_r)} \mathrm{d}W_c + \int_{(\vec{0},\,\theta_r)}^{(\vec{i},\,\theta_r)} \mathrm{d}W_c$$

The first term on the right-hand side is zero as no energy is being exchanged between the mechanical system and the coupling field when no current is flowing through the electrical circuits. Owing to the above consideration, the coenergy value resulting from the state vector $(\vec{i},\,\theta_r)$ is:

$$\begin{aligned}
W_c(\vec{i},\,\theta_r) &= \int_{(0,\cdots,0)}^{(i_0,\cdots,0)} \sum_{k=0}^{m_s+m_r-1} \frac{\partial W_c}{\partial i'_k}\,\mathrm{d}i'_k + \cdots + \int_{(i_0,\cdots,i_{m_s+m_r-2},\,i_{m_s+m_r-1})}^{(i_0,\cdots,i_{m_s+m_r-2},\,0)} \sum_{k=0}^{m_s+m_r-1} \frac{\partial W_c}{\partial i'_k}\,\mathrm{d}i'_k \\
&= \int_{i'=0}^{i_0} \widetilde{\psi}_0(i',0,\cdots,0,\,\theta_r)\,\mathrm{d}i' + \cdots + \int_{i'=0}^{i_k} \widetilde{\psi}_k(i_0,\cdots,i_{k-1},\,i',\,0,\cdots,0,\,\theta_r)\,\mathrm{d}i' \\
&\quad + \cdots + \int_{i'=0}^{i_{m_s+m_r-1}} \widetilde{\psi}_{m_s+m_r-1}(i_0,\cdots,i_{m_s+m_r-2},\,i',\,\theta_r)\,\mathrm{d}i' \\
&= \sum_{k=0}^{m_s+m_r-1} \int_{i'=0}^{i_k} \widetilde{\psi}_k(i_0,\cdots,i_{k-1},\,i',\,0,\cdots,0,\,\theta_r)\,\mathrm{d}i'
\end{aligned} \tag{A.8}$$

Given the expression of the main flux vector (3.47), $W_c(\vec{i},\,\theta_r)$ can be further simplified in the considered case:

$$\begin{aligned}
W_c(\vec{i},\,\theta_r) &= \sum_{k=0}^{m_s+m_r-1} \int_{i'=0}^{i_k} \left(\sum_{l=0}^{k-1} \widetilde{L}_{kl}(\theta_r) i_l + \widetilde{L}_{kk}(\theta_r) i' \right) \mathrm{d}i' \\
&= \sum_{k=0}^{m_s+m_r-1} \left(\sum_{l=0}^{k-1} \widetilde{L}_{kl}(\theta_r) i_l i_k + \frac{1}{2} \widetilde{L}_{kk}(\theta_r) i_k^2 \right)
\end{aligned}$$

As $\widetilde{\mathbf{L}}(\theta_r)$ is symmetric, $\displaystyle\sum_{l=0}^{k-1} \widetilde{L}_{kl}(\theta_r) i_l i_k = \sum_{l=k+1}^{m_s+m_r-1} \widetilde{L}_{kl}(\theta_r) i_l i_k$, which yields:

$$\begin{aligned}
W_c(\vec{i},\,\theta_r) &= \sum_{k=0}^{m_s+m_r-1} \left(\frac{1}{2} \sum_{l=0}^{k-1} \widetilde{L}_{kl}(\theta_r) i_l i_k + \frac{1}{2} \widetilde{L}_{kk}(\theta_r) i_k^2 + \frac{1}{2} \sum_{l=k+1}^{m_s+m_r-1} \widetilde{L}_{kl}(\theta_r) i_l i_k \right) \\
&= \frac{1}{2} \sum_{k=0}^{m_s+m_r-1} \sum_{l=0}^{m_s+m_r-1} \widetilde{L}_{kl}(\theta_r) i_l i_k \\
&= \frac{1}{2} \vec{i}^{\top} \widetilde{\mathbf{L}}(\theta_r) \vec{i} = \frac{1}{2} \vec{i}^{\top} \vec{\widetilde{\Psi}}
\end{aligned} \tag{A.9}$$

As expected for a linear system, the coenergy W_c is equal to the energy W_f. The electromagnetic torque is calculated using (A.9) and (A.7):

$$\begin{aligned}
M_M &= \frac{\partial}{\partial \theta_r} \left(\frac{1}{2} \vec{i}^{\top} \widetilde{\mathbf{L}}(\theta_r) \vec{i} \right) \\
&= \frac{1}{2} \vec{i}^{\top} \frac{\partial \widetilde{\mathbf{L}}(\theta_r)}{\partial \theta_r} \vec{i} = \frac{1}{2} \vec{i}^{\top} \frac{\partial \vec{\widetilde{\Psi}}}{\partial \theta_r}
\end{aligned} \tag{A.10}$$

A.2.2 Linear geometric model (chapter 3)

Proposition 4 (p. 46): Properties of the matrix $\widetilde{\mathbf{L}}_{\mathbf{h}}(\theta_r)$, $h \in \mathbb{N}^\star$

- $\widetilde{\mathbf{L}}_{\mathbf{h}}(\theta_r)$ *is symmetric.*

$$\widetilde{\mathbf{L}}_{\mathbf{h}}^\top(\theta_r) = \begin{bmatrix} \widetilde{\mathbf{L}}_{\mathbf{s\,h}}^\top & \widetilde{\mathbf{L}}_{\mathbf{sr\,h}}^\top(\theta_r) \\ \widetilde{\mathbf{L}}_{\mathbf{rs\,h}}^\top(\theta_r) & \widetilde{\mathbf{L}}_{\mathbf{r\,h}}^\top \end{bmatrix} = \begin{bmatrix} \widetilde{\mathbf{L}}_{\mathbf{s\,h}} & \widetilde{\mathbf{L}}_{\mathbf{rs\,h}}(\theta_r) \\ \widetilde{\mathbf{L}}_{\mathbf{sr\,h}(\theta_\mathbf{r})} & \widetilde{\mathbf{L}}_{\mathbf{r\,h}} \end{bmatrix} = \widetilde{\mathbf{L}}_{\mathbf{h}}(\theta_r) \tag{A.11}$$

□

- $\widetilde{\mathbf{L}}_{\mathbf{h}}(\theta_r)$ *is positive semidefinite.*

For $\vec{i} = \begin{bmatrix} \vec{i}_s^\top & \vec{i}_r^\top \end{bmatrix}^\top \in \mathbb{R}^{m_s+m_r}$ with $\vec{i}_s \in \mathbb{R}^{m_s}$ and $\vec{i}_r \in \mathbb{R}^{m_r}$,

$$\begin{aligned} \vec{i}^\top \widetilde{\mathbf{L}}_{\mathbf{h}}(\theta_r)\vec{i} &= \begin{bmatrix} \vec{i}_s^\top & \vec{i}_r^\top \end{bmatrix} \begin{bmatrix} \widetilde{\mathbf{L}}_{\mathbf{s\,h}}\vec{i}_s + \widetilde{\mathbf{L}}_{\mathbf{rs\,h}}(\theta_r)\vec{i}_r \\ \widetilde{\mathbf{L}}_{\mathbf{sr\,h}}(\theta_r)\vec{i}_s + \widetilde{\mathbf{L}}_{\mathbf{r\,h}}\vec{i}_r \end{bmatrix} \\ &= \vec{i}_s^\top \widetilde{\mathbf{L}}_{\mathbf{s\,h}}\vec{i}_s + \vec{i}_s^\top \widetilde{\mathbf{L}}_{\mathbf{rs\,h}}(\theta_r)\vec{i}_r + \vec{i}_r^\top \widetilde{\mathbf{L}}_{\mathbf{sr\,h}}(\theta_r)\vec{i}_s + \vec{i}_r^\top \widetilde{\mathbf{L}}_{\mathbf{r\,h}}\vec{i}_r \end{aligned}$$

Given the expressions (3.36), (3.37) as well as (3.43) and (3.44), we have:

$$\begin{aligned} \vec{i}^\top \widetilde{\mathbf{L}}_{\mathbf{h}}(\theta_r)\vec{i} &= \widetilde{L}_{s,h}\vec{i}_s^\top \widetilde{\mathbf{T}}_{\mathbf{Cs\,h}}^\top \widetilde{\mathbf{T}}_{\mathbf{Cs\,h}}\vec{i}_s + L_{M,h}\vec{i}_s^\top \widetilde{\mathbf{T}}_{\mathbf{Cs\,h}}^\top \mathbf{T}(h\theta_r - \varphi_h)\widetilde{\mathbf{T}}_{\mathbf{Cr\,h}}\vec{i}_r \\ &\quad + L_{M,h}\vec{i}_r^\top \widetilde{\mathbf{T}}_{\mathbf{Cr\,h}}^\top \mathbf{T}(-h\theta_r + \varphi_h)\widetilde{\mathbf{T}}_{\mathbf{Cs\,h}}\vec{i}_s + \widetilde{L}_{r,h}\vec{i}_r^\top \widetilde{\mathbf{T}}_{\mathbf{Cr\,h}}^\top \widetilde{\mathbf{T}}_{\mathbf{Cr\,h}}\vec{i}_r \\ &= \widetilde{L}_{s,h}\left[\widetilde{\mathbf{T}}_{\mathbf{Cs\,h}}\vec{i}_s\right]^\top \left[\widetilde{\mathbf{T}}_{\mathbf{Cs\,h}}\vec{i}_s\right] + L_{M,h}\left[\widetilde{\mathbf{T}}_{\mathbf{Cs\,h}}\vec{i}_s\right]^\top \mathbf{T}(h\theta_r - \varphi_h)\left[\widetilde{\mathbf{T}}_{\mathbf{Cr\,h}}\vec{i}_r\right] \\ &\quad + L_{M,h}\left[\left[\widetilde{\mathbf{T}}_{\mathbf{Cr\,h}}\vec{i}_r\right]^\top \mathbf{T}(-h\theta_r + \varphi_h)\left[\widetilde{\mathbf{T}}_{\mathbf{Cs\,h}}\vec{i}_s\right]\right]^\top + \widetilde{L}_{r,h}\left[\widetilde{\mathbf{T}}_{\mathbf{Cr\,h}}\vec{i}_r\right]^\top \left[\widetilde{\mathbf{T}}_{\mathbf{Cr\,h}}\vec{i}_r\right] \\ &= \widetilde{L}_{s,h}\left\|\widetilde{\mathbf{T}}_{\mathbf{Cs\,h}}\vec{i}_s\right\|^2 + L_{M,h}\left[\widetilde{\mathbf{T}}_{\mathbf{Cs\,h}}\vec{i}_s\right]^\top \mathbf{T}(h\theta_r - \varphi_h)\left[\widetilde{\mathbf{T}}_{\mathbf{Cr\,h}}\vec{i}_r\right] \\ &\quad + L_{M,h}\left[\widetilde{\mathbf{T}}_{\mathbf{Cs\,h}}\vec{i}_s\right]^\top \mathbf{T}(h\theta_r - \varphi_h)\left[\widetilde{\mathbf{T}}_{\mathbf{Cr\,h}}\vec{i}_r\right] + \widetilde{L}_{r,h}\left\|\widetilde{\mathbf{T}}_{\mathbf{Cr\,h}}\vec{i}_r\right\|^2 \\ &= \widetilde{L}_{s,h}\left\|\widetilde{\mathbf{T}}_{\mathbf{Cs\,h}}\vec{i}_s\right\|^2 + 2L_{M,h}\left[\widetilde{\mathbf{T}}_{\mathbf{Cs\,h}}\vec{i}_s\right]^\top \mathbf{T}(h\theta_r - \varphi_h)\left[\widetilde{\mathbf{T}}_{\mathbf{Cr\,h}}\vec{i}_r\right] + \widetilde{L}_{r,h}\left\|\widetilde{\mathbf{T}}_{\mathbf{Cr\,h}}\vec{i}_r\right\|^2 \end{aligned}$$

The second term on the right-hand side requires particular attention:

$$\begin{aligned} 2L_{M,h}\left[\widetilde{\mathbf{T}}_{\mathbf{Cs\,h}}\vec{i}_s\right]^\top \mathbf{T}(h\theta_r - \varphi_h)\left[\widetilde{\mathbf{T}}_{\mathbf{Cr\,h}}\vec{i}_r\right] &\geqslant -2L_{M,h}\left\|\widetilde{\mathbf{T}}_{\mathbf{Cs\,h}}\vec{i}_s\right\|\left\|\mathbf{T}(h\theta_r - \varphi_h)\widetilde{\mathbf{T}}_{\mathbf{Cr\,h}}\vec{i}_r\right\| \\ &\geqslant -2L_{M,h}\left\|\widetilde{\mathbf{T}}_{\mathbf{Cs\,h}}\vec{i}_s\right\|\left\|\widetilde{\mathbf{T}}_{\mathbf{Cr\,h}}\vec{i}_r\right\| \end{aligned}$$

As a result,

$$\vec{i}^\top \widetilde{\mathbf{L}}_{\mathbf{h}}(\theta_r)\vec{i} \geqslant \widetilde{L}_{s,h}\left\|\widetilde{\mathbf{T}}_{\mathbf{Cs\,h}}\vec{i}_s\right\|^2 - 2L_{M,h}\left\|\widetilde{\mathbf{T}}_{\mathbf{Cs\,h}}\vec{i}_s\right\|\left\|\widetilde{\mathbf{T}}_{\mathbf{Cr\,h}}\vec{i}_r\right\| + \widetilde{L}_{r,h}\left\|\widetilde{\mathbf{T}}_{\mathbf{Cr\,h}}\vec{i}_r\right\|^2$$

Using (3.33), a meaningful expression can be gained:

$$\begin{aligned}\vec{i}^{\top}\widetilde{\mathbf{L}}_{\mathbf{h}}(\theta_r)\vec{i} &\geqslant 4\pi r l\frac{\mu_0}{\delta_0}\Big[c_h^2(W_{s0})\Big\|\widetilde{\mathbf{T}}_{\mathbf{Cs\,h}}\vec{i}_s\Big\|^2 - 2c_h(W_{r0})c_h(W_{s0})\Big\|\widetilde{\mathbf{T}}_{\mathbf{Cs\,h}}\vec{i}_s\Big\|\Big\|\widetilde{\mathbf{T}}_{\mathbf{Cr\,h}}\vec{i}_r\Big\| \\ &\qquad + c_h^2(W_{r0})\Big\|\widetilde{\mathbf{T}}_{\mathbf{Cr\,h}}\vec{i}_r\Big\|^2\Big] \\ &\geqslant 4\pi r l\frac{\mu_0}{\delta_0}\Big(c_h(W_{s0})\Big\|\widetilde{\mathbf{T}}_{\mathbf{Cs\,h}}\vec{i}_s\Big\| - c_h(W_{r0})\Big\|\widetilde{\mathbf{T}}_{\mathbf{Cr\,h}}\vec{i}_r\Big\|\Big)^2 \\ &\geqslant 0 \end{aligned} \tag{A.12}$$

The validity of eq. (A.12) for every $\vec{i}\in\mathbb{R}^{m_s+m_r}\setminus\{\vec{0}\}$ ensures the positive semidefiniteness of $\widetilde{\mathbf{L}}_{\mathbf{h}}$. $\widetilde{\mathbf{L}}_{\mathbf{h}}$ is, however, not positive definite. As $\operatorname{rank}(\widetilde{\mathbf{T}}_{\mathbf{Cs\,h}})\leqslant 2$ and $\operatorname{rank}(\widetilde{\mathbf{T}}_{\mathbf{Cr\,h}})\leqslant 2$, the rank-nullity theorem leads to $\dim\Big[\ker(\widetilde{\mathbf{T}}_{\mathbf{Cs\,h}})\Big]\geqslant m_s+m_r-2$ and $\dim\Big[\ker(\widetilde{\mathbf{T}}_{\mathbf{Cr\,h}})\Big]\geqslant m_s+m_r-2$.
Hence, $\exists\,\vec{i}\in\mathbb{R}^{m_s+m_r}\setminus\{\vec{0}\}$, $\vec{i}^{\top}\widetilde{\mathbf{L}}_{\mathbf{h}}(\theta_r)\vec{i}=0$.

□

Proposition 6 (p. 48): Properties of the matrices $\widetilde{\mathbf{L}}'_{\mathbf{h}}(\theta_r)$, $(h\in\mathbb{N}^\star)$, $\widetilde{\mathbf{L}}'(\theta_r)$ and $\mathbf{L}'(\theta_r)$

• *For $h\in\mathbb{N}^\star$, $\widetilde{\mathbf{L}}'_{\mathbf{h}}(\theta_r)=\mathbf{C}^{\top}\widetilde{\mathbf{L}}_{\mathbf{h}}(\theta_r)\mathbf{C}$ is symmetric positive semidefinite.*

$\widetilde{\mathbf{L}}'^{\top}_{\mathbf{h}}(\theta_r)=\Big[\mathbf{C}^{\top}\widetilde{\mathbf{L}}_{\mathbf{h}}(\theta_r)\mathbf{C}\Big]^{\top}=\mathbf{C}^{\top}\widetilde{\mathbf{L}}^{\top}_{\mathbf{h}}(\theta_r)\mathbf{C}=\widetilde{\mathbf{L}}'_{\mathbf{h}}(\theta_r)$ as $\widetilde{\mathbf{L}}_{\mathbf{h}}$ is symmetric.

For $\vec{i}'=\begin{bmatrix}\vec{i}_s'^{\top} & \vec{i}_r'^{\top}\end{bmatrix}^{\top}\in\mathbb{R}^{m'_s+m'_r}$ with $\vec{i}'_s\in\mathbb{R}^{m'_s}$ and $\vec{i}'_r\in\mathbb{R}^{m'_r}$,

$$\begin{aligned}\vec{i}'^{\top}\widetilde{\mathbf{L}}'_{\mathbf{h}}(\theta_r)\vec{i}' &= \begin{bmatrix}\vec{i}_s'^{\top} & \vec{i}_r'^{\top}\end{bmatrix}\begin{bmatrix}\mathbf{C}_{\mathbf{s}}^{\top} & \mathbf{0}\\ \mathbf{0} & \mathbf{C}_{\mathbf{r}}^{\top}\end{bmatrix}\begin{bmatrix}\widetilde{\mathbf{L}}_{\mathbf{s\,h}} & \widetilde{\mathbf{L}}_{\mathbf{rs\,h}}(\theta_r)\\ \widetilde{\mathbf{L}}_{\mathbf{sr\,h}}(\theta_r) & \widetilde{\mathbf{L}}_{\mathbf{r\,h}}\end{bmatrix}\begin{bmatrix}\mathbf{C}_{\mathbf{s}} & \mathbf{0}\\ \mathbf{0} & \mathbf{C}_{\mathbf{r}}\end{bmatrix}\begin{bmatrix}\vec{i}'_s\\ \vec{i}'_r\end{bmatrix} \\ &= \begin{bmatrix}\vec{i}_s'^{\top} & \vec{i}_r'^{\top}\end{bmatrix}\begin{bmatrix}\mathbf{C}_{\mathbf{s}}^{\top}\widetilde{\mathbf{L}}_{\mathbf{s\,h}}\mathbf{C}_{\mathbf{s}} & \mathbf{C}_{\mathbf{s}}^{\top}\widetilde{\mathbf{L}}_{\mathbf{rs\,h}}(\theta_r)\mathbf{C}_{\mathbf{r}}\\ \mathbf{C}_{\mathbf{r}}^{\top}\widetilde{\mathbf{L}}_{\mathbf{sr\,h}}(\theta_r)\mathbf{C}_{\mathbf{s}} & \mathbf{C}_{\mathbf{r}}^{\top}\widetilde{\mathbf{L}}_{\mathbf{r\,h}}\mathbf{C}_{\mathbf{r}}\end{bmatrix}\begin{bmatrix}\vec{i}'_s\\ \vec{i}'_r\end{bmatrix} \\ &= \vec{i}_s'^{\top}\Big[\mathbf{C}_{\mathbf{s}}^{\top}\widetilde{\mathbf{L}}_{\mathbf{s\,h}}\mathbf{C}_{\mathbf{s}}\vec{i}'_s + \mathbf{C}_{\mathbf{s}}^{\top}\widetilde{\mathbf{L}}_{\mathbf{rs\,h}}(\theta_r)\mathbf{C}_{\mathbf{r}}\vec{i}'_r\Big] + \vec{i}_r'^{\top}\Big[\mathbf{C}_{\mathbf{r}}^{\top}\widetilde{\mathbf{L}}_{\mathbf{sr\,h}}(\theta_r)\mathbf{C}_{\mathbf{s}}\vec{i}'_s + \mathbf{C}_{\mathbf{r}}^{\top}\widetilde{\mathbf{L}}_{\mathbf{r\,h}}\mathbf{C}_{\mathbf{r}}\vec{i}'_r\Big] \\ &= \widetilde{L}_{s,h}\Big[\widetilde{\mathbf{T}}_{\mathbf{Cs\,h}}\mathbf{C}_{\mathbf{s}}\vec{i}'_s\Big]^{\top}\widetilde{\mathbf{T}}_{\mathbf{Cs\,h}}\mathbf{C}_{\mathbf{s}}\vec{i}'_s + L_{M,h}\Big[\widetilde{\mathbf{T}}_{\mathbf{Cs\,h}}\mathbf{C}_{\mathbf{s}}\vec{i}'_s\Big]^{\top}\mathbf{T}(h\theta_r-\varphi_h)\widetilde{\mathbf{T}}_{\mathbf{Cr\,h}}\mathbf{C}_{\mathbf{r}}\vec{i}'_r \\ &\quad + L_{M,h}\Big[\widetilde{\mathbf{T}}_{\mathbf{Cr\,h}}\mathbf{C}_{\mathbf{r}}\vec{i}'_r\Big]^{\top}\mathbf{T}(-h\theta_r+\varphi_h)\widetilde{\mathbf{T}}_{\mathbf{Cs\,h}}\mathbf{C}_{\mathbf{s}}\vec{i}'_s + \widetilde{L}_{r,h}\Big[\widetilde{\mathbf{T}}_{\mathbf{Cr\,h}}\mathbf{C}_{\mathbf{r}}\vec{i}'_r\Big]^{\top}\widetilde{\mathbf{T}}_{\mathbf{Cr\,h}}\mathbf{C}_{\mathbf{r}}\vec{i}'_r \\ &\geqslant \widetilde{L}_{s,h}\Big\|\widetilde{\mathbf{T}}_{\mathbf{Cs\,h}}\mathbf{C}_{\mathbf{s}}\vec{i}'_s\Big\|^2 + \widetilde{L}_{r,h}\Big\|\widetilde{\mathbf{T}}_{\mathbf{Cr\,h}}\mathbf{C}_{\mathbf{r}}\vec{i}'_r\Big\|^2 - 2L_{M,h}\Big\|\widetilde{\mathbf{T}}_{\mathbf{Cs\,h}}\mathbf{C}_{\mathbf{s}}\vec{i}'_s\Big\|\Big\|\widetilde{\mathbf{T}}_{\mathbf{Cr\,h}}\mathbf{C}_{\mathbf{r}}\vec{i}'_r\Big\| \\ &\geqslant 4\pi r l\frac{\mu_0}{\delta_0}\Big(c_h(W_{s0})\Big\|\widetilde{\mathbf{T}}_{\mathbf{Cs\,h}}\mathbf{C}_{\mathbf{s}}\vec{i}'_s\Big\| - c_h(W_{r0})\Big\|\widetilde{\mathbf{T}}_{\mathbf{Cr\,h}}\mathbf{C}_{\mathbf{r}}\vec{i}'_r\Big\|\Big)^2 \\ &\geqslant 0\end{aligned}$$

□

• $\widetilde{\mathbf{L}}'(\theta_r)$ *is positive semidefinite.*

For $N \in \mathbb{N}^\star$, $\sum_{h=1}^{N} \widetilde{\mathbf{L}}'_{\mathbf{h}}(\theta_r)$ is positive semidefinite as the sum of positive semidefinite matrices. The positive semidefiniteness of $\widetilde{\mathbf{L}}'(\theta_r)$ is then gained from the fact that

$$\widetilde{\mathbf{L}}'(\theta_r) = \lim_{N \longrightarrow +\infty} \sum_{h=1}^{N} \widetilde{\mathbf{L}}'_{\mathbf{h}}(\theta_r)$$

exists and, for $\vec{i'} \in \mathbb{R}^{m'_s+m'_r}$, the map

$$\begin{array}{rccc} \phi_{\vec{i'}}: & \mathcal{M}_{m'_s+m'_r}(\mathbb{R}) & \longrightarrow & \mathbb{R} \\ & \mathbf{M} & \longmapsto & \phi_{\vec{i'}}(\mathbf{M}) = \vec{i'}^{\top}\mathbf{M}\vec{i'} \end{array}$$

is a linear form in a finite dimensional vector space and therefore continuous. □

• $\mathbf{L}'(\theta_r)$ *is positive definite.*

$\mathbf{L}(\theta_r)$ being the sum of a positive semidefinite and a positive definite matrix, $\widetilde{\mathbf{L}}'(\theta_r)$ and $\mathbf{L}_\sigma$ respectively, it is positive definite. Hence, there exists a unique upper triangular matrix with strictly positive diagonal coefficients $\mathbf{\Delta}$ such that $\mathbf{L}(\theta_r) = \mathbf{\Delta}^\top\mathbf{\Delta}$ (Cholesky). For $\vec{i'} \in \mathbb{R}^{m'_s+m'_r}$

$$\vec{i'}^{\top}\mathbf{L}'(\theta_r)\vec{i'} = \vec{i'}^{\top}\mathbf{C}^\top\mathbf{\Delta}^\top\mathbf{\Delta}\mathbf{C}\vec{i'} = \left[\mathbf{\Delta}\mathbf{C}\vec{i'}\right]^\top\mathbf{\Delta}\mathbf{C}\vec{i'} = \left\|\mathbf{\Delta}\mathbf{C}\vec{i'}\right\|^2$$

Owing to the shape of matrix $\mathbf{C}$, $\vec{i'} \neq \vec{0} \Longrightarrow \mathbf{C}\vec{i'} \neq \vec{0}$. As $\mathbf{\Delta}$ is invertible, $\vec{i'} \neq \vec{0} \Longrightarrow \vec{i'}^{\top}\mathbf{L}'(\theta_r)\vec{i'} > 0$. Hence, $\mathbf{L}'(\theta_r)$ is positive definite.

□

A.2.3 Transformed linear geometric model (chapter 4)

Transformed stator main inductance matrix of wavelength h, $\widetilde{\mathbf{L}}^{\natural}_{\mathbf{s\,h}}$ (p. 86)

In order to find a simpler expression of $\widetilde{\mathbf{L}}^{\natural}_{\mathbf{s\,h}}$, the matrix product $\widetilde{\mathbf{T}}_{\mathbf{Cs\,k_0}}\mathcal{W}_{\mathrm{m_s}}$ is now being investigated. To do so, the coefficients of $\widetilde{\mathbf{T}}_{\mathbf{Cs\,k_0}}$ are expressed using complex exponentials:

$$\begin{aligned} \widetilde{\mathbf{T}}_{\mathbf{Cs\,k_0}} &= \frac{1}{2}\left(\begin{bmatrix} 1 & \cdots & e^{jk_0m\frac{2\pi}{m_s}} & \cdots & e^{jk_0(m_s-1)\frac{2\pi}{m_s}} \\ 0 & \cdots & -je^{jk_0m\frac{2\pi}{m_s}} & \cdots & -je^{jk_0(m_s-1)\frac{2\pi}{m_s}} \end{bmatrix}\right. \\ &\quad \left. + \begin{bmatrix} 1 & \cdots & e^{-jk_0m\frac{2\pi}{m_s}} & \cdots & e^{-jk_0(m_s-1)\frac{2\pi}{m_s}} \\ 0 & \cdots & je^{-jk_0m\frac{2\pi}{m_s}} & \cdots & je^{-jk_0(m_s-1)\frac{2\pi}{m_s}} \end{bmatrix}\right) \\ &= \frac{1}{2}\left(\begin{bmatrix} 1 & 0 \\ 0 & -j \end{bmatrix}\begin{bmatrix} 1 & \cdots & W_{-m_s}^{k_0m} & \cdots & W_{-m_s}^{k_0(m_s-1)} \\ 0 & \cdots & W_{-m_s}^{k_0m} & \cdots & W_{-m_s}^{k_0(m_s-1)} \end{bmatrix}\right. \\ &\quad \left. + \begin{bmatrix} 1 & 0 \\ 0 & j \end{bmatrix}\begin{bmatrix} 1 & \cdots & W_{m_s}^{k_0m} & \cdots & W_{m_s}^{k_0(m_s-1)} \\ 0 & \cdots & W_{m_s}^{k_0m} & \cdots & W_{m_s}^{k_0(m_s-1)} \end{bmatrix}\right) \end{aligned}$$

$$= \frac{1}{2}\left(\begin{bmatrix} 1 & 0 \\ 0 & -j \end{bmatrix} \begin{bmatrix} 1 & \cdots & \cdots & 1 \\ 0 & 1 & \cdots & 1 \end{bmatrix} \begin{bmatrix} 1 & & & 0 \\ & \ddots & & \\ & & W_{m_s}^{k_0 m} & \\ & & & \ddots \\ 0 & & & W_{m_s}^{k_0(m_s-1)} \end{bmatrix} \right.$$

$$\left. + \begin{bmatrix} 1 & 0 \\ 0 & j \end{bmatrix} \begin{bmatrix} 1 & \cdots & \cdots & 1 \\ 0 & 1 & \cdots & 1 \end{bmatrix} \begin{bmatrix} 1 & & & 0 \\ & \ddots & & \\ & & W_{m_s}^{k_0 m} & \\ & & & \ddots \\ 0 & & & W_{m_s}^{k_0(m_s-1)} \end{bmatrix} \right) \tag{A.13}$$

Defining the following matrices,

$$\mathbf{M_{m_s,\,k_0}} = \begin{bmatrix} 1 & & & 0 \\ & \ddots & & \\ & & W_{m_s}^{k_0 m} & \\ & & & \ddots \\ 0 & & & W_{m_s}^{k_0(m_s-1)} \end{bmatrix} \qquad \mathbf{N} = \begin{bmatrix} 1 & \cdots & \cdots & 1 \\ 0 & 1 & \cdots & 1 \end{bmatrix} \qquad \mathbf{P} = \begin{bmatrix} 1 & 0 \\ 0 & j \end{bmatrix}$$

we obtain:

$$\widetilde{\mathbf{T}}_{\mathbf{Cs\,k_0}} = \frac{1}{2}\left(\overline{\mathbf{P}}\mathbf{N}\overline{\mathbf{M_{m_s,\,k_0}}} + \mathbf{P}\mathbf{N}\mathbf{M_{m_s,\,k_0}}\right) \tag{A.14}$$

At first, we focus on the product $\mathbf{M_{m_s,\,k_0}}\mathcal{W}_{\mathrm{m_s}}$:

$$\mathbf{M_{m_s,\,k_0}}\mathcal{W}_{\mathrm{m_s}} = \frac{1}{\sqrt{m_s}} \begin{bmatrix} 1 & & & 0 \\ & \ddots & & \\ & & W_{m_s}^{k_0 m} & \\ & & & \ddots \\ 0 & & & W_{m_s}^{k_0(m_s-1)} \end{bmatrix}$$

$$\times \begin{bmatrix} 1 & 1 & \cdots & \cdots & \cdots & 1 \\ 1 & W_{m_s} & \cdots & W_{m_s}^{m} & \cdots & W_{m_s}^{m_s-1} \\ \vdots & \vdots & \vdots & \vdots & \vdots & \vdots \\ 1 & W_{m_s}^{k} & \cdots & W_{m_s}^{mk} & \cdots & W_{m_s}^{(m_s-1)k} \\ \vdots & \vdots & \vdots & \vdots & \vdots & \vdots \\ 1 & W_{m_s}^{m_s-1} & \cdots & W_{m_s}^{m(m_s-1)} & \cdots & W_{m_s}^{(m_s-1)^2} \end{bmatrix}$$

$$= \frac{1}{\sqrt{m_s}} \begin{bmatrix} 1 & \cdots & \cdots & \cdots & 1 \\ W_{m_s}^{k_0} & \cdots & W_{m_s}^{k_0+m} & \cdots & W_{m_s}^{k_0+m_s-1} \\ \vdots & \vdots & \vdots & \vdots & \vdots \\ W_{m_s}^{kk_0} & \cdots & W_{m_s}^{k(k_0+m)} & \cdots & W_{m_s}^{k(k_0+m_s-1)} \\ \vdots & \vdots & \vdots & \vdots & \vdots \\ W_{m_s}^{(m_s-1)k_0} & \cdots & W_{m_s}^{(m_s-1)(k_0+m)} & \cdots & W_{m_s}^{(m_s-1)(k_0+m_s-1)} \end{bmatrix}$$

In order to calculate the product $\mathbf{NM_{m_s,k_0}}\mathcal{W}_{\mathrm{m_s}}$, it is necessary to determine the sum

$$\sum_{k=0}^{m_s-1} W_{m_s}^{k(k_0+m)} = \sum_{k=0}^{m_s-1} \left[e^{-j(k_0+m)\frac{2\pi}{m_s}}\right]^k$$

depending on $(k_0,\, m) \in [\![0,\, m_s-1]\!]^2$. The following two cases have to be distinguished:

- **Case 1:** $k_0 + m \equiv 0 \pmod{m_s}$

  $\exists \lambda \in \mathbb{Z}, \quad k_0 + m = \lambda m_s$

  $$\Longrightarrow e^{-j(k_0+m)\frac{2\pi}{m_s}} = e^{-j\lambda m_s \frac{2\pi}{m_s}} = e^{-j\lambda 2\pi} = 1$$

  $$\Longrightarrow \sum_{k=0}^{m_s-1} W_{m_s}^{k(k_0+m)} = m_s$$

  As $(k_0,\, m) \in [\![0,\, m_s-1]\!]^2$, the only possible values of λ are 0 and 1:

  $\lambda = 0 \Longrightarrow k_0 + m = 0 \Longrightarrow m = k_0 = 0$ (only relevant if $k_0 = 0$)

  $\lambda = 1 \Longrightarrow k_0 + m = m_s \Longrightarrow m = m_s - k_0$ (only relevant if $k_0 \neq 0$)

- **Case 2:** $k_0 + m \not\equiv 0 \pmod{m_s}$

  $$\sum_{k=0}^{m_s-1} W_{m_s}^{k(k_0+m)} = \frac{1 - \left[e^{-j(k_0+m)\frac{2\pi}{m_s}}\right]^{m_s}}{1 - e^{-j(k_0+m)\frac{2\pi}{m_s}}} = 0$$

As a result, if $k_0 = 0$,

$$\mathbf{NM_{m_s,k_0}}\mathcal{W}_{\mathrm{m_s}} = \frac{1}{\sqrt{m_s}} \begin{bmatrix} \overset{m=0}{m_s} & 0 & \cdots & \overset{m=m_s-1}{0} \\ m_s - 1 & -1 & \cdots & -1 \end{bmatrix}$$

and

$$\mathbf{PNM_{m_s,k_0}}\mathcal{W}_{\mathrm{m_s}} = \frac{1}{\sqrt{m_s}} \begin{bmatrix} \overset{m=0}{m_s} & 0 & \cdots & \overset{m=m_s-1}{0} \\ j(m_s - 1) & -j & \cdots & -j \end{bmatrix}$$

In contrast, if $k_0 \neq 0$,

$$\mathbf{NM_{m_s,k_0}}\mathcal{W}_{\mathrm{m_s}} = \frac{1}{\sqrt{m_s}} \begin{bmatrix} \overset{m=0}{0} & \cdots & 0 & \overset{m=m_s-k_0}{m_s} & 0 & \cdots & \overset{m=m_s-1}{0} \\ -1 & \cdots & -1 & m_s - 1 & -1 & \cdots & -1 \end{bmatrix}$$

and

$$\mathbf{PNM_{m_s,k_0}}\mathcal{W}_{\mathrm{m_s}} = \frac{1}{\sqrt{m_s}} \begin{bmatrix} \overset{m=0}{0} & \cdots & 0 & \overset{m=m_s-k_0}{m_s} & 0 & \cdots & \overset{m=m_s-1}{0} \\ -j & \cdots & -j & j(m_s - 1) & -j & \cdots & -j \end{bmatrix}$$

Considering now the remaining term in (A.14), the product $\overline{\mathbf{M_{m_s,\,k_0}}}\mathcal{W}_{\mathrm{m_s}}$ needs to be calculated:

$$\overline{\mathbf{M_{m_s,\,k_0}}}\mathcal{W}_{\mathrm{m_s}} = \frac{1}{\sqrt{m_s}}\begin{bmatrix} 1 & & & 0 \\ & \ddots & & \\ & & W_{-m_s}^{k_0 k} & \\ 0 & & & \ddots \\ & & & W_{-m_s}^{k_0(m_s-1)} \end{bmatrix}$$

$$\times \begin{bmatrix} 1 & 1 & \cdots & \cdots & \cdots & 1 \\ 1 & W_{m_s} & \cdots & W_{m_s}^{m} & \cdots & W_{m_s}^{m_s-1} \\ \vdots & \vdots & \vdots & \vdots & \vdots & \vdots \\ 1 & W_{m_s}^{k} & \cdots & W_{m_s}^{mk} & \cdots & W_{m_s}^{(m_s-1)k} \\ \vdots & \vdots & \vdots & \vdots & \vdots & \vdots \\ 1 & W_{m_s}^{m_s-1} & \cdots & W_{m_s}^{m(m_s-1)} & \cdots & W_{m_s}^{(m_s-1)^2} \end{bmatrix}$$

$$= \frac{1}{\sqrt{m_s}}\begin{bmatrix} 1 & \cdots & \cdots & \cdots & 1 \\ W_{m_s}^{-k_0} & \cdots & W_{m_s}^{m-k_0} & \cdots & W_{m_s}^{m_s-1-k_0} \\ \vdots & \vdots & \vdots & \vdots & \vdots \\ W_{m_s}^{-kk_0} & \cdots & W_{m_s}^{k(m-k_0)} & \cdots & W_{m_s}^{k(m_s-1-k_0)} \\ \vdots & \vdots & \vdots & \vdots & \vdots \\ W_{m_s}^{-(m_s-1)k_0} & \cdots & W_{m_s}^{(m_s-1)(m-k_0)} & \cdots & W_{m_s}^{(m_s-1)(m_s-1-k_0)} \end{bmatrix}$$

The computation of $\mathbf{N}\overline{\mathbf{M}_{\mathbf{m_s,\,k_0}}}\mathcal{W}_{\mathrm{m_s}}$ requires a closer look at the sum

$$\sum_{k=0}^{m_s-1} W_{m_s}^{k(m-k_0)} = \sum_{k=0}^{m_s-1}\left[e^{-j(m-k_0)\frac{2\pi}{m_s}}\right]^k$$

which depends on $(k_0,\, m) \in [\![0,\, m_s-1]\!]^2$.

- **Case 1:** $m - k_0 \equiv 0 \pmod{m_s}$

  $\exists \lambda \in \mathbb{Z}, \quad m - k_0 = \lambda m_s$

  $$\Longrightarrow e^{-j(m-k_0)\frac{2\pi}{m_s}} = e^{-j\lambda m_s \frac{2\pi}{m_s}} = e^{-j\lambda 2\pi} = 1$$

  $$\Longrightarrow \sum_{k=0}^{m_s-1} W_{m_s}^{k(m-k_0)} = m_s$$

  $(k_0,\, m) \in [\![0,\, m_s-1]\!]^2 \Longrightarrow \lambda = 0$

  $$\Longrightarrow k_0 - m = 0 \Longrightarrow m = k_0$$

- **Case 2:** $k_0 - m \not\equiv 0 \pmod{m_s}$

  $$\sum_{k=0}^{m_s-1} W_{m_s}^{k(m-k_0)} = \frac{1 - \left[e^{-j(m-k_0)\frac{2\pi}{m_s}}\right]^{m_s}}{1 - e^{-j(m-k_0)\frac{2\pi}{m_s}}} = 0$$

Following these results:

$$\mathbf{N}\overline{\mathbf{M}_{\mathbf{m_s},\mathbf{k_0}}}\mathcal{W}_{\mathrm{m_s}} = \frac{1}{\sqrt{m_s}} \begin{bmatrix} \overset{m=0}{0} & \cdots & 0 & \overset{m=k_0}{m_s} & 0 & \cdots & \overset{m=m_s-1}{0} \\ -1 & \cdots & -1 & m_s-1 & -1 & \cdots & -1 \end{bmatrix}$$

and

$$\overline{\mathbf{P}}\mathbf{N}\overline{\mathbf{M}_{\mathbf{m_s},\mathbf{k_0}}}\mathcal{W}_{\mathrm{m_s}} = \frac{1}{\sqrt{m_s}} \begin{bmatrix} \overset{m=0}{0} & \cdots & 0 & \overset{m=k_0}{m_s} & 0 & \cdots & \overset{m=m_s-1}{0} \\ j & \cdots & j & -j(m_s-1) & j & \cdots & j \end{bmatrix}$$

According to the previous considerations, the value of k_0 has an influence on the product $\widetilde{\mathbf{T}}_{\mathbf{Cs\,k_0}}\mathcal{W}_{\mathrm{m_s}}$ and the case $k_0 = 0$, i.e. the wavelength order h is a multiple of the number of stator circuits m_s, has to be examined separately.

$$k_0 = 0 \Longrightarrow \widetilde{\mathbf{T}}_{\mathbf{Cs\,k_0}}\mathcal{W}_{\mathrm{m_s}} = \frac{1}{2}\overline{\mathbf{P}}\mathbf{N}\overline{\mathbf{M}_{\mathbf{m_s},\mathbf{k_0}}}\mathcal{W}_{\mathrm{m_s}} + \frac{1}{2}\mathbf{P}\mathbf{N}\mathbf{M}_{\mathbf{m_s},\mathbf{k_0}}\mathcal{W}_{\mathrm{m_s}}$$

$$= \frac{1}{2\sqrt{m_s}} \begin{bmatrix} \overset{m=0}{2m_s} & 0 & \cdots & \overset{m=m_s-1}{0} \\ 0 & \cdots & \cdots & 0 \end{bmatrix}$$

$$= \sqrt{m_s} \begin{bmatrix} \overset{m=0}{1} & 0 & \cdots & \overset{m=m_s-1}{0} \\ 0 & \cdots & \cdots & 0 \end{bmatrix}$$

$$k_0 \neq 0 \Longrightarrow \widetilde{\mathbf{T}}_{\mathbf{Cs\,k_0}}\mathcal{W}_{\mathrm{m_s}} = \frac{1}{2}\overline{\mathbf{P}}\mathbf{N}\overline{\mathbf{M}_{\mathbf{m_s},\mathbf{k_0}}}\mathcal{W}_{\mathrm{m_s}} + \frac{1}{2}\mathbf{P}\mathbf{N}\mathbf{M}_{\mathbf{m_s},\mathbf{k_0}}\mathcal{W}_{\mathrm{m_s}}$$

$$= \frac{1}{2\sqrt{m_s}} \left(\begin{bmatrix} \overset{m=0}{0} & \cdots & 0 & \overset{m=k_0}{m_s} & 0 & \cdots & \overset{m=m_s-1}{0} \\ j & \cdots & j & -j(m_s-1) & j & \cdots & j \end{bmatrix} \right.$$

$$\left. + \begin{bmatrix} \overset{m=0}{0} & \cdots & 0 & \overset{m=m_s-k_0}{m_s} & 0 & \cdots & \overset{m=m_s-1}{0} \\ -j & \cdots & -j & j(m_s-1) & -j & \cdots & -j \end{bmatrix} \right)$$

In case $k_0 \neq m_s - k_0$,

$$\widetilde{\mathbf{T}}_{\mathbf{Cs\,k_0}}\mathcal{W}_{\mathrm{m_s}} = \frac{\sqrt{m_s}}{2} \begin{bmatrix} \overset{m=0}{0} & \cdots & 0 & \overset{m=k_0}{1} & 0 & \cdots & 0 & \overset{m=m_s-k_0}{1} & 0 & \cdots & \overset{m=m_s-1}{0} \\ 0 & \cdots & 0 & -j & 0 & \cdots & 0 & j & 0 & \cdots & 0 \end{bmatrix}$$

however, if $k_0 = m_s - k_0$ (i.e. $k_0 = m_s/2$),

$$\widetilde{\mathbf{T}}_{\mathbf{Cs\,k_0}}\mathcal{W}_{\mathrm{m_s}} = \sqrt{m_s} \begin{bmatrix} \overset{m=0}{0} & \cdots & 0 & \overset{m=k_0}{1} & 0 & \cdots & \overset{m=m_s-1}{0} \\ 0 & \cdots & 0 & 0 & 0 & \cdots & 0 \end{bmatrix}$$

The latter case may only occur if the number of stator circuits is even, for example when considering the wavelength of order 3 in a 6 phase machine.

Getting back to the transformed stator main inductance of wavelength h, $\widetilde{\mathbf{L}}^{\natural}_{\mathbf{s\,h}}$, the previous results lead to:

• $k_0 = 0$, i.e. the wavelength order h is a multiple of the number of circuits m_s:

$$\widetilde{\mathbf{L}}^{\natural}_{\mathbf{s\,h}} = \widetilde{L}_{s,\,h}\overline{\widetilde{\mathbf{T}}_{\mathbf{Cs\,k_0}}\mathcal{W}_{\mathrm{m_s}}}^{\top}\widetilde{\mathbf{T}}_{\mathbf{Cs\,k_0}}\mathcal{W}_{\mathrm{m_s}}$$

$$= \widetilde{L}_{s,\,h}\sqrt{m_s} \begin{matrix} k=0 \\ \\ \\ k=m_s-1 \end{matrix} \begin{bmatrix} 1 & 0 \\ 0 & \vdots \\ \vdots & \vdots \\ 0 & 0 \end{bmatrix} \sqrt{m_s} \begin{matrix} m=0 & & & m=m_s-1 \end{matrix} \begin{bmatrix} 1 & 0 & \cdots & 0 \\ 0 & \cdots & \cdots & 0 \end{bmatrix}$$

$$= m_s\widetilde{L}_{s,\,h} \begin{matrix} m=0 & & & m=m_s-1 \\ k=0 & & & \\ & & & \\ k=m_s-1 & & & \end{matrix} \begin{bmatrix} 1 & 0 & \cdots & 0 \\ 0 & \cdots & \cdots & 0 \\ \vdots & \vdots & \vdots & \vdots \\ 0 & \cdots & \cdots & 0 \end{bmatrix} \tag{A.15}$$

• $k_0 \neq 0$:

If $k_0 = m_s - k_0$, an expression similar to the previous one is obtained:

$$\widetilde{\mathbf{L}}^{\natural}_{\mathbf{s\,h}} = \widetilde{L}_{s,\,h}\overline{\widetilde{\mathbf{T}}_{\mathbf{Cs\,k_0}}\mathcal{W}_{\mathrm{m_s}}}^{\top}\widetilde{\mathbf{T}}_{\mathbf{Cs\,k_0}}\mathcal{W}_{\mathrm{m_s}}$$

$$= \widetilde{L}_{s,\,h}\sqrt{m_s} \begin{matrix} k=0 \\ \\ k=k_0 \\ \\ k=m_s-1 \end{matrix} \begin{bmatrix} 0 & 0 \\ \vdots & \vdots \\ 0 & \vdots \\ 1 & \vdots \\ 0 & \vdots \\ \vdots & \vdots \\ 0 & 0 \end{bmatrix} \sqrt{m_s} \begin{matrix} m=0 & & & m=k_0 & & & m=m_s-1 \end{matrix} \begin{bmatrix} 0 & \cdots & 0 & 1 & 0 & \cdots & 0 \\ 0 & \cdots & \cdots & \cdots & \cdots & \cdots & 0 \end{bmatrix}$$

$$= m_s\widetilde{L}_{s,\,h} \begin{matrix} m=0 & & & m=k_0 & & & m=m_s-1 \\ k=0 & & & & & & \\ & & & & & & \\ k=k_0 & & & & & & \\ & & & & & & \\ & & & & & & \\ k=m_s-1 & & & & & & \end{matrix} \begin{bmatrix} 0 & \cdots & 0 & 0 & 0 & \cdots & 0 \\ \vdots & \ddots & \vdots & \vdots & \vdots & \ddots & 0 \\ 0 & \cdots & 0 & 0 & 0 & \cdots & 0 \\ 0 & \cdots & 0 & 1 & 0 & \cdots & 0 \\ 0 & \cdots & 0 & 0 & 0 & \cdots & 0 \\ \vdots & \ddots & \vdots & \vdots & \vdots & \ddots & 0 \\ 0 & \cdots & 0 & 0 & 0 & \cdots & 0 \end{bmatrix} \tag{A.16}$$

If $k_0 \neq m_s - k_0$, we have:

$$\widetilde{\mathbf{L}}^{\natural}_{\mathbf{s\,h}} = \widetilde{L}_{s,\,h}\overline{\widetilde{\mathbf{T}}_{\mathbf{Cs\,k_0}}\mathcal{W}_{\mathrm{m_s}}}^{\top}\widetilde{\mathbf{T}}_{\mathbf{Cs\,k_0}}\mathcal{W}_{\mathrm{m_s}}$$

$$
= \widetilde{L}_{s,h}\frac{\sqrt{m_s}}{2}
\begin{array}{c}
\\ k{=}0 \\ \\ \\ k{=}k_0 \\ \\ \\ k{=}m_s{-}k_0 \\ \\ \\ k{=}m_s{-}1
\end{array}
\begin{bmatrix}
0 & 0 \\ \vdots & \vdots \\ 0 & \vdots \\ 1 & j \\ 0 & 0 \\ \vdots & \vdots \\ 0 & 0 \\ 1 & -j \\ 0 & 0 \\ \vdots & \vdots \\ 0 & 0
\end{bmatrix}
$$

$$
\times \frac{\sqrt{m_s}}{2}
\begin{array}{c}
\\ m{=}0 \\ \\ \\ m{=}k_0 \\ \\ \\ m{=}m_s{-}k_0 \\ \\ \\ m{=}m_s{-}1
\end{array}
\begin{bmatrix}
0 & \cdots & 0 & 1 & 0 & \cdots & 0 & 1 & 0 & \cdots & 0 \\
0 & \cdots & 0 & -j & 0 & \cdots & 0 & j & 0 & \cdots & 0
\end{bmatrix}
$$

$$
= \frac{m_s}{2}\widetilde{L}_{s,h}
\begin{array}{c}
\\ \\ \\ k{=}k_0 \\ \\ \\ \\ k{=}m_s{-}k_0 \\ \\ \\ \\
\end{array}
\begin{array}{c}
\begin{array}{ccccccccccc}
 & & & m{=}k_0 & & & & m{=}m_s{-}k_0 & & & \\
\end{array} \\
\begin{bmatrix}
 & & & 0 & & & & 0 & & & \\
 & 0 & & \vdots & & 0 & & \vdots & & 0 & \\
 & & & 0 & & & & 0 & & & \\
0 & \cdots & 0 & 1 & 0 & \cdots & 0 & 0 & 0 & \cdots & 0 \\
 & & & 0 & & & & 0 & & & \\
 & 0 & & \vdots & & 0 & & \vdots & & 0 & \\
 & & & 0 & & & & 0 & & & \\
0 & \cdots & 0 & 0 & 0 & \cdots & 0 & 1 & 0 & \cdots & 0 \\
 & & & 0 & & & & 0 & & & \\
 & 0 & & \vdots & & 0 & & \vdots & & 0 & \\
 & & & 0 & & & & 0 & & &
\end{bmatrix}
\end{array}
\tag{A.17}
$$

Transformed rotor main inductance matrix of wavelength h, $\widetilde{\mathbf{L}}^{\natural}_{\mathbf{r\,h}}$ (p. 86)

As in section A.2.3, three cases have to be distinguished, depending on the value of l_0:

- $l_0 = 0$, i.e. the considered wavelength order is a multiple of the number of rotor circuits m_r:

$$
\widetilde{\mathbf{T}}_{\mathbf{Cr\,l_0}}\mathcal{W}_{\mathrm{m_r}} = \frac{1}{2}\overline{\mathbf{P}}\overline{\mathbf{N}}\overline{\mathbf{M}_{\mathbf{m_r,\,l_0}}}\mathcal{W}_{\mathrm{m_r}} + \frac{1}{2}\mathbf{P}\mathbf{N}\mathbf{M}_{\mathbf{m_r,\,l_0}}\mathcal{W}_{\mathrm{m_r}} = \sqrt{m_r}
\begin{array}{c}
\begin{array}{cccc}
n{=}0 & & & n{=}m_r{-}1
\end{array} \\
\begin{bmatrix}
1 & 0 & \cdots & 0 \\ 0 & \cdots & \cdots & 0
\end{bmatrix}
\end{array}
$$

$$
\widetilde{\mathbf{L}}^{\natural}_{\mathbf{r\,h}} = m_r\widetilde{L}_{r,h}
\begin{array}{c}
\begin{array}{cccc}
n{=}0 & & & n{=}m_r{-}1
\end{array} \\
\begin{array}{c}
l{=}0 \\ \\ \\ l{=}m_r{-}1
\end{array}
\begin{bmatrix}
1 & 0 & \cdots & 0 \\ 0 & \cdots & \cdots & 0 \\ \vdots & \vdots & \vdots & \vdots \\ 0 & \cdots & \cdots & 0
\end{bmatrix}
\end{array}
\tag{A.18}
$$

- $l_0 \neq 0 \quad \wedge \quad l_0 = m_r - l_0$:

$$\widetilde{\mathbf{T}}_{\mathbf{Cr\,l_0}} \mathcal{W}_{\mathrm{m_r}} = \sqrt{m_r} \begin{bmatrix} \overset{n=0}{0} & \cdots & 0 & \overset{n=l_0}{1} & 0 & \cdots & \overset{n=m_r-1}{0} \\ 0 & \cdots & 0 & 0 & 0 & \cdots & 0 \end{bmatrix}$$

$$\widetilde{\mathbf{L}}^{\natural}_{\mathbf{r\,h}} = m_r \widetilde{L}_{r,h} \begin{matrix} \\ l=0 \\ \\ l=l_0 \\ \\ \\ l=m_r-1 \end{matrix} \begin{bmatrix} \overset{n=0}{0} & \cdots & 0 & \overset{n=l_0}{0} & 0 & \cdots & \overset{n=m_r-1}{0} \\ \vdots & \ddots & \vdots & \vdots & \vdots & \ddots & 0 \\ 0 & \cdots & 0 & 0 & 0 & \cdots & 0 \\ 0 & \cdots & 0 & 1 & 0 & \cdots & 0 \\ 0 & \cdots & 0 & 0 & 0 & \cdots & 0 \\ \vdots & \ddots & \vdots & \vdots & \vdots & \ddots & 0 \\ 0 & \cdots & 0 & 0 & 0 & \cdots & 0 \end{bmatrix}$$

- $l_0 \neq 0 \quad \wedge \quad l_0 \neq m_r - l_0$:

$$\widetilde{\mathbf{T}}_{\mathbf{Cr\,l_0}} \mathcal{W}_{\mathrm{m_r}} = \frac{\sqrt{m_r}}{2} \begin{bmatrix} \overset{n=0}{0} & \cdots & 0 & \overset{n=l_0}{1} & 0 & \cdots & 0 & \overset{n=m_r-l_0}{1} & 0 & \cdots & \overset{n=m_r-1}{0} \\ 0 & \cdots & 0 & -j & 0 & \cdots & 0 & j & 0 & \cdots & 0 \end{bmatrix}$$

$$\widetilde{\mathbf{L}}^{\natural}_{\mathbf{r\,h}} = \frac{m_r}{2} \widetilde{L}_{r,h} \begin{matrix} \\ \\ l=l_0 \\ \\ \\ l=m_r-l_0 \\ \\ \\ \end{matrix} \begin{bmatrix} & & & \overset{n=l_0}{0} & & & & \overset{n=m_r-l_0}{0} & & & \\ & 0 & & \vdots & & 0 & & \vdots & & 0 & \\ & & & 0 & & & & 0 & & & \\ 0 & \cdots & 0 & 1 & 0 & \cdots & 0 & 0 & 0 & \cdots & 0 \\ & & & 0 & & & & 0 & & & \\ & 0 & & \vdots & & 0 & & \vdots & & 0 & \\ & & & 0 & & & & 0 & & & \\ 0 & \cdots & 0 & 0 & 0 & \cdots & 0 & 1 & 0 & \cdots & 0 \\ & & & 0 & & & & 0 & & & \\ & 0 & & \vdots & & 0 & & \vdots & & 0 & \\ & & & 0 & & & & 0 & & & \end{bmatrix} \tag{A.19}$$

Transformed mutual inductance matrix of wavelength h (p. 87)

It is useful to express the coefficients of the matrix $\mathbf{T}(\theta'_{r,h})$ using complex exponentials:

$$\begin{aligned} \mathbf{T}(\theta'_{r,h}) &= \begin{bmatrix} \cos(\theta'_{r,h}) & -\sin(\theta'_{r,h}) \\ \sin(\theta'_{r,h}) & \cos(\theta'_{r,h}) \end{bmatrix} = \frac{1}{2} \begin{bmatrix} e^{j\theta'_{r,h}} + e^{-j\theta'_{r,h}} & j\left[e^{j\theta'_{r,h}} - e^{-j\theta'_{r,h}}\right] \\ -j\left[e^{j\theta'_{r,h}} + e^{-j\theta'_{r,h}}\right] & e^{j\theta'_{r,h}} + e^{-j\theta'_{r,h}} \end{bmatrix} \\ &= \frac{1}{2} e^{j\theta'_{r,h}} \begin{bmatrix} 1 & j \\ -j & 1 \end{bmatrix} + \frac{1}{2} e^{-j\theta'_{r,h}} \begin{bmatrix} 1 & -j \\ j & 1 \end{bmatrix} \end{aligned} \tag{A.20}$$

Following the results obtained in the foregoing sections, nine different computation schemes of $\widetilde{\mathbf{L}}^{\natural}_{\mathbf{rs\,h}}$ need to be distinguished depending on the wavelength order h and, consequently, the values of k_0 and l_0:

1.) $k_0 = 0 \wedge\ l_0 = 0$

$$\frac{1}{2}e^{j\theta'_{r,\,h}}\begin{bmatrix}1 & j\\ -j & 1\end{bmatrix}\widetilde{\mathbf{T}}_{\mathbf{Cr\,l_0}}\mathcal{W}_{\mathrm{m_r}} = \frac{\sqrt{m_r}}{2}e^{j\theta'_{r,\,h}}\begin{bmatrix}1 & j\\ -j & 1\end{bmatrix}\begin{bmatrix}\overset{n=0}{1} & 0 & \cdots & \overset{n=m_r-1}{0}\\ 0 & 0 & \cdots & 0\end{bmatrix}$$

$$= \frac{\sqrt{m_r}}{2}e^{j\theta'_{r,\,h}}\begin{bmatrix}\overset{n=0}{1} & 0 & \cdots & \overset{n=m_r-1}{0}\\ -j & 0 & \cdots & 0\end{bmatrix}$$

$$\frac{1}{2}e^{-j\theta'_{r,\,h}}\begin{bmatrix}1 & -j\\ j & 1\end{bmatrix}\widetilde{\mathbf{T}}_{\mathbf{Cr\,l_0}}\mathcal{W}_{\mathrm{m_r}} = \frac{\sqrt{m_r}}{2}e^{-j\theta'_{r,\,h}}\begin{bmatrix}1 & -j\\ j & 1\end{bmatrix}\begin{bmatrix}\overset{n=0}{1} & 0 & \cdots & \overset{n=m_r-1}{0}\\ -j & 0 & \cdots & 0\end{bmatrix}$$

$$= \frac{\sqrt{m_r}}{2}e^{-j\theta'_{r,\,h}}\begin{bmatrix}\overset{n=0}{1} & 0 & \cdots & \overset{n=m_r-1}{0}\\ j & 0 & \cdots & 0\end{bmatrix}$$

As a result,

$$\mathbf{T}(\theta'_{r,\,h})\widetilde{\mathbf{T}}_{\mathbf{Cr\,l_0}}\mathcal{W}_{\mathrm{m_r}} = \frac{\sqrt{m_r}}{2}\begin{bmatrix}\overset{n=l_0}{e^{j\theta'_{r,\,h}} + e^{-j\theta'_{r,\,h}}} & 0 & \cdots & \overset{n=m_r-1}{0}\\ -je^{j\theta'_{r,\,h}} + je^{-j\theta'_{r,\,h}} & 0 & \cdots & 0\end{bmatrix}$$

and hence,

$$\widetilde{\mathbf{L}}^{\natural}_{\mathbf{rs\,h}} = L_{M,\,h}\sqrt{m_s}\begin{bmatrix}\overset{k=0}{1} & 0\\ 0 & \vdots\\ \vdots & \vdots\\ \underset{k=m_s-1}{0} & 0\end{bmatrix}\frac{\sqrt{m_r}}{2}\begin{bmatrix}\overset{n=l_0}{e^{j\theta'_{r,\,h}} + e^{-j\theta'_{r,\,h}}} & 0 & \cdots & \overset{n=m_r-1}{0}\\ -je^{j\theta'_{r,\,h}} + je^{-j\theta'_{r,\,h}} & 0 & \cdots & 0\end{bmatrix}$$

$$= L_{M,\,h}\sqrt{m_s m_r}\begin{bmatrix}\overset{k=0}{\overset{n=0}{\cos(\theta'_{r,\,h})}} & 0 & \cdots & \overset{n=m_r-1}{0}\\ 0 & & & \\ \vdots & & \mathbf{0} & \\ \underset{k=m_s-1}{0} & & & \end{bmatrix} \tag{A.21}$$

2.) $k_0 = 0\ \wedge\ l_0 = m_r - l_0$

- $$\frac{1}{2}e^{j\theta'_{r,\,h}}\begin{bmatrix}1 & j\\ -j & 1\end{bmatrix}\widetilde{\mathbf{T}}_{\mathbf{Cr\,l_0}}\mathcal{W}_{\mathrm{m_r}} = \frac{\sqrt{m_r}}{2}e^{j\theta'_{r,\,h}}\begin{bmatrix}1 & j\\ -j & 1\end{bmatrix}\begin{bmatrix}\overset{n=0}{0} & \cdots & 0 & \overset{n=l_0}{1} & 0 & \cdots & \overset{n=m_r-1}{0}\\ 0 & \cdots & 0 & 0 & 0 & \cdots & 0\end{bmatrix}$$

$$= \frac{\sqrt{m_r}}{2}e^{j\theta'_{r,\,h}}\begin{bmatrix}\overset{n=0}{0} & \cdots & 0 & \overset{n=l_0}{1} & 0 & \cdots & \overset{n=m_r-1}{0}\\ 0 & \cdots & 0 & -j & 0 & \cdots & 0\end{bmatrix}$$

- $\frac{1}{2}e^{-j\theta'_{r,h}}\begin{bmatrix}1 & -j\\ j & 1\end{bmatrix}\widetilde{\mathbf{T}}_{\mathbf{Cr\,l_0}}\mathcal{W}_{\mathrm{m_r}} = \frac{\sqrt{m_r}}{2}e^{-j\theta'_{r,h}}\begin{bmatrix}1 & -j\\ j & 1\end{bmatrix}\begin{bmatrix}\overset{n=0}{0} & \cdots & 0 & \overset{n=l_0}{1} & 0 & \cdots & \overset{n=m_r-1}{0}\\ 0 & \cdots & 0 & 0 & 0 & \cdots & 0\end{bmatrix}$

$$= \frac{\sqrt{m_r}}{2}e^{-j\theta'_{r,h}}\begin{bmatrix}\overset{n=0}{0} & \cdots & 0 & \overset{n=l_0}{1} & 0 & \cdots & \overset{n=m_r-1}{0}\\ 0 & \cdots & 0 & j & 0 & \cdots & 0\end{bmatrix}$$

As a result,

$$\mathbf{T}(\theta'_{r,h})\widetilde{\mathbf{T}}_{\mathbf{Cr\,l_0}}\mathcal{W}_{\mathrm{m_r}} = \frac{\sqrt{m_r}}{2}\begin{bmatrix}\overset{n=0}{0} & \cdots & 0 & \overset{n=l_0}{e^{j\theta'_{r,h}}+e^{-j\theta'_{r,h}}} & 0 & \cdots & \overset{n=m_r-1}{0}\\ 0 & \cdots & 0 & -je^{j\theta'_{r,h}}+je^{-j\theta'_{r,h}} & 0 & \cdots & 0\end{bmatrix}$$

and hence,

$$\widetilde{\mathbf{L}}^{\natural}_{\mathbf{rs\,h}} = L_{M,h}\sqrt{m_s}\begin{matrix}\overset{k=0}{}\\ \\ \\ \underset{k=m_s-1}{}\end{matrix}\begin{bmatrix}1 & 0\\ 0 & \vdots\\ \vdots & \vdots\\ 0 & 0\end{bmatrix}\frac{\sqrt{m_r}}{2}\begin{bmatrix}\overset{n=0}{0} & \cdots & 0 & \overset{n=l_0}{e^{j\theta'_{r,h}}+e^{-j\theta'_{r,h}}} & 0 & \cdots & \overset{n=m_r-1}{0}\\ 0 & \cdots & 0 & -je^{j\theta'_{r,h}}+je^{-j\theta'_{r,h}} & 0 & \cdots & 0\end{bmatrix}$$

$$= L_{M,h}\sqrt{m_s m_r}\begin{matrix}\overset{k=0}{}\\ \\ \\ \underset{k=m_s-1}{}\end{matrix}\begin{bmatrix}\overset{n=0}{0} & \cdots & 0 & \overset{n=l_0}{cos(\theta'_{r,h})} & 0 & \cdots & \overset{n=m_r-1}{0}\\ & & & 0 & & & \\ & \mathbf{0} & & \vdots & & \mathbf{0} & \\ & & & 0 & & & \end{bmatrix} \tag{A.22}$$

3.) $k_0 = 0 \ \wedge \ \neg(l_0 = 0 \ \vee \ l_0 = m_r - l_0)$

- $\frac{1}{2}e^{j\theta'_{r,h}}\begin{bmatrix}1 & j\\ -j & 1\end{bmatrix}\widetilde{\mathbf{T}}_{\mathbf{Cr\,l_0}}\mathcal{W}_{\mathrm{m_r}}$

$$= \frac{\sqrt{m_r}}{4}e^{j\theta'_{r,h}}\begin{bmatrix}1 & j\\ -j & 1\end{bmatrix}\begin{bmatrix}\overset{n=0}{0} & \cdots & 0 & \overset{n=l_0}{1} & 0 & \cdots & 0 & \overset{n=m_r-l_0}{1} & 0 & \cdots & \overset{n=m_r-1}{0}\\ 0 & \cdots & 0 & -j & 0 & \cdots & 0 & j & 0 & \cdots & 0\end{bmatrix}$$

$$= \frac{\sqrt{m_r}}{2}e^{j\theta'_{r,h}}\begin{bmatrix}\overset{n=0}{0} & \cdots & 0 & \overset{n=l_0}{1} & 0 & \cdots & \overset{n=m_r-1}{0}\\ 0 & \cdots & 0 & -j & 0 & \cdots & 0\end{bmatrix}$$

- $\frac{1}{2}e^{-j\theta'_{r,h}}\begin{bmatrix}1 & -j\\ j & 1\end{bmatrix}\widetilde{\mathbf{T}}_{\mathbf{Cr\,l_0}}\mathcal{W}_{\mathrm{m_r}}$

$$= \frac{\sqrt{m_r}}{4} e^{-j\theta'_{r,\,h}} \begin{bmatrix} 1 & -j \\ j & 1 \end{bmatrix} \begin{bmatrix} \overset{n=0}{0} & \cdots & 0 & \overset{n=l_0}{1} & 0 & \cdots & 0 & \overset{n=m_r-l_0}{1} & 0 & \cdots & \overset{n=m_r-1}{0} \\ 0 & \cdots & 0 & -j & 0 & \cdots & 0 & j & 0 & \cdots & 0 \end{bmatrix}$$

$$= \frac{\sqrt{m_r}}{2} e^{-j\theta'_{r,\,h}} \begin{bmatrix} \overset{n=0}{0} & \cdots & 0 & \overset{n=m_r-l_0}{1} & 0 & \cdots & \overset{n=m_r-1}{0} \\ 0 & \cdots & 0 & j & 0 & \cdots & 0 \end{bmatrix}$$

Consequently,

$$\mathbf{T}(\theta'_{r,\,h})\widetilde{\mathbf{T}}_{\mathbf{Cr\,l_0}}\mathcal{W}_{\mathrm{m_r}} = \frac{\sqrt{m_r}}{2} \begin{bmatrix} \overset{n=0}{0} & \cdots & 0 & \overset{n=l_0}{e^{j\theta'_{r,\,h}}} & 0 & \cdots & 0 & \overset{n=m_r-l_0}{e^{-j\theta'_{r,\,h}}} & 0 & \cdots & \overset{n=m_r-1}{0} \\ 0 & \cdots & 0 & -je^{j\theta'_{r,\,h}} & 0 & \cdots & 0 & je^{-j\theta'_{r,\,h}} & 0 & \cdots & 0 \end{bmatrix}$$

and

$$\widetilde{\mathbf{L}}^{\natural}_{\mathbf{rs\,h}} = L_{M,\,h}\sqrt{m_s} \begin{matrix} \overset{k=0}{} \\ \\ \\ \underset{k=m_s-1}{} \end{matrix} \begin{bmatrix} 1 & 0 \\ 0 & \vdots \\ \vdots & \vdots \\ 0 & 0 \end{bmatrix}$$

$$\times \frac{\sqrt{m_r}}{2} \begin{bmatrix} \overset{n=0}{0} & \cdots & 0 & \overset{n=l_0}{e^{j\theta'_{r,\,h}}} & 0 & \cdots & 0 & \overset{n=m_r-l_0}{e^{-j\theta'_{r,\,h}}} & 0 & \cdots & \overset{n=m_r-1}{0} \\ 0 & \cdots & 0 & -je^{j\theta'_{r,\,h}} & 0 & \cdots & 0 & je^{-j\theta'_{r,\,h}} & 0 & \cdots & 0 \end{bmatrix}$$

$$\widetilde{\mathbf{L}}^{\natural}_{\mathbf{rs\,h}} = L_{M,\,h}\frac{\sqrt{m_s m_r}}{2} \begin{matrix} \overset{k=k_0}{} \\ \\ \underset{k=m_s-1}{} \end{matrix} \begin{bmatrix} 0 & \cdots & 0 & \overset{n=l_0}{e^{j\theta'_{r,\,h}}} & 0 & \cdots & 0 & \overset{n=m_r-l_0}{e^{-j\theta'_{r,\,h}}} & 0 & \cdots & 0 \\ & & & 0 & & & & 0 & & & \\ & 0 & & \vdots & & 0 & & \vdots & & 0 & \\ & & & 0 & & & & 0 & & & \end{bmatrix} \tag{A.23}$$

4.) $k_0 = m_s - k_0 \ \wedge \ l_0 = 0$

$$\mathbf{T}(\theta'_{r,\,h})\widetilde{\mathbf{T}}_{\mathbf{Cr\,l_0}}\mathcal{W}_{\mathrm{m_r}} = \frac{\sqrt{m_r}}{2} \begin{bmatrix} \overset{n=l_0}{e^{j\theta'_{r,\,h}} + e^{-j\theta'_{r,\,h}}} & 0 & \cdots & \overset{n=m_r-1}{0} \\ -je^{j\theta'_{r,\,h}} + je^{-j\theta'_{r,\,h}} & 0 & \cdots & 0 \end{bmatrix}$$

$$\widetilde{\mathbf{L}}^{\natural}_{\mathbf{rs\,h}} = L_{M,\,h}\sqrt{m_s} \begin{matrix} \overset{k=0}{} \\ \\ \\ \underset{k=k_0}{} \\ \\ \\ \underset{k=m_s-1}{} \end{matrix} \begin{bmatrix} 0 & 0 \\ \vdots & \vdots \\ 0 & \vdots \\ 1 & \vdots \\ 0 & \vdots \\ \vdots & \vdots \\ 0 & 0 \end{bmatrix} \mathbf{T}(\theta'_{r,\,h})\widetilde{\mathbf{T}}_{\mathbf{Cr\,l_0}}\mathcal{W}_{\mathrm{m_r}}$$

$$= L_{M,h}\sqrt{m_s m_r} \begin{matrix} \\ k{=}0 \\ \\ k{=}k_0 \\ \\ k{=}m_s{-}1 \end{matrix} \begin{matrix} \begin{matrix} n{=}0 & & & & n{=}m_r{-}1 \end{matrix} \\ \begin{bmatrix} 0 & & & \\ \vdots & & 0 & \\ 0 & & & \\ \cos(\theta'_{r,h}) & 0 & \cdots & 0 \\ 0 & & & \\ \vdots & & 0 & \\ 0 & & & \end{bmatrix} \end{matrix} \tag{A.24}$$

5.) $k_0 = m_s - k_0 \ \wedge \ l_0 = m_r - l_0$

$$\mathbf{T}(\theta'_{r,h})\widetilde{\mathbf{T}}_{\mathbf{Cr\,l_0}}\mathcal{W}_{\mathrm{m_r}} = \frac{\sqrt{m_r}}{2} \begin{matrix} \begin{matrix} n{=}0 & & & & n{=}l_0 & & & & n{=}m_r{-}1 \end{matrix} \\ \begin{bmatrix} 0 & \cdots & 0 & e^{j\theta'_{r,h}} + e^{-j\theta'_{r,h}} & 0 & \cdots & 0 \\ 0 & \cdots & 0 & -je^{j\theta'_{r,h}} + je^{-j\theta'_{r,h}} & 0 & \cdots & 0 \end{bmatrix} \end{matrix}$$

$$\widetilde{\mathbf{L}}^{\natural}_{\mathbf{rs\,h}} = L_{M,h}\sqrt{m_s} \begin{matrix} \\ k{=}0 \\ \\ k{=}k_0 \\ \\ k{=}m_s{-}1 \end{matrix} \begin{bmatrix} 0 & 0 \\ \vdots & \vdots \\ 0 & \vdots \\ 1 & \vdots \\ 0 & \vdots \\ \vdots & \vdots \\ 0 & 0 \end{bmatrix} \mathbf{T}(\theta'_{r,h})\widetilde{\mathbf{T}}_{\mathbf{Cr\,l_0}}\mathcal{W}_{\mathrm{m_r}}$$

$$= L_{M,h}\sqrt{m_s m_r} \begin{matrix} \\ k{=}0 \\ \\ k{=}k_0 \\ \\ k{=}m_s{-}1 \end{matrix} \begin{matrix} \begin{matrix} & & n{=}l_0 & & \end{matrix} \\ \begin{bmatrix} & & 0 & & \\ & 0 & \vdots & 0 & \\ & & 0 & & \\ 0 & \cdots & \cos(\theta'_{r,h}) & \cdots & 0 \\ & & 0 & & \\ & 0 & \vdots & 0 & \\ & & 0 & & \end{bmatrix} \end{matrix} \tag{A.25}$$

6.) $k_0 = m_s - k_0 \ \wedge \ \neg(l_0 = 0 \ \vee \ l_0 = m_r - l_0)$

$$\mathbf{T}(\theta'_{r,h})\widetilde{\mathbf{T}}_{\mathbf{Cr\,l_0}}\mathcal{W}_{\mathrm{m_r}} = \frac{\sqrt{m_r}}{2} \begin{matrix} \begin{matrix} n{=}0 & & & n{=}l_0 & & & & n{=}m_r{-}l_0 & & & n{=}m_r{-}1 \end{matrix} \\ \begin{bmatrix} 0 & \cdots & 0 & e^{j\theta'_{r,h}} & 0 & \cdots & 0 & e^{-j\theta'_{r,h}} & 0 & \cdots & 0 \\ 0 & \cdots & 0 & -je^{j\theta'_{r,h}} & 0 & \cdots & 0 & je^{-j\theta'_{r,h}} & 0 & \cdots & 0 \end{bmatrix} \end{matrix}$$

$$\widetilde{\mathbf{L}}^{\natural}_{\mathbf{rs\,h}} = L_{M,h}\sqrt{m_s} \begin{matrix} \\ k{=}0 \\ \\ k{=}k_0 \\ \\ \\ k{=}m_s{-}1 \end{matrix} \begin{bmatrix} 0 & 0 \\ \vdots & \vdots \\ 0 & \vdots \\ 1 & \vdots \\ 0 & \vdots \\ \vdots & \vdots \\ 0 & 0 \end{bmatrix} \mathbf{T}(\theta'_{r,\,h})\widetilde{\mathbf{T}}_{\mathbf{Cr\,l_0}}\mathcal{W}_{\mathrm{m_r}}$$

$$= L_{M,h}\frac{\sqrt{m_s m_r}}{2} \begin{matrix} \\ k{=}0 \\ \\ k{=}k_0 \\ \\ k{=}m_s{-}1 \end{matrix} \begin{bmatrix} & & \overset{n=l_0}{0} & & & \overset{n=m_r-l_0}{0} & & \\ & 0 & \vdots & & 0 & \vdots & & 0 & \\ & & 0 & & & 0 & & & \\ 0 & \cdots & e^{j\theta'_{r,\,h}} & 0 & \cdots & e^{-j\theta'_{r,\,h}} & 0 & \cdots & 0 \\ & & 0 & & & 0 & & & \\ & 0 & \vdots & & 0 & \vdots & & 0 & \\ & & 0 & & & 0 & & & \end{bmatrix} \tag{A.26}$$

7.) $\neg(k_0 = 0 \ \vee \ k_0 = m_s - k_0) \ \wedge \ l_0 = 0$

$$\mathbf{T}(\theta'_{r,\,h})\widetilde{\mathbf{T}}_{\mathbf{Cr\,l_0}}\mathcal{W}_{\mathrm{m_r}} = \frac{\sqrt{m_r}}{2} \begin{bmatrix} \overset{n=0}{e^{j\theta'_{r,\,h}} + e^{-j\theta'_{r,\,h}}} & 0 & \cdots & \overset{n=m_r-1}{0} \\ -je^{j\theta'_{r,\,h}} + je^{-j\theta'_{r,\,h}} & 0 & \cdots & 0 \end{bmatrix}$$

$$\widetilde{\mathbf{L}}^{\natural}_{\mathbf{rs\,h}} = L_{M,h}\frac{\sqrt{m_s}}{2} \begin{matrix} \\ k{=}0 \\ \\ k{=}k_0 \\ \\ \\ k{=}m_s{-}k_0 \\ \\ k{=}m_s{-}1 \end{matrix} \begin{bmatrix} 0 & 0 \\ \vdots & \vdots \\ 0 & 0 \\ 1 & j \\ 0 & 0 \\ \vdots & \vdots \\ 0 & 0 \\ 1 & -j \\ 0 & 0 \\ \vdots & \vdots \\ 0 & 0 \end{bmatrix} \frac{\sqrt{m_r}}{2} \begin{bmatrix} \overset{n=0}{e^{j\theta'_{r,\,h}} + e^{-j\theta'_{r,\,h}}} & 0 & \cdots & \overset{n=m_r-1}{0} \\ -je^{j\theta'_{r,\,h}} + je^{-j\theta'_{r,\,h}} & 0 & \cdots & 0 \end{bmatrix}$$

$$= L_{M,h}\frac{\sqrt{m_s m_r}}{2}\begin{array}{c} \\ \\ \\ k=k_0 \\ \\ \\ k=m_s-k_0 \\ \\ \end{array}\begin{array}{c} n=0 \qquad\qquad\qquad\qquad n=m_r-1 \\ \begin{bmatrix} 0 & & \\ \vdots & & 0 \\ 0 & & \\ e^{j\theta'_{r,h}} & 0 \cdots & 0 \\ 0 & & \\ \vdots & & 0 \\ 0 & & \\ e^{-j\theta'_{r,h}} & 0 \cdots & 0 \\ 0 & & \\ \vdots & & 0 \\ 0 & & \end{bmatrix} \end{array} \tag{A.27}$$

8.) $\neg(k_0 = 0 \ \vee \ k_0 = m_s - k_0) \ \wedge \ l_0 = m_r - l_0$

$$\mathbf{T}(\theta'_{r,h})\widetilde{\mathbf{T}}_{\mathbf{Cr\,l_0}}\mathcal{W}_{\mathrm{m_r}} = \frac{\sqrt{m_r}}{2}\begin{array}{c} n=0 \qquad\qquad n=l_0 \qquad\qquad\qquad n=m_r-1 \\ \begin{bmatrix} 0 & \cdots & 0 & e^{j\theta'_{r,h}} + e^{-j\theta'_{r,h}} & 0 & \cdots & 0 \\ 0 & \cdots & 0 & -je^{j\theta'_{r,h}} + je^{-j\theta'_{r,h}} & 0 & \cdots & 0 \end{bmatrix} \end{array}$$

$$\widetilde{\mathbf{L}}^{\natural}_{\mathbf{rs\,h}} = L_{M,h}\frac{\sqrt{m_s}}{2}\begin{array}{c} \\ k=0 \\ \\ k=k_0 \\ \\ \\ k=m_s-k_0 \\ \\ k=m_s-1 \end{array}\begin{bmatrix} 0 & 0 \\ \vdots & \vdots \\ 0 & 0 \\ 1 & j \\ 0 & 0 \\ \vdots & \vdots \\ 0 & 0 \\ 1 & -j \\ 0 & 0 \\ \vdots & \vdots \\ 0 & 0 \end{bmatrix}\frac{\sqrt{m_r}}{2}\begin{array}{c} n=0 \qquad\qquad n=l_0 \qquad\qquad\qquad n=m_r-1 \\ \begin{bmatrix} 0 & \cdots & 0 & e^{j\theta'_{r,h}} + e^{-j\theta'_{r,h}} & 0 & \cdots & 0 \\ 0 & \cdots & 0 & -je^{j\theta'_{r,h}} + je^{-j\theta'_{r,h}} & 0 & \cdots & 0 \end{bmatrix} \end{array}$$

$$= L_{M,h}\frac{\sqrt{m_s m_r}}{2}\begin{array}{c} \\ \\ \\ k=k_0 \\ \\ \\ k=m_s-k_0 \\ \\ \end{array}\begin{array}{c} n=l_0 \\ \begin{bmatrix} & 0 & & & & 0 & \\ & & & 0 & & & \\ & & & \vdots & & & \\ & & & 0 & & & \\ 0 & \cdots & 0 & e^{j\theta'_{r,h}} & 0 & \cdots & 0 \\ & & & 0 & & & \\ & 0 & & \vdots & & 0 & \\ & & & 0 & & & \\ 0 & \cdots & 0 & e^{-j\theta'_{r,h}} & 0 & \cdots & 0 \\ & & & 0 & & & \\ & 0 & & \vdots & & 0 & \\ & & & 0 & & & \end{bmatrix} \end{array} \tag{A.28}$$

9.) $\neg(k_0 = 0 \;\vee\; k_0 = m_s - k_0) \;\wedge\; \neg(l_0 = 0 \;\vee\; l_0 = m_r - l_0)$

$$\mathbf{T}(\theta'_{r,\,h})\widetilde{\mathbf{T}}_{\mathbf{Cr}\,\mathbf{l_0}}\mathcal{W}_{\mathrm{m_r}} = \frac{\sqrt{m_r}}{2}\begin{bmatrix} \overset{n=0}{0} & \cdots & 0 & \overset{n=l_0}{e^{j\theta'_{r,\,h}}} & 0 & \cdots & 0 & \overset{n=m_r-l_0}{e^{-j\theta'_{r,\,h}}} & 0 & \cdots & \overset{n=m_r-1}{0} \\ 0 & \cdots & 0 & -je^{j\theta'_{r,\,h}} & 0 & \cdots & 0 & je^{-j\theta'_{r,\,h}} & 0 & \cdots & 0 \end{bmatrix}$$

$$\widetilde{\mathbf{L}}^{\natural}_{\mathbf{rs\,h}} = L_{M,\,h}\frac{\sqrt{m_s}}{2}\begin{array}{r} {\scriptstyle k=0} \\ \\ \\ {\scriptstyle k=k_0} \\ \\ \\ \\ {\scriptstyle k=m_s-k_0} \\ \\ \\ {\scriptstyle k=m_s-1} \end{array}\begin{bmatrix} 0 & 0 \\ \vdots & \vdots \\ 0 & 0 \\ 1 & j \\ 0 & 0 \\ \vdots & \vdots \\ 0 & 0 \\ 1 & -j \\ 0 & 0 \\ \vdots & \vdots \\ 0 & 0 \end{bmatrix}$$

$$\times\frac{\sqrt{m_r}}{2}\begin{bmatrix} \overset{n=0}{0} & \cdots & 0 & \overset{n=l_0}{e^{j\theta'_{r,\,h}}} & 0 & \cdots & 0 & \overset{n=m_r-l_0}{e^{-j\theta'_{r,\,h}}} & 0 & \cdots & \overset{n=m_r-1}{0} \\ 0 & \cdots & 0 & -je^{j\theta'_{r,\,h}} & 0 & \cdots & 0 & je^{-j\theta'_{r,\,h}} & 0 & \cdots & 0 \end{bmatrix}$$

$$\widetilde{\mathbf{L}}^{\natural}_{\mathbf{rs\,h}} = L_{M,\,h}\frac{\sqrt{m_s m_r}}{2}\begin{array}{r} \\ \\ \\ {\scriptstyle k=k_0} \\ \\ \\ \\ {\scriptstyle k=m_s-k_0} \\ \\ \\ \\ \end{array}\begin{bmatrix} & & & \overset{n=l_0}{0} & & & & \overset{n=m_r-l_0}{0} & & & \\ & \mathbf{0} & & \vdots & & \mathbf{0} & & \vdots & & \mathbf{0} & \\ & & & 0 & & & & 0 & & & \\ 0 & \cdots & 0 & e^{j\theta'_{r,\,h}} & 0 & \cdots & 0 & 0 & 0 & \cdots & 0 \\ & & & 0 & & & & 0 & & & \\ & \mathbf{0} & & \vdots & & \mathbf{0} & & \vdots & & \mathbf{0} & \\ & & & 0 & & & & 0 & & & \\ 0 & \cdots & 0 & 0 & 0 & \cdots & 0 & e^{-j\theta'_{r,\,h}} & 0 & \cdots & 0 \\ & & & 0 & & & & 0 & & & \\ & \mathbf{0} & & \vdots & & \mathbf{0} & & \vdots & & \mathbf{0} & \\ & & & 0 & & & & 0 & & & \end{bmatrix} \tag{A.29}$$

It turns out that the expressions of $\widetilde{\mathbf{L}}^{\natural}_{\mathbf{rs\,h}}$ obtained in cases 1 to 8 are a particular form of (A.29). Hence, (A.29) can be treated as the general form of $\widetilde{\mathbf{L}}^{\natural}_{\mathbf{rs\,h}}$ for any wavelength $h \in \mathbb{N}^{\star}$.

Bibliography

[1] Gabriel Kron. *Equivalent Circuits of Electric Machinery.* John Wiley & Sons, 1951 (cit. on pp. 4 sq., 8 sq., 37).

[2] Gabriel Kron. 'Induction Motor Slot Combinations Rules to Predetermine Crawling, Vibration, Noise and Hooks in the Speed-Torque Curve'. In: *Transactions of the AIEE* 50.2 (06/1931), pp. 757–767 (cit. on pp. 4, 7).

[3] M. M. Liwschitz. 'Field Harmonics in Induction Motors'. In: *Transactions of the AIEE* 61.11 (11/1942), pp. 797–803 (cit. on p. 4).

[4] Philip L. Alger. *The nature of polyphase induction machines.* Wiley, 1951 (cit. on p. 4).

[5] David C. White and Herbert H. Woodson. *Electromechanical Energy Conversion.* John Wiley & Sons, 1959 (cit. on pp. 4, 82, 118).

[6] G. Joksimovic, M. Djurovic and J. Penman. 'Cage Rotor MMF: Winding Function Approach'. In: *IEEE Power Engineering Review* 21.4 (04/2001), pp. 64–66 (cit. on p. 5).

[7] Gojko M. Joksimovic, Jaksa Riger, Thomas M. Wolbank, Nedjeljko Peric and Mario Vasak. 'Stator-Current Spectrum Signature of Healthy Cage Rotor Induction Machines'. In: *IEEE Transactions on Industrial Electronics* 60.9 (09/2013), pp. 4025–4033 (cit. on pp. 5, 10, 14).

[8] J. R. Cameron, W. T. Thomson and A. B. Dow. 'Vibration and current monitoring for detecting airgap eccentricity in large induction motors'. In: *IEE Proceedings B Electric Power Applications* 133.3 (05/1986), p. 155 (cit. on p. 5).

[9] G. M. Joksimovic. 'Dynamic simulation of cage induction machine with air gap eccentricity'. In: *IEE Proceedings - Electric Power Applications* 152.4 (07/2005), p. 803 (cit. on pp. 5, 10).

[10] Subhasis Nandi, Thirumarai Chelvan Ilamparithi, Sang Bin Lee and Doosoo Hyun. 'Detection of Eccentricity Faults in Induction Machines Based on Nameplate Parameters'. In: *IEEE Transactions on Industrial Electronics* 58.5 (05/2011), pp. 1673–1683 (cit. on pp. 5 sq.).

[11] Julio C. Moreira and Thomas A. Lipo. 'Modeling of Saturated ac Machines Including Air Gap Flux Harmonic Components'. In: *IEEE Transactions on Industry Applications* 28.2 (03/1992), pp. 343–349 (cit. on pp. 5, 9 sq., 14).

[12] Kevin D. Hurst and Thomas G. Habetler. 'Sensorless Speed Measurement Using Current Harmonic Spectral Estimation in Induction Machine Drives'. In: *IEEE Transactions on Power Electronics* 11.1 (01/1996), pp. 66–73 (cit. on p. 6).

[13] K. D. Hurst and T. G. Habetler. 'A comparison of spectrum estimation techniques for sensorless speed detection in induction machines'. In: *IEEE Transactions on Industry Applications* 33.4 (07/1997), pp. 898–905 (cit. on p. 6).

[14] D.R. McGaughey, M. Tarbouchi, K. Nutt and A. Chikhani. 'Speed Sensorless Estimation of AC Induction Motors Using the Fast Orthogonal Search Algorithm'. In: *IEEE Transactions on Energy Conversion* 21.1 (03/2006), pp. 112–120 (cit. on p. 6).

[15] Zhi Gao, Larry Turner, Roy S. Colby and Benoit Leprettre. 'A Frequency Demodulation Approach to Induction Motor Speed Detection'. In: *IEEE Transactions on Industry Applications* 47.4 (07/2011), pp. 1632–1642 (cit. on p. 6).

[16] Michael W. Degner and Robert D. Lorenz. 'Using Multiple Saliencies for the Estimation of Flux, Position, and Velocity in AC Machines'. In: *IEEE Transactions on Industry Applications* 34.5 (09/1998), pp. 1097–1104 (cit. on pp. 6, 8).

[17] Michael W. Degner and Robert D. Lorenz. 'Position Estimation in Induction Machines Utilizing Rotor Bar Slot Harmonics and Carrier-Frequency Signal Injection'. In: *IEEE Transactions on Industry Applications* 36.3 (05/2000), pp. 736–742 (cit. on pp. 6, 8).

[18] Nikolas Teske, Greg M. Asher, Mark Sumner and Keith J. Bradley. 'Encoderless Position Estimation for Symmetric Cage Induction Machines Under Loaded Conditions'. In: *IEEE Transactions on Industry Applications* 37.6 (11/2001), pp. 1793–1800 (cit. on pp. 6, 8).

[19] Qiang Gao, Greg M. Asher and Mark Sumner. 'Sensorless Position and Speed Control of Induction Motors Using High-Frequency Injection and Without Offline Precommissioning'. In: *IEEE Transactions on Industrial Electronics* 54.5 (10/2007), pp. 2474–2481 (cit. on p. 6).

[20] Reiko Raute, Cedric Caruana, Cyril Spiteri Staines, Joseph Cilia, Mark Sumner and Greg M. Asher. 'Sensorless Control of Induction Machines at Low and Zero Speed by Using PWM Harmonics for Rotor-Bar Slotting Detection'. In: *IEEE Transactions on Industry Applications* 46.5 (09/2010), pp. 1989–1998 (cit. on pp. 6, 8).

[21] Markus A. Vogelsberger, Stefan Grubic, Thomas G. Habetler and Thomas M. Wolbank. 'Using PWM-Induced Transient Excitation and Advanced Signal Processing for Zero-Speed Sensorless Control of AC Machines'. In: *IEEE Transactions on Industrial Electronics* 57.1 (01/2010), pp. 365–374 (cit. on p. 6).

[22] Mohamed K. Metwaly, Nagy I. Elkalashy, Mohamed S. Zaky and Thomas M. Wolbank. 'Slotting Saliency Extraction For Sensorless Torque Control of Standard Induction Machines'. In: *IEEE Transactions on Energy Conversion* 33.1 (03/2018), pp. 68–77 (cit. on p. 6).

[23] Hamid A. Toliyat and Thomas A. Lipo. 'Transient Analysis of Cage Induction Machines Under Stator, Rotor Bar and End Ring Faults'. In: *IEEE Transactions on Energy Conversion* 10.2 (06/1995), pp. 241–247 (cit. on pp. 6, 9, 25).

[24] Gojko M. Joksimovic and Jim Penman. 'The Detection of Inter-Turn Short Circuits in the Stator Windings of Operating Motors'. In: *IEEE Transactions on Industrial Electronics* 47.5 (10/2000), pp. 1078–1084 (cit. on pp. 6, 21).

[25] Subhasis Nandi and Hamid A. Toliyat. 'Novel Frequency-Domain-Based Technique to Detect Stator Interturn Faults in Induction Machines Using Stator-Induced Voltages After Switch-Off'. In: *IEEE Transactions on Industry Applications* 38.1 (01/2002), pp. 101–109 (cit. on p. 6).

[26] Jafar Milimonfared, Homayoun Meshgin Kelk, Subhasis Nandi and Artin Der Minassiansand Hamid A. Toliyat. 'A Novel Approach for Broken-Rotor-Bar Detection in Cage Induction Motors'. In: *IEEE Transactions on Industry Applications* 35.5 (09/1999), pp. 1000–1006 (cit. on p. 6).

[27] A. Bellini, A. Yazidi, F. Filippetti, C. Rossi and G.-A. Capolino. 'High Frequency Resolution Techniques for Rotor Fault Detection of Induction Machines'. In: *IEEE Transactions on Industrial Electronics* 55.12 (12/2008), pp. 4200–4209 (cit. on p. 6).

[28] Gojko Joksimovic, Jaksa Riger, Thomas Wolbank, Nedjeljko Peric and Mario Vasak. 'Stator Line Current Spectrum Content of a Healthy Cage Rotor Induction Machine'. In: *8th IEEE Symposium on Diagnostics for Electrical Machines, Power Electronics & Drives*. IEEE, 09/2011, pp. 113–118 (cit. on p. 6).

[29] Vincent Choqueuse, Mohamed El Hachemi Benbouzid, Yassine Amirat and Sylvie Turri. 'Diagnosis of Three-Phase Electrical Machines Using Multidimensional Demodulation Techniques'. In: *IEEE Transactions on Industrial Electronics* 59.4 (04/2012), pp. 2014–2023 (cit. on p. 6).

[30] Subhasis Nandi, Shehab Ahmed and Hamid A. Toliyat. 'Detection of Rotor Slot and Other Eccentricity Related Harmonics in a Three Phase Induction Motor with Different Rotor Cages'. In: *IEEE Transactions on Energy Conversion* 16.3 (09/2001), pp. 253–260 (cit. on p. 6).

[31] Thomas M. Wolbank, Peter Nussbaumer, Hao Chen and Peter E. Macheiner. 'Monitoring of Rotor-Bar Defects in Inverter-Fed Induction Machines at Zero Load and Speed'. In: *IEEE Transactions on Industrial Electronics* 58.5 (05/2011), pp. 1468–1478 (cit. on p. 6).

[32] Mohamed Sahraoui, Antonio J. Marques Cardoso and Adel Ghoggal. 'The Use of a Modified Prony Method to Track the Broken Rotor Bar Characteristic Frequencies and Amplitudes in Three-Phase Induction Motors'. In: *IEEE Transactions on Industry Applications* 51.3 (05/2015), pp. 2136–2147 (cit. on p. 6).

[33] Arunava Naha, Anik Kumar Samanta, Aurobinda Routray and Alok Kanti Deb. 'A Method for Detecting Half-Broken Rotor Bar in Lightly Loaded Induction Motors Using Current'. In: *IEEE Transactions on Instrumentation and Measurement* 65.7 (07/2016), pp. 1614–1625 (cit. on p. 6).

[34] Eshaan Ghosh, Aida Mollaeian, Weusong Hu and Narayan C. Kar. 'A Novel Control Strategy for Online Harmonic Compensation in Parametrically Unbalanced Induction Motor'. In: *IEEE Transactions on Magnetics* 52.7 (07/2016), pp. 1–4 (cit. on p. 7).

[35] Eshaan Ghosh, Aida Mollaeian, Seog Kim, Jimi Tjong and Narayan C. Kar. 'DNN-Based Predictive Magnetic Flux Reference for Harmonic Compensation Control in Magnetically Unbalanced Induction Motor'. In: *IEEE Transactions on Magnetics* 53.11 (11/2017), pp. 1–7 (cit. on p. 7).

[36] Wolfgang Bischof. *Noise Optimized Control of an Electrical Drive with Induction Machine. Harmonics Modeling and Control Strategies*. Cuvillier, 07/08/2019. 214 pp. (cit. on p. 7).

[37] D. W. Novotny. *Vector Control and Dynamics of AC Drives*. Clarendon Press, 25/07/1996. 464 pp. (cit. on p. 7).

[38] Gabriel Kron. 'The Application of Tensors to the Analysis of Rotating Electrical Machinery'. In: *General Electric Review* I-XVI (1938) (cit. on pp. 8, 15, 21 sq.).

[39] F. Vernet, F. Heliodore, J.-L. Thomas and S. Poullain. 'Tensorial Analysis of Electrical Machine : A Modeling Tool for Electro-Mechanical Active Filtering and Diagnosis'. In: *International Conference on Electrical Machines*. 2002 (cit. on pp. 8 sq.).

[40] F. Vernet, F. Heliodore, J.-L. Thomas and S. Poullain. 'Space harmonics in electrical machines: extended state-space model and Kalman filter'. In: *Proceedings of 2003 IEEE Conference on Control Applications, 2003. CCA 2003.* IEEE, 2003, pp. 909–914 (cit. on p. 9).

[41] H. A. Toliyat, T. A. Lipo and J. C. White. 'Analysis of a concentrated winding induction machine for adjustable speed drive applications. I. Motor analysis'. In: *IEEE Transactions on Energy Conversion* 6.4 (12/1991), pp. 679–683 (cit. on p. 9).

[42] Xiaogang Luo, Yuefeng Liao, Hamid A. Toliyat, Ahmed El-Antably and Thomas A. Lipo. 'Multiple Coupled Circuit Modeling of Induction Machines'. In: *IEEE Transactions on Industry Applications* 31.2 (03/1995), pp. 311–318 (cit. on pp. 9, 21, 25).

[43] Jawad Faiz and Iman Tabatabaei. 'Extension of Winding Function Theory for Nonuniform Air Gap in Electric Machinery'. In: *IEEE Transactions on Magnetics* 38.6 (11/2002), pp. 3654–3657 (cit. on pp. 9, 18 sq.).

[44] Gojko M. Joksimovic, Momir D. Durovic and Aleksandar B. Obradovic. 'Skew and Linear Rise of MMF Across Slot Modeling - Winding Function Approach'. In: *IEEE Transactions on Energy Conversion* 14.3 (09/1999), pp. 315–320 (cit. on p. 10).

[45] G. Bossio, C. De Angelo, J. Solsona, G. Garcia and M. I. Valla. 'A 2-D Model of the Induction Machine: An Extension of the Modified Winding Function Approach'. In: *IEEE Transactions on Energy Conversion* 19.1 (03/2004), pp. 144–150 (cit. on p. 10).

[46] Gojko Joksimovic, Jaksa Riger, Thomas Wolbank, Nedjeljko Peric, Mario Vasak, Goran Stojvic and Vinko Lesic. 'Dynamic induction machine model accounting for stator and rotor slotting'. In: *2012 XXth International Conference on Electrical Machines*. IEEE, 09/2012 (cit. on p. 10).

[47] Q. Hecker, J. Igelspacher and H.-G. Herzog. 'Parameter identification of an axial-flux induction machine by winding functions'. In: *The XIX International Conference on Electrical Machines - ICEM 2010*. IEEE, 09/2010 (cit. on p. 10).

[48] J. Igelspacher, Q. Hecker and H.-G. Herzog. 'Simulation of an axial-flux induction machine with squirrel cage based on the winding function theory'. In: *2012 Electrical Systems for Aircraft, Railway and Ship Propulsion*. IEEE, 10/2012 (cit. on p. 10).

[49] Hamid A. Toliyat, Mohammed S. Arefeen and Alexander G. Parlos. 'A Method for Dynamic Simulation of Air-Gap Eccentricity in Induction Machines'. In: *IEEE Transactions on Industry Applications* 32.4 (07/1996), pp. 910–918 (cit. on pp. 10, 21).

[50] J. Faiz and M. Ojaghi. 'Unified winding function approach for dynamic simulation of different kinds of eccentricity faults in cage induction machines'. In: *IET Electric Power Applications* 3.5 (09/2009), pp. 461–470 (cit. on p. 10).

[51] P. C. Krause, O. Wasynczuk and S. D. Sudhoff. *Analysis of electric machinery and drive systems*. IEEE Press series on power engineering. IEEE Press, 2002 (cit. on pp. 20, 140).

[52] William H. Press, Saul A. Teukolsky, William T. Vetterling and Brian P. Flannery. *Numerical Recipes in C - The Art of Scientific Computing (2nd ed.)* Cambridge University Press, 1992 (cit. on p. 21).

[53] Jakob Igelspacher, Stephan Willerich and H.-G. Herzog. 'Simulation of an axial-flux squirrel-cage induction machine under stator fault conditions using winding functions'. In: *2013 International Electric Machines & Drives Conference*. IEEE, 05/2013, pp. 1283–1288 (cit. on p. 21).

[54] A. R. Munoz and T. A. Lipo. 'Complex vector model of the squirrel-cage induction machine including instantaneous rotor bar currents'. In: *IEEE Transactions on Industry Applications* 35.6 (1999), pp. 1332–1340 (cit. on pp. 21, 25, 28, 118).

[55] Gojko Joksimovic. 'Line current spectrum analysis in saturated three-phase cage induction machines'. In: *Electrical Engineering* 91 (04/2010), pp. 425–437 (cit. on p. 21).

[56] Gojko Joksimović. 'Dynamic model of cage induction motor with number of rotor bars as parameter'. In: *The Journal of Engineering* 2017.6 (06/2017), pp. 205–211 (cit. on p. 21).

[57] A. K. Wallace and A. Wright. 'Novel Simulation of Cage Windings Based on Mesh Circuit Model'. In: *IEEE Transactions on Power Apparatus and Systems* PAS-93.1 (01/1974), pp. 377–382 (cit. on p. 25).

[58] N. Gule and M. J. Kamper. 'Evaluation of rotor bar and end ring current waveform of brush DC equivalent controlled multiphase cage rotor induction machine'. In: *2012 XXth International Conference on Electrical Machines*. 09/2012, pp. 946–952 (cit. on p. 25).

[59] Julien Cordier and Ralph Kennel. 'A Simple and Efficient State-Space Model of Induction Machines with Interconnected Windings Including Space Harmonics'. In: *2018 IEEE Energy Conversion Congress and Exposition (ECCE)*. IEEE, 2018, pp. 1595–1602 (cit. on p. 30).

[60] Georgi P. Tolstov. *Fourier Series*. Dover Publications Inc., 01/02/1977. 352 pp. (cit. on p. 35).

[61] S. A. Nasar. 'Electromechanical Energy Conversion in nm-Winding Double Cylindrical Structures in Presence of Space Harmonics'. In: *IEEE Transactions on Power Apparatus and Systems* PAS-87.4 (04/1968), pp. 1099–1106 (cit. on pp. 47, 82, 118).

[62] Fengxiang Wang, Zhe Chen, Peter Stolze, Jean-Francois Stumper, Jose Rodriguez and Ralph Kennel. 'Encoderless Finite-State Predictive Torque Control for Induction Machine With a Compensated MRAS'. In: *IEEE Transactions on Industrial Informatics* 10.2 (05/2014), pp. 1097–1106 (cit. on p. 58).

[63] Petros Karamanakos, Peter Stolze, Ralph M. Kennel, Stefanos Manias and Hendrik du Toit Mouton. 'Variable Switching Point Predictive Torque Control of Induction Machines'. In: *IEEE Journal of Emerging and Selected Topics in Power Electronics* 2.2 (06/2014), pp. 285–295 (cit. on p. 58).

[64] Narpat Singh Gehlot and Pablo Javier Alsina. 'A Discrete Model of Induction Motors for Real-Time Control Applications'. In: *IEEE Transactions on Industrial Electronics* 40.3 (06/1993), pp. 317–325 (cit. on p. 58).

[65] Hernán Miranda, Patricio Cortés, Juan I. Yuz and José Rodríguez. 'Predictive Torque Control of Induction Machines Based on State-Space Models'. In: *IEEE Transactions on Industrial Electronics* 56.6 (06/2009), pp. 1916–1924 (cit. on p. 58).

[66] Christian A. Rojas, Juan I. Yuz, Cesar A. Silva and Jose Rodriguez. 'Comments on "Predictive Torque Control of Induction Machines Based on State-Space Models"'. In: *IEEE Transactions on Industrial Electronics* 61.3 (03/2014), pp. 1635–1638 (cit. on p. 58).

[67] Pavel Vaclavek and Petr Blaha. 'Enhanced discrete time model for AC induction machine model predictive control'. In: *IECON 2012 - 38th Annual Conference on IEEE Industrial Electronics Society*. IEEE, 10/2012 (cit. on p. 58).

[68] Bernardino Castillo-Toledo, Stefano Di Gennaro, Alexander G. Loukianov and Jorge Rivera. 'Hybrid Control of Induction Motors via Sampled Closed Representations'. In: *IEEE Transactions on Industrial Electronics* 55.10 (10/2008), pp. 3758–3771 (cit. on p. 58).

[69] Jorge Rivera Dominguez. 'Discrete-Time Modeling and Control of Induction Motors by Means of Variational Integrators and Sliding Modes - Part I: Mathematical Modeling'. In: *IEEE Transactions on Industrial Electronics* 62.9 (09/2015), pp. 5393–5401 (cit. on p. 58).

[70] David F. Griffiths and Desmond J. Higham. *Numerical Methods for Ordinary Differential Equations*. Springer London, 2010 (cit. on p. 58).

[71] Julien Cordier, Stefan Klass and Ralph Kennel. 'A Discrete-Time Model of Induction Machines Including Winding Distribution Harmonics'. In: *13th IEEE International Conference on Power Electronics and Drive Systems (PEDS 2019)*. IEEE, 2019 (cit. on pp. 60, 67).

[72] Julien Cordier, Stefan Klass and Ralph Kennel. 'A Real-Time Compliant State-Space Model of Induction Machines Including Winding Distribution Harmonics and Winding Interconnections'. In: *2019 21st European Conference on Power Electronics and Applications (EPE'19 ECCE Europe)*. IEEE, 09/2019 (cit. on p. 60).

[73] James E. Gentle. *Matrix Algebra - Theory, Computations and Applications in Statistics*. Springer, 2017 (cit. on p. 80).

[74] Stephan Ramon Garcia and Roger A. Horn. *A Second Course in Linear Algebra*. Cambridge University Press, 05/2017 (cit. on p. 80).

[75] P. Drozdowski and T. J. Sobczyk. 'On a mathematical model of squirrel-cage induction motors'. In: *Archiv fuer Elektrotechnik* 70.6 (11/1987), pp. 371–382 (cit. on pp. 82, 84, 118).

[76] Julien Cordier, Stefan Klass and Ralph Kennel. 'A General Coordinate Transformation Based on Fourier Matrices for Modelling Space Harmonics in Induction Machines'. In: *2019 IEEE Energy Conversion Congress and Exposition (ECCE)*. IEEE, 2019 (cit. on p. 92).

[77] Tzon-Tzer Lu and Sheng-Hua Shiou. 'Inverses of 2 x 2 block matrices'. In: *Computers & Mathematics with Applications* 43.1-2 (01/2002), pp. 119–129 (cit. on pp. 103, 124).

[78] H. R. Fudeh and C. M. Ong. 'Modeling and Analysis of Induction Machines Containing Space Harmonics - Part I: Modeling and Transformation'. In: *IEEE Transactions on Power Apparatus and Systems* PAS-102.8 (08/1983), pp. 2608–2615 (cit. on pp. 118, 122).

[79] H. R. Fudeh and C. M. Ong. 'Modeling and Analysis of Induction Machines Containing Space Harmonics - Part III: Three-Phase Cage Rotor Induction Machines'. In: *IEEE Transactions on Power Apparatus and Systems* PAS-102.8 (08/1983), pp. 2621–2628 (cit. on p. 118).

[80] H. R. Fudeh and C. M. Ong. 'Modeling and Analysis of Induction Machines Containing Space Harmonics - Part II: Analysis of Asynchronous and Synchronous Actions'. In: *IEEE Transactions on Power Apparatus and Systems* PAS-102.8 (08/1983), pp. 2616–2620 (cit. on p. 118).

[81] Yifan Zhao and T.A. Lipo. 'Space vector PWM control of dual three-phase induction machine using vector space decomposition'. In: *IEEE Transactions on Industry Applications* 31.5 (1995), pp. 1100–1109 (cit. on p. 119).

[82] E. Levi, R. Bojoi, F. Profumo, H.A. Toliyat and S. Williamson. 'Multiphase induction motor drives – a technology status review'. In: *IET Electric Power Applications* 1.4 (2007), p. 489 (cit. on p. 119).

[83] Robert Hermann and Arthur J. Krener. 'Nonlinear Controllability and Observability'. In: *IEEE Transactions on Automatic Control* AC-22.5 (10/1977), pp. 728–740 (cit. on p. 122).

[84] C. Canudas De Wit, A. Youssef, J.P. Barbot, P. Martin and F. Malrait. 'Observability conditions of induction motors at low frequencies'. In: *Proceedings of the 39th IEEE Conference on Decision and Control (Cat. No.00CH37187)*. IEEE, 2000 (cit. on p. 128).

[85] Pavel Vaclavek, Petr Blaha and Ivo Herman. 'AC Drive Observability Analysis'. In: *IEEE Transactions on Industrial Electronics* 60.8 (08/2013), pp. 3047–3059 (cit. on p. 128).